FORMING BEHAVIOR OF FRICTION STIR WELDED SHEETS

A Thesis Submitted in Partial Fulfillment of the Requirements

for the Degree of

DOCTOR OF PHILOSOPHY

by

Perumalla Janaki Ramulu

(Roll No. 08610306)

Department of Mechanical Engineering

Indian Institute of Technology Guwahati

Guwahati–781039

INDIA

September 2012

Department of Mechanical Engineering
Indian Institute of Technology Guwahati
Guwahati-781039 INDIA

CERTIFICATE

It is certified that the work contained in the thesis entitled "**FORMING BEHAVIOR OF FRICTION STIR WELDED SHEETS**" submitted by **Mr. Perumalla Janaki Ramulu** to the Indian Institute of Technology Guwahati for the award of the degree of Doctor of Philosophy has been carried out under my supervision in the Department of Mechanical Engineering, Indian Institute of Technology Guwahati. This work has not been submitted elsewhere for the award of any other degree or diploma.

(Dr. R. Ganesh Narayanan)
Assistant Professor
Department of Mechanical Engineering,
Indian Institute of Technology Guwahati,
Guwahati– 781039,
INDIA

Dedicated to……

MY NATION

ACKNOWLEDGEMENT

First of all, I express my deepest gratitude to my supervisor, Dr. R. Ganesh Narayanan for his invaluable guidance, encouragement, inspiration and support throughout my PhD work. I can never forget the vigor and attention bestowed by him in taking my research ahead. His innovative ideas and acumen helped me in truly understanding what research means, and how with a focused mind, with patience and perseverance, an unsolved problem can be solved and its results physically interpreted and analyzed. His personal character combined with professional ethics will remain a source of inspiration for the rest of my life.

I am thankful to my Doctoral Committee members, Prof. U.S. Dixit, Dr. S. Senthilvelan, Prof. Ananthakrishnan Srinivasan and Dr. Perumal Alagarsamy for their insightful comments and valuable suggestions during my progress seminars, and on other occasions too. I would like to express my sincere thanks to Prof. D**.** Chakraborty, ex HOD and Prof. P. Mahanta, HOD and all other faculty members of the Department of Mechanical Engineering for their encouragement and support.

I am extremely grateful to Prof. Satish V. Kailas IISc Bangalore and Prof K. Narasimhan IIT Bombay for their support and guidance to carry out a part of my experimental work. I spent four productive months at IISc and three months at IIT Bombay in their laboratory. In a short time, I could experience what research culture is, and with what great enthusiasm the researchers there work, and how Professors truly support their students. I express my sincere thanks to all the members and staff of IISc Bangalore and IIT Bombay for their kind cooperation and help during my stay. Special thanks to Jayachandra Reddy, BVS Raju, Dilip, M. Bhargav and Swami Babu who helped during experiments in the lab.

I am thankful to DST for funding the project through FASTTRACK scheme and travelling abroad to attend the conference. I also thank Aeronautics Research and Development Board, India for funding a project.

I thank IIT Guwahati administration for providing all facilities and Mechanical Engineering department technical staffs Dr. D. K. Sharma, N. K. Das, Basumatari, Rituraj Sakia, Sanjib Sharma, Pranjal Poul, Nip Bora, Bhaishya, Chatri, Tithlahari for helping me.

Last but not the least, the patience and forbearance of my wife, my parents, my sister, my brothers, my father-in-law, mother-in-law and my whole family members need special mention. Leaving rest other things aside, their continued moral support and blessings,

allowed me to concentrate on my work for long hours. It is their trust and confidence in me that I am in a position to write this acknowledgement.

The company of my friends at IIT Guwahati made my four years of stay enjoyable. My friends especially C. Subramanian, Eswaran, Satheesh, Ratnakar Das, S. Mahato, Chandra Shekaran, Mohit, Rakesh, Sateesh Kumar, Rama Srikanth, Purnendu Mandal, Ravi, Satya Shekar, Sudharshan Kumar, Anbarasu, Parida Biswajit, Yadaiah, Anil, Deepak, Arpan, Ravichandra, Muthuraja, Sivarama Krishnan, Durga Rao, Shanti Raju, Yadav, Chenchaiah, Laxman, Sai Kumar, Himanshu Jha, Guptha, Nagesh, Kanchana, Tanveera, Mukesh Singh, Vijay Singh, Arun, Biplav, Shukanto, Jagannath Sardar, Amitava Ghatak, Rajendhra, etc... Here, I learned not only the academics and research, but many other things which are needed in personal and professional lives. They indeed made me realize, what the life is. Each of them deserves special thanks.

September 2012 **Perumalla Janaki Ramulu (*Swapnam*)**
IIT Guwahati

Publications from the present work

Journals

Published:

1. **P. Janaki Ramulu**, R. Ganesh Narayanan, Satish V. Kailas, Jayachandra Reddy, "Internal defect and process parameter analysis during friction stir welding of Al 6061 sheets". International Journal of Advanced Manufacturing Technology, (**2012**), DOI: 10.1007/S00170-012-4276-Z.
2. **Perumalla Janaki Ramulu** and R. Ganesh Narayanan **2012**, "Weld zone representation during the formability prediction of friction stir welded blanks with dissimilar thickness", Materials Science and Engineering Technology, Volume 43: 241-252.
3. **P. Janaki Ramulu**, R. Ganesh Narayanan, Satish V. Kailas, Jayachandra Reddy, **2012**, "Formability evaluation of FSW blanks made of aluminum sheet: Influence of welding speed and tool rotation speed" Advanced Materials Research Vol. 410:287-290.
4. **Perumalla Janaki Ramulu** and R. Ganesh Narayanan **2011**, "Weld zone representation during the formability prediction of friction stir welded blanks with similar thickness". The Journal of Strain Analysis for Engineering Design, Volume 46: 456-478.

Under review:

1. **P. Janaki Ramulu**, R. Ganesh Narayanan, Satish V. Kailas, "Influence of shoulder diameter and plunge depth on forming limit of friction stir welded sheets".
2. **P. Janaki Ramulu**, R. Ganesh Narayanan, Satish V. Kailas, "Influence of tool rotation speed and welding speed on forming limit of friction stir welded sheets".
3. **P. Janaki Ramulu**, R. Ganesh Narayanan, "Effect of friction stir welding process parameters on the mechanical properties of welded sheets".
4. **P. Janaki Ramulu**, Satish V. Kailas, R. Ganesh Narayanan, "Influence of different weld location and orientation on forming limit of friction stir welded sheets".

Under documentation:

1. **P. Janaki Ramulu**, R. Ganesh Narayanan, "Forming limit prediction of friction stir welded blanks with different weld locations and orientation".

Conferences

1. **P. Janaki Ramulu**, R. Ganesh Narayanan, Satish V. Kailas, "Influence of weld location and orientation on the formability of friction stir welded sheets made of Al 6061 alloy", International deep drawing research group (IDDRG), November 25-28, **2012**, IIT Mumbai, India.
2. **P. Janaki Ramulu,** R. Ganesh Narayanan, "Sensitivity analysis of mechanical and geometric properties for weld zone representation of friction stir welded blanks during formability prediction, International Conference on Computational Methods in Manufacturing, December 15-16, **2011**, IIT Guwahati, India.
3. **P. Janaki Ramulu**, R. Ganesh Narayanan, Satish V. Kailas, Jayachandra Reddy, "Formability evaluation of FSW blanks made of aluminum sheet: Influence of welding speed and tool rotation speed", Twentieth International Symposium on Processing and Fabrication of Advanced Materials (PFAM XX) December 15-18, **2011**, Hong Kong.
4. **P. Janaki Ramulu**, R. Ganesh Narayanan, Satish V. Kailas, Jayachandra Reddy, "Tensile behavior of FSW blanks made of aluminum sheet: Influence of welding speed and rotation speed. International conference on advances in materials and materials processing (ICAMMP-2011) pp.193, **2011**. Kharagpur, India.
5. **P. Janaki Ramulu**, R. Ganesh Narayanan, Satish V. Kailas, Jayachandra Reddy, "Formability evaluation of FSW blanks made of aluminum sheet: Influence of shoulder diameter and plunge depth" 49th National Metallurgists' day and 65th annual technical meeting of the Indian Institute of Metals, 13-16 November **2011**
6. **Perumalla Janaki Ramulu** and R. Ganesh Narayanan, "Comparing the weld zone representation methods during the formability prediction of friction stir welded blanks", The 14th International ESAFORM Conference on Material Forming AIP Conf. Proc. 1353, 213-218 (**2011**).
7. **Perumalla Janaki Ramulu** and R. Ganesh Narayanan, "Predicting the forming limit of friction stir welded blanks", The 14th International ESAFORM Conference on Material Forming AIP Conf. Proc. 1353, 219-223 (**2011**).
8. **Perumalla Janaki Ramulu,** Nilesh Bondre and R Ganesh Narayanan, **2010**, "Weld zone representation during the formability prediction of friction stir welded blanks with equal thickness", 3rd International & 24th National conference, All India Manufacturing Technology, Design and Research (AIMTDR) 2010, Volume 2: 989-994.
9. **Perumalla Janaki Ramulu** and R Ganesh Narayanan, **2009**, "Representing weld zone during friction stir welded blank formability prediction", 3rd International Congress on Computational Mechanics and Simulation (ICCMS-09), pp. 231-232.
10. **Perumalla Janaki Ramulu** and R Ganesh Narayanan, **2009**, "Forming limit prediction of friction stir welded blanks", 3rd International Congress on Computational Mechanics and Simulation (ICCMS-09), pp. 233-234.

ABSTRACT

The difficulty of making welds of aluminum alloys by conventional (fusion) welding process is due to poor solidification microstructure, porosity in the fusion zone, the loss in mechanical properties, more expensive surface preparation techniques, and also formation of surface oxides. Friction stir welding (FSW) is proven process to fabricate defect free welds and high strength joints, under optimized conditions. This process fabricates the joints in solid state, such that it is advantageous over conventional processes. It has been successfully used to weld similar and dissimilar metals by varying many process parameters. The joining technique can be used to produce butt, corner, lap, T, spot, fillet, hem joints and hollow objects, and parts with 3D profiles, so that it is applicable for automobile and other industries. The complexity of the process lies in the selection of the process parameters upon which the joint formation and strength depends on. The main process parameters are distinguished with respect to tool geometry, welding parameters and joint design. Tool geometry is varied with respect to shoulder diameter and pin profile; welding parameters like tool rotation speeds and welding speeds play important role in the process along with axial load and tilt angle. Each parameter has its own significance during joint formation, change in microstructure and mechanical properties.

The main objective of the present thesis is to study the influence of shoulder diameter, plunge depth, tool rotation speed and welding speed on the formability of FSW sheets made of 2.1 mm thick AA 6061-T6 alloy. Later the formability of FSW sheets is also predicted by using few necking criteria and validated with experimental results. The parameters mentioned are changed in a specific range by conducting many experimental trials. The effect of welding speed, rotation speed, plunge depth, and shoulder diameter on the formation of internal defects during welding is also analyzed. It is observed that at higher welding speed, higher rotation speed and higher plunge depth, the welds are defect free. The effect on axial force and torque during welding is studied. The axial force and torque are not constant and a large variation is seen with respect to FSW parameters that produced defective welds and they are almost constant while defective welds are formed. The optimized welding parameters for producing internal defect free welds are found. A simple criterion, $(\partial\tau/\partial p)_{\text{defective}} > (\partial\tau/\partial p)_{\text{defect free}}$ and $(\partial F/\partial p)_{\text{defective}} > (\partial F/\partial p)_{\text{defect free}}$, is proposed with this observation for identifying the onset of defect free weld formation.

The influence of optimized plunge depth, tool rotation speed, welding speed and shoulder diameter on the tensile behavior namely flow strength, elongation, hardness, and forming

behavior of FSW sheets in different welding conditions like weld orientation and weld orientation are studied. Formability evaluation is performed through limit dome height tests. The forming limit curve (only in stretching region), thickness distribution, and strain hardening exponent of weld region are monitored during formability studies. The influence of three different weld orientations, 0°, 45° and 90° and weld locations, at centre, at 5 mm offset, and at 10 mm offset in the longitudinal weld orientation are deformed. The experimental forming limit results are compared with predicted limit strain results.

Micro-hardness showed a decreasing trend, from the base material to the centre of the nugget zone, except near the transition zone. With increase in shoulder diameter and welding speed, hardness has increased. But with increase in plunge depth and rotational speed, hardness has decreased. The FSW sheets showed a decreased flow stress, improved elongation and formability when compared to base material. The overall elongation of FSW sheets and weld zone has improved with increase in plunge depth, shoulder diameter, and rotational speed, while welding speed has shown insignificant effect. With increase in shoulder diameter, plunge depth and tool rotation speed the forming limit is found to improve considerably, whereas reverse effect is seen with increasing welding speed.

The relation between thickness gradient of FSW sheets developed during forming and strain hardening exponent of weld zone to elongation and forming limit improvement has been developed. The thickness gradient is found to be severe in un-welded blanks as compared to FSW blanks. With increase in shoulder diameter, plunge depth and rotation speed, the thickness gradient is found to decrease, while welding speed showed negligible effect. With decrease in thickness gradient severity and with increase in strain hardening exponent of weld region, the overall elongation and the forming limit is found to increase. The improvement in strain hardening exponent in weld zone is believed to occur because of lower dislocation density in the recrystallized weld zone. There is not much variation in dome height among the FSW sheets tested. When compared with un-welded sheets, dome height of FSW sheets is higher in near plane-strain condition, but it is lesser in stretching strain paths.

The influence of weld orientation and weld location on the formability of FSW blanks during stretching operation is also analyzed. Three different weld orientations, 0°, 45° and 90° and weld locations, at centre, at 5 mm offset, and at 10 mm offset in the longitudinal weld orientation are deformed. The formability of FSW sheets with 0° weld orientation is better than 45° and 90° orientations. The FSW sheets with weld at centre location show better formability, followed by 5 mm offset and 10 mm offset locations.

During formability prediction of friction stir welded (FSW) blanks, it is necessary to incorporate nugget zone and heat affected zone (HAZ) properties separately for better accuracy. In this work, it is proposed that there should be a domain of weld conditions where in the single zone assumption breaks down and double zone assumption should be followed for both similar and dissimilar thickness FSW sheets. This is accomplished by performing limit dome height test simulation in PAM STAMP 2G, an elastio-plastic finite element code, with single and double zone assumptions. The progression at failure and maximum load are compared between FSW blanks modeled with single and double zone assumptions. It is observed that modeling FSW blanks with double zone assumption plays a vital role for accurate formability prediction. It is found that there exists relationship between the thickness distribution and availability of single zone or double zone models. Whenever the thickness distribution of a particular double zone is closer to reference case modeled with single zone, it is sufficient to model that weld zone case with single zone. Double zone representation is required in cases when thickness distribution is very different. The number of single zone models has increased in transverse weld orientation and number of double zone models has increased in longitudinal weld orientation in the case of FSW blanks with dissimilar thickness as compared to similar thickness FSW blanks.

The forming limit of FSW sheets under different weld orientation and locations are predicted using thickness gradient based necking criterion (TGNC) and major strain-rate ratio based necking criterion (MSRC). The predictions are compared with experimental results. It is found that TGNC predictions are better than MSRC in most of the cases, though MSRC predictions are comparable with TGNC predictions. The significance of single zone and double zone modeling of weld region is also discussed here by comparing with experimental results.

ABBREVIATIONS

AS	Advancing side
BHF	Blank holding force
BM/PM	Base material
FLC	Forming limit curve
FLD	Forming limit diagram
FSP	Friction stir process
FSW	Friction stir welding
HAZ	Heat affected zone
HDS	Hot die steel
HF	Hydro fluoric
LDH	Limiting dome height
MSRC	Major strain-rate ratio criterion
PD	Plunge depth
PP	Pin profile
RS	Retreating side
SD	Shoulder diameter
TE	Total elongation
TGNC	Thickness gradient necked criterion
TMAZ	Thermo-mechanically affected zone
TRS	Tool rotation speed
TWB	Tailor welded blank
TWI	The welding institute
UE	Uniform elongation
UTS	Ultimate tensile strength
WN/NZ	Weld nugget/nugget zone
WS	Welding speed
YS	Yield strength

NOMENCLATURE

w_r	weld width ratio
w_{NZ}	width of nugget zone
w_{HAZ}	width of heat affected zone
YS_r	yield strength ratio
YS_{NZ}	yield strength of nugget zone in MPa
YS_{HAZ}	yield strength of heat affected zone in MPa
n_r	strain hardening exponent ratio
n_{NZ}	strain hardening exponent of nugget zone
n_{HAZ}	strain hardening exponent of heat affected zone
σ	True stress in MPa
K	Material strength coefficient in MPa
ε	True strain
n	strain hardening exponent
t	Thickness in mm
$R_{\text{thickness gradient}}$	Thickness gradient necking ratio
R	Plastic strain ratio
∂p	change in welding speed or tool rotation speed or plunge depth
∂F	change in the axial force
$\partial \tau$	change in the torque
R_1	Major strain-rate ratio

CONTENTS

List of Figures

List of Tables

Chapter 1

Introduction, Literature review, Significance and Objective of work

1.1 Introduction

Friction stir welding (FSW) is a solid state welding process and it was invented in 1991 by the Welding Institute (TWI), Cambridge, UK. This process joins two different metals by fusing them from the heat produced by a rotating tool. FSW has many advantages over conventional processes and it has also replaced the fastened joints, due to its significant weight and cost reductions. It has been successfully used to weld similar and dissimilar metals by varying many process parameters. Many studies have been carried out about the effect of process parameters on the joint properties like mechanical properties, microstructure, forming behavior and their prediction. These process parameters are distinguished with respect to tool geometry, welding parameters and joint design. Tool geometry is varied with respect to shoulder diameter and pin profile, welding parameters are tool rotation speeds and welding speeds play important role in the process along with axial load and tilt angle.

Various studies have been investigated such as the influence of shoulder diameter, pin profile, tool rotation speed, welding speed, axial load/force, and tilt angle on the FSW process, material flow during welding, microstructural variations, and mechanical properties. It has been observed that all these process parameters have significant impact on generating frictional heat, gripping on the plasticized materials, material flow field, temperature in the weld region, contact between tool and work-pieces and defects positions in joints. The optimization of these parameters with respect to base materials proved the quality welded joints with defect free microstructure and high strength.

FSW joint microstructure consists of four different zones namely- base metal, heat affected zone (HAZ), thermo mechanical affected zone (TMAZ) and weld nugget (WN). These zones have different grain structure along with different mechanical properties. But, TMAZ is combined with WN because it is small in size. By this, weld zone is distinguished with HAZ and WN only. Due to different properties in weld zone, FSW joints will have impact on failure location and mechanical behaviour modelling, especially forming FSW sheets.

There are a few studies which were focussed on numerical modelling and simulation of FSW process. From their studies material flow formation in weld zone, temperature variations, residual stresses and strains can be evaluated. This evaluation is with respect to the effect various process parameters and their significance in FSW process. Few prediction works are seen related to the forming behaviour of FSW blanks, in which, formability prediction of FSW blanks was studied by considering weld zone as single entity i.e., weld zone modelled as single zone without considering HAZ and WN properties separately. This is not acceptable when accurate formability is required.

The main objectives of the present work is to study the effect of different shoulder diameters, plunge depths, tool rotation speed and welding speeds on the formability of FSW sheets and predicting the formability of FSW sheets using different failure criteria. For this, few process parameter ranges was identified to fabricate defect free welds of AA 6061-T6 aluminum alloy with 2.1 mm thickness. The important varied parameters were shoulder diameter, plunge depth, tool rotation speed and welding. The individual effect of these parameters on formability was seen by constructing forming limit diagrams obtained from limit dome height test and monitoring the dome height. The effect of weld location and weld orientation on formability of FSW blanks is also observed. The FSW blanks formability is predicted and compared with experimental FLCs by using different failure criteria. During prediction the weld zone in FSW blanks is represented as single zone model (without considering HAZ separately) and double zone model (with considering HAZ separately).
Literature review, significance of the work, objectives of the work, and tasks involved is presented in Chapter 1. Weld zone representation in FSW blanks made of similar and dissimilar thickness during formability prediction and its essentiality during forming prediction is presented in Chapter 2 and 3. Internal defects formation in FSW joints made of AA 6061-T6 and identified the process parameter range for making defect welds is presented in Chapter 4. Tensile behavior and micro hardness of FSW sheets are presented Chapter 5. The influence of shoulder diameter, plunge depth, tool rotation speed, and welding speed on formability of FSW sheets is presented in Chapter 6 and 7. The effect of weld location and orientation on the forming behavior of FSW sheets is presented in Chapter 8. Predicting the forming limit strains of FSW blanks made at different weld orientations and weld locations is presented in Chapter 9.

1.2 Literature review

1.2.1 Introduction to friction stir welding

Friction stir welding (FSW) is an addition to friction welding; a solid state welding process and it was invented in 1991 by the Welding Institute (TWI), Cambridge, UK. This technique utilizes a non consumable rotating welding tool to generate frictional heat and deformation at the welding location, thereby affecting the formation of a joint, while the material is in the solid state. It is defined as "FSW is a solid state welding process that joins to different metals by fusing them from the heat produced by a rotating tool."

1.2.1.1 Background: It is difficult to make welds of aluminum alloys by conventional process. It is due to poor solidification microstructure, porosity in the fusion zone, and loss in mechanical properties, more expensive on surface preparation and also surface oxides. FSW process is used to weld aluminum alloys without any defects. More over this process is used to weld similar and dissimilar cast and wrought aluminum alloys, steels, titanium, copper, magnesium alloys, dissimilar metal group alloys and metal matrix composites (Mishra and Ma, 2005).

1.2.1.2 Working principle: The basic concept of FSW is a non-consumable rotating tool with pin and shoulder is inserted into the abutting edges of sheets or plates to be joined and traversed along the line of joint. During joint formation the tool serves two primary functions: (a) heating of work piece, and (b) movement to the material. The heating is accomplished by friction between the tool and the work-piece. There were many tools used to fabricate the joints of different materials. The selection of the tool is depending on the base materials (Rai *et al.*, 2011). The plastic deformation happens at tool contacting area in work-piece. The material flow from the front side of the pin to backside of the pin is due to combination of tool rotation and tool movement (Mishra and Ma, 2005; Nandan *et al.*, 2008). The working principle of this process is shown in Fig. 1.1.

In general, welds produced by FSW are asymmetric. On one side of the weld called as advancing side (AS), the direction of rotation of the tool coincides with the welding direction, while on the other side, the retreating side (RS), the direction of rotation of the tool is opposite to the welding direction (Heurtier *et al.*, 2006). Therefore, a plasticized material on

the advancing spends a longer time than on the retreating side. This is influenced by the vortex velocity field.

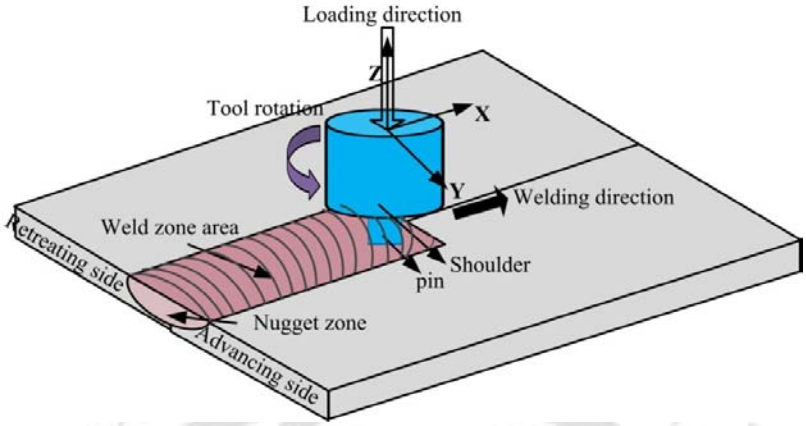

Fig. 1.1 Schematic representation of friction stir welding process

1.2.1.3 Advantages: The process is simple since welding is at low temperatures, simple joint preparation, no fused-on spatters, fume or dust, no inert protective gas, low power requirement, low distortion of the welded parts, very good mechanical behavior of the welds, material mix of different aluminum alloys. By comparing with other welding processes, low cost process and no yielding due to less heat input.

1.2.1.4 Disadvantages: This process is not suitable for high melting point materials, complicated joints are not possible, need proper selection of process parameters, improper bond formation between tool metal, not applicable for more thickness plates, key hole at the end of operation, pieces must be rigidly clamped, requires a backing bar. Inspite of these disadvantages, recently materials like steel, titanium etc. are FS welded with proper selection on of tool materials and process parameters (Reynolds *et al.*, 2003; Lee *et al.*, 2005; Sato *et al.*, 2005 and Ahn *et al.*, 2012).

1.2.1.5 Applications: The process can be used to produce butt, corner, lap, T, spot, fillet, hem joints and hollow objects, like tanks and tube/pipe, and parts with 3D profiles so that it is applicable for all types of automobile and other type of industries. Some of them are welding of long length of materials in aerospace, shipbuilding, railway industries, formula 1 race cars, large fuel tanks, containers for space launch vehicles, cargo decks for high-speed ferries, and roofs for railway carriages (Thomas and Nicholas, 1997; Heinz *et al.*, 2000).

1.2.2 Different types of process parameters in FSW process

FSW process involves complex material movement and plastic deformation. Due to this selected process parameters play an important role during the process. In general, process

parameters in FSW are classified in three different manners like tool geometry, welding parameters, and joint design. In tool geometry variable parameters are tool profile, shoulder diameter, pin profile, plunge depth, overlap and tilt angle. The welding parameters are mainly tool rotation speed and welding speed. All of these parameters are represented schematically in Fig.1.2. Apart from these parameters, some other parameters like axial force, and base metal properties also affect the process. The effect of these process parameters during FSW joint formation was discussed by FU Zhi-hong *et al.*, 2004; Mishra and Ma, 2005; Greitmann and Deimel, 2005; Ma, 2008; Ghosh *et al.*, 2010. Every parameter has its own significance and has combined effect during weld formation. In whole process parameters like shoulder diameter (SD), pin profile (PP), plunge depth (PD), welding speed (WS), tool rotational speed (TRS), axial load and tilt angle are the important parameters which are controlling the total FSW process.

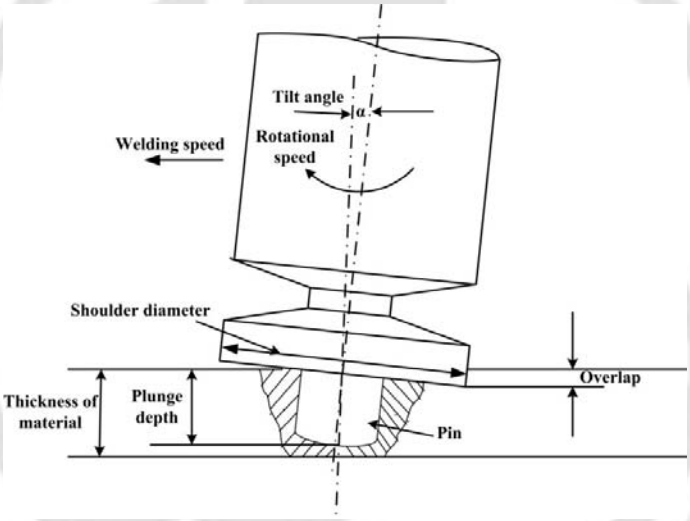

Fig. 1.2 Schematic representation of main process parameters involved during Friction Stir Welding

1.2.3 Material flow and defect formation in FSW process

The material flow pattern is a complex phenomenon in this process and depends on the process parameters chosen. This varies from AS to RS. In FSW material flow occurs through the RS and the transport of the plasticized material behind the tool makes the welded joint. Material flow formation is depending on the three types of flow. In which, near the tool, a slug of plasticized material rotates around the tool. This motion is driven by the rotation of the tool and the resulting friction between the tool and the work-piece. Second, rotational

motion of the pin tends to push material downward close to the pin which drives an upward motion of an equivalent amount of material. Finally, there is a relative motion between the tool and the work-piece (Nandan *et al.*, 2008; Kumar and Kailas, 2008 b). In whole, the material flow varies material to material depending on the tool geometry and welding parameters chosen for welding.

Li *et al.*, 1999; Guerra *et al.*, 2003; Schmidt *et al.*, 2006; Zhang *et al.*, 2007; Arbegast, 2008; Chen *et al.*, 2008; Hamilton *et al.*, 2008; Kumar and Kailas 2008 b; Leal *et al.*, 2008; Reynolds, 2008 were studied and the materials flow pattern in different materials like AA2024-T4 to AA 6061-T6, AA6061, AA2024-T3, AA 6061-T6, AA 5085-O, 6061-T6, AA 7020-T6, AA 5182-H111 to AA 6016-T4 aluminum alloys using different process parameters were examined. From these studies, they suggested that internal defects free joints are possible only by the selection of proper process parameters. Improper selection leads to the external and internal defects like flash due to the excess heat input, cavity or groove by insufficient heat input; and cavity by the abnormal stirring (Kim *et al.*, 2006), channel and kissing-bond due to small or large tool tilt angle, Lazy S by improper mixing of the oxide layer (Chen *et al.*, 2006), root flaws by insufficient heat input (Zhou *et al.*, 2006), wormhole due to inadequate fill of AS (Arbegast, 2008), original joint line with severe plastic deformation, tunnel, kissing bond, and zigzag line in T-joints (Cui *et al.*, 2012).

1.2.4 Effect of FSW process on Microstructure and Mechanical properties of FSW joints

From the last decade onwards many studies have been carried out based on the effect of FSW process on the microstructure and mechanical properties of various materials joints. It is seen that microstructure of FSW joints consist of four different regions as shown in Fig. 1.3 irrespective of the base material**.** They are: (a) unaffected base metal, (b) heat affected zone (HAZ), (c) thermo-mechanically affected zone (TMAZ) and (d) friction stir processed (FSP)/weld nugget (WN) zone. The formations of above regions are affected by the material flow under the action of tool rotation. However, the material flow behavior is predominantly influenced by the process parameters.

HAZ: Heat Affected Zone, TMAZ: Thermo-Mechanically Affected Zone, WN: Weld Nugget

Fig. 1.3 Schematic of cross sectional view of FSW joint

In any material FSW joint, the microstructure in weld zone is characterized by grain size, dislocation density, texture variation and mechanical properties in different zones. The microstructural changes were observed by Rhodes *et al.*, 1997; Murr *et al.*, 1998; Jones *et al.*, 2005; Ouyang *et al.*, 2006; Cabibbo *et al.*, 2007; Woo *et al.*, 2008; Woo *et al.*, 2009; Xu *et al.*, 2009 b; Sirong *et al.*, 2010 in AA 7075-T6, AA 6061-T6, AA 2024-T351, AA 6061-T6 to Cu, AA 6056-T6, AA 6061-T6, AA 2219-O aluminium alloys and AZ31B magnesium alloy. The microstructure of these joints was observed as dynamic recrystallization and grain growth in weld zone. During FSW process strengthening precipitates appeared and re-precipitates happened on cooling. Due to this precipitates in weld zone each zone has different grain structure with different mechanical properties. The overall mechanical properties were decreased in the weld zone as compared to base metal and also the dislocation density in weld zone was less as compared to base metal. Microstructure formation and mechanical properties in weld zone can be described through the texture or grain orientation. The texture was correlated with the onion ring formations in the weld nugget. The welding parameters like tool rotation speeds and welding speeds are more responsible for the variation of texture (Lima *et al.*, 2003; Fonda and Bingert, 2007; Zadpoor *et al.*, 2008 b).

The mechanical properties of FSW joints were investigated by measuring microhardness and conducting tensile tests in longitudinal direction i.e., along the weld direction and transverse direction i.e., perpendicular to the weld. The strength of weld was compared with parent/base metal and identified the failure locations in the weld zone. For example, Mahoney *et al.*, 1998 welded 7075-T651 aluminium alloy and performed tensile test in both the longitudinal and transverse directions. Results showed that weld nugget strength was decreased, and increased in ductility compared to base metal. Failure occurred in HAZ in transverse direction. Liu *et al.*, 2004 evaluated the tensile fracture location characterizations of the friction stir welded joints of AA1050-H24 and AA6061-T6 alloys. The AA1050-H24 joints are fractured in the HAZ and TMAZ on the AS, while the AA6061-T6 joints are fractured in the HAZ on the RS. Sirong *et al.*, 2010 welded the AZ31B magnesium alloy and evaluated the mechanical properties in transverse direction. The results showed that the fracture locations of joints were in the HAZ. The microhardness in the weld nugget zone was slightly lower than that of the base metal and more than TMAZ and HAZ.

Lockwood *et al.*, 2002 examined the global and local mechanical response of AA 2024-T351 by transverse tensile tests and suggested that the mechanical response in the weld zone is governed by the response of the HAZ and WN constituents. Liu and Chao, 2005 evaluated global (total weld zone) and local (HAZ and WN) mechanical properties through rule of mixture method of AA 2024-T351 by transverse tensile tests. Results showed that the mechanical properties were different for HAZ and WN. Afrin *et al.*, 2007 evaluated the effect of FSW on the strain hardening behaviour of AZ31B Mg alloy. The hardening capacity and strain hardening exponent of the FSW samples were twice and three times more than that of the base metal. Gan *et al.*, 2008 welded the AA 5083-H18 and AA 6111-T4 alloys. They measured the hardness as well as tensile properties of the base and weld materials and related to their microstructures. The overall strength of the FSW was reduced compared to base metal. Derry and Robson, 2008 investigated the effect of the FSW process on the toughness properties of AA6013-T6 sheet and observed that minimum toughness occurs at the boundary between the WN and the HAZ. Moreira *et al.*, 2008 investigated the influence of FSW on the fatigue life of specimens of aluminium alloy 6063-T6 and compared with base material specimens. FSW specimens have longer fatigue lives compared to base metal.

Zadpoor *et al.*, 2008 b and 2010 studied the microstructure and mechanical properties of friction stir welds made in different thickness/material combinations from 2024-T3 and 7075-T6 sheets. From mechanical properties results, the hardness was more in AS and extends more into the RS and the local and global mechanical properties decrease as the thickness ratio increases. Haşim and Nuran, 2009 characterized the microstructure of the WN and HAZ through hardness and compared with the base material of AA 6013-T6. Results showed that FSW weld zone has small grain size with less hardness than base metal. Cerri *et al.*, 2011 investigated the mechanical behaviour of 6082 T6 – 6082 T6, 2024 T3 - 2024 T3, and 6082 T6 - 2024 T3 joints at varied temperatures. The tensile stress–strain curves showed a decrease of the flow stress with increasing temperature and decreasing strain rate. Aval *et al.*, 2011 investigated thermo-mechanical behaviour in similar and dissimilar friction stir welding of AA6061-T6 and AA5086-O. It is found that different strengthening mechanisms in AA5086 and AA6061 resulted in complex behaviours in hardness of the welded cross section. Nourani *et al.*, 2011 optimized the process parameters for 6061-T6 through Taguchi method.

From the above studies, it is observed that the mechanical properties of FSW joints were reduced compared to base metal. Whereas the strength and hardness of FSW joint can be improved by the post weld heat treatments like aging, solution heat treatment and combination of both treatments. The improvement in the properties was seen in joints made

of 6063-T5, 6013-T4 and T6, AA2024-T4, AA7075-T6, and 60613-T6 aluminum alloys by the heat treatments in which dislocation density and grain formation was improved (Sato and Kokawa, 2001; Heinz and Skrotzki, 2002; Barcellona *et al.*, 2006; Elangovan and Balasubramanian, 2008 a).

All the results discussed about the fracture locations of the joints, tensile behaviour, joint strength, fatigue life, and micro-hardness for the different materials. All these properties of FSW joints are depending on the process parameters used for welding. The important process parameters are shoulder diameter, pin profile, tool rotation speed, welding speed, axial load, tilt angle which were responsible for changing the microstructure and mechanical properties. The influence of these parameters is in synergetic manner as well as they affect individually. The individual effect of these parameters is discussed in the following section.

1.2.5 Effect of process parameters on joint formation, microstructures and mechanical properties of FSW joints

In this section the effect of the tool shoulder diameter, pin profile, plunge depth, welding speed, tool rotation speed, axial load and tilt angle on joint formation, microstructure, and mechanical properties variation in different materials joints are discussed.

1.2.5.1 Shoulder diameter and pin profile

The shoulder diameter and pin profile of the tool is an important parameter. They generate most of the heat, hold the plasticized material and establish the material flow field. They play a vital role to make high strength joints. It has been reported in many studies about the effect of tool shoulder diameter on microstructure, mechanical properties, weld formation and temperature evolution in aluminum alloys and other materials and their essentiality to fabricate quality welded joints have been explained.

Boz and Kurt, 2004 studied the effect of stirrer geometry on the weldability and mechanical properties of AA 1080 aluminum alloy. Five different stirrers with a square cross-sectioned and cylindrical with 0.85, 1.10, 1.40 and 2.1 mm screw pitched were used. Better bonding effect along with microstructure and mechanical properties was seen with the square, and screw 0.85 and 1.10 mm pitched stirrers. Zhao *et al.*, 2005 investigated the effect of four different pins, two of them are column pin and taper pin and the other two are the same size but with screw thread on the weldability and mechanical properties FSW of AA 2014 alloy plates. The microstructures mechanical properties and the best bonding were obtained with screw pitched taper stir pin. Fujii *et al.*, 2006 worked on the effect of the simplest pin shape

(column without threads), the ordinary pin shape (column with threads) and the triangular prism shaped pin tool shapes on the mechanical properties and microstructures of AA 1050-H24, AA 5083-O and AA 6061-T6 aluminum alloys. For 1050-H24, a columnar tool without threads produced weld with the best mechanical properties; for 6061-T6, the tool shape has not shown significant effect on the microstructures and mechanical properties; for 5083-O, the weld ability was significantly affected by the rotation speed. For a lower rotation speed, the tool shape showed insignificant effect on the microstructures and mechanical properties of the joints. Ma *et al.*, 2006 investigated the effect of tool geometry and FSP parameters on microstructure and mechanical properties of cast aluminum alloy A356. The FSP made a uniform distribution of Si particles in the aluminum matrix with significant microstructural refinement which leads to a significant improvement in both strength and ductility. But the effect of tool geometry was complicated and no systematic trend was observed.

Scialpi *et al.*, 2007 studied the effect of three tools differed from shoulders with scroll and fillet, cavity and fillet, and only fillet on the mechanical and microstructural properties of AA 6082-T6 aluminum alloy. The results showed that the best joint was achieved by a shoulder with fillet and cavity. Liu and Ma, 2008 studied the effect of different tool geometries under a wide range of parameters on microstructure and mechanical properties of AA 6061-T651. The results showed that the tensile strength of the welds increased with increasing the welding speed and was independent of the tool dimension and the rotation rate. Elangovan and Balasubramanian, 2007; Elangovan *et al.*, 2008 b, c, d studied the effect of tool profiles on FS process zone formation of AA 6061 and AA 2219 aluminum alloy joints. Five different tool pin profiles (straight cylindrical, tapered cylindrical, threaded cylindrical, triangular and square) with three different shoulder (15, 18, and 21 mm) diameters were used to fabricate the joints. From their investigation it was found that the square pin profiled tool with 18 mm shoulder diameter produced mechanically sound and metallurgically defect free welds compared to other tool pin profiles.

In similar manner Leal *et al.*, 2008; Giorgi *et al.*, 2009; D'Urso *et al.*, 2009; Aval *et al.*, 2010; Arora *et al.*, 2011; Malarvizhi and Balasubramanian, 2012; Mohanty *et al.*, 2012; Akinlabi, 2012; Longo *et al.*, 2012 studied the influence of shoulders diameter on material flow, residual stresses, fatigue life, based on maximum utilization of torque, microstructure and mechanical properties in AA 5182-H111 to AA 6016-T4 dissimilar joint, AA 6082-T6, AA 6060, AA5086, AA6061 to AZ31 dissimilar joint, commercial aluminum alloy, AA 5754 to C11000 dissimilar joint and AA 6060-T6. It was observed the shoulder size and shape have impact on more material flow, less residual stress, more fatigue life for higher shoulder

diameters and also better microstructure and mechanical properties. Zhang *et al.*, 2009 developed a thermo-mechanical model and studied the effect of different shoulder size on the temperature distributions and the material deformations in friction stir welding of AA 6061-T6. Numerical results indicated that the temperature was increased with the increase of the shoulder diameter. The stirring zone was enlarged by the increasing the shoulder size.

Chowdhury *et al.*, 2010; Palanivel *et al.*, 2012 studied the effect of pin profile on the microstructure, tensile strength and strain hardening behavior of the FSW joints made of AZ31BH24 magnesium alloy, AA5083-H111 and AA6351-T6 aluminum alloys. Vijay and Murugan, 2010 developed the different tool pin profiles to weld Al–TiB_2 metal matrix composites and studied the effect of tool pin profile on metallurgical and mechanical properties of the welded joint. Rajakumar *et al.*, 2011 investigated the tensile strength and hardness along with the corrosion rate of friction-stir- welded joints of AA6061-T6 aluminum alloy by varying shoulder diameter and pin diameter. Forcellese *et al.*, 2012b investigated the effect of different shoulder diameters with pin and without pin on friction stir welding of AZ31 magnesium alloy.

Some of the studies about effect of the tool geometry along with a few process parameters on microstructure and mechanical properties of FSW lap joints made of AA2198-T4 aluminum alloy, AZ31 magnesium alloy, commercial aluminum alloy, AA 6022-T4, AZ31B-H24 and AZ31 magnesium alloy was discussed by Buffa *et al.*, 2009; Chen and Nakata, 2009; Zhang, 2010; D'Urso and Giardini, 2010, Cao and Jahazi, 2011; Yang *et al.*, 2011. From all the studies it is shown about the significance of the tool geometry and welding parameters on the lap joint formation and its properties. In similar manner Tozaki *et al.*, 2007; Badarinarayan *et al.*, 2009 a; b; Yuan *et al.*, 2011, Bilici and Yukler, 2012 studied on 6061, 5083, 6016-T4, 5754 aluminum alloys and high density polyethylene friction stir spot welds and effect tool geometry and welding parameters on the joint properties.

From all these studies, it can be understood that the selection of shoulder diameter and pin profile is very important to have better mechanical properties, joint quality of different types of joints with different materials.

1.2.5.2 Tool rotation speed and welding speed

Tool rotation speed (TRS) is one of the main factors affecting the frictional heat. If the rotating speed is too low, the frictional heat is not enough to induce plasticized flow which leads to defects in the weld. The plasticized layer increases from top to the underside, resulting in smaller defects in weld region by increasing TRS.

Another main factor is welding speed (WS). When the welding speed is too small, the frictional heat makes the temperature too high. When the weld speed increases the material just below the tool softens to such a degree that it acts as a lubricant, lowering the friction and reduces the temperature. When the welding speed is low the temperature rise would be higher as the heat input to a given control volume of material would be for a longer time. On the other hand, when the welding speed is too large, the frictional heat is not enough to plasticize the materials beneath the tool shoulder and around the probe, resulting in improper welding. (FU Zhi-hong *et al.*, 2004; Mishra and Ma, 2005). So both tool rotation speed and welding speed are responsible for the frictional heat to join perfect defect free welds.

Sato *et al.*, 2002 examined the microstructure and hardness of AA 6063-T5 and T4 aluminum alloys at varied TRSs from 800 to 3600 rpm. Different TRS values did not result in significant differences in the hardness profile. Post weld aging raised the hardness, but the increase in hardness was small in the stir zone at the lower TRS values. James *et al.*, 2003 studied the influence of WS in the range of 80–200 mm/min on defect formation, fatigue crack initiation and life in 5083-H321 aluminum alloy. The occurrence of 'onion-skin' forging-type defects known as 'kissing bonds' was seen in single pass friction stir welds, and fatigue crack initiation and decreased overall life. Ericsson and Sandstrom, 2003 investigated the influence of 700 and 1400 mm/min WSs on the fatigue strength of AA 6082 in T6 and T4 conditions and compared the fatigue results with results for conventional arc-welding like MIG and TIG. Results showed that lower welding speed improved the fatigue performance of FSW joints than the MIG and TIG welds. Peel *et al.*, 2003 presented results of microstructural/mechanical property investigations and residual stresses of AA5083. In which four samples were welded using three 100, 150 and 200 mm/min WSs. It was found that the weld properties were at lower welding speed.

Lee *et al.*, 2004 investigated the microstructural change related with the mechanical properties of AA 6061-T6 Al alloy under varied TRS of 1250-3600 rpm and 87-267 mm/min WS. The hardness of the weld zone at a higher tool rotation speed was higher. Lim *et al.*, 2004 examined the tensile behavior of AA 6061-T651 at different TRSs 1000, 1400, 1600, 2000, and 2500 rpm and WSs 0.1, 0.2, 0.3, to 0.4 m/min. It was found that the tensile elongation of AA 6061-T651 decreased with decreasing welding speed or increasing rotating speed. Low welding speed or high rotating speed tended to encourage the plastic flow per unit time and consequently the clustering of coarse precipitates. Lim *et al.*, 2005 studied the mechanical properties of AA 6061-T651 and AA 7075-T6 and AA5083-H32 with varying TRS from 1000 to 2500 rpm and WS from 0.1 to 0.4 m/min. The tensile elongation of FSW

Al 6061-T651 and Al 7075-T6 increased while the tensile strength decreased, with increasing welding speed and/or decreasing rotating speed.

In similar manner the combine defect of TRS and WS was studied on the effect of mechanical, microstructural properties, torque, fracture characteristics and strain hardening behavior of AA 6056 and cast A356, AA 6061–T651, AA 6016-T4, AA 2219-T6, AA6351, AA6082-T651 aluminum alloys, AZ31BH24 magnesium alloy (Cavaliere *et al.*, 2006; Ma *et al.*, 2006; Ren *et al.*, 2007; Feng *et al.*, 2009; Rodrigues *et al.*, 2009; Xu *et al.*, 2009 a; Cui *et al.*, 2010; Hussain and Quadri, 2010; Gurmeet Singh *et al.*, 2011; Chowdhury *et al.*, 2010), optimization for the dissimilar joints of AA5083-AA6082 and AA2024-T351-AA6056-T4 and AA6061-T6 aluminum alloy (Peel *et al.*, 2006; Amancio-Filho *et al.*, 2008; Rani *et al.*, 2011), influence on residual stresses, and temperature distribution in the welds of AA5083–AA6082 and AA2014 alloys (Steuwer *et al.*, 2006; Rajamanickam *et al.*, 2009), corrosion behavior of AA 2219-T87, AA 6061-T6 alloy welds (Surekha *et al.*, 2009; Rajakumar *et al.*, 2011). It was observed that microstructural, mechanical properties and strain hardening behavior were better at lower welding speed and higher tool rotation speed. Torque and residual stresses were more affected by TRS than WS. The influence of different ratios of TRS/WS on mechanical properties of different zones and resulting residual stresses of FSW AZ31 magnesium alloy studied by Gharacheh *et al.*, 2006 and Commin *et al.*, 2009. It was found that increase in ratio leads to decrease in strength of the weld zone and increases the weld nugget size. Decrease in ratio leads to incomplete root penetration.

Only the effect of TRS on microstructure and mechanical properties of joints of AA 2219 aluminum alloy, joint quality of AZ31B-H24 magnesium alloy, AZ31/Al_2O_3 nano-composites, AA 7056-T6, AA5083 with reinforced layers using copper particles, AA5083-H111 and AA6351-T6 was studied by Elangovan and Balasubramanian, 2007; Cao and Jahazi, 2011; Azizieh *et al.*, 2011; Rezaei *et al.*, 2011; Zohoor *et al.*, 2012; Palanivel *et al.*, 2012. Their results showed that better microstructure and quality joints were obtained by increasing TRS.

The influence of welding speed was also seen in various studies on microstructure, mechanical properties, weld formation, force and torque development, and weld at under water of AA 6082, AA 2219, AA 6005A-T6, AA 6000 alloy, Ni base alloy, Inconel 600, AA 2219 alloys(Cavaliere *et al.*, 2008; Elangovan and Balasubramanian, 2008 b; Simar *et al.*, 2008; Zimmer *et al.*, 2009; Sakthivel *et al.*, 2009; Zhang and Zhang, 2009; Song *et al.*, 2009; Liu *et al.*, 2011). It was observed that better microstructure and quality joints were obtained at lower WS.

1.2.5.3 Axial load/force and Tilt angle

The axial load/force affects the contact state between tool and work-pieces. If the axial force is not enough then surface metal of the weld come out from weld zone area, resulting in holes at the bottom of the welding. When the axial force is high, the frictional force increases between the tool and the work-pieces surface, leading to flashes and burs on the weld surface.

Here some description has been made directly about effect of axial force/load and tilt angle on the FSW joints. Melendez *et al.*, 2003 described a technique for measuring the various forces and the torque during FSW. They made welds with 6061-T6 and 2195-T6 aluminum alloys and distinguished three types like downward force, a longitudinal force in the direction of the weld, and transverse force in direction. Kim *et al.*, 2006 examined the weldability of aluminum die casting alloy joints obtained by the varied axial force from 6.9 to 14.2 kN. For each given axial force, the sound joints were obtained at appropriate tool rotation speeds and welding speeds. At the highest axial force of 14.2 kN, the range of the optimum FSW conditions were wider. Kumar and Kailas, 2008a investigated the influence of axial load on friction stir welded joint of AA 7020-T6. The axial force was varied linearly increasing from 4 to 8.8 kN and found an optimal axial load at 8.1kN, above which the weld is defect-free. Similarly, Elangovan *et al.*, 2008 d; Rajakumar *et al.*, 2011; Rose *et al.*, 2011 studied the effect of axial force on AA6061-T6 aluminium alloy and AZ61A magnesium alloy and obtained an optimal axial force at corresponding parameters.

The tool tilt angle has an essential influence on the heat input into the material and the position of the defects in the weld. At lower tilt angle, the plastic material cannot flow sufficiently and be driven down near the end of the pin during welding. At larger tool tilt angle, weld flash can generate on the retreated side, and no sufficient plastic material fill up the cavity in the nugget zone. Chen *et al.*, 2006 analyzed and discussed about the welding defects formation with respect to tilt angle (α) variation from 1.5º to 4.5º in FSW joint made of AA 5456. From the microscopic examination of the nugget zone and fracture location of the weld confirms that the tilt angle can change the plastic material flow patterns in the stir zone. The defects like channel is formed at $\alpha \leq 1.5º$ and $\alpha \geq 4.5º$ due to small and larger tool tilt angle and kissing bond is seen at low tilt angle $\alpha = 2.5º$ which cause reduction in tensile strength.

1.2.6 Modeling and simulation of FSW process

The material flow formation during welding and the measurement of the temperature, strain, strain rate, stresses in the weld zone, axial force and torque developed by tool and

power utilization during process is a tedious job with respect to process parameters. It is possible by numerical modeling and simulations of FSW process. There are a few models such as three-dimensional visco-plastic model, heat transfer model, and thermo-mechanical model to determine the effect of TRS on temperature, force acting on tool, the trajectory of each material element of the weld, the strain, strain rates and estimations of the temperatures and micro-hardness in the different weld zones developed by Ulysse, 2002; Song and Kovacevic, 2003; Heurtier *et al.*, 2006; Zhang and Zhang, 2009; Cui *et al.*, 2010. Lockwood *et al.*, 2002 modeled the global and local mechanical response of friction stir welded AA2024 and measured the local strains. Colligan and Mishra, 2008 proposed a conceptual model to specifically distinguish between plastic work and friction in the generation of heat and to describe relationships between the independent and dependant process variables in FSW. Zhang et al. (2007) simulated material flow in friction stir welding under different process parameters by using the finite element technique based on the nonlinear continuum mechanics. Fersini and Pirondi (2008) predicted fatigue failure of AA 2024-T3 friction stir welded over lap joint through a finite element analysis. Kim *et al.*, 2009 numerically simulated the plastic deformation; thermal history and microstructure evolution of AA 6111-T4 alloy.

Paul *et al.*, 2005 demonstrated the benefits and pitfalls of using CFD to model FSW. Schmidt and Hattel, 2006 analyzed the primary conditions under which the cavity behind the tool is filled. For this, a fully coupled thermo-mechanical three-dimensional FE model has been developed. Similarly Buffa *et al.*, 2006 proposed a continuum based FEM model for friction stir welding process that is 3D Lagrangian implicit, coupled, rigid-viscoplastic. Colligan and Mishra, 2008 proposed a conceptual model to specifically distinguish between plastic work and friction in the generation of heat and to describe relationships between the independent and dependant process variables in FSW. Zhang et al. (2007) simulated material flow in friction stir welding under different process parameters by using the finite element technique based on the nonlinear continuum mechanics. Fersini and Pirondi (2008) predicted fatigue failure of AA 2024-T3 friction stir welded over lap joint through a finite element analysis. Kim *et al.*, 2009 numerically simulated the plastic deformation; thermal history and microstructure evolution of AA 6111-T4 alloy. Guerdoux and Fourment, 2009 developed an Arbitrary Lagrangian Eulerian (ALE) formulation to simulate the different stages of the FSW process. Using this formulation Assidi *et al.*, 2010 identified a robust and accurate friction model for FSW simulations using calibrations with experiments, for the Al 6061 aluminum.

1.2.7 Formability Analysis

1.2.7.1 Introduction to formability of sheets

The formability is a measure of its ability to deform plastically during a forming process in order to produce a part with definite requirements on mechanics, dimension and appearance, being mainly limited by the occurrence of flow localization or instability.

The formability of any sheet material depends on the materials properties, process parameters, and strain bounding criteria. The formability can be evaluated through simulating tests like stretching, deep drawing and drawing processes, mechanical tests, limiting dome height (LDH) and forming limit diagrams. (Banabic *et al.*, 2000; Miles, 2006 a; Kazanowski, 2006; Banabic, 2010). The concept of forming limit diagrams (FLD) was introduced by Keeler from the theoretical point of view. This diagram is the graphical representation of a curve in the plane of the principal logarithmic major and minor strains. The maximum values of the true strains can be determined by measuring the strains at failure on sheets (Banabic, 2010). The concept of FLD is applied to various tailored blanks made of different joining processes apart from base metal sheets.

1.2.8 Forming behavior Tailor welded blanks (TWBs)

Tailor welded blanks (TWBs) are made of multiple sheets that differ in terms of thickness, grade/strength, and coating of the material and are welded together before the forming process. From its beginning in mid 1980s to present status, the TWBs process has become an important element of automotive component manufacture. The prime advantage of TWBs process is reduction in cost and weight which are most important in industries. There are different types of welding processes used for making TWBs such as Laser, Resistance mash seam, High-frequency induction, Electron beam, and FSW. Many of these processes are suitable for steel sheets only except FSW which is meant for aluminum alloys only. Later it has been applied to many other materials also (Semiatin, 2006).

Forming TWBs is a challenging task due to a significant reduction of formability associated with type of blank. The forming behavior of TWBs is affected by weld conditions such as weld properties, weld orientation, and weld location, thickness difference and strength difference between the sheets. The weld region in a TWB causes serious concerns in formability because of material discontinuity and additional inhomogeneous property distribution. (Choi *et al.*, 2000; Kinsey *et al.*, 2001 a, b; 2004; Kinsey and Cao, 2005; Cheng

et al., 2005; Ganesh Narayanan and Narasimhan, 2008 a, b; Panda and Kumar, 2009; Panda *et al.*, 2010).

1.2.8.1 Forming behavior of FSW sheets

There are a few studies which were related to the formability of FSW sheets with respect to microstructural changes, joints with dissimilar materials, and comparison with other welded sheets. Sato *et al.*, 2004; Hirata *et al.*, 2007 a, b examined the relationship between the microstructure of the FS welds and their formability of AA 5052 and AA5083 aluminum alloys. They suggested that the fracture limit strains were associated to the microstructure grain size, dislocation density and sub-boundaries in the stir zone. Kang *et al.*, 2007 studied the mechanical behavior of AA 5052-H32 alloy subjected to one-pass FS process. They observed that microstructural modification in local regions in weld zone and resulted in the improvement of formability.

Miles *et al.*, 2004; 2005 analyzed the formability of similar and dissimilar TWBs obtained by FSW of the AA 5754-O, AA 5182-O and AA 6022-T4 aluminum alloys. The sheets joined using friction stir welding had better formability than those joined using gas tungsten arc welding (Miles *et al.*, 2004). The formability of FSW sheets made of dissimilar materials with same gage showed that the properties of welded 5182/5754 alloy pairs retained reasonably good formability compared to base material performance whereas the 5182/6022 and 5754/6022 alloy pairs reduced formability compared to the base material. It was due to failures occurred in the heat-affected zone of the 6022 or in the weld nugget itself (Miles *et al.* 2005). Grant *et al.*, 2005 studied the effect of the FSW process parameters on mechanical properties and formability of FSW TWBs made with different dissimilar aluminum alloys of 5182-O, 6022-T4, 5052-H111 and 5052-H32 with same/different thicknesses. Results showed that FSW TWBs have higher formability, higher ductility, and lower defect content than other joining processes. Miles *et al.*, 2006b investigated the formability of welded dual phase 590 (DP 590) steel sheets of similar and dissimilar thicknesses, and Buffa *et al.*, 2007 evaluated the local mechanical properties and the formability of FSW blanks of AA6016-T4 blanks of different thicknesses welded using FSW and laser welding. Results showed that FSW has better mechanical behavior and formability compared to laser welding.

Leitao *et al.*, 2009 analyzed the formability of FSW TWBs with similar and dissimilar of AA 5182-H111 and AA 6016-T4 Al alloys. They concluded that the formability of the TWBs is influenced by the mismatch in mechanical properties between the weld and the base

materials, and also, by the initial size of the blanks. Silva *et al.*, 2009 focused on the single point incremental forming of TWBs of AA1050-H111 alloy. Results showed that single point incremental forming with TWB produced by FSW is capable in high forming depths. Recently Yuan *et al.*, 2012; Forcellese and Simoncini, 2012 a evaluated the formability of FSW tube made of AA 2024-O and blanks made of AZ31 magnesium alloy. The tube exhibited high formability and elongation was two times higher compared to extruded tube. Formability of the AZ31 magnesium alloy welded joint has lower formability than the base material.

1.2.8.2 Formability prediction of FSW sheets

There are a few studies on the modeling and formability predictions of FSW blanks and are described here. Lockwood *et al.*, 2002 modeled the weld zone as double zone entities and studied the effect of HAZ and WN on mechanical properties locally and compared with total weld zone parameters, and suggested that the mechanical response in the weld zone is governed by the response of the HAZ and WN constituents. Zadpoor *et al.,* 2007 a, b; 2008 a; 2009 studied the effects of the implementation of the weld details on the accuracy of the failure prediction, strain distribution, and spring-back behavior of FSW TWBs. They modeled the weld zone as double zone (i.e., WZ and HAZ separately) and finally suggested that implementation of the global mechanical properties of the weld zone (i.e., single zone) is sufficient for reasonably accurate predictions of the spring back behavior.

Lee *et al.*, 2009 evaluated the formability performance of FSW TWB automotive sheets made of 6111-T4, 5083-H18, 5083-O, dual-phase steel (DP590) and AZ31 magnesium alloy, through numerical simulation and experiments. Similar type of works were carried out (Chung *et al.*, 2010; Kim *et al.*, 2010) to investigate the formability performance for four automotive sheets viz., 6111-T4, 5083-H18, 5083-O and DP590 steel sheets, each having one or two different thicknesses. For all the FSW blanks, weld zone was modeled as single zone model in the numerical simulation and studied the forming performances of welded blanks compared to those of base metal blanks. It was observed from LDH prediction that when failure occurred at base metal region, experimental and predicted FLD showed good results; while failure when occurred at weld zone area, FLC prediction was not accurate. Another study (Kim *et al.*, 2010) on the formability performance with respect to material directional combination in friction stir welded aluminum alloy 6111-T4 sheet. Experimental measurements were compared with the numerical predictions. The failures were initiated on a similar location in the weld zone for all the combinations.

1.3 Significance of work

From the literature, it is observed that many of the researchers have studied about the effect of process parameters like shoulder diameter, pin profile, tool rotational speed, welding speed, axial force, and tilt angle on FSW process, material flow formation, defects formation in joints, microstructural changes, and mechanical properties in different similar and dissimilar materials. From all the studies, it has been noticed that each parameter has its own significance in changing the joints properties. Specifically tool design influences the heat generation, plastic flow, the power required, and the uniformity of the welded joint. It creates the uniform microstructure and comparable mechanical properties with base material. Along with tool design, the welding parameters like rotational speed, transverse speed, tilt angle and axial load will also affect the microstructure and mechanical properties of the joints. From all the studies a common conclusion was made as proper selection of these parameters has to be chosen for the welding of similar and dissimilar materials with same gauge or dissimilar gauge for the better material flow formation, temperature development, microstructure integrity, mechanical properties, formability.

Many studies are already focused on flow formation, temperature development, microstructure integrity, mechanical properties of different materials during FSW. But still there is deficiency in literature about the effect of different process and tool parameters like shoulder diameter, plunge depth, tool rotation speed and welding speed, axial force, tilt angle, pin profile etc., on formability of the FSW blanks. There are a few studies about formability of FSW blanks with respect to the formability related to grain size (Sato *et al.*, 2004; Hitara *et al.*, 2007a; Kang *et al.*, 2007), formability of FSW blanks in comparison with other conventional process (Miles *et al.*, 2006; Hitara *et al.*, 2007b), and formability of dissimilar materials (Miles *et al.*, 2005; Leitao et al. 2009).

The formability prediction of FSW blanks of different materials with similar and dissimilar thickness was discussed by modeling weld zone as single entity (Zadpoor *et al.*, 2007 a; b; 2008 a; 2009; Lee *et al*., 2009; Chung *et al.*, 2010; Kim *et al.*, 2010 a, b). The results concluded that whenever failure happened in the base metal or weld nugget zone, prediction results were close to the experimental results. The prediction results were not close and more error was seen with experimental results when failure happened in the HAZ zone. This results in inaccurate formability prediction if weld zone is modeled without HAZ separately. It is clear from the literature that weld region has three zones (HAZ, TMAZ, WN)

with different mechanical properties (Lockwood *et al.*, 2002; Liu and Chao, 2005) because of which they behave differently during forming. So, it is mandatory for weld zone to model as double zone model for accurate formability prediction for different materials with similar and dissimilar thickness.

Hence in this work the effect of welding speed, rotation speed, shoulder diameter and plunge depth on the formability of FSW sheets is studied. The formability is also predicted and validated with experimental results.

1.4 Objectives of thesis

The main objectives of the thesis are to, (i) investigate the effect of shoulder diameter, plunge depth, tool rotation speed, and welding speed on the formability of friction stir welded blanks, and (ii) predict the formability of friction stir welded blanks having different weld locations and orientations by using different failure criteria and validating with experimental results.

The important sub-tasks to achieve the objectives are to,

(i) Identify the optimum shoulder diameter, plunge depth, tool rotation speed, and welding speed for fabricating defects free FSW joints.

(ii) Study the influence of chosen shoulder diameter, plunge depth, tool rotation speed, and welding speed on the tensile behavior and formability of FSW sheets.

(iii) Study the effect of weld conditions namely weld orientation and weld location on the formability of FSW sheets.

(iv) Critically investigate the effect of weld zone representation methods, i.e., through single zone model or double zone models, for accurate formability prediction of FSW sheets.

(v) Predict the forming limit of friction stir welded sheets using different failure criteria and validating with experimental results.

1.5 Organization of Thesis

The thesis consists of ten chapters, which are organized as follows:

- The first chapter has provided an introduction and literature review of FSW process, significance and objectives of the present work.

- Chapter 2 presents the weld zone representation during formability prediction of FSW blanks with same thickness. In this study weld zone is modelled with single zone and double zone in transverse and longitudinal weld orientations. The geometrical and mechanical properties are varied hypothetically during prediction. From the simulation results it is showed that double zone model is essential for accurate formability prediction of FSW sheets in both weld orientations.
- Chapter 3 presents the weld zone representation during formability prediction of FSW blanks with dissimilar thickness. In this case also weld zone is modelled with single zone and double zone and then varied the geometrical and mechanical properties hypothetically during prediction like in Chapter 2. The number of single zone models has increased in transverse weld orientation and number of double zone models has increased in longitudinal weld orientation in the case of FSW blank with dissimilar thicknesses as compared to similar thickness FSW blanks. This is due to the change in failure location during forming of FSW blanks.
- In Chapter 4, internal defects formation in FSW sheets made of AA 6061-T651 with 2.1 mm thickness under different process parameters like shoulder diameter, plunge depth, tool rotation speed and welding speed is shown. An optimum range is identified by which defect free welds are fabricated. The effect of process parameters on the axial force and toque is observed and a simple criterion is proposed by observing the variation of axial force and torque with respect to welding parameters for identifying the onset of defect free weld region.
- Chapter 5 deals with the tensile behaviour and micro-hardness distribution of AA 6061 welded joints at optimized process parameters from Chapter 4. Effect of each parameters on the tensile properties like yield strength, tensile strength, uniform and total elongation, strain hardening exponent and strength coefficient has been seen. The effect of these parameters on thinning distribution is also observed.
- In Chapter 6, the effect of shoulder diameter and plunge depth on the formability of FSW sheets is observed. The limit dome height test is conducted to evaluate formability through forming limit diagram and monitored the dome height. The change in forming limit curve is related to thickness distribution, weld zone strain hardening exponent and dislocation density of weld zone.

- Chapter 7 explains about the effect of welding speed and tool rotation speed on the formability of FSW sheets. The limit dome height test is conducted to evaluate formability through forming limit diagram and monitored the dome height. The change in forming limit curve is related to thickness distribution, weld zone strain hardening exponent and dislocation density of weld zone.
- The influence of weld location and weld orientation on formability is presented in Chapter 8, in which weld is kept at three different locations (centre, 5 mm and 10 mm offset to centre) and three orientations (0º, 45º and 90º) by keeping weld at geometric centre. The LDH test is conducted and forming limit curves are constructed for each FSW case and compared with each other and with un-welded sheet for analysis.
- In Chapter 9 the formability predicted by using two different failure criteria for FSW sheets are compared with experimental results. The accuracy of FLC prediction by the two necking criteria is discussed. During prediction, weld zone is modelled as single zone and double zone like in Chapter 2 and 3 and explained the essentiality of the weld zone model for accurate formability prediction in FSW sheets.
- Conclusions from the thesis work are presented in Chapter 10 followed by scope for future work and references.

Chapter 2

Weld Zone Representation during the Formability Prediction of Friction Stir Welded Blanks with Similar Thickness Sheets

2.1 Methodology

Representing weld zone in FSW blanks involves accurate evaluation of the mechanical properties of WN and HAZ. Because of the practical difficulties in evaluating the nugget and HAZ properties separately, the entire weld zone is generally modeled as the single entity, which is expected to show profound effect on the accuracy of formability prediction. In nutshell, the FSW blanks are modeled in two ways - (i) single zone model, where WN and HAZ are modeled as single entity, and (ii) double zone model, where WN and HAZ are modeled separately, for formability simulation and prediction.

Single zone model: The single zone model is shown schematically in Fig. 2.1 (a). In this model, weld zone includes WN and HAZ as single entity and global mechanical properties are defined in weld zone and base material during modeling. The maximum and optimum weld width of 30 mm (Lockwood *et al.*, 2002; Zadpoor *et al.*, 2008) is considered for simulation (Fig. 2.1 (a)). The single zone model is considered as the reference model, in which the base material and weld properties (including weld width) are kept constant. Table 2.1 gives the properties of weld zone and base material (AA 6111-T4) used for simulation of single zone case. The mechanical properties and anisotropy values shown in the Table 2.1 are obtained from the literature (Lockwood *et al.*, 2002; Liu and Chao, 2005; Ganesh Narayanan and Narasimhan, 2006; 2008; Zadpoor *et al.*, 2008; Veera Babu *et al.*, 2009; Naik *et al.*, 2010). Same thickness is considered for the base material and weld zone, so that the intrinsic effect of the weld on forming behavior of FSW blanks can be established.

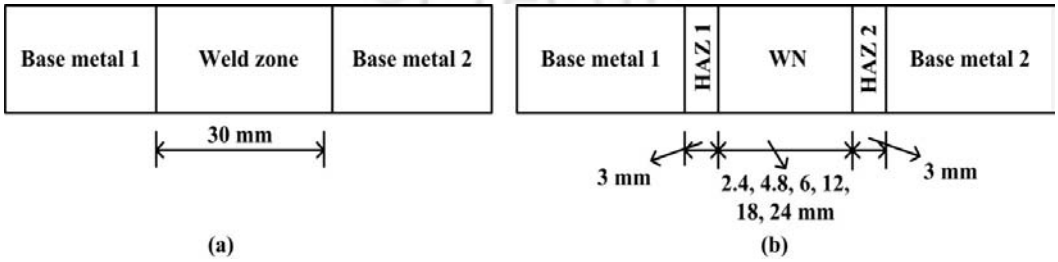

Fig. 2.1 Schematic representation of (a) single zone model and (b) double zone model

Double zone model: In this model, weld zone includes WN and HAZ as shown in Fig. 2.1 (b), and separate mechanical properties are defined for WN and HAZ during modeling. The minimum weld width of FSW blanks considered from the literature is 8 mm (WN+HAZ) (Chen *et al.*, 2008). For this model simulation, width of HAZ is fixed at 3 mm on both sides of WN, as the weld zone is assumed symmetric for the present investigation. The width of WN is modified as 2.4, 4.8, 6, 12, 18 and 24 mm (Fig. 2.1 (b)), in order to have varied combinations of WN and HAZ widths. Similarly yield strength and strain hardening exponent of WN and HAZ are also modified. Here the combination of geometric and the mechanical properties of WN and HAZ is quantified by three different ratios, namely weld width ratio (w_r), yield strength ratio (YS_r) and strain hardening exponent ratio (n_r). They are defined as,

(a) Ratio of NZ width (w_{NZ}) to HAZ width (w_{HAZ}) i.e., $w_r = w_{NZ} / w_{HAZ}$

(b) Ratio of yield strength of NZ (YS_{NZ}) to HAZ (YS_{HAZ}) i.e., $YS_r = YS_{NZ} / YS_{HAZ}$

(c) Ratio of strain hardening exponent of NZ (n_{NZ}) to HAZ (n_{HAZ}) i.e., $n_r = n_{NZ} / n_{HAZ}$

Table 2.1 Base material (AA 6111-T4) and weld zone properties used for single zone model case

Base/Weld	E (GPa)	γ	σ_{YS}^{*} (MPa)	K (MPa)	n	R_0	R_{45}	R_{90}	t (mm)
Base	69.44	0.33	380	1616	0.233	0.894	0.611	0.66	1.5
Weld**	69.44	0.33	258	1057	0.227	1	1	1	1.5

*obtained from flow equation $\boldsymbol{\sigma = K \varepsilon^n}$; ** weld width = 30 mm

The three ratios, w_r, YS_r and n_r, are varied at regular intervals in order to simulate variety of FSW blanks conditions. The ratios, w_r, YS_r and n_r, are varied as shown in the Table 2.2. Based on the availability of mechanical properties of WN and HAZ from the literature (Liu and Chao, 2005; Zadpoor *et al.*, 2008; 2009), the mechanical properties are quantified for WN and HAZ, without changing base material properties. The quantification of mechanical properties for HAZ and NZ is based on the probable failure locations in FSW blanks during simulation. In general, the failure location is expected to occur in WN or HAZ or in BM. In case of transverse weld orientation, failure has strictly occurred either in WN or in HAZ, which consequently influenced the weld zone representation. In longitudinal weld orientation, failure always occur normal to the weld zone, such that HAZ, WN and BM will participate during forming.

Table 2.2 Different weld zone properties used for double zone model case

Weld width (w) in mm		Ratio (w_r)	Yield Strength (YS) in MPa		Ratio (YS_r)	Strain Hardening coefficient (n)		Ratio (n_r)
NZ	HAZ	w_{NZ}/w_{HAZ}	NZ	HAZ	YS_{NZ}/YS_{HAZ}	NZ	HAZ	n_{NZ}/n_{HAZ}
2.4	6	0.4	206.4	258	0.80	0.159	0.227	0.70
4.8	6	0.8	232.2	258	0.90	0.181	0.227	0.80
6	6	1	258	258	1.00	0.204	0.227	0.90
12	6	2	283.8	258	1.10	0.227	0.227	1
18	6	3	309.6	250	1.24	0.272	0.219	1.24
24	6	4	335.4	240	1.40	0.341	0.213	1.6

2.1.1 Modeling simulation of LDH testing of friction stir welded blanks

In LDH test, the sheet is deformed by a hemispherical punch (diameter: 101.6mm) inside a die opening of diameter 105.7mm. Simulations were performed for near plane-strain (Sheet sample dimension: 100 X 200 mm) strain path only. The LDH setup used for simulation of FSW blank with transverse and longitudinal weld orientations is shown in Fig. 2.2. The tools required for LDH test, punch, die, blank holder, draw bead and blank were generated in Solid works, a CAD package, and meshed using Delta Mesh facility in PAM STAMP 2G. The base material and weld zone model were comprised of quadrilateral shell elements of Belytschko-Tsay formulation with five through thickness integration points. Hollomon's strain hardening law and Hill's 1948 isotropic hardening yield criterion was used as the plasticity model. Fig. 2.2 (b) shows a closer look at the meshed TWB used in the simulations. The meshed blank was divided into five regions viz., base metal 1, HAZ 1, HAZ 2, NZ, base metal 2 in double zone modeling case. A uniform mesh size of 1 mm was used throughout the simulations. The thickness gradient based necking criterion is sensitive to mesh size and it was found that for accurate prediction of limit strain 1-5 mm mesh size is optimum. Friction coefficient "μ" was assumed to be 0.12 and is kept constant throughout the study. Blank Holder Force (BHF) (~ 60 to 80 kN) was chosen such that the blank neither draws in nor tears near drawbeads during forming prediction. In total, 216 simulations were performed with double zone model and compared with single zone model (reference) case. The standard limit dome height test was simulated in PAMSTAMP 2G for each FSW blank case and the load-displacement behavior were predicted. From the load-displacement curve, the maximum displacement at failure was obtained from the thickness gradient based necking criterion (a criterion for predicting limit strain) and the corresponding load was considered as maximum load. The maximum load and corresponding displacement were compared between single zone and double zone cases for obtaining the domain of the weld conditions where single zone assumption breaks down and double zone assumption can be followed.

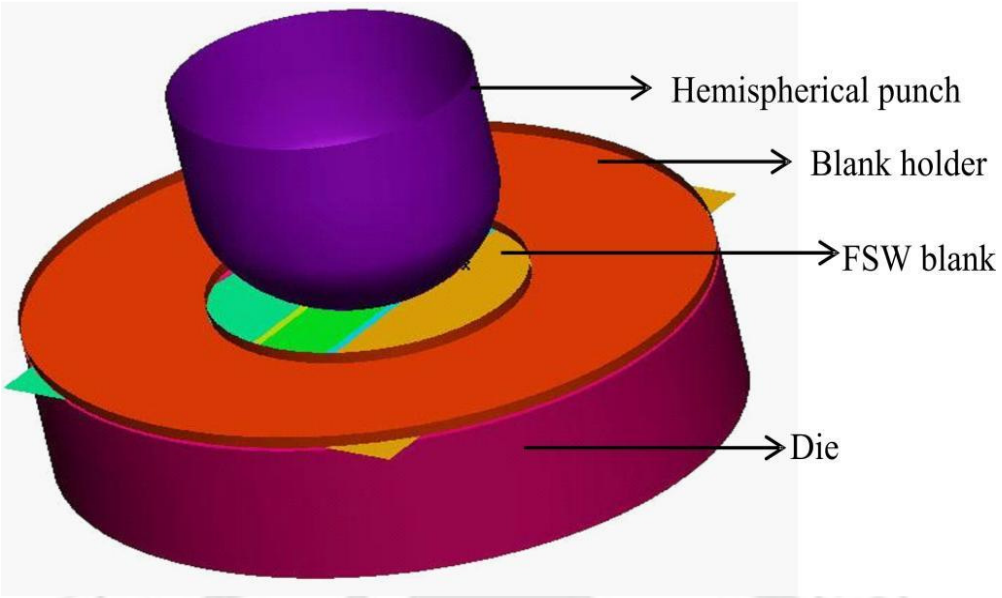

(a)

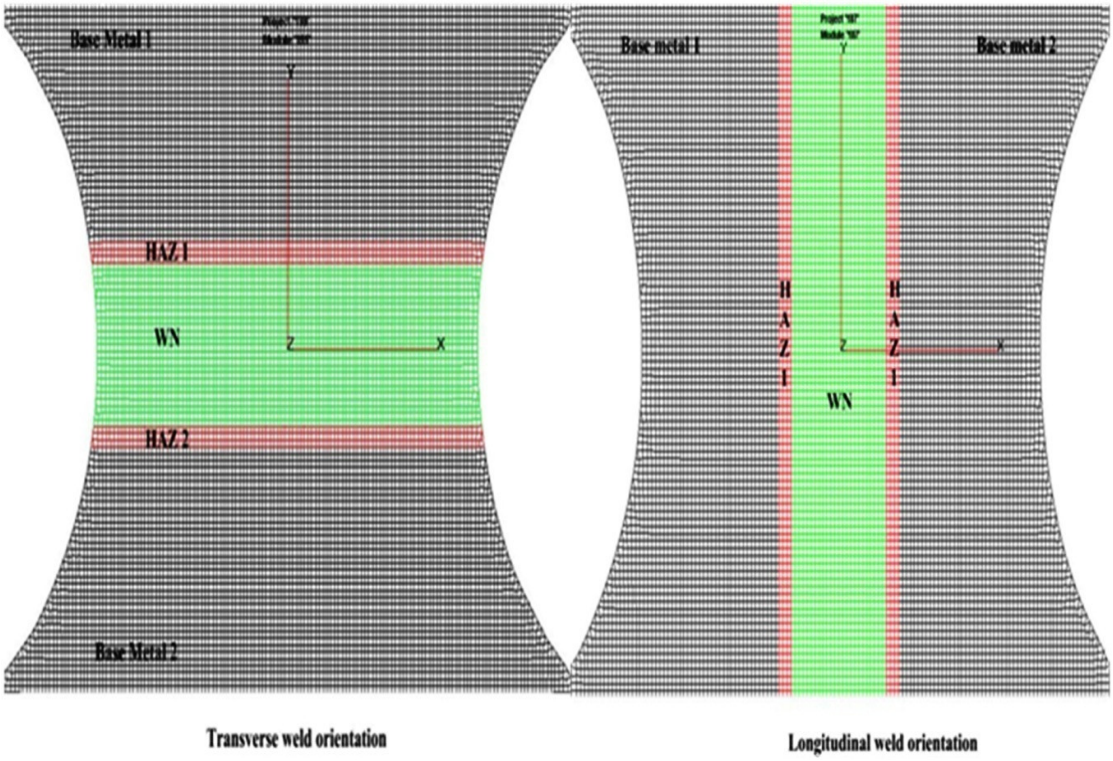

(b)

Fig. 2.2 (a) Assembly of LDH setup in PAM STAMP 2G with friction stir welded blanks (b) Mesh models of friction stir welded blanks with different zones (WN: weld nugget; HAZ: heat affected zone) [Note: Only the deforming region of 100x200 mm strain path is shown in Fig. 2.2 (b)]

2.1.2 Criterion for breaking down of single zone modeling assumption

The domain of weld conditions at which the single zone assumption breaks down was obtained by comparing the load-displacement behavior of single zone modeling and double zone modeling. The maximum displacement and corresponding loads were monitored in each simulation. The maximum displacement is obtained from thickness gradient based necking criterion (a criterion for predicting failure and limit strain) and corresponding load from load-displacement curve is termed as maximum load. From the literature (Lee et al., 2009), it was observed that the error percentage limit for the experimental and predicted forming behavior of FSW blanks modeled with single zone for five different materials (6111-T4, 5083-H18, 5083-O aluminum alloy, dual-phase steel (DP590) and AZ31 magnesium alloy) lies between 5.3 % to 37.03 % for maximum displacement at failure and 2.5 % to 43.54 % for maximum load in plane strain conditions. In all five materials, one of the material is AA 5083-H18 which has error percentage difference of 15.87% with maximum displacement. This error percentage difference is approximated to 16% and as an optimum acceptable limit for both displacement at failure and maximum load in the present work. If the difference is more than 16%, between the single zone and double zone data, then for that particular weld condition, the single zone assumption is considered to be invalid. The percentage difference in maximum load and displacement are evaluated and represented such that it is positive throughout analyses. In whole, four cases, viz., transverse weld orientation based on maximum load, transverse weld orientation based on maximum displacement, longitudinal weld orientation based on maximum load, and longitudinal weld orientation based on maximum displacement are considered for the work.

2.1.3 Thickness gradient based necking criterion

A novel thickness gradient-based necking criterion is used to obtain the displacement at failure. It is found from the experiments that necking occurs in the sheet metal when the thickness gradient (ratio of thickness of neighboring elements or circles) falls below 0.92 (Nandedkar, 2000). Hence, in the present simulations, element pairs where the thickness ratio equals or falls below 0.92 are considered as necked elements. In general, necking can be understood as a thinning phenomenon and it basically perceives necking as a localized thinning phenomenon i.e., a localized region within the deforming sheet where a steep gradient in thickness develops. A local critical thickness gradient (R_c) must exist at the onset of a local visible neck. In the simulations, the thickness gradient developing in the adjoining elements (of size about 2-5 mm) is monitored, when this gradient (R_{actual}) drops below a

critical value, it is concluded that the local neck has initiated in the element where thickness is lower. The maximum load and displacement at failure is noted down when the necking criterion is satisfied. Similar procedure is followed for both transverse and longitudinal weld orientations of FSW blanks during LDH tests. This criterion is related to the physical necking phenomenon and hence can be associated with finite element simulations directly. Moreover, the criterion followed in this work is simple and easy for applicability in sheet-forming processes to identify necking onset. This limit strain criterion is sensitive to 'mesh size'. From the previous study, it was found that the mesh size should be 1–5 mm to follow this necking failure criterion. Moreover, it is logical to say this because in experiments we use circle grid size of 2.5 mm for strain measurements. The schematic of applicability of this criterion is shown in Fig. 2.3.

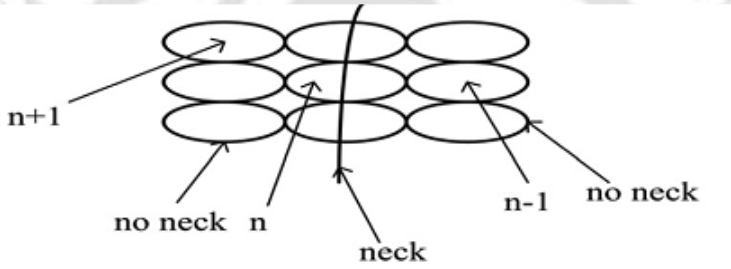

$$R_{\text{thickness gradient}} = \frac{\text{thickness}_{\text{Necking element}}}{\text{thickness}_{\text{Neighboring element}}} = \frac{t_n}{t_{n-1}} \; or \; \frac{t_n}{t_{n+1}} \leq R_{\text{Cri}} \Rightarrow \text{material failure or necking}$$

$$R_{\text{Critical}} \leq 0.92$$

Fig. 2.3 Schematic representation of deformed grids and applicability of thickness gradient based necking criterion

2.2 Results and discussion

2.2.1 Transverse weld orientation based on maximum load

In this case, transverse weld orientation is considered and only maximum load is compared between single zone and double zone assumptions. The maximum load at failure data for single zone and few double zone cases are shown in Table 2.3 for discussion. The data monitored are compared between FSW blank models with 'single zone (reference)' and double zone assumption and percentage error is quantified. For example, by considering the maximum load attained as criterion in transverse weld orientation, w_r = 2-4, n_r = 1, YS_r = 1 and w_r = 3-4, YS_r = 1.1, n_r = 0.9 are the two domains within which 'single zone' assumption is valid. Though the two domains are modeled as double zone, since the percentage error is

less than 16%, they are categorized in single zone. This also means that 'double zone' model is valid only outside the specified domains for this FSW blank condition. This is indicated in Table 2.3 in which the weld conditions (w_r, YS_r, n_r) with the above said domains exhibit load difference less than 16% and all the other conditions have difference greater than 16%.

In order to understand why the single zone model is valid only within the domains stated, the thickness distribution is observed from one end of sheet along the major strain direction and normal to the necking region. Fig. 2.4 shows the thickness distribution from one end of sheet for different weld conditions comparing the single zone model (reference model) assumption; YS_r=1, n_r=1, w_r= 4 and double zone models. Only few weld conditions are shown in Fig. 2.5 for maintaining the clarity. Here thickness distribution is measured normal to the weld zone just after the maximum load is reached. It can be understood from Fig. 2.4 that the weld condition w_r= 4, YS_r= 1, n_r= 1, belonging to double zone model case (curve 4) have same thickness distribution as that of single zone model case (reference model). This case exhibits a very less error percentage of 0.19% (Table 2.3) when maximum load is compared with reference model case. The failure location is also same as that of reference model. The other weld conditions (w_r= 3, YS_r= 1.1, n_r= 0.9; w_r= 2, YS_r= 1, n_r= 1 and w_r= 4, YS_r= 1.1, n_r= 0.9) belonging to the single zone model cases (curves 1, 2, 3) and reference case are closer to each other, showing lesser difference between them and exhibit error percentage of 15.48 %, 14.58 %, and 2.58 % (Table 2.3) when maximum load is compared with reference model case. On the other hand, the weld conditions (w_r= 0.8, YS_r= 1.1, n_r= 1; w_r= 0.8, YS_r= 1.24, n_r= 1 and w_r= 0.8, YS_r= 1.4, n_r= 1) belonging to double zone model cases (curves 5, 6, 7) are very different when compared to reference cases, showing more difference between them. These weld conditions (w_r= 0.8, YS_r= 1.1, n_r= 1; w_r= 0.8, YS_r= 1.24, n_r= 1 and w_r= 0.8, YS_r= 1.4, n_r= 1) belonging to double zone modeling case exhibit error percentage of 42.58 %, 57.03 % and 64.9 % in maximum load (Table 2.3) with respect to the reference case. It is observed that whenever the error percentage in maximum load is below 16%, the weld conditions, say w_r= 3, YS_r= 1.1, n_r= 0.9; w_r= 2, YS_r= 1, n_r= 1 and w_r= 4, YS_r= 1.1, n_r= 0.9, exhibit thickness distribution and failure location similar to that of reference model. It can be said that in these weld conditions double zone model behaves like single zone model and hence it is sufficient to represent FSW blank as single zone model without incorporating separate mechanical properties in HAZ and WN. In other weld conditions like w_r= 0.8, YS_r= 1.1, n_r= 1; w_r= 0.8, YS_r= 1.24, n_r= 1 and w_r= 0.8, YS_r= 1.4, n_r= 1, where the error percentage in maximum load is more than 16%, the thickness distributions are very different when compared to reference case, though the failure location is within the weld zone (Fig. 2.4). In these weld conditions,

one has to treat weld zone as double zone by incorporating separate mechanical properties in HAZ and WN.

Table 2.3 Maximum load at failure for LDH test simulation of transverse weld orientation

Weld conditions			Maximum load (kN)	% difference in load
w_r	YS_r	n_r		
FSW blank modeled with single zone assumption (reference)			155	0.00
0.8	1.1	1	89	42.58
0.8	1.24	1	66.6	57.03
0.8	1.4	1	54.4	64.90
1	1	0.9	60.1	61.23
1	1	1	120.4	22.32
1	1	1.24	64.2	58.58
2	1	0.9	69.4	55.23
2	**1**	**1**	**132.4**	**15.48**
2	1	1.24	55.1	64.45
3	1	0.9	66.3	57.23
3	**1**	**1**	**141.8**	**8.52**
3	**1.1**	**0.9**	**131**	**15.48**
3	1.1	1	89.6	42.19
4	**1**	**1**	**155.3**	**0.19**
4	**1.1**	**0.9**	**159**	**2.58**
4	1.1	1.24	60.6	60.9

Figure 2.5 shows the error percentage variation of double zone modeled FSW blanks with transverse weld and maximum load at failure as criteria at different weld conditions. The maximum error percentage among all the cases is 93.66% at w_r= 0.4, YS_r= 0.8, n_r= 0.7 weld condition and minimum is 0.19% at w_r= 4, YS_r= 1, n_r= 1 weld condition. It is clear from Fig. 2.5 that most of the weld conditions are above 16% limit and few are below the limit. One of the case is close to 16 % limit with 15.48 error percentage at w_r= 3, YS_r= 1.1, n_r= 0.9 weld condition. All the weld conditions whose error percentages are less than or greater than 16% can be represented in terms single zone or double zone model validity. Fig. 2.6 depicts the weld conditions representation for single zone and double zone model validity. In Fig. 2.6, the domains of weld conditions, viz., w_r= 2-4, n_r= 1, YS_r= 1 and w_r= 3-4, YS_r= 1.1, n_r= 0.9 represent the validity of single zone model for simulating FSW blanks when maximum load at failure is considered as the criteria for transverse weld case. This means that within these weld conditions, it is sufficient to incorporate global weld zone properties during FSW blanks formability prediction, while WN and HAZ properties should be incorporated separately when the weld conditions are outside the indicated domain, i.e., double zone representation has to be followed in these cases. As shown in Fig. 2.6, the domains are represented by straight lines which indicate that out of three weld conditions, only weld width (w_r) is varying

continuously within the finite range and other two conditions (YS_r, n_r) are constant at different levels.

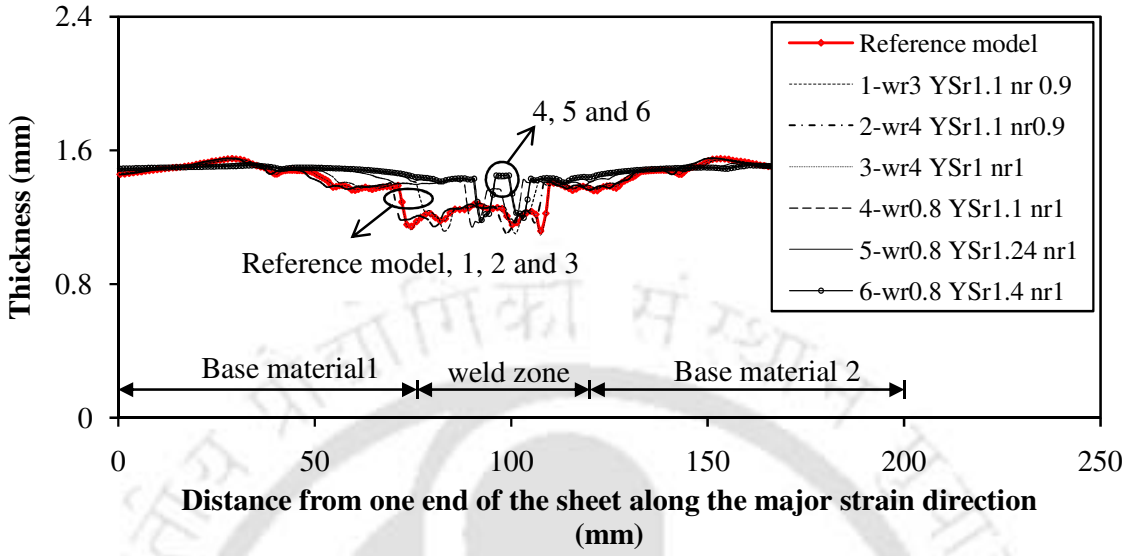

Fig. 2.4 Thickness distribution for FSW blanks with transverse weld and maximum load at failure as criterion

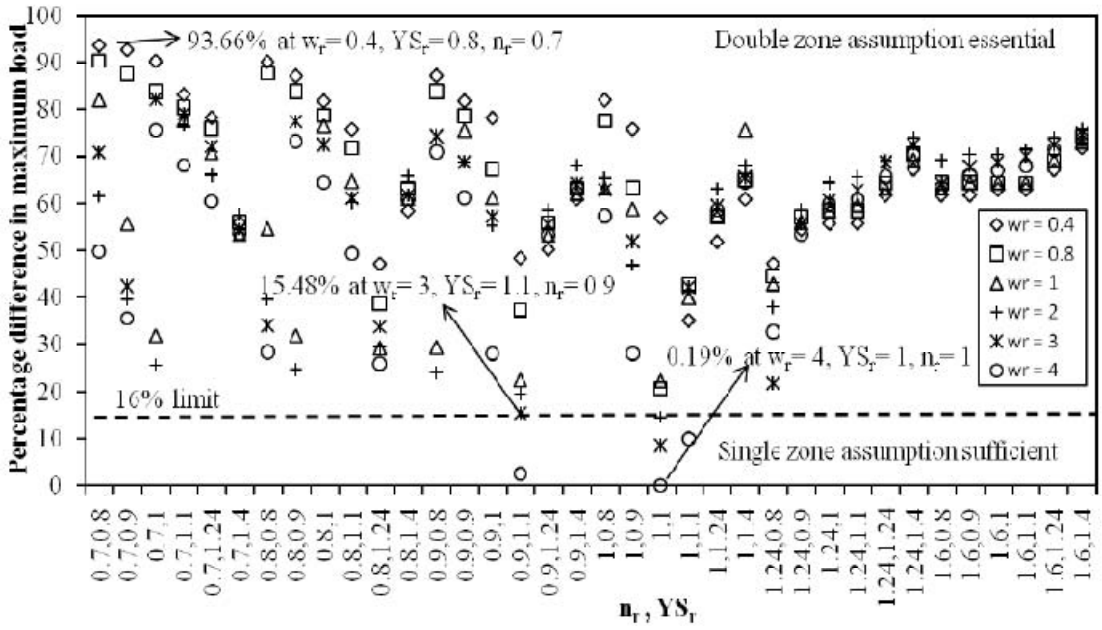

Fig. 2.5 Error percentage variations of double zone modeled FSW blanks with transverse weld and maximum load at failure as criterion at different weld conditions

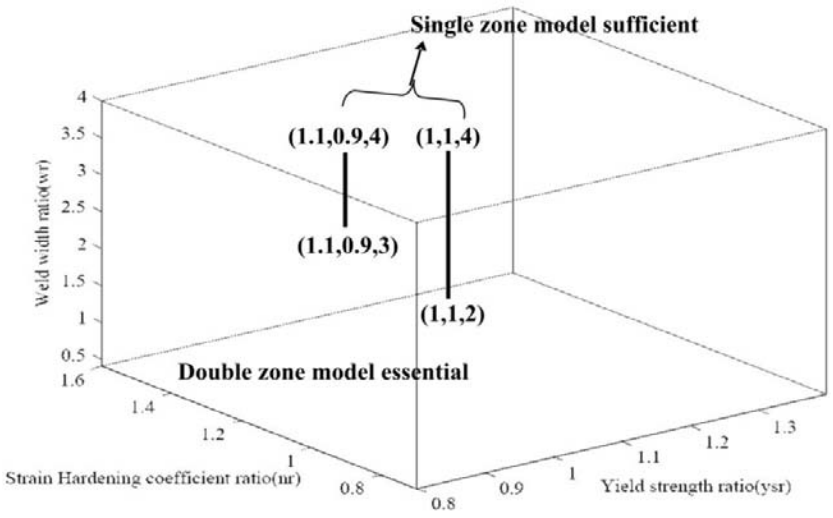

Fig. 2.6 Domains of weld conditions for representing the single zone and double zone model validity with maximum load as criterion (transverse weld orientation)

2.2.2 Transverse weld orientation based on displacement at failure

The domain at which the single zone assumption breaks down is obtained for transverse weld orientation by considering displacement at failure as the criterion. In this case, it is observed that multiple weld domains are possible where single zone assumption is invalid. The displacement at failure data for single zone and few double zone cases are shown in Table 2.4 for discussion. One of the domain, w_r=0.8-4, YS_r=1, n_r =1 is indicated in Table 2.4 in which the weld conditions within the above said domain exhibit displacement difference less than 16%. Similarly there are multiple domains where single zone assumption is valid. They are w_r=0.8-4, YS_r=1, n_r=1; w_r=1-2, YS_r=0.8, n_r=0.9; w_r=1-2, YS_r=0.9, n_r=0.8; w_r=2-4, YS_r=0.8, n_r=0.8; w_r=1-2, YS_r=1, n_r=0.7; w_r=1-4, YS_r=1.1, n_r=0.9 and w_r=2-4, YS_r=0.9, n_r=0.7. All other weld conditions outside the specified range are greater than 16%, and hence double zone model should be followed.

The thickness distribution is observed (Fig. 2.7), from one end of sheet along the major strain direction i.e., normal to the neck to validate the single zone model within the domains stated. The single zone model (i.e., reference model) assumption, YS_r=1, n_r=1, and w_r=4 double zone models are compared. Only few weld conditions are shown for maintaining the clarity. Here thickness distribution is measured normal to the weld zone just after the maximum load is reached. It can be understood from the Fig. 2.7 that a weld condition w_r= 4, YS_r= 1, n_r= 1 belonging to single zone model case (curve 2) exhibits same thickness

distribution as that of reference model. In this case, zero error percentage is witnessed when displacement is compared with the reference model. The failure location is also found to be same as that of reference model. The other weld condition (curve 1: w_r= 4, YS_r= 1.1, n_r= 0.9) belonging to the single zone model case is also closer to reference each other, showing lesser difference between them. This condition exhibit an error percentage of 3.57 (shown in Table 2.4) when displacement is compared with reference model case. On the other hand, the weld conditions w_r= 4, YS_r= 0.8, n_r= 1; w_r= 4, YS_r= 0.9, n_r= 1; w_r= 4, YS_r= 1.24, n_r= 1 and w_r= 4, YS_r= 1.4, n_r= 1, belonging to double zone model cases (curves 3, 4, 5 and 6) are very different when compared to reference cases, showing more difference between them. These weld conditions belong to double zone model and exhibit error percentage of 41.67%,19.05%, 44.05% and 50% (shown in Table 2.4) with the reference case. It is observed that whenever the error percentage in maximum displacement is below 16%, the weld conditions exhibit thickness distribution and failure location similar to that of reference model. In these weld conditions, viz., w_r= 4, YS_r= 1.1, n_r= 0.9 and w_r= 4, YS_r= 1, n_r= 1 double zone model behaves like single zone model only and it is sufficient to represent FSW blank as single zone model without incorporating separate mechanical properties in HAZ and WN. In other weld conditions like w_r= 4, YS_r= 0.8, n_r= 1; w_r= 4, YS_r= 0.9, n_r= 1; w_r= 4, YS_r= 1.24, n_r= 1 and w_r= 4, YS_r= 1.4, n_r= 1, the error percentage in displacement at failure is more than 16% and the thickness distributions are very different when compared to reference case, though the failure location is within the weld zone (Fig. 2.8). In these weld conditions, one has to treat weld zone as double zone by incorporating separate mechanical properties in HAZ and WN.

Figure 2.8 shows the error percentage variation of double zone modeled FSW blanks with transverse weld and displacement at failure as criteria at different weld conditions. The maximum error percentage among all the cases is 83.33% at w_r= 0.4, YS_r= 0.8, n_r= 0.7 weld condition and minimum is zero percentage at w_r= 4, YS_r= 1, n_r= 1 weld condition, which behaves like the reference model. It is clear from Fig. 2.8 that most of the cases are above to 16% limit and few are below the limit. All the weld conditions whose error percentages are less than or greater than 16% can be represented as single zone or double zone model validity. Fig. 2.9 depicts the weld conditions representation for single zone and double zone model validity. The possible multiple domains are w_r=0.8-4, YS_r=1, n_r=1; w_r=1-2, YS_r=0.8, n_1=0.9; w_r=1-2, YS_r=0.9, n_r=0.8; w_r=2-4, YS_r=0.8, n_r=0.8; w_r=1-2, YS_r=1, n_r=0.7; w_r=2-4, YS_r=1.1, n_r=0.9 and w_r=2-4, YS_r=0.9, n_r=0.7 in which the single zone model is valid when displacement at failure is considered as the criteria for transverse weld case. This means that within these weld conditions, it is sufficient to incorporate global weld zone properties during

FSW blanks formability prediction, while WN and HAZ properties should be incorporated separately if weld conditions are outside the indicated domain, i.e., double zone representation has to be followed. As shown in Fig. 2.9, the domains are represented by straight lines which indicate that out of three weld conditions only one parameter (w_r) is changing within the finite range and other two conditions (YS_r, n_r) are constant at different levels.

Table 2.4 Displacement till failure for LDH test simulation of transverse weld orientation under varied weld conditions

Weld conditions			Displacement at failure (mm)	% difference in displacement
w_r	YS_r	n_r		
FSW blank modeled with single zone assumption (reference)			42	0.00
0.8	1	0.9	20	52.38
0.8	**1**	**1**	**36**	**14.29**
0.8	1	1.24	23.5	44.05
1	1	0.9	22.5	46.50
1	**1**	**1**	**35.5**	**15.48**
1	1	1.24	23.5	44.05
2	1	0.9	25	40.48
2	**1**	**1**	**38**	**9.52**
2	1	1.24	21	50.00
3	1	0.9	24	42.86
3	**1**	**1**	**39.5**	**5.95**
3	1	1.24	22.5	46.43
4	0.8	1	24.5	41.67
4	0.9	1	34	19.05
4	**1**	**1**	**42**	**0.00**
4	1.1	0.9	43.5	3.57
4	1	1.24	23	45.24
4	1.24	1	23.5	44.05
4	1.4	1	21	50

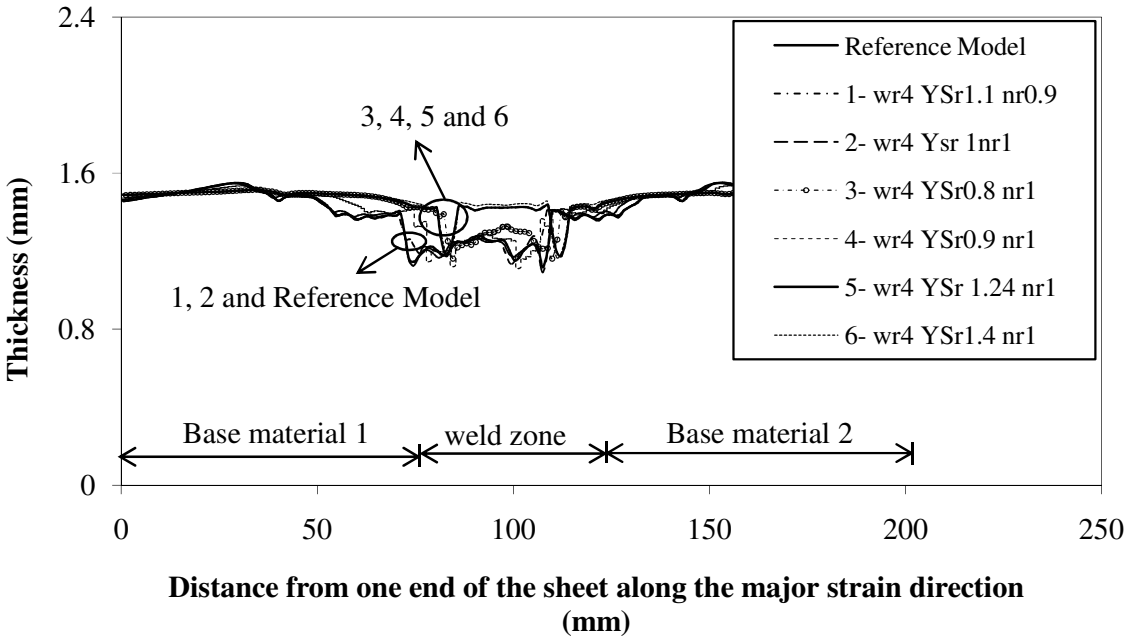

Fig. 2.7 Thickness distribution for FSW blanks with transverse weld and displacement at failure as criterion

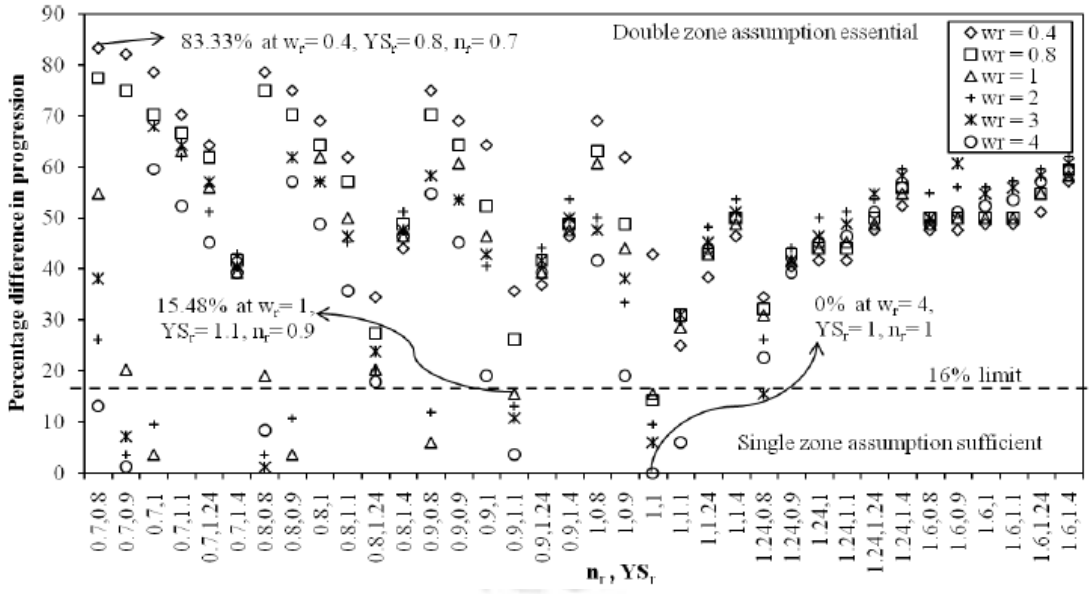

Fig. 2.8 Error percentage variations of double zone modeled FSW blanks with transverse weld and displacement at failure as criterion at different weld conditions

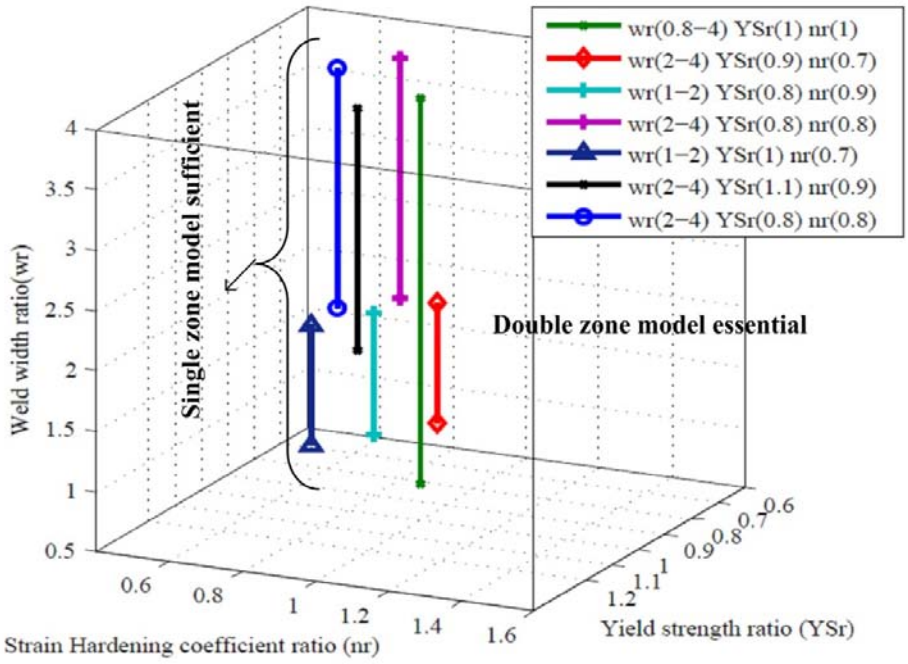

Fig. 2.9 Domains of weld conditions for representing the single zone and double zone model validity with displacement at failure as criterion (transverse weld orientation)

2.2.3 Longitudinal weld orientation with maximum load as criterion

In this case, longitudinal weld orientation is considered and maximum load at failure is compared between single zone and double zone assumptions. The maximum load at failure data for single zone and few double zone cases are shown in Table 2.5 for discussion. In this case, it is observed that multiple weld domains are possible where double zone assumption is invalid. One of the domain w_r=3-4, YS_r=1.24 and n_r=1 is indicated in Table 2.5 in which the weld conditions within the above said domain exhibit maximum load difference more than 16%. Similarly there are multiple domains where double zone assumption is valid. They are w_r=0.4, YS_r=0.8-1, n_r=0.7-0.9; w_r=0.8-4, YS_r=0.8, n_r=0.7-0.8; w_r=0.8-1, YS_r=0.8, n_r=0.9; w_r=0.8-3, YS_r=0.9-1, n_r=0.7; w_r=0.8-1, YS_r=0.9, n_r=0.8; w_r=0.8, YS_r=1-1.24, n_r=1.24-1.6; w_r=0.8-1, YS_r=1.4, n_r=1.6; w_r=2-4, YS_r=0.9-1.24, n_r=1.6; w_r=2-4, YS_r=1.4, n_r=0.7-1.24; w_r=3-4, YS_r=0.8, n_r=1.6 and w_r=3-4, YS_r=1.24, n_r=1. All other weld conditions outside the specified range are less than 16%, and hence single zone model should be followed.

The thickness distribution is observed (Fig. 2.10), from one end of sheet along the major strain direction, i.e., normal to the neck to validate the double zone model within the domains stated. Only few weld conditions are shown in Fig. 2.10 for maintaining the clarity. It can be understood from the Fig. 2.10 that the weld conditions, w_r= 4, YS_r= 1, n_r= 1 (curve 1), of

double zone model case has same thickness distribution as that the single zone model (i.e., reference model). In this case, zero error percentage is witnessed when maximum load is compared with reference model and failure location is same as that of reference model. The other weld conditions viz., w_r= 3, YS_r= 0.9, n_r=1 and w_r= 3, YS_r= 1.1, n_r=1 belonging to the single zone model (curves 2 and 3) and the reference case are closer to each other, showing lesser difference between them. These conditions (w_r= 3, YS_r= 0.9, n_r=1 and w_r= 3, YS_r= 1.1, n_r=1) exhibit error percentage of 1.09% and 11.96% when maximum load is compared with reference model case. On the other hand, the weld conditions (w_r= 3, YS_r= 1.24, n_r=1 and w_r= 3, YS_r= 1.4, n_r=1) belonging to double zone model cases (curves 4 and 5) are very different when compared to reference case, showing more difference between them. These weld conditions belong to double zone model and exhibit error percentage of 18.26% and 21.51% (shown in Table 2.5) with reference case. It is observed that whenever the error percentage in maximum load is below 16%, the weld conditions viz., w_r= 4, YS_r= 1, n_r= 1; w_r= 3, YS_r= 1.24, n_r=1 and w_r= 3, YS_r= 1.4, n_r=1, exhibit thickness distribution and failure location similar to that of reference model. In these weld conditions, double zone model behaves like single zone model and it is sufficient to represent FSW blank as single zone model without incorporating separate mechanical properties in HAZ and WN. In other weld conditions like w_r= 3, YS_r= 1.24, n_r=1 and w_r= 3, YS_r= 1.4, n_r=1, the error percentage in displacement is more than 16% and the thickness distributions are very different when compared to reference case, though the failure location is within the weld zone (Fig. 2.10). In these weld conditions, one has to treat weld zone as double zone by incorporating separate mechanical properties in HAZ and WN.

Figure 2.11 shows the error percentage variation of double zone modeled FSW blanks with longitudinal weld and maximum load at failure as criteria at different weld conditions. The maximum error percentage among all the cases is 75.90% at w_r= 0.4, YS_r= 0.8, n_r= 0.7 weld condition and minimum is zero percentage at w_r=4, YS_r=1, n_r=1 weld condition, which behaves like the reference model. All the weld conditions whose error percentages are less than or greater than 16% can be represented for single zone or double zone model validity. Fig. 2.12 depicts the weld conditions representation for single zone and double zone model validity. The multiple domains, viz., w_r=0.4, YS_r=0.8-1, n_r=0.7-0.9; w_r=0.8-4, YS_r=0.8, n_r=0.7-0.8; w_r=0.8-1, YS_r=0.8, n_r=0.9; w_r=0.8-3, YS_r=0.9-1, n_r=0.7; w_r=0.8-1, YS_r=0.9, n_r=0.8; w_r=0.8, YS_r=1-1.24, n_r=1.24-1.6; w_r=0.8-1, YS_r=1.4, n_r=1.6; w_r=2-4, YS_r=0.9-1.24, n_r=1.6; w_r=2-4, YS_r=1.4, n_r=0.7-1.24; w_r=3-4, YS_r=0.8, n_r=1.6 and w_r=3-4, YS_r=1.24, n_r=1 are the weld conditions where double zone model is valid when maximum load at failure is

considered as the criteria for longitudinal weld case. This means that within these weld conditions, it is essential to incorporate local weld zone properties (HAZ, WN) during FSW blanks formability prediction. If the weld conditions are outside the indicated domain, single zone representation has to be followed. As shown in Fig. 2.12, the domains are represented by straight lines and plane surfaces within the finite range of weld conditions at different levels. Among all the domains, few domains form straight lines in which one parameter is changing out of three weld conditions. They are w_r=0.8-1, YS_r=0.8, n_r=0.9; w_r=0.8-1, YS_r=0.9, n_r=0.8; w_r=0.8-1, YS_r=1.4, n_r=1.6; w_r=3-4, YS_r=0.8, n_r=1.6 and w_r=3-4, YS_r=1.24, n_r=1. The other domains form plane surfaces in which two parameters are changing out of three weld conditions, like w_r=0.4, YS_r=0.8-1, n_r=0.7-0.9; w_r=0.8-4, YS_r=0.8, n_r=0.7-0.8; w_r=0.8-3, YS_r=0.9-1, n_r=0.7; w_r=0.8, YS_r=1-1.24, n_r=1.24-1.6; w_r=2-4, YS_r=0.9-1.24, n_r=1.6 and w_r=2-4, YS_r=1.4, n_r=0.7-1.24.

Table 2.5 Maximum load at failure for LDH test simulation of longitudinal weld

Weld conditions			Maximum load (kN)	% difference in load
w_r	YS_r	n_r		
FSW blank modeled with single zone assumption (reference)			199	0.00
2	0.8	1	207.3	3.70
2	0.9	1	216.4	8.25
2	1	1	229	14.56
2	1.1	1	205.1	2.60
2	1.24	1	171	14.46
2	1.4	1	165	17.46
3	0.8	1	175.5	12.21
3	0.9	1	197.8	1.05
3	1	1	190.5	4.70
3	1.1	1	176	11.96
3	**1.24**	**1**	**163.4**	**18.26**
3	1.4	1	156.9	21.51
4	0.8	1	189.8	5.05
4	0.9	1	201.3	0.7
4	1	1	199.9	0.00
4	1.1	1	171.2	14.36
4	**1.24**	**1**	**167.1**	**16.41**
4	1.4	1	160.6	19.50

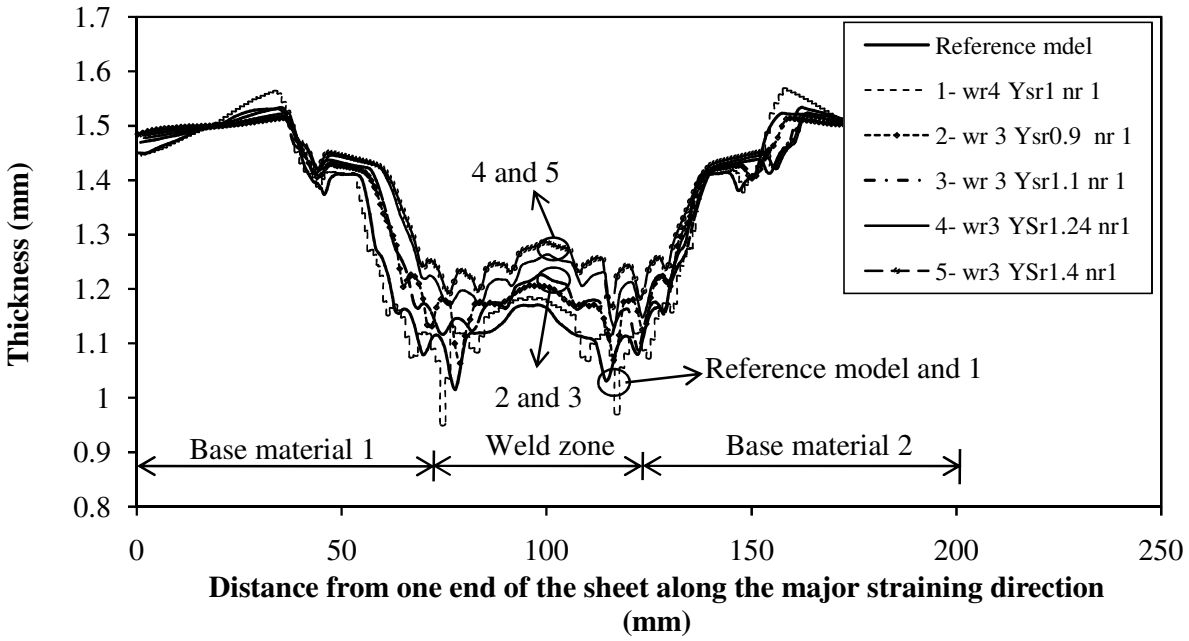

Fig. 2.10 Thickness distribution for FSW blanks with longitudinal weld orientation and maximum load at failure as criterion

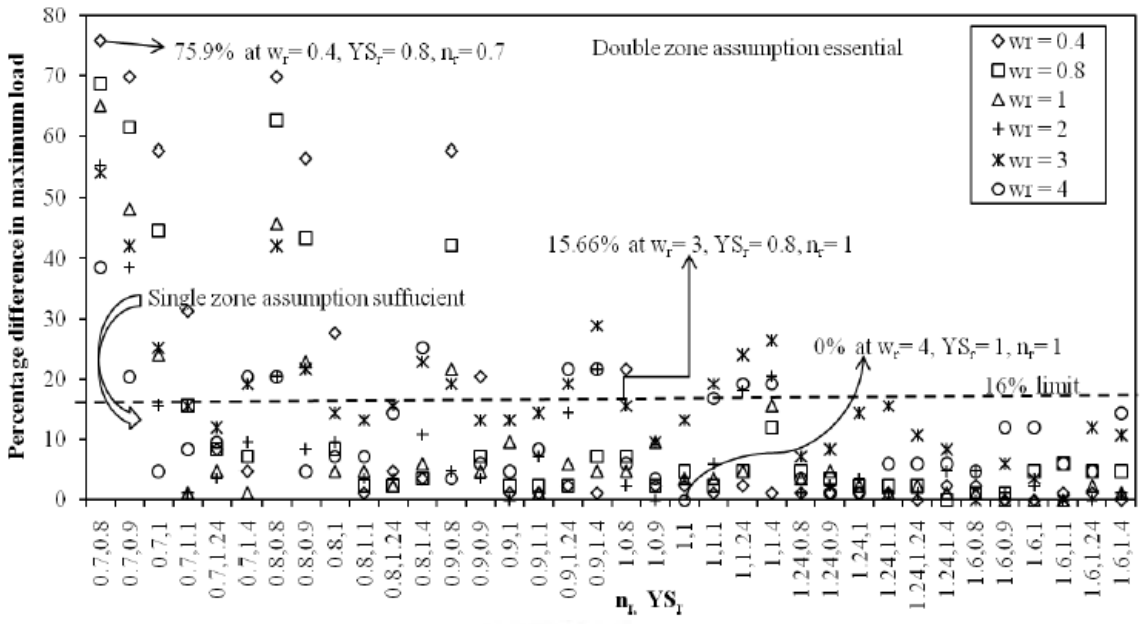

Fig. 2.11 Error percentage variation of double zone modeled FSW blanks with longitudinal weld and maximum load at failure as criterion at different weld conditions

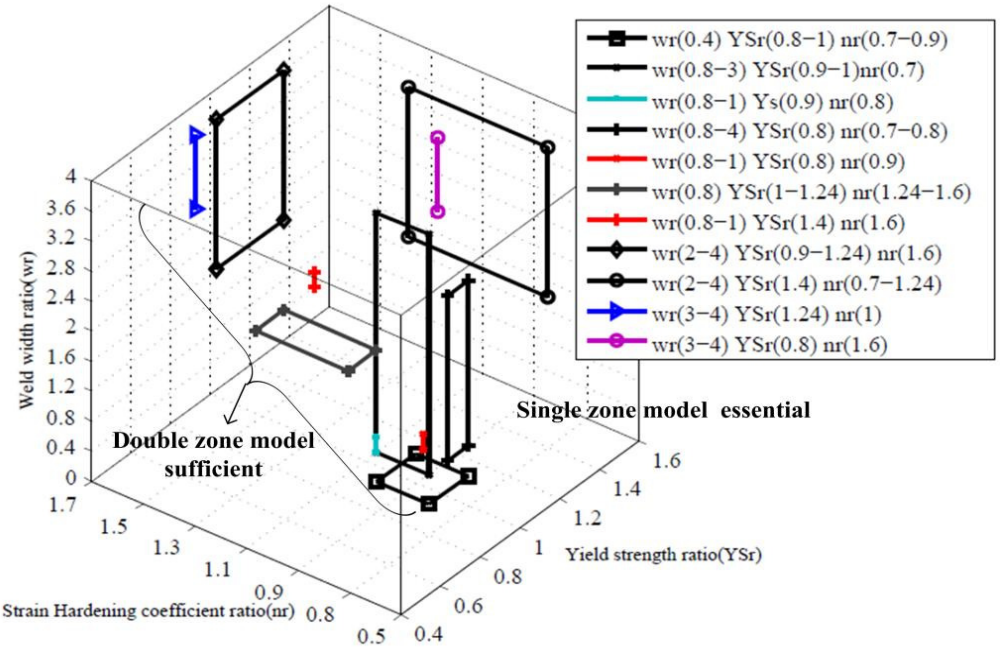

Fig. 2.12 Domains of weld conditions for representing the double zone modeling validity with maximum load at failure as criterion (longitudinal weld orientation)

2.2.4 Longitudinal weld orientation with displacement at failure as criterion

Here longitudinal weld orientation is considered and only displacement at failure is compared between single zone and double zone assumptions (Table 2.6). The weld condition, w_r=0.4-4, YS_r=0.8, n_r=0.7-0.8, is shown in the Table 2.6 in which the difference in displacement at failure is more than 16%. In this case, it is essential to model weld zone as double zone with HAZ, NZ properties separately. Similarly, it is found that there are multiple domains where double zone assumption is essential. They are w_r=0.4-4, YS_r=0.8, n_r=0.7-0.8; w_r=0.4-4, YS_r=0.9, n_r=0.7; w_r=0.4-1, YS_r=0.8-0.9, n_r=0.8-0.9; w_r=0.4, YS_r=1, n_r=0.7-0.8; w_r=0.8-3, YS_r=1, n_r=0.7; w_r=0.4-0.8, YS_r=1, n_r=0.7; w_r=2-4, YS_r=1.4, n_r=0.9-1; w_r=2-4, YS_r=1.24, n_r=1; w_r=3-4, YS_r=1.1, n_r=1; w_r=3-4, YS_r=1.24, n_r=0.9 and w_r=3-4, YS_r=1.4, n_r=0.7-0.8. All the other weld conditions have difference less than 16% and hence it is sufficient to follow single zone assumption.

The thickness distribution (Fig. 2.13) is observed from one end of sheet along the major strain direction and normal to the neck to validate the double zone model within the domains stated. The single zone model assumption (reference model) and double zone models are compared with each other. Only few data conditions are shown in Fig. 2.13 for maintaining the clarity. It can be understood from the Fig. 2.13 that the weld conditions, w_r= 4, YS_r= 1,

n_r= 1 (curve 1) which is actually modeled with double zone has same thickness distribution as that of single zone model (i.e., reference model) case. In this case, error percentage of zero (shown in Table 2.6) is witnessed when displacement at failure is compared with reference model case. The failure location is also same as that of reference model. The other weld conditions like w_r= 4, YS_r= 0.8, n_r=1 and w_r= 4, YS_r= 0.9, n_r=1, belonging to the double zone model (curves 2 and 3) are closer to reference case, showing lesser difference between them and exhibit error percentage of 6.02% and 3.61% (Table 2.6) when displacement is compared. On the other hand, the weld conditions like w_r= 4, YS_r= 1.24, n_r=1 and w_r= 4, YS_r= 1.4, n_r=1, belonging to double zone model cases (curves 4 and 5) are very different when compared to reference cases, showing more difference between them. These weld conditions (w_r= 4, YS_r= 1.24, n_r=1 and w_r= 4, YS_r= 1.4, n_r=1) belong to double zone model case and exhibit error percentage of 19.28% and 19.28% (Table 2.6) in displacement at failure with reference case. It can be said that whenever the error percentage in displacement is below 16%, the weld conditions exhibit thickness distribution and failure location similar to that of reference model. In these weld conditions, double zone model behaves like single zone model and hence it is sufficient to represent FSW blank with single zone without incorporating separate mechanical properties in HAZ and WN. In other weld conditions like w_r= 4, YS_r= 1.24, n_r=1 and w_r= 4, YS_r= 1.4, n_r=1, the error percentage in displacement is more than 16% and the thickness distributions are very different when compared to reference case, though the failure location is within the weld zone (Fig. 2.14). In these weld conditions; one has to follow double zone assumption by incorporating separate mechanical properties in HAZ and WN.

Figure 2.14 shows the error percentage variation of double zone modeled FSW blanks with longitudinal weld and displacement at failure as criteria for different weld conditions. The maximum error percentage 89.44% among all the cases is seen in w_r= 0.4, YS_r= 0.8, n_r= 0.7 weld condition and minimum is zero percentage at w_r= 4, YS_r= 1, n_r= 1 weld condition, which indicate that it is behaving like the reference model. It is clear from Fig. 2.14 that some of the cases are above 16% limit and many are in below the limit. All the weld conditions whose error percentages are less than or greater than 16% can be represented as single zone or double zone domains. Figure 2.15 depicts the weld condition domains representing single zone and double zone model validity. The multiple domains, w_r=0.4-4, YS_r=0.8, n_r=0.7-0.8; w_r=0.4-4, YS_r=0.9, n_r=0.7; w_r=0.4-1, YS_r=0.8-0.9, n_r=0.8-0.9; w_r=0.4, YS_r=1, n_r=0.7-0.8; w_r=0.8-3, YS_r=1, n_r=0.7; w_r=0.4-0.8, YS_r=1, n_r=0.7; w_r=2-4, YS_r=1.4, n_r=0.9-1; w_r=2-4, YS_r=1.24, n_r=1; w_r=3-4, YS_r=1.1, n_r=1; w_r=3-4, YS_r=1.24, n_r=0.9 and w_r=3-4, YS_r=1.4,

n_r=0.7-0.8 are represented, in which the double zone model is valid when displacement at failure is considered as the criteria for longitudinal weld orientation. This means that within these weld condition domains, it is essential to incorporate HAZ, WN properties separately during FSW blanks formability prediction, while single zone model is essential if the weld conditions (w_r, YS_r, n_r) are outside the indicated domains. As shown in Fig. 2.15, the domains are represented by straight lines, plane surfaces and cube within the finite range of weld conditions at different levels. Among all the domains, few domains form straight lines in which only one parameter (either w_r or YS_r or n_r) is changing out of three weld parameters, few other domains form plane surfaces in which two parameters (either w_r and YS_r or YS_r and n_r or w_r and n_r) are changing out of three weld parameters and only one domain form cube shape in which all three parameters (w_r, YS_r, n_r) are changing within finite limits.

Table 2.6 Displacement till failure for LDH test simulation of longitudinal weld

Weld conditions			Displacement at failure (mm)	% difference in displacement
w_r	YS_r	n_r		
FSW blank modeled with single zone assumption (reference)			41.5	0.00
0.4	**0.8**	**0.7**	**10**	**75.90**
0.4	**0.8**	**0.8**	**12.5**	**69.88**
0.4	0.8	1.24	42	1.20
0.8	**0.8**	**0.7**	**13**	**68.67**
0.8	**0.8**	**0.8**	**15.5**	**62.65**
0.8	0.8	1	38.5	7.23
1	**0.8**	**0.7**	**14.5**	**65.05**
1	**0.8**	**0.8**	**22.5**	**45.78**
1	0.8	1	39.5	4.82
2	**0.8**	**0.7**	**18.5**	**55.42**
2	**0.8**	**0.8**	**33**	**20.48**
2	0.8	0.9	39.5	4.82
3	**0.8**	**0.7**	**19**	**54.22**
3	**0.8**	**0.8**	**24**	**42.17**
3	0.8	1	35	15.66
4	**0.8**	**0.7**	**25.5**	**38.55**
4	**0.8**	**0.8**	**33**	**20.48**
4	0.8	0.9	40	3.61
4	0.8	1	39	6.02
4	0.9	1	40	3.61
4	1	1	41.5	0.00
4	1.24	1	33.5	19.28
4	1.4	1	33.5	19.28

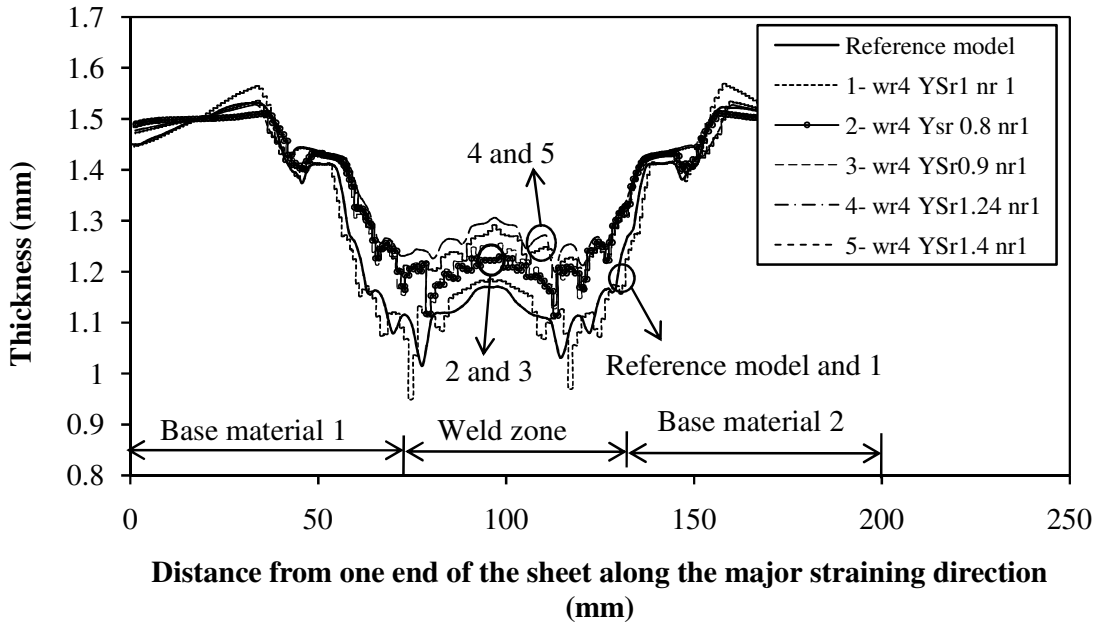

Fig. 2.13 Thickness distribution for FSW blanks with longitudinal weld and displacement at failure as criterion

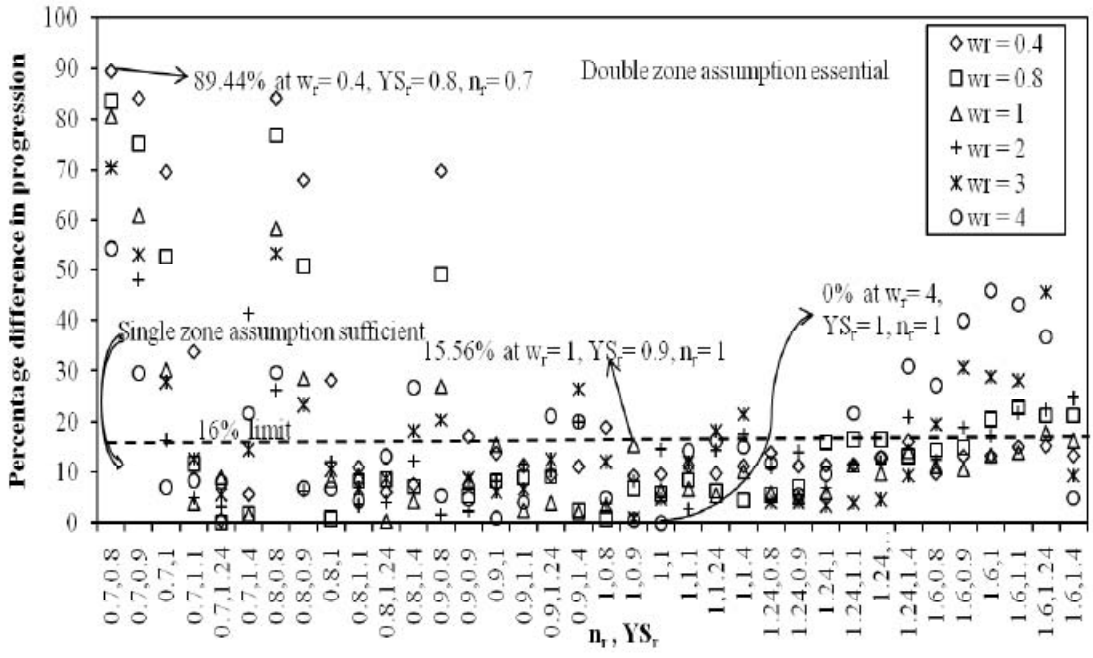

Fig. 2.14 Error percentage variations of double zone modeled FSW blanks with longitudinal weld and displacement at failure as criterion at different weld conditions

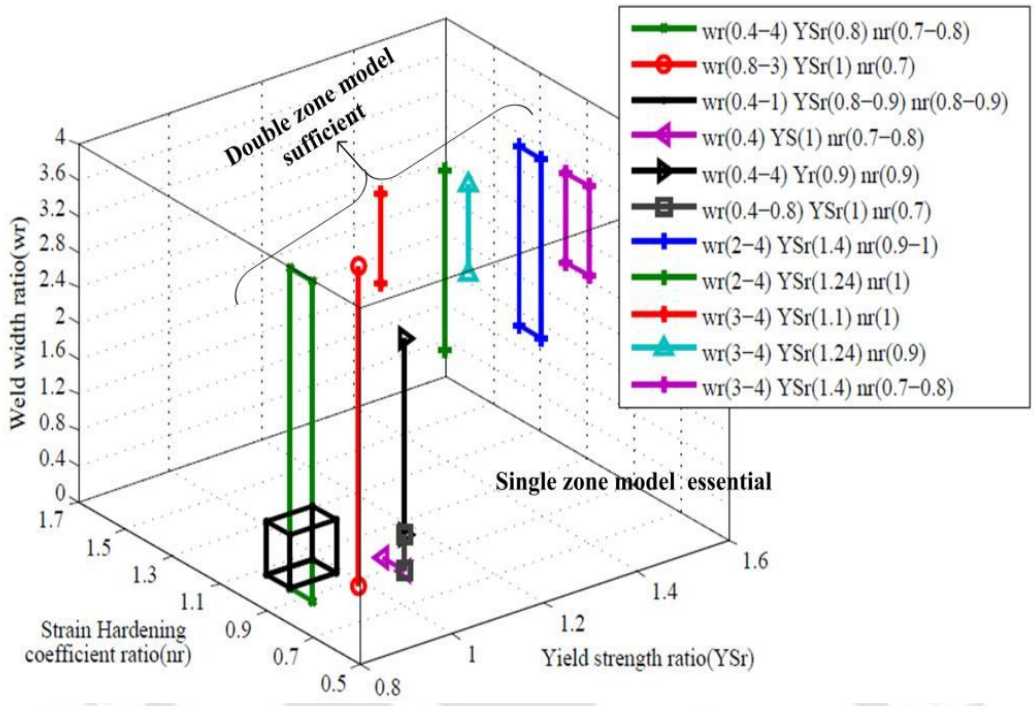

Fig. 2.15 Domains of weld conditions for representing the double zone model validity with displacement at failure as criterion (longitudinal weld orientation)

2.2.5 Relating failure location with weld zone representation

The failure location is another critical factor in deciding the methods of weld zone representation of FSW blanks in both weld orientations. Based on the simulation results, there are three types of failure locations observed in double zone modeled FSW blanks, where as only weld zone failures are seen in the single zone (reference) models as shown in Fig. 2.16 schematically. In case of transverse weld orientation, failure occurs either in WN or in HAZ depending on the relative mechanical properties. In the case of longitudinal weld orientation, failure occurs normal to the weld region. The failure initiation could be in the weld region or at the interface of base material and weld region. The failure location pattern is found to show profound effect on the representation of weld zone in FSW blank, i.e., as single zone or double zone model.

2.2.5.1 Transverse weld orientation: From the simulation results, it is observed that failure location in single zone model FSW blank with transverse weld orientation is in weld zone (Fig. 2.16 (a)). In double zone model cases, failure occurs either in WN or in HAZ depending on the relative mechanical properties. Table 2.7 shows some of the double zone model cases where failure location is in WN and compared with the single zone model. The reference

model case has failed at displacement of 42 mm, whereas double zone model cases like w_r=4, YS_r=1.1, n_r=0.9; w_r=4, YS_r=1.1, n_r=1; w_r=4, YS_r=0.8, n_r=1 and w_r=4, YS_r=0.9, n_r=1 failed at displacement of 43.5 mm, 39.5 mm, 24.5 mm and 34 mm respectively and in all cases failure location is in weld nugget (WN). When these cases are compared with reference model, it is observed that two of the cases w_r=4, YS_r=1.1, n_r=0.9 and w_r=4, YS_r=1.1, n_r=1 have the error percentage difference of 3.57% and 5.95%. In these cases single zone model is sufficient. The other two cases have error percentage difference of 41.67 % and 19.05 % and hence double zone model is necessary. According to single zone model representation, when failure location is in WN, it should be modeled as single zone. But, it is not always true as depicted in Table 2.7. The cases like, w_r=4, YS_r=0.8, n_r=1; and w_r=4, YS_r=0.9, n_r=1, have error percentage more than 16% (41.67% and 19.05 %) and hence double zone model is essential though failure location seen in WN.

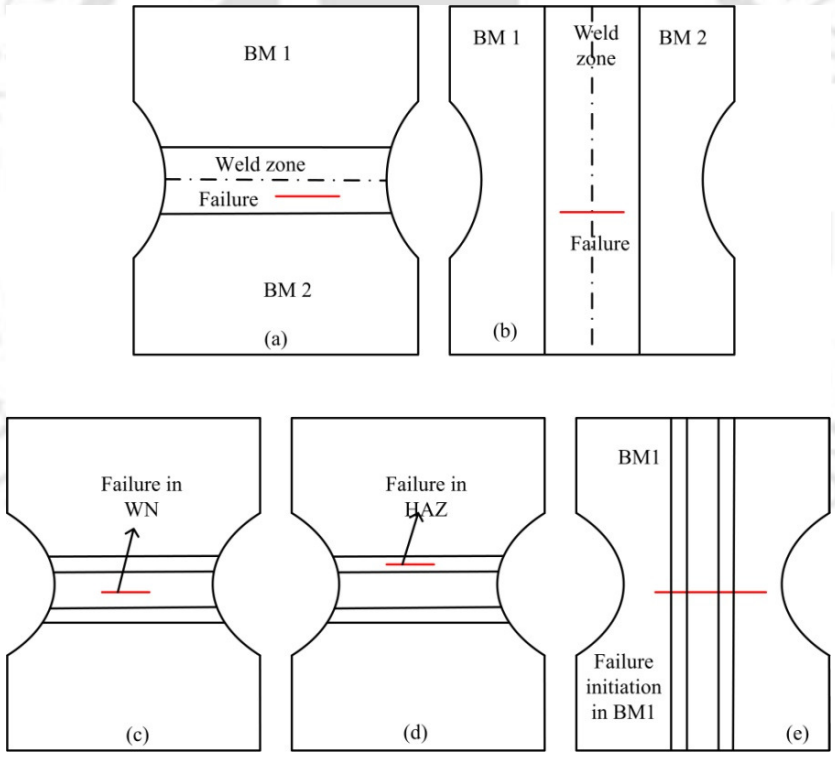

(a) single zone model (reference) with transverse weld orientation; (b) single zone model (reference) with longitudinal weld orientation; (c) & (d) double zone models failure locations in transverse weld orientation; (e) double zone model failure locations in longitudinal weld orientation

Fig. 2.16 Schematic representation of typical failure zones for FSW blanks in LDH tests simulation

Table 2.7 Failure location in WN for LDH test simulation at displacement at failure as criterion

Weld conditions			Displacement at failure (mm)	% difference in displacement	Failure initiation
w_r	YS_r	n_r			
FSW blank modeled with single zone assumption (reference)			42	0.00	Weld zone
4	1.1	0.9	43.5	3.57	WN
4	1.1	1	39.5	5.95	WN
4	0.8	1	24.5	41.67	WN
4	0.9	1	34	19.05	WN

Table 2.8 Failure location in HAZ for LDH test simulation at displacement at failure as criterion

Weld conditions			Displacement at failure (mm)	% difference in displacement	Failure initiation
w_r	YS_r	n_r			
FSW blank modeled with single zone assumption (reference)			42	0.00	Weld zone
0.8	1	1	36	14.29	HAZ
2	1	1	38	9.52	HAZ
0.8	1.4	1.6	17	59.52	HAZ
2	1.1	1	29.5	29.76	HAZ

The other comparison is between the single zone model case where failure is in weld zone and double zone case failing in HAZ. As shown in Table 2.8, the reference model case is failed at displacement of 42 mm, whereas other double zone model cases like w_r=0.8, YS_r=1, n_r=1; w_r=2, YS_r=1, n_r=1; w_r=0.8, YS_r=1.4, n_r=1.6 and w_r=2, YS_r=1.1, n_r=1 are failing at displacement of 36 mm, 38 mm, 17 mm and 29.5 mm respectively and with failure initiation is in HAZ only. When these cases are compared with reference model displacement at failure, it is observed that two weld conditions w_r=0.8, YS_r=1, n_r=1; w_r=2, YS_r=1, n_r=1 have error percentage difference of 14.29% and 9.52 % and other cases (w_r=0.8, YS_r=1.4, n_r=1.6; w_r=2, YS_r=1.1, n_r=1) exhibit error percentage difference of 59.52 % and 29.76 %. According to double zone model representation, when failure location is in HAZ, it should be modeled as double zone. But, it is not always true as depicted in Table 2.8. The cases like, w_r=0.8, YS_r=1, n_r=1 and w_r=2, YS_r=1, n_r=1, have error percentage less than 16% (14.29% and 9.52 %) and hence single zone model is sufficient. But for other two cases, w_r=0.8, YS_r=1.4, n_r=1.6 and w_r=2, YS_r=1.1, n_r=1 double zone model is necessary, though failure location is seen in HAZ.

2.2.5.2 Longitudinal orientation: From the simulation results, it is observed that failure in FSW blank modeled with single zone longitudinal weld orientation is normal to the weld zone. Even in double zone model cases, failure is seen normal to the weld zone, but initiation

is found to be either in base material or WN or HAZ. Table 2.9 shows weld conditions exhibiting failure in WN of double zone model cases compared with single zone model. The reference model case has failed at maximum load of 199.9 kN, whereas double zone model cases like w_r=4, YS_r=1.24, n_r=0.8; w_r=4, YS_r=0.9, n_r=1.24; w_r=4, YS_r=0.8, n_r=0.7 and w_r= 4, YS_r= 1.4, n_r= 0.8 failed at maximum load of 173.4 kN, 211.1 kN, 91.1 kN and 146.3 kN respectively and with failure location in WN. When these cases are compared with reference model, it is observed that two of the cases w_r=4, YS_r=1.24, n_r=0.8; w_r=4, YS_r=0.9, n_r=1.24 have the error percentage difference of 13.26% and 5.26%. For these cases, single zone model is sufficient. The other two cases (w_r=4, YS_r=0.8, n_r=0.7; w_r=4, YS_r=1.4, n_r=0.8) exhibit error percentage difference of 54.43 % and 26.81 % shown in Table 9. For these cases double zone model is essential. According to single zone model representation, when failure location is in WN, it can be modeled as single zone. But, it is not always true as depicted in Table 2.9. The cases like, w_r=4, YS_r=0.9, n_r=0.7; and w_r=4, YS_r=1.4, n_r=0.8, have error percentage more than 16% (54.43% and 26.81 %) and hence double zone model is essential though failure location seen in WN.

The other comparison is between the single zone model case where failure is in weld zone and double zone case failing in HAZ. In Table 2.10, the double zone model cases failing in HAZ and single zone model failing in WZ are compared. The reference model case has failed at maximum load of 199.9 kN, whereas double zone model cases- w_r=3, YS_r=1.1, n_r=0.8; w_r=4, YS_r=1.4, n_r=1.6; w_r=3, YS_r=1.24, n_r=1.6 and w_r=4, YS_r=1, n_r=1.6 failed at maximum load of 186.3 kN, 210 kN, 291.1kN and 291.8kN respectively and failure initiation is in HAZ only. When these cases are compared with reference model, it is observed that two of the cases, w_r=3, YS_r=1.1, n_r=0.8; w_r=4, YS_r=1.4, n_r=1.6, have the error percentage difference of 6.80 % and 5.05 % and other cases, viz., w_r=3, YS_r=1.24, n_r=1.6; w_r=4, YS_r=1, n_r=1.6 are having error percentage difference of 45.62 % and 45.97 %. According to double zone model representation when failure initiation is in HAZ, then it should be modeled with double zone model. But, it is not always true as depicted in Table 2.10. From Table 2.10, the cases w_r=0.8, YS_r=1, n_r=1; w_r=2, YS_r=1, n_r=1, have error percentage less than 16% (6.80% and 5.05 %) and hence single zone model is sufficient. For other two cases (w_r=0.8, YS_r=1.4, n_r=1.6 and w_r=2, YS_r=1.1, n_r=1) double zone model is essential, though failure initiation is seen in HAZ.

Table 2.9 Failure location in WN for LDH test simulation at maximum load at failure as criterion

Weld conditions			Maximum load (kN)	% difference in load	Failure initiation
w_r	YS_r	n_r			
FSW blank modeled with single zone assumption (reference)			199.9	0.00	Weld zone
4	1.24	0.8	173.4	13.26	WN
4	0.8	1.24	211.1	5.60	WN
4	0.9	0.7	91.1	54.43	WN
4	1.4	0.8	146.3	26.81	WN

Table 2.10 Failure location in HAZ for LDH test simulation at maximum load at failure as criterion

Weld conditions			Maximum load (kN)	% difference in load	Failure initiation
w_r	YS_r	n_r			
FSW blank modeled with single zone assumption (reference)			199.9	0.00	Weld zone
3	1.1	0.8	186.3	6.80	HAZ
4	1.4	1.6	210	5.05	HAZ
3	1.24	1.6	291.1	45.62	HAZ
4	1	1.6	291.8	45.97	HAZ

The last comparison is between reference model and double zone model cases with failure initiation in base metal. Table 2.11 shows some of the cases, where failure initiation is in BM of double zone model cases compared with single zone model failing at weld zone. The reference model case is failing at maximum load of 199.9 kN, whereas double zone model cases like w_r=0.4, YS_r=1.4, n_r=0.7; w_r=0.8, YS_r=1, n_r=0.9; w_r=2, YS_r=0.8, n_r=0.8 and w_r=4, YS_r=0.8, n_r=1.6 fail at maximum load of 211.3, 216.5, 147.5 and 254.3 respectively and with failure initiation in BM only as shown in Table 2.10. When these cases are compared with reference model, it is observed that two cases viz., w_r=0.4, YS_r=1.4, n_r=0.7; w_r=0.8, YS_r=1, n_r=0.9 weld are having the error percentage difference of 5.70 % and 8.30 % and other cases (w_r=2, YS_r=0.8, n_r=0.8, w_r=4, YS_r=0.8, n_r=1.6) are having error percentage difference of 26.21 % and 27.21 %. For these cases (w_r=0.4, YS_r=1.4, n_r=0.7; w_r=0.8, YS_r=1, n_r=0.9) single zone model is sufficient. In the other two cases (w_r=2, YS_r=0.8, n_r=0.8; w_r=4, YS_r=0.8, n_r=1.6) double zone model is essential.

Table 2.11 Failure initiation in BM for LDH test simulation at maximum load at failure as criterion

Weld conditions			Maximum load (kN)	% difference in load	Failure initiation
w_r	YS_r	n_r			
FSW blank modeled with single zone assumption (reference)			199.9	0.00	Weld zone
0.4	1.4	0.7	211.3	5.70	BM
0.8	1	0.9	216.5	8.30	BM
2	0.8	0.8	147.5	26.21	BM
4	0.8	1.6	254.3	27.21	BM

Finally, the weld zone representation of FSW blanks as single zone or double zone is dependent on failure location and its dependence on weld width and mechanical properties of different zones are already known. In this work, the failure initiations are observed at different locations of weld in transverse and longitudinal orientations for different weld conditions of FSW blanks. In general, the failure locations are observed in WN and HAZ. These failure locations have distinguished the weld zone model that can be followed in FSW blanks during forming simulation. The failure initiation is dependent on the total weld width and mechanical properties of different zones with respect to reference model, i.e., if the weld conditions of the double zone model is same or nearly equal to reference model, then failure initiation is seen in the same zone. Similarly if the weld conditions of the double zone model are very different than the single zone model, the failure locations are in different zones of weld region. Though failure locations are same, in the present work, weld zone representation is distinguished based on critical error percentage limit between reference model (single zone) and double zone model FSW blanks formability parameters. The formability comparison of reference model to double zone model is done with fixed an error percentage of 16%. From literature, the available error percentage range is between 5.3 % to 37.03% for maximum displacement at failure and 2.5% to 43.54% for maximum load in plane- strain stretching between experiment and simulation results condition. In the present work, the error percentage is fixed as 16%, which is found to be optimum within the available ranges. Whereas, this may not be applicable for all the weld conditions, materials and forming behavior monitored. In such cases, the weld conditions at which double zone or single zones are valid will be different. From the results of present work, if the error percentage limit is fixed other than 16%, then few of the double zone model cases will become single zone models and vice versa. So weld conditions, failure location and error percentage fixed affect the weld zone representation methods in a synergistic fashion.

2.2.6 Implications of weld zone representation on TWB formability prediction

In FSW blanks, single zone or double zone model decides the accuracy with which formability can be predicted. The weld zone properties (n, σ_{YS}, width of HAZ and WN), weld orientation (transverse, longitudinal or any other angle), weld location (center or at some offset) affect the weld zone representation in a compounding fashion. For example, whenever the weld zone properties are very different as compared to the base material, double zone model is essential. When weld properties are closer to base material, single zone model could be sufficient. In other words, FSW that generates heterogeneous properties in the weld zone

(HAZ, WN) for a particular base material should be represented as double zone. For example, it is understood from Miles *et al.*, 2004; Liu and Chao, 2005 studies that HAZ and WN have different mechanical properties as compared to base material. In these cases, it is advisable to follow double zone model during formability prediction. Similarly the contribution of HAZ, WN width (Zadpoor *et al.*, 2008 c; Xu *et al.*, 2009) to total weld width also affect the weld zone representation. Due to these variations in the mechanical properties and widths of weld zones in FSW blanks, weld zone should be modeled with double zone assumption which will give accurate formability prediction results.

In the case of weld orientation, it is observed that double zone models are more in transverse weld, while single zone models are more than in longitudinal welds. This is due to change in the failure locations with weld orientations. It is seen that with transverse weld FSW blanks, either HAZ or WN fails during forming, resulting in the emergence of gauge effect. This resulted in deviation between the forming behavior of reference case and individual FSW cases. In longitudinal weld, both HAZ and WN and base metal take part in the forming and hence failure occur normal to weld region. So in this case, the ductility of HAZ or WN decides the weld zone representation along with other weld properties. In the present work, only transverse and longitudinal weld orientations are simulated for FSW blanks formability prediction. Any other weld orientation (say 45°) will behave in a mixed pattern (combining both 0° and 90° welds) and one would select the double zone model for formability prediction.

When placed at critical locations (or offset locations), formability is found to decrease significantly and hence it is always safe to follow double zone modeling for accurate evaluation of formability. One may choose single zone model in this case if the accuracy is not compromised. In the case of industrial sheet parts, weld can be at any location and orientation depending on the part requirement. Generally weld is placed at safe region of the sheet part. It would be sufficient to follow single zone model since the individual sheet parts are very large in size. Above all, the forming test performed, forming behavior monitored, dissimilar thickness and strength of sheet materials and range fixed for selecting single or double zone welds affect the weld zone representation in a compounding manner.

In the present work, the two different methods of representing the weld zone in FSW blanks are analyzed by giving importance to the accuracy of formability prediction. There are other equally important issues like determining the mechanical properties of weld zone, CPU time, simplicity of preparing the models etc. that can be compared between the single and double zone assumptions. In the case of double zone models, it is difficult to evaluate the

mechanical properties of nugget and HAZ separately. But it is relatively easy to evaluate the global mechanical properties of weld zone in the case of single zone models with the existing methods. The existing methods, viz., (i) evaluating the tensile properties of the weld zone (as a single entity) using a miniature size sample made from the weld region, and (ii) applying iso-strain principle to the TWB tensile sample with longitudinal weld zone, are used by few research groups to determine the properties of weld zone, as a single entity, in FSW blanks. For evaluating the mechanical properties of local weld regions, small notch can be made on tensile specimen at the nugget or HAZ, which is a tedious procedure and may finally compromise on the accuracy with which the properties are evaluated. Due to these difficulties in double zone model assumption, many of the researchers are modeling the weld zone as a single entity only.

When CPU time is considered, it is observed from the simulations of the present work that both the models take almost same time for simulation. It is also concluded by Zadpoor *et al*., 2009 that CPU time for LDH tests are independent of the methods by which weld zone is represented during forming simulation. It is also said that considerable difference in CPU time was seen only in the 'springback' stage of S-rail problem, and not in the stamping stage. Moreover, it is time consuming, but not difficult to make double zone models in any FE code and CAD package as compared to single zone models. From these three comparisons, it can be said that single zone model is always convenient than double zone model during FSW blank forming prediction, but this is not always acceptable when forming prediction accuracy is concerned.

2.3 Conclusions

From the present work, the following conclusions are made.

- For representing the single zone or double zone models, multiple domains are possible due to the parametric changes in weld conditions and such changes affects the local and global deformation influencing the model representation.

- The three weld conditions (YS_r, n_r, w_r) influence the validity of single zone or double zone in a compounding fashion. By considering the maximum load attained as criterion in transverse weld orientation, w_r = 2-4, n_r = 1, YS_r = 1 and w_r = 3-4, YS_r = 1.1, n_r= 0.9 are the two domains within which 'single zone' assumption is valid.

Similarly, single zone and double zone valid domains are obtained with displacement at failure as criteria in both the weld orientations.

- When the weld conditions are closer to reference model weld condition, single zone model is found to be valid. If the weld conditions are very different from the reference model, it breaks down the single zone model and double zone model is valid in those conditions.

- In the cases where weld conditions are near to reference model and error percentage difference is less than 16%, the thickness distribution is found to be closer to reference model thickness distribution in both transverse and longitudinal weld orientations. Single zone model is found to be valid under these circumstances.

- It is seen that by defining the properties for WN and HAZ separately, it makes a significant contribution to the accuracy of the forming prediction

- The failure initiations are observed at different locations of weld in transverse and longitudinal orientations for different weld conditions of FSW blanks. In the case of transverse weld orientation, failure initiations are in weld nugget and HAZ only. In longitudinal weld orientation, failure initiation is not only in weld zones but also in base materials, and failure is normal to the weld zone.

- These failure locations or initiations also affect the weld zone representation along with the critical error percentage difference between reference model (single zone) and double zone model FSW blanks.

- The critical weld conditions (width, properties) where the single zone model assumption breaks down are not unique. It depends on the mode of deformation and weld orientation. In addition, the base metal properties and thickness could also affect the methods of weld zone representation during formability prediction.

Chapter 3

Weld zone representation methods during the stretching of friction stir welded blanks with dissimilar sheet thickness: A study using numerical simulations

3.1 Methodology

The FSW blanks with dissimilar thicknesses (and similar thickness) are modeled in two ways - (i) single zone model, where WN and HAZ are modeled as single entity, and (ii) double zone model, where WN and HAZ are modeled separately, for formability simulation and prediction. The single zone model, which is a reference model, is shown schematically in Fig. 3.1 (a). In this model, weld zone includes WN and HAZ as single entity and global mechanical properties are defined in weld zone and base material during modeling. A maximum weld width of 30 mm (Buffa *et al.*, 2008; Zadpoor *et al.*, 2008) is considered for simulation analyses (Fig. 3.1 (a)). The thickness of the base materials considered for FSW blanks are 1.1 mm and 1.5 mm and for weld zone, an average thickness of 1.3 mm is used.

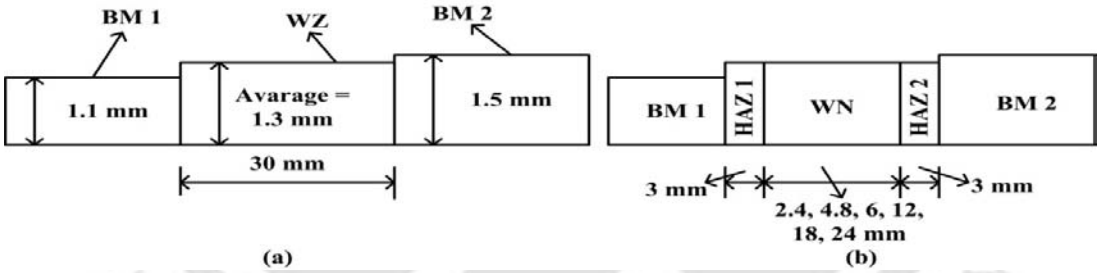

Fig. 3.1 Schematic representation of (a) single zone model, and (b) double zone model

"The same **methodology** of **Chapter 2** in section **2.1** is followed for this study also".

3.2 Results and Discussion

3.2.1 Transverse weld orientation based on maximum load

The domain at which the single zone assumption breaks down is obtained for transverse weld orientation by considering maximum load at failure as the criterion. In this case, it is observed that multiple domains of weld conditions are possible where single zone assumption is invalid. The maximum load at failure data for single zone and few double zone cases are shown in Table 3.1 for discussion. One of the domains, w_r=4, YS_r =0.9-1.1, n_r =1 is indicated in Table 3.1 in which the weld conditions within the above said domain exhibit stroke difference less than 16%. Similarly there are multiple domains where single zone assumption

is valid. They are w_r=0.8-2, YS_r=1, n_r=1; w_r=1-3, YS_r=1.1, n_r=0.9; w_r=3-4, YS_r=0.8, n_r=1.24; w_r=4, YS_r=0.9-1.1, n_r=1; w_r=1-2, YS_r=1.24, n_r=0.8; and w_r =4, YS_r=0.8-1, n_r=0.9. All other weld conditions outside the specified range are greater than 16%, and hence double zone model should be followed.

Table 3.1 Maximum Load at failure for LDH test simulation of transverse weld orientation

Weld conditions			Maximum load (kN)	% difference in load
w_r	YS_r	n_r		
FSW blank modeled with single zone assumption (reference)			59	0.00
0.8	1	0.9	30.9	47.60
0.8	1	1	55.9	5.25
0.8	1.1	1	47.3	19.8
1	0.9	1	43	33.6
1	1	1	65.7	11.36
1	1	1.24	32.4	45.08
2	0.9	0.9	27	54.24
2	0.9	1	36.5	38.14
2	1	1	65.9	11.7
2	1.1	1.24	26.6	54.92
2	1.4	1.6	26.6	54.92
3	0.9	1	45.1	23.56
3	1	1	70.5	19.49
3	1.1	1.24	30.3	48.64
3	1.4	1.6	20.1	65.93
4	0.8	0.9	61.2	3.73
4	**0.9**	**1**	**53.2**	**9.83**
4	1	0.9	51.5	12.71
4	**1**	**1**	**58.4**	**1.02**
4	1	1.24	37.2	36.95
4	**1.1**	**1**	**63**	**6.78**
4	1.1	1.24	34.3	41.86
4	1.4	1.6	20.2	65.75

The thickness distribution is observed from one end of sheet along the major strain direction, i.e., normal to the neck to validate the single zone model within the domains stated. Figure 3.2 shows the thickness distribution of different weld conditions comparing the single zone model (i.e., reference model) assumption, YS_r=1, n_r=1, w_r=4 and double zone models. Here thickness distribution is measured just after the maximum load is reached. It can be understood from the Fig. 3.2 that weld conditions w_r= 4, YS_r= 0.8, n_r= 0.9; w_r= 4, YS_r= 1, n_r= 0.9; w_r= 4, YS_r= 1.1, n_r= 1 belonging to single zone model case (curves 1, 2 and 3) are closer to reference model, showing lesser difference between them. These conditions exhibit an error percentage of 3.73 %, 12.71 %, 6.78 % (shown in Table 3.1) when maximum load is compared with the reference model. The failure location is also found to be same as that of reference model. On the other hand, the weld conditions, w_r= 4, YS_r= 1, n_r= 1.24; w_r= 4, YS_r=

1.1, n_r=1.24; and w_r= 4, YS_r= 1.4, n_r= 1.6, belonging to double zone model cases (curves 4, 5 and 6) are very different when compared to reference cases, showing more difference between them. These weld conditions belong to double zone model and exhibit error percentage of 36.95 %, 41.86 %, 65.75 % and 50% (shown in Table 3.1) with the reference case. It is observed that whenever the error percentage in maximum load is below 16%, the weld conditions exhibit thickness distribution and failure location similar to that of reference model. In these weld conditions, double zone models behaves like single zone model, and it is sufficient to represent FSW blank as single zone model without incorporating separate mechanical properties in HAZ and WN. In other weld conditions like w_r= 4, YS_r= 1, n_r= 1.24; w_r= 4, YS_r= 1.1, n_r=1.24; and w_r= 4, YS_r= 1.4, n_r= 1.6, the error percentage in stroke is more than 16% and the thickness distributions are very different when compared to reference case, though the failure location is within the weld zone (Fig. 3.3). In these weld conditions, one has to treat weld zone as double zone by incorporating separate mechanical properties in HAZ and WN.

Figure 3.3 shows the error percentage variation of double zone modeled FSW blanks with transverse weld and stroke at failure as criteria at different weld conditions. The maximum error percentage among all the cases is 92.59 % at w_r= 0.4, YS_r= 0.8, n_r= 0.7 weld condition and minimum is 1.02 % percentage at w_r= 4, YS_r= 1, n_r= 1 weld condition, which behaves like the reference model. It is clear from Fig. 3.3 that most of the cases are above 16% limit and few are below the limit. All the weld conditions whose error percentages are less than or greater than 16% can be represented as single zone or double zone model validity. Figure 3.4 depicts the weld conditions representation for single zone and double zone model validity. The possible multiple domains are w_r=0.8-2, YS_r=1, n_r=1; w_r=1-3, YS_r=1.1, n_r=0.9; w_r=3-4, YS_r=0.8, n_r=1.24; w_r=4, YS_r=0.9-1.1, n_r=1; w_r=1-2, YS_r=1.24, n_r=0.8; and w_r=4, YSr=0.8-1, n_r=0.9. In which the single zone model is valid when maximum load at failure considered as the criteria for transverse weld case. This means that within these weld conditions, it is sufficient to incorporate global weld zone properties during FSW blanks formability prediction, while WN and HAZ properties should be incorporated separately if weld conditions are outside the indicated domain, i.e., double zone representation has to be followed. As shown in Fig. 3.4, the domains are represented by straight lines which indicate that out of three weld conditions only one parameter (w_r) is changing within the finite range and other two conditions (YS_r, n_r) are constant at different levels.

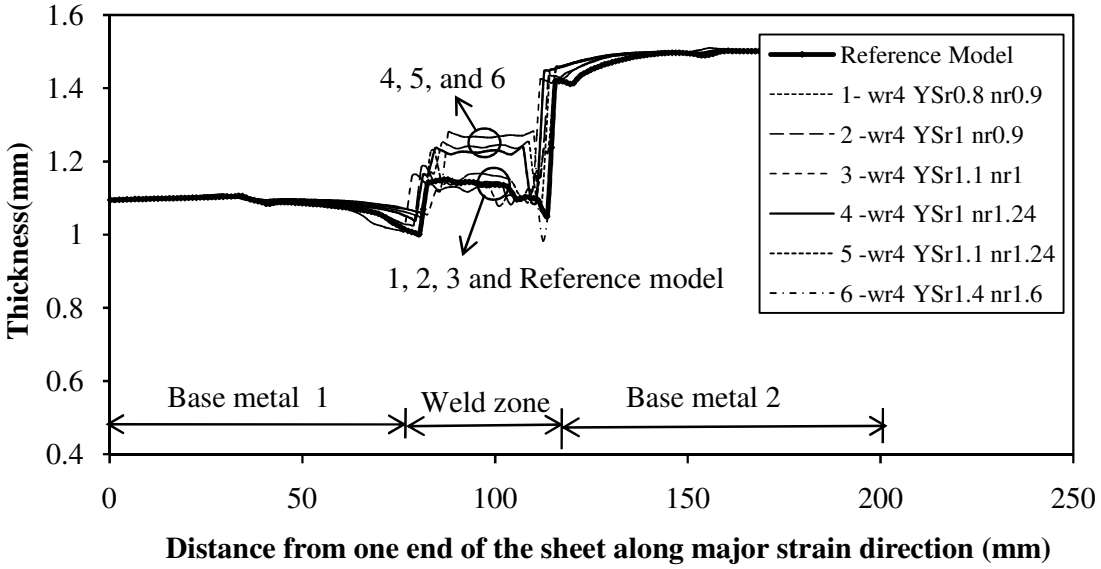

Fig. 3.2 Thickness distribution for FSW blanks with transverse weld and maximum load at failure as criterion

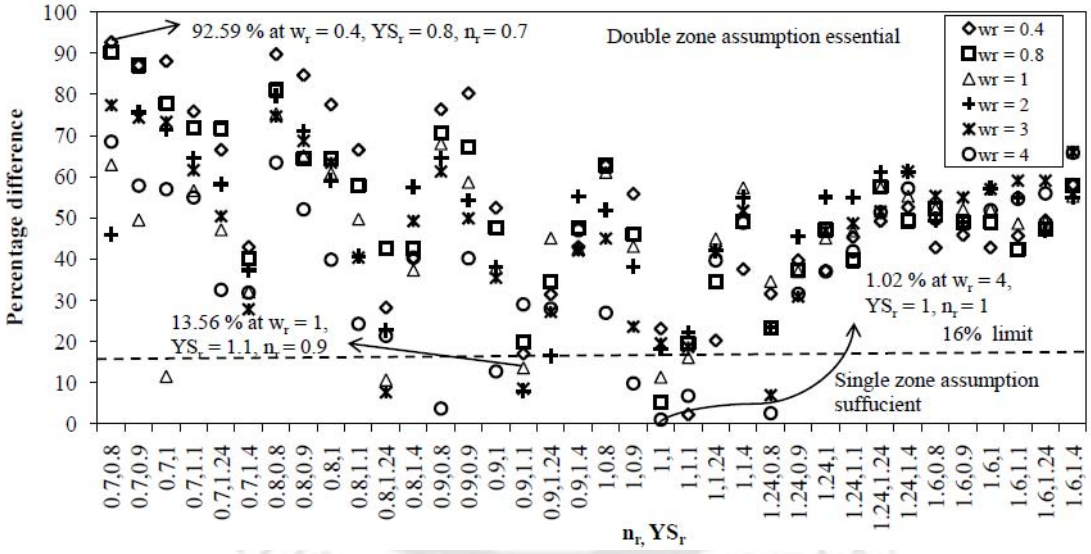

Fig. 3.3 Error percentage variations of double zone modeled FSW blanks with transverse weld and maximum load at failure as criterion at different weld conditions

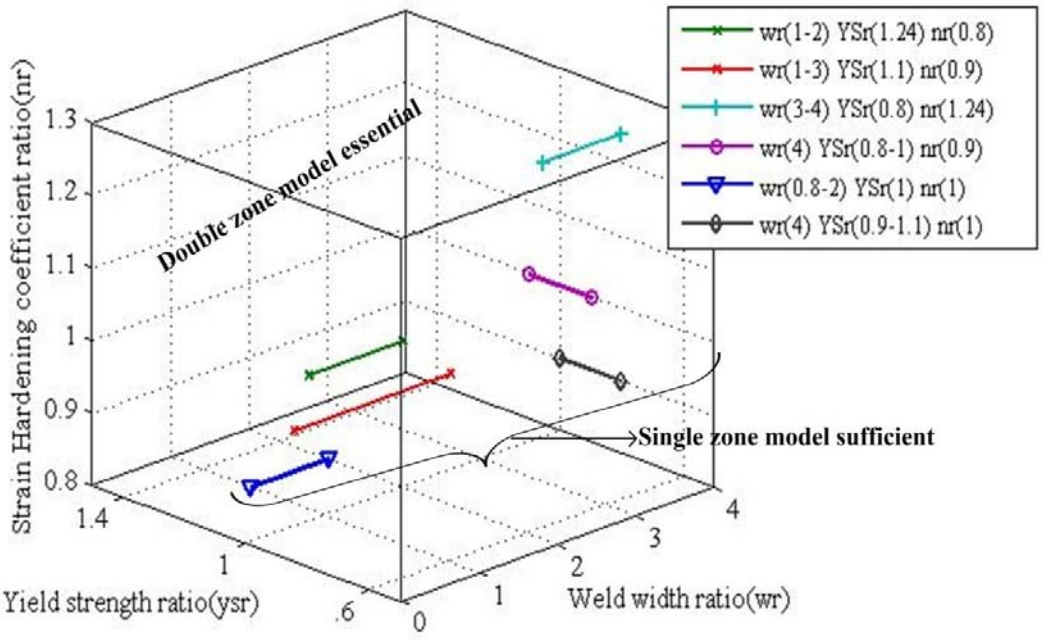

Fig. 3.4 Domains of weld conditions for representing the single zone and double zone model validity with maximum load as criterion (transverse weld orientation)

3.2.2 Transverse weld orientation based on punch stroke at failure

The domain at which the single zone assumption breaks down is obtained for transverse weld orientation by considering punch stroke at failure as the criterion. In this case, it is observed that multiple domains of weld conditions are possible where single zone assumption is invalid. The stroke at failure data for single zone and few double zone cases are shown in Table 3.2 for discussion. One of the domains, w_r=3-4, YS_r=0.9, n_r=1-1.24 is indicated in Table 3.2 in which the weld conditions within the above said domain exhibit stroke difference less than 16%. Similarly there are multiple domains where single zone assumption is valid. They are: w_r=0.4-0.8, YS_r=0.8, n_r=1.24; w_r=0.4-0.8, YS_r=1, n_r=1; w_r=0.4-2, YS_r=1.1, n_r=0.9-1; w_r=0.4, YS_r=1.24, n_r=0.8-1; w_r=1-2, YS_r=0.8, n_r=0.7; w_r=1-2, YS_r=0.8, n_r=1.24; w_r=1-3, YS_r=1.24, n_r=0.8; w_r=2-4, YS_r=1.24, n_r=0.8-0.9; w_r=3-4, YS_r=0.9, n_r=1-1.24; w_r=3-4, YS_r=1.4, n_r=0.7; and w_r=4, YS_r=1, n_r=0.9-1. All other weld conditions outside the specified range are greater than 16%, and hence double zone model should be followed.

Table 3.2 Punch stroke till failure for LDH test simulation of transverse weld orientation under varied weld conditions

Weld conditions			Stroke (mm)	% difference in stroke
w_r	YS_r	n_r		
FSW blank modeled with single zone assumption (reference)			21.5	0.00
2	1	0.9	17.5	18.6
2	0.8	1	15	30.23
2	0.9	1	17.5	18.6
2	0.9	1.24	16	25.58
2	1.4	1	14	34.88
2	1.1	1.6	14	34.88
2	1.4	1.6	14	34.88
3	1	0.9	18	16.28
3	0.8	1	16.5	23.26
3	**0.9**	**1**	**20**	**6.98**
3	**0.9**	**1.24**	**18.5**	**13.95**
3	1.4	1	14.5	32.56
3	1.1	1.6	13	39.53
2	1.4	1.6	11.5	46.51
4	1	0.9	22	2.33
4	0.8	1	20	6.98
4	**0.9**	**1**	**22.5**	**4.65**
4	**0.9**	**1.24**	**18.5**	**13.95**
4	1.4	1	15	30.23
4	1.1	1.6	14	34.88
4	1.4	1.6	11.5	46.51

The thickness distribution is observed from one end of sheet along the major strain direction, i.e., normal to the neck to validate the single zone model within the domains stated. Figure 3.5 shows the thickness distribution of different weld conditions comparing the single zone model (i.e., reference model) assumption, YS_r=1, n_r=1, w_r=4 and double zone models. It can be understood from the Fig. 3.5 that weld conditions w_r= 4, YS_r= 1, n_r= 0.9; w_r= 4, YS_r= 0.8, n_r= 1; and w_r= 4, YS_r= 0.9, n_r= 1 belonging to single zone model cases (curves 1, 2 and 3) are closer to reference model, showing lesser difference between them. These conditions exhibit an error percentage of 2.33 %, 6.98 %, 4.65 % (shown in Table 3.2) when stroke at failure is compared with the reference model. The failure location is also found to be same as that of reference model. On the other hand, the weld conditions, w_r= 4, YS_r= 1.4, n_r= 1; w_r= 4, YS_r= 1.1, n_r= 1.6; w_r= 4, and YS_r= 1.4, n_r= 1.6, belonging to double zone model cases (curves 4, 5 and 6) are very different when compared to reference cases, showing more difference between them. These weld conditions belong to double zone model and exhibit error percentage of 30.23 %, 34.88 %, and 46.51 % (shown in Table 3.2) with the reference case. It is observed that whenever the error percentage in maximum stroke is below 16%, the weld conditions exhibit thickness distribution and failure location similar to that of reference

model. In these weld conditions, double zone models behaves like single zone model and it is sufficient to represent FSW blank as single zone model. In other weld conditions like w_r= 4, YS_r= 1.4, n_r= 1; w_r= 4, YS_r= 1.1, n_r= 1.6; w_r= 4, YS_r= 1.4, n_r= 1.6, the error percentage in stroke is more than 16% and the thickness distributions are very different when compared to reference case, though the failure location is within the weld zone. In these weld conditions, one has to treat weld zone as double zone by incorporating separate mechanical properties in HAZ and WN.

Figure 3.6 depicts the weld conditions representation for single zone and double zone model validity. The possible multiple domains are: w_r=0.4-0.8, YS_r=0.8, n_r=1.24; w_r=0.4-0.8, YS_r=1, n_r=1; w_r=0.4-2, YS_r=1.1, n_r=0.9-1; w_r=0.4, YS_r=1.24, n_r=0.8-1; w_r=1-2, YS_r=0.8, n_r=0.7; w_r=1-2, YS_r=0.8, n_r=1.24; w_r=1-3, YS_r=1.24, n_r=0.8; w_r=2-4, YS_r=1.24, n_r=0.8-0.9; w_r=3-4, YS_r=0.9, n_r=1-1.24; w_r=3-4, YS_r=1.4, n_r=0.7; and w_r=4, YS_r=1, n_r=0.9-1. In which the single zone model is valid when stroke at failure is considered as the criterion for transverse weld case. This means that within these weld conditions, it is sufficient to incorporate global weld zone properties during FSW blanks formability prediction, while WN and HAZ properties should be incorporated separately if weld conditions are outside the indicated domain.

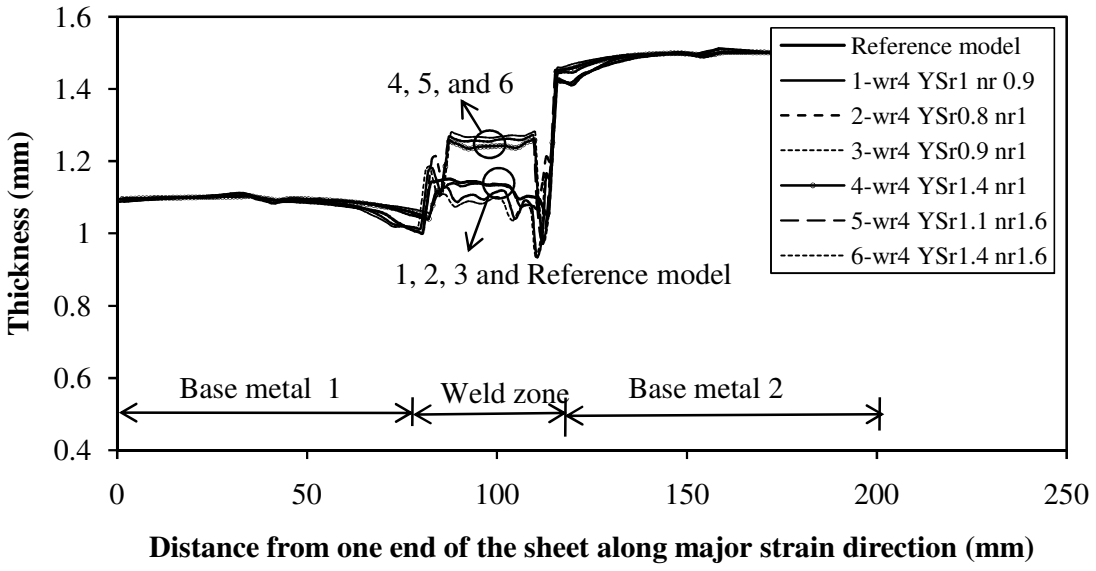

Fig. 3.5 Thickness distribution for FSW blanks with transverse weld and punch stroke at failure as criterion

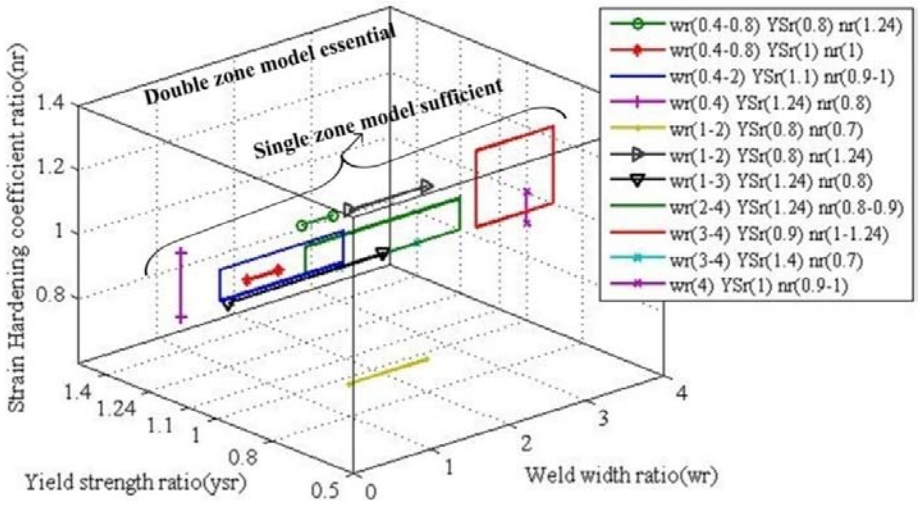

Fig. 3.6 Domains of weld conditions for representing the single zone model with punch stroke at failure as criterion in transverse weld

3.2.3 Longitudinal weld orientation with maximum load and punch stroke at failure as criterion

In this case, longitudinal weld orientation is considered and maximum load at failure is compared between single zone and double zone models. The maximum load at failure data for single zone and few double zone cases are shown in Table 3.3. In this case, it is observed that multiple domains of weld conditions are possible where double zone assumption is invalid. One of the domains w_r=3-4, YS_r=1 and n_r=0.8-1 is indicated in Table 3.3 in which the weld conditions within the above said domain exhibit maximum load difference less than 16%. Similarly, there are multiple domains where single zone assumption is valid. They are: w_r=0.4-1, YS_r=1.24, n_r=0.7; w_r=0.8-1, YS_r=1.4, n_r=1.6; w_r=1-3, YS_r=0.8, n_r=1; w_r=2, YS_r=0.9-1, n_r=0.9; w_r=2, YS_r=1.24, n_r=0.7-0.9; w_r=2-4, YS_r=1.24, n_r=1.6; w_r=2-4, YS_r=1.1, n_r=0.7-1.24; w_r=3-4, YS_r=0.9-1, n_r=0.9-1; w_r=3-4, YS_r=1, n_r=0.8; w_r=3-4, YS_r=1.24, n_r=0.8-1; w_r=3, YS_r=1.4, n_r=0.7-1.24 and w_r=4, YS_r=0.8, n_r=0.9-1. All other weld conditions outside the specified range exhibit error more than 16%, and hence double zone model should be followed.

The thickness distribution is observed (Fig. 3.7), from one end of sheet along the major strain direction, i.e., normal to the neck to validate the double zone model within the domains stated. It can be understood that the weld conditions - w_r= 4, YS_r= 1, n_r= 1 (curve 2) of double zone model case has same thickness distribution as that of single zone model (i.e., reference model). In this case, 3.18 % is witnessed when maximum load is compared with reference model and failure location is same as that of reference model. The other weld conditions, viz.,

w_r= 4, YS_r= 0.9, n_r=0.9 and w_r= 4, YS_r= 1, n_r=0.9 (curves 1 and 3) belonging to the single zone model and the reference case are closer to each other, showing lesser difference between them. These conditions exhibit error percentage of 1.15 % and 9.06 % (shown in Table 3.3) when maximum load is compared with reference model case. On the other hand, the weld conditions like w_r= 4, YS_r= 0.8, n_r=1.24; w_r= 4, YS_r= 0.9, n_r=1.24 and w_r= 4, YS_r= 1, n_r=1.24 belonging to double zone model cases (curves 4 and 5) are very different when compared to reference case, showing more difference between them. These weld conditions belong to double zone model and exhibit error percentage of 26.02 %, 31.49 % and 36.38 % (shown in Table 3.3) with reference case. It is observed that whenever the error percentage in maximum load is below 16%, the weld conditions exhibit thickness distribution and failure location similar to that of reference model. In these weld conditions, it is sufficient to represent FSW blank as single zone model without incorporating separate mechanical properties in HAZ and WN. In other weld conditions like w_r= 4, YS_r= 0.8, n_r=1.24; w_r= 4, YS_r= 0.9, n_r=1.24 and w_r= 4, YS_r= 1, n_r=1.24, the error percentage in stroke is more than 16% and the thickness distributions are very different when compared to reference case, though the failure location is same. In these weld conditions, one has to treat weld zone as double zone by incorporating separate mechanical properties in HAZ and WN.

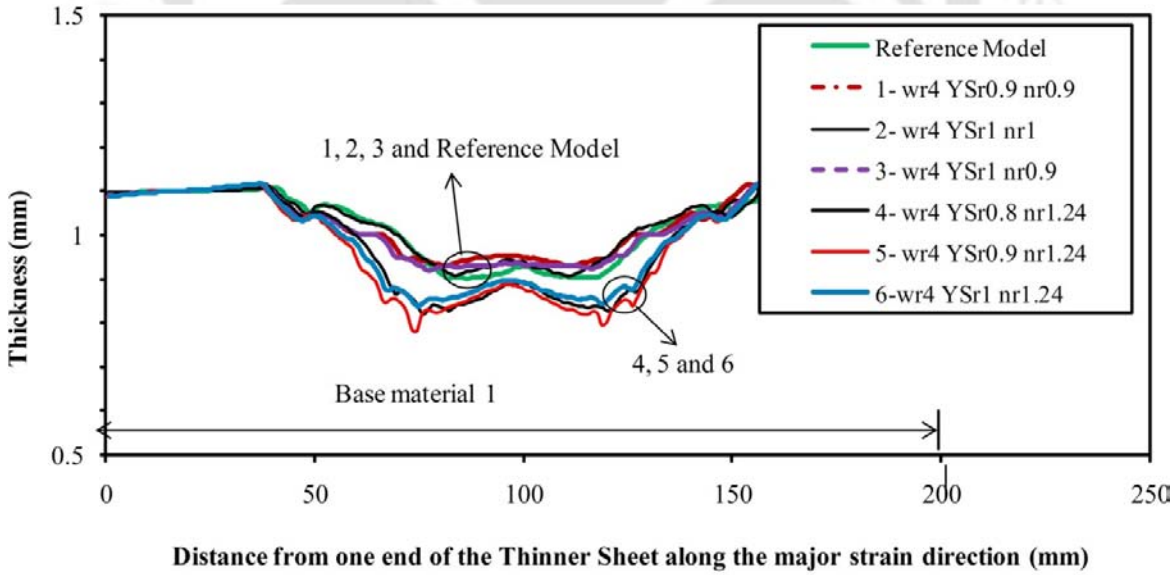

Fig. 3.7 Thickness distribution for FSW blanks with longitudinal weld and maximum load at failure as criterion

Table 3.3 Maximum load at failure for LDH test simulation of longitudinal weld

Weld conditions			Maximum load(kN)	% difference in load
w_r	YS_r	n_r		
FSW blank modeled with single zone assumption (reference)			139.1	0.00
2	0.9	0.9	121.8	12.44
2	1	0.8	115.3	17.11
2	1	0.9	155.6	11.86
2	1	1	167.9	20.70
2	0.8	1.24	174	25.09
2	0.9	1.24	169.6	21.93
2	1	1.24	175	25.81
3	0.9	0.9	139.2	0.07
3	**1**	**0.8**	**133.3**	**4.17**
3	**1**	**0.9**	**149.4**	**7.40**
3	**1**	**1**	**160.2**	**15.17**
3	0.8	1.24	161.8	16.32
3	0.9	1.24	175.2	25.95
3	1	1.24	164.6	18.33
4	0.9	0.9	140.7	1.15
4	**1**	**0.8**	**137.2**	**1.37**
4	**1**	**0.9**	**151.7**	**9.06**
4	**1**	**1**	**144.4**	**3.81**
4	0.8	1.24	175.3	26.02
4	0.9	1.24	182.9	31.49
4	1	1.24	189.7	36.38

Figure 3.8 depicts the weld conditions representation for single zone and double zone model validity. The multiple domains namely w_r=0.4-1, YS_r=1.24, n_r=0.7; w_r=0.8-1, YS_r=1.4, n_r=1.6; w_r=1-3, YS_r=0.8, n_r=1; w_r=2, YS_r=0.9-1, n_r=0.9; w_r=2, YS_r=1.24, n_r=0.7-0.9; w_r=2-4, YS_r=1.24, n_r=1.6; w_r=2-4, YS_r=1.1, n_r=0.7-1.24; w_r=3-4, YS_r=0.9, n_r=1; w_r=3-4, YS_r=1, n_r=0.8-1; w_r=3-4, YS_r=1.24, n_r=0.8-1; w_r=3, YS_r=1.4, n_r=0.7-1.24; and w_r=4, YS_r=0.8, n_r=0.9-1 are the weld conditions where single zone model is valid when maximum load at failure is considered as the criteria for longitudinal weld case. This means that within these weld conditions, single zone model is sufficient and hence it is not required to incorporate local weld zone properties (HAZ, WN) during FSW blanks formability prediction. If the weld conditions are outside the indicated domain, double zone representation has to be followed.

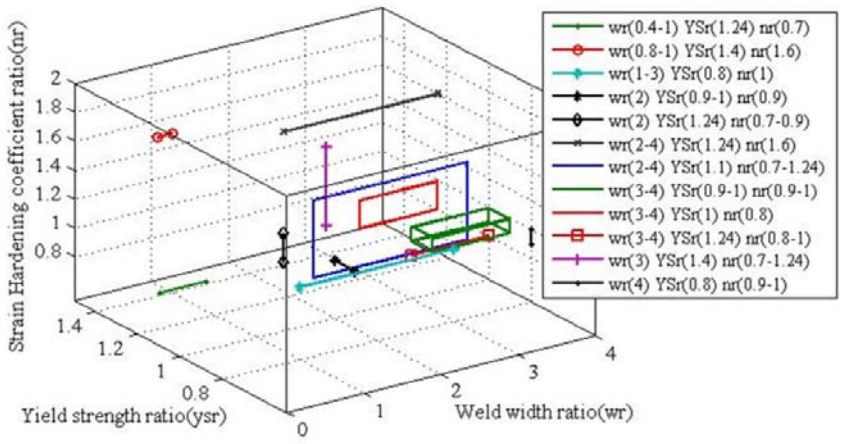

Fig. 3.8 Domains of weld conditions for representing the single zone model with maximum load at failure as criterion (longitudinal weld orientation)

Similar work is extended with stroke at failure as criterion for longitudinal weld orientation and it is found that there are multiple domains where double zone assumption is essential (Fig. 3.9). Like the earlier cases, thickness distribution were monitored and it is observed that the thickness distribution of double zone models are very different when compared to reference model, while single zone models showed almost the same behavior.

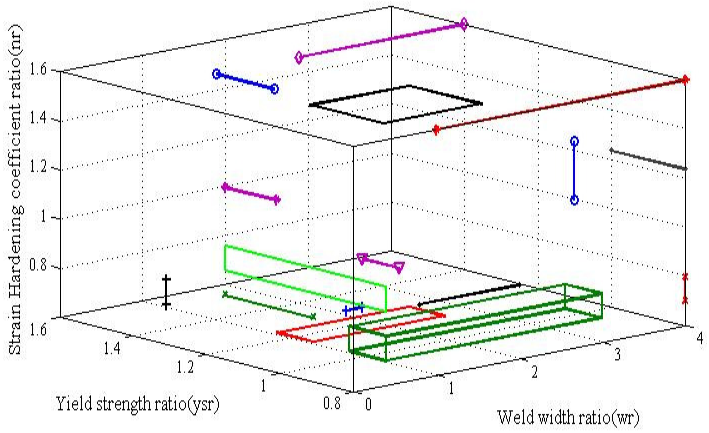

Fig. 3.9 Domains of weld conditions for representing the double zone models with punch stroke at failure as criterion (longitudinal weld orientation)

3.2.4 Comparison of similar thickness to dissimilar thickness FSW blanks in weld zone representation

In this section, the weld zone representation of FSW blanks during formability prediction as single zone or double zone models with similar and dissimilar thicknesses are compared and analyzed. The analyses of similar thickness sheets can be obtained from the previous

chapter 2. In similar thickness case, the sheet thicknesses of 1.5 mm are assumed for both the base metals and the weld region (nugget zone and HAZ). In dissimilar thickness case, a thickness of 1.1 mm for base metal 1 and 1.5 mm for base metal 2 are assumed, while weld zone has an average of 1.3 mm thickness.

In the case of transverse weld orientation, Tables 3.4 and 3.5 show the comparison of number of single zone and double zone models available for similar and dissimilar thickness FSW blanks with stroke at failure and maximum load at failure as criteria respectively. Out of 216 weld conditions, in Table 3.4, 20 weld conditions represent single zone model and 196 weld conditions represent double zone model in similar thickness case, where as in dissimilar thickness case, 35 weld conditions represent single zone model and 181 represent double zone model. Similar behavior is depicted when maximum load at failure is considered as criterion (Table 3.5). It is clear from both the Tables that the number of single zone models has increased when the FSW blanks are changed from similar to dissimilar thickness combination. The failure location is found only in weld zone in the case of similar thickness FSW blanks. In the dissimilar thickness case, some of the blanks show failure in thinner base material (1.1 mm thick) also. Whenever failure is seen in the weld region, double zone model becomes essential. When failure location is shifted to thinner (or weaker) base material, single zone model would be sufficient to have acceptable prediction of formability. Hence the number of single zone models has increased in dissimilar FSW blank cases. The increase in single zone models is independent of the output monitored, i.e., either with stroke at failure or with maximum load at failure as criteria.

In the case of longitudinal weld orientation, the number of weld conditions in single zone and double zone models with maximum load at failure and punch stroke till failure as criteria are shown in Tables 3.6 and 3.7 respectively. In similar thickness case, there are 146 weld conditions representing single zone model and 70 weld conditions represent double zone model, where as in dissimilar thickness case 54 weld conditions are in single zone model case and 162 are in double zone model case. So the number of single zone models has decreased and hence double zone models have increased when the similar thickness FSW blank is changed to dissimilar thickness. Similar behavior is seen in Table 3.7 with punch stroke till failure as criterion. This behavior is just opposite to what is seen in the case of transverse weld orientation. In the case of longitudinal weld orientation, failure is generally seen normal to the weld zone. This is independent of similar or dissimilar thickness sheet combinations. The presence of sheets with dissimilar thicknesses becomes a severe case, in which the failure initiation could be at the interface of thinner sheet and HAZ closer to the thinner sheet.

This makes the double zone modeling mandatory and the number of double zone models increases with increase in dissimilarity between the sheet thicknesses. It is expected that the number of double zone models will increase further with reduction in thinner blank thickness from 1.1 mm to say 0.9 or 0.8 mm.

Table 3.4 Comparison of punch stroke at failure as criterion in transverse weld orientation

FSW blanks	Total number of weld conditions	Weld region representation		Reference failure location
		Single zone model	Double zone model	
Similar Thickness (1.5:1.5)	216	20	196	Weld zone
Dissimilar Thickness (1.5:1.1)		35	181	Weld zone

Table 3.5 Comparison of maximum load at failure in transverse weld orientation

FSW blanks	Total number of weld conditions	Weld conditions representing		Reference failure location
		Single zone model	Double zone model	
Similar Thickness (1.5:1.5)	216	5	211	Weld zone
Dissimilar Thickness (1.5:1.1)		15	201	Weld zone

Table 3.6 Comparison of maximum load at failure in longitudinal weld orientation

FSW blanks	Total number of weld conditions	Weld conditions representing		Reference failure location
		Single zone model	Double zone model	
Similar Thickness (1.5:1.5)	216	146	70	Weld zone
Dissimilar Thickness (1.5:1.1)		54	162	Base metal 1

Table 3.7 Comparison of punch stroke till failure in longitudinal weld orientation

FSW blanks	Total number of weld conditions	Weld region representation		Reference failure location
		Single zone model	Double zone model	
Similar Thickness (1.5:1.5)	216	161	55	Weld zone
Dissimilar Thickness (1.5:1.1)		139	77	Base metal 1

From the comparison of similar and dissimilar thickness FSW blanks with different weld orientations, it is seen that the increase and decrease of number of single zone models

depends mainly on the failure location. From the simulation results, it is observed that failure locations occur in base material, HAZ and weld nugget region. If failure initiation is in base material, single zone model is sufficient and if it is in HAZ then double zone model is essential. As shown by Miles *et al.*, 2006 the failure of FSW blanks has occurred in HAZ during LDH test. In this case, double zone modeling would be essential. Further, this depends on the critical error percentage followed to identify the single and double zone models. Suppose the critical error percentage is changed from 16% (followed in the present work) to 20%, the domains of weld conditions for single and double zone models will be modified. In this case, more number of single zones will be available. Overall, FSW blanks with dissimilar thickness sheets should always be modeled with double zone, i.e., nugget zone and HAZ modeled separately. But when failure is seen in thinner material, the double zone model can be relaxed and single zone model would be sufficient for reasonably accurate prediction of formability.

3.2.5 Single zone Vs double zone weld: Forming limit strain comparison

In the previous sections, the domain of weld conditions where in double zone assumption is valid and single zone assumption is invalid were obtained for friction stir welded blanks with dissimilar thickness sheets. It is observed that there are multiple domains where in double zone assumption is valid. This exercise was performed by comparing the load-punch stroke behavior of FSW blanks modeled with single zone and double zone assumptions. Later the validity of double zone assumption was rationalized by analyzing the thickness distribution during forming. It was observed that the thickness distribution of FSW blanks which follow single zone assumption is closer to the reference case. The double zone cases showed more difference when compared to reference case.

In this section, a comparative analysis of forming limit strains is performed between the reference case and FSW blanks with single zone and double zone assumptions. The main motive behind this analysis is to demonstrate that the weld zone representation methods are important, not only in load-punch stroke behavior prediction, but also in forming limit strain prediction. For this, the forming limit strains of few weld conditions that falls under single zone assumption category and few other weld conditions that falls under double zone category are compared with reference case following single zone assumption. The forming limit strains are predicted for FSW blanks by thickness gradient based necking criterion (Nandedkar, 2000). The LDH test is simulated only in the plane-strain strain path for limit strain prediction.

It can be understood from the Fig. 3.10 and Fig. 3.11, for transverse and longitudinal weld orientations respectively, that the forming limit strains of single zone models, for which the error percentage in load-punch stroke behavior is less than 16%, are closer to reference model. The forming limit strains of double zone model are away from the reference model in which error percentage is more than 16%. This demonstrates that the FSW blank cases whose limit strains are closer to reference case can be modeled with single zone assumption, while it is mandatory to follow double zone model if it is far away from the reference case. The limit strain values will not be accurate if double zone models are assumed as single zone models.

The limit strain comparison performed in plane-strain condition can be extended for the whole forming limit curve (FLC) of FSW blanks. The incorrect assumption of single zone model in place of double zone model will yield incorrect (or inaccurate) FLC, and the incorrect assumption of double zone model will result in evaluating the HAZ properties separately. The domain of weld conditions in which double zone modeling is mandatory, is independent of the forming behavior that is monitored. Similar results are seen while predicting load-punch stroke behavior, thickness distribution, and forming limit strain. From the experimental observation of Miles *et al.*, 2005 during the forming of dissimilar FSW blanks, it is seen that failure occurs in HAZ region, for which double zone model becomes mandatory. If HAZ is not modeled separately, then limit strains may show variation and formability prediction may not be accurate. Finally it is better that FSW blanks with dissimilar thickness sheets be modeled with double zones, i.e., nugget zone and HAZ modeled separately for more accurate formability prediction, but not always. There exists a compromise between accuracy and practical limitations during formability prediction of FSW blanks.

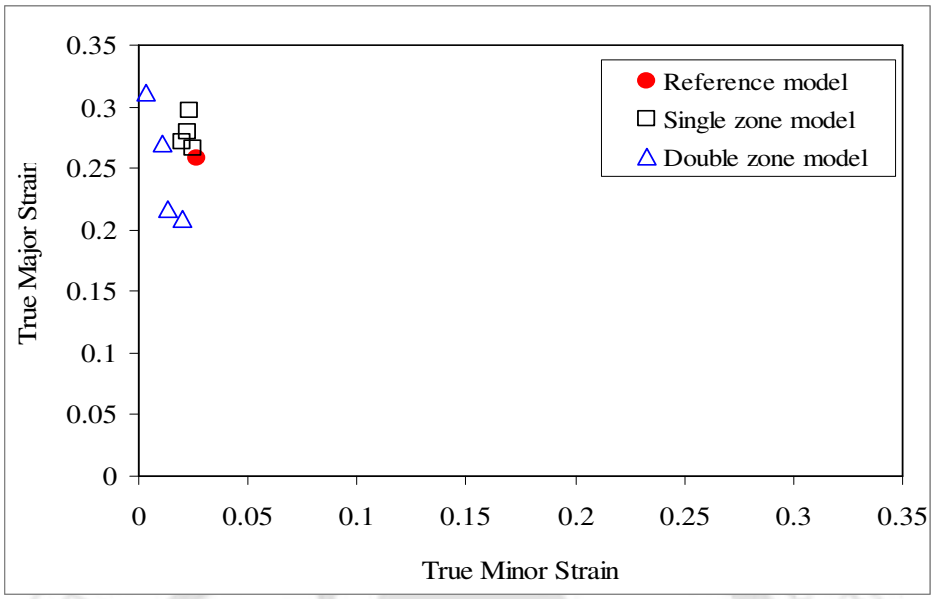

Fig. 3.10 Forming limit strains of dissimilar FSW blank with transverse weld

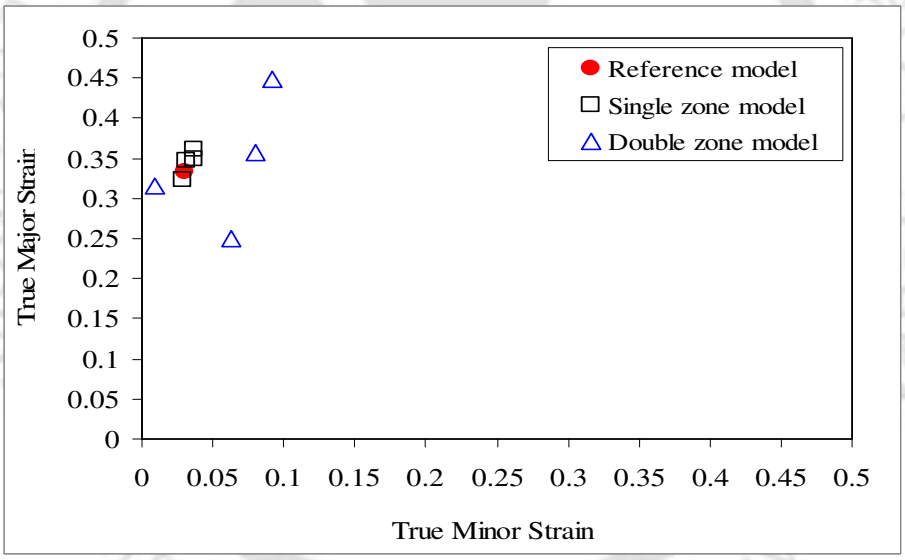

Fig. 3.11 Forming limit strains of dissimilar FSW blank with longitudinal weld

3.2.6 Guidelines to represent weld zone during the stretching simulation of FSW blanks

In FSW blanks, single zone or double zone model decides the accuracy with which formability can be predicted. The weld zone properties (n, σ_{YS}, widths of HAZ and WN), weld orientation (transverse, longitudinal or any other angle), weld location (center or at some offset) affect the weld zone representation in a compounding fashion. In the case of weld orientation, for FSW blanks with similar thickness sheets, the double zone models are

more in transverse weld, while single zone models are more in longitudinal welds. Just by introducing thickness heterogeneity in TWB, i.e., for FSW blanks with dissimilar thickness sheets, it is seen that the number of single zone models had increased in transverse weld orientation, and number of double zone models had increased in longitudinal weld orientation. This suggests the importance of thickness heterogeneity in the weld zone representation methods during the forming simulation of FSW blanks. In the present work, only transverse and longitudinal weld orientations are simulated for FSW blanks formability prediction. Any other weld orientation (say 45°) will behave in a mixed pattern (combining both 0° and 90° welds) and one would select the double zone model for formability prediction for better accuracy.

When placed at critical locations (or offset locations), formability is found to decrease significantly. In the case of industrial sheet parts, weld can be at any location and orientation depending on the part requirement. Generally weld is placed at safe region of the sheet part. It would be sufficient to follow single zone model since the individual sheet parts are large. Above all, the forming test performed, forming behavior monitored, thickness and strength heterogeneity of sheet materials and range fixed for selecting single or double zone welds affect the weld zone representation in a compounding manner.

In the present work, the two different methods of representing the weld zone in FSW blanks are analyzed by giving importance to the accuracy of formability prediction. There are other equally important issues like determining the mechanical properties of weld zone, CPU time, simplicity of preparing the models etc. that can be compared between the single and double zone model assumptions. In the case of double zone models, it is difficult to evaluate the mechanical properties of nugget and HAZ separately. But it is relatively easy to evaluate the global mechanical properties of weld zone in the case of single zone models with the existing methods. Hence single zone modeling is commonly seen in literature.

When CPU time is considered, it is observed from the simulations of the present work that both the models take almost same time for simulation in case of similar and dissimilar gage FSW blanks. Moreover, it is time consuming, but not difficult to make double zone models in any FE code and CAD package as compared to single zone models. From these three comparisons, it can be said that single zone model is always convenient than double zone model during FSW blank forming prediction, but this is not always acceptable when forming prediction accuracy is concerned.

3.3 Conclusions

The following are the conclusions made from the present work.

- The implementation of weld zone properties as single zone or double zone significantly affects the formability prediction of friction stir welded blanks. The double zone model is valid in multiple domains and single zone model is found to be valid outside these domains. Some specific domains for double zone modeling are obtained for a representative base material with dissimilar (1.1:1.5 mm) thicknesses by considering punch stroke at failure and maximum load at failure as criteria.

- Whenever the thickness distribution of FSW blank with double zone model is closer to reference case, the error percentage is less than 16% and single zone model is sufficient in this case. When the thickness distribution is very different compared to the reference case, the error percentage is more than 16% and double zone model should be followed in this case.

- The number of single zone models has increased in transverse weld orientation and number of double zone models has increased in longitudinal weld orientation in the case of FSW blank with dissimilar thicknesses as compared to similar thickness FSW blanks. This is due to the change in failure location during forming of FSW blanks.

- The weld zone representation methods affect the accuracy of forming limit prediction significantly. The forming limit strains are compared between the single zone and double zone representation methods with reference FSW blank case. The limit strains in the single zone model category are closer to reference FSW blank, while large difference is seen in the case of double zone model category.

- The domain of weld conditions in which double zone modeling is mandatory, is independent of the forming behavior that is monitored. Similar results are seen in predicting load-punch stroke behavior, thickness distribution, and forming limit strain.

Chapter 4

Internal defect and process parameter analysis during friction stir welding of Al 6061 sheets

4.1 Experimental Methodology

The base material in the present investigation is AA 6061-T651 alloy with 2.1 mm thickness. The nominal chemical composition of the base material is given in Table 4.1.

Table 4.1 Chemical composition of base material (AA 6061-T651) in wt. %

Si	Fe	Cu	Mn	Mg	Cr	Zn	Ti	Al
0.65	0.3	0.27	0.02	1.0	0.17	0.04	0.02	Remaining

The base metal was laser cut in different rolling directions like 0°, 15°, 30°, 45°, 60°, 75°, 90° and the mechanical properties and plastic strain ratio (R) were evaluated through tensile tests as per ASTM-B557M and ASTM-E517 standards. The schematic of samples used for evaluating mechanical properties and plastic strain ratio are shown in Fig. 4.1 and Fig. 4.2 respectively. Tensile tests were performed at a nominal cross-head speed of 1 mm/min, at room temperature on an INSTRON 8801 tensile testing machine and repeated twice for each set to check the reproducibility. Failure from grip or slippage during testing was not observed. The mechanical properties of FSW sheets like yield strength, ultimate tensile strength, total elongation, uniform elongation, strain hardening coefficient (n) and strength coefficient (K) were evaluated as per the standard procedure after testing the samples till failure. The load-stroke behavior obtained during testing was converted into engineering stress - strain and true stress - strain plot for evaluating the mechanical properties. The plastic strain ratios at different rolling directions were obtained after testing the base material to 10% plastic strain. Table 4.2 summarizes the mechanical properties of AA 6061 base material obtained in the present work.

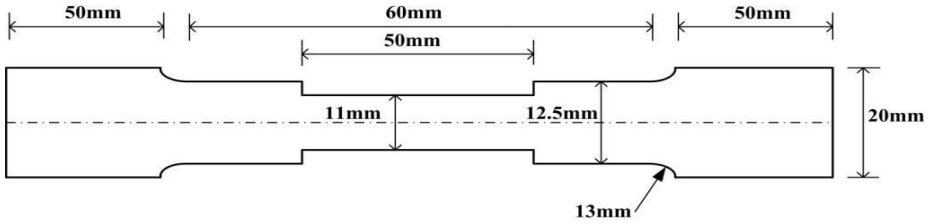

Fig. 4.1 Tensile test specimen dimensions as per ASTM-B557 M

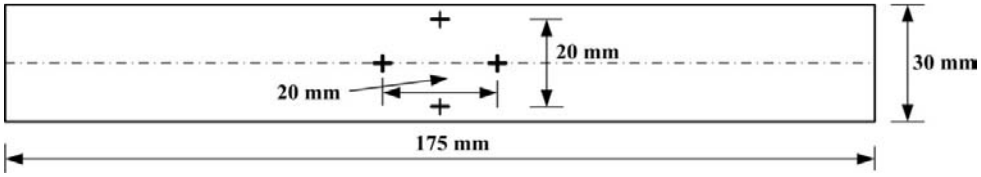

Fig. 4.2 Sheared rectangular tension test specimen, parallel strip as per ASTM-E517

Table 4.2 Tensile properties of base metal (AA 6061- T651)

Rolling direction→ Mechanical properties↓	0°	15°	30°	45°	60°	75°	90°
YS (MPa)	265±5	272±7	265±4	264±15	266±12	279±8	257±17
UTS (MPa)	300±8	309±6	300±4	297±14	300±9	333±7	292±9
UE (%)	8.9	8.6	9.1	8.8	8.5	8.9	9.6
TE (%)	11.2	11.5	11.5	11.6	11.3	11.5	11.9
K (MPa)	427±30	421±15	410±7	406±17	411±10	424±10	426±15
n	0.101	0.094	0.095	0.094	0.095	0.096	0.12
R	0.79	0.74	0.78	0.95	0.84	0.93	0.85

YS: yield strength; UTS: ultimate tensile strength; UE: uniform elongation; TE: total elongation; K: strength coefficient; n: strain hardening coefficient; R: plastic strain ratio

The friction stir welding was carried out on a machine designed and developed by the Indian Institute of Science, Bangalore and ETA Technologies, Bangalore. The machine had a unique capability in that the plunge depth, rotational speed, or weld speed could be varied within a test. In the present work, only one parameter is changed by keeping other parameters constant in each experiment. The process parameters varied were tool rotational speed, welding speed, plunge depth and shoulder diameter, while the tool tilt angle (2.5°) was kept constant throughout the process. Three types of tools with flat shoulder having different diameters and pin with equal probe lengths were used for all the welding trials. These three tools were made of hot die steel (HDS) with shoulder diameter 12, 15 and 18 mm, pin of frustum shape with base diameter 6 mm, top diameter 4 mm and length 1.7 mm as shown schematically in Fig. 4.3. The base material sheets were clamped rigidly over the vertical bed from four sides to avoid vibration or displacement during processing. The welding trials were done under varied plunge depths, welding speeds and tool rotation speeds within a specified range by three tools having different shoulder diameters as listed in Table 4.3. The parameter range was fixed based on the available ranges in the literature and from earlier experience such that it gives both the defect free and defective welds. In a single trial, either plunge depth or welding speed or tool rotation speed was changed for same shoulder diameter which is shown in Fig. 4.4. The same has been followed for other two parameter variation also.

For example, in trial I FSW tool with 18 mm shoulder diameter was used as listed in Table 4.3. All the parameters were selected such that both defective and defect free welds are generated and with prior experience. Parameters were varied linearly during welding, due to this linearity some of the parameters were selected in a specified distances and transverse section has been taken for internal defect characterization. The specimens for metallographic examination were sectioned to the required sizes from the joint comprising of FSW zone, and base metal regions and polished using different grades of emery sheets (200-1200 grades). Final polishing has been done using the diamond compound (1µm particle size) in the disc polishing machine. Specimens were etched with 1:20 of hydro fluoric (HF) acid and distilled water mixture. Specimens were examined in stereo microscope and all the macrostructures were captured at different process parameters. From these macrostructures, FSW joints were observed for the presence of defects. During each trial, the axial force and torque were also monitored directly from the machine.

Table 4.3 Process parameters for fabricating FSW joints before optimization

Trial	**Parameters**									
	Pin length (mm)	Shoulder diameter (mm)	Plunge depth (mm)		Tool rotational speed (rpm)				Welding speed (mm/min)	
			min	max	min		max		min	max
I	1.7	18	**1.5**	**1.9**	1100				90	
			1.9		**800**		**1600**			
					1350				**50**	**100**
II		15	**1.7**	**2.0**	1100				90	
			1.9		**1200**		**1500**			
					1350				**90**	**130**
III		12	**1.75**	**2.0**	1300				90	
			2		**1300**		**1600**		120	
			1.9		1300				**90**	**130**

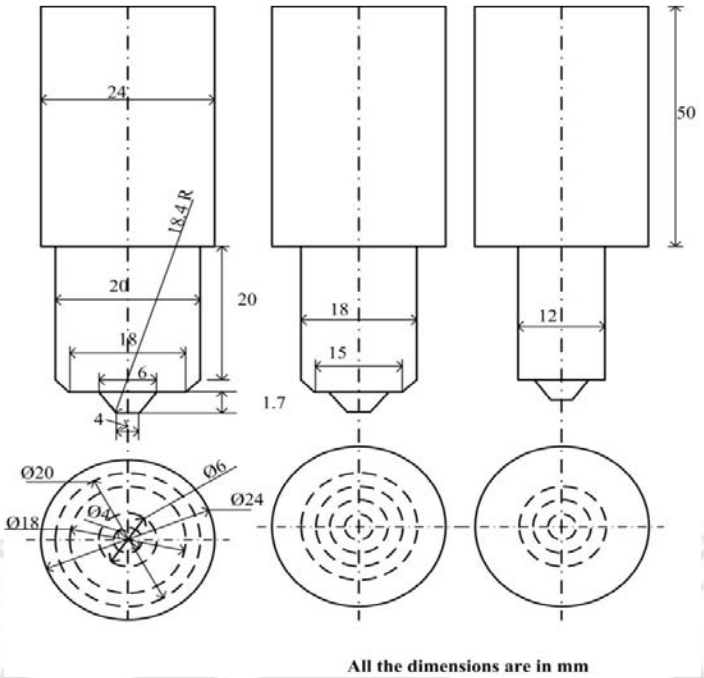

Fig. 4.3 Schematic representation of tools used for FSW

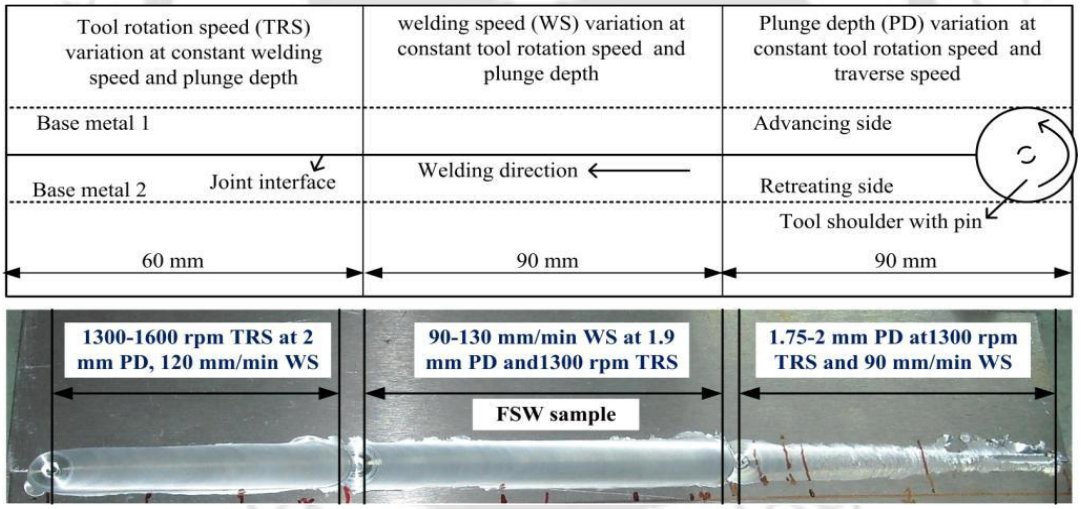

Fig. 4.4 Top: Representation of process parameters variation during FSW in a single trial; **Bottom:** FSW sample with varying welding parameters for 12 mm shoulder diameter

4.2 Results and Discussion

4.2.1 Effect of FSW process parameters on the formation FS welds

The effect of tool dimensions (like shoulder diameter) and welding parameters (welding speed, tool rotation speed and plunge depth) on the joint quality is observed through defect analysis with an aim of fabricating defect free joints. In general, friction stir welded joints are

known to be free from defects like porosity, slag inclusion, solidification cracks etc. that are generated in fusion welding of aluminum alloys and these defects disintegrate the weld quality and joint properties (Fujii *et al.*, 2006). Since FSW is solid state process, the base metals are joined in solid state due to the heat generated by the friction and flow of metal by the stirring action. But FSW joints are prone to other defects like pin hole, tunnel defect, piping defect, kissing bond, cracks etc. due to improper plastic flow and insufficient consolidation of metal in the FS process region (Rhodes *et al.*, 1997). The internal defects in FS joints are observed through macrostructures at different parameter combinations. The macrostructure of the joints and parameters used are presented in Tables 4.4–4.6.

Table 4.4 Macrostructures (with 10 x magnification) of weld region at different plunge depths

PD (mm)	Parameters	Macrostructures of FSW joint	Observation
1.6	TRS:1100 rpm; WS: 90 mm/min; SD: 18 mm	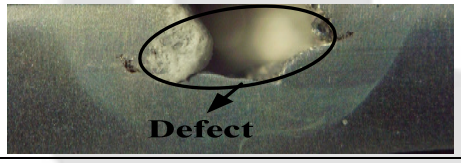	Defect due to less tool plunge, insufficient heat generation, and plastic deformation. Defect type is void.
1.8	TRS:1100 rpm; WS:90mm/min; SD: 18 mm		Defect due to insufficient tool plunge, heat generation, and plastic deformation; Defect size is reduced; Defect type is void.
1.9	TRS: 1100 rpm; WS:90 mm/min; SD:18 mm		Defect due to insufficient tool plunge, heat generation, and plastic deformation; Defect size is less; Defect type is void.
1.85	TRS:1300 rpm; WS:90 mm/min; SD: 15 mm		No defect
1.9	TRS:1300 rpm; WS:90 mm/min; SD: 12 mm	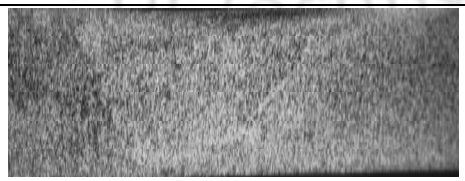	No defect

PD: plunge depth; TRS: tool rotation speed; WS: welding speed; SD: shoulder diameter

Table 4.5 Macrostructures (with 10 x magnification) of weld region at different welding speeds

WS (mm/min)	Parameters	Macrostructures of FSW joint	Observation
60	TRS:1350 rpm; PD:1.9 mm; SD:18 mm	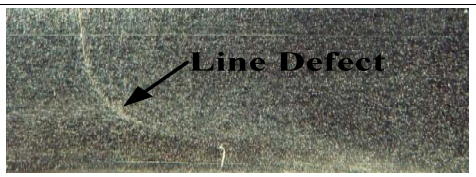	Line defect formed at the transition zone
80	TRS:1350 rpm; PD:1.9 mm; SD:18 mm		No defect
100	TRS:1350 rpm; PD:1.9 mm; SD:18 mm		No defect
120	TRS:1350 rpm; PD:1.9 mm; SD:18 mm		No defect

PD: plunge depth; TRS: tool rotation speed; WS: welding speed; SD: shoulder diameter

Table 4.6 Macrostructures (with 10x magnification) of weld region at different tool rotation speeds

TRS (rpm)	Parameters	Weld zone macrostructures	Observation
900	WS:90 mm/min; PD: 1.9 mm; SD: 18 mm;	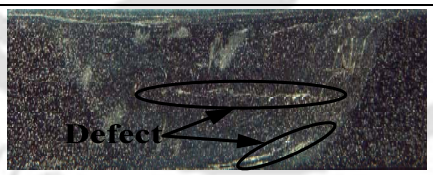	Cracks are found in the stirring zone duo incomplete plastic flow of material because of inadequate heat input at lower speeds.
1200	WS:90 mm/min; PD:1.9 mm; SD:18 mm	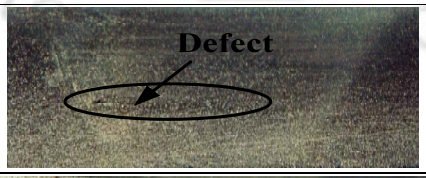	Small hole in stirred zone due inadequate heat input
1300	WS:90 mm/min; PD: 1.9 mm; SD: 18 mm		No defect

1400	WS:90 mm/min; PD: 1.9 mm; SD: 18 mm		No defect
1300	WS:90 mm/min; PD: 1.9 mm SD: 15 mm	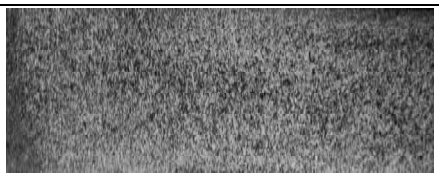	No defect
1500	WS:90 mm/min; PD: 1.9 mm; SD: 15 mm	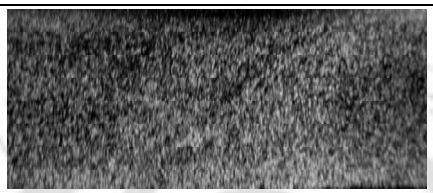	No defect

PD: plunge depth; TRS: tool rotation speed; WS: welding speed; SD: shoulder diameter

Formation of defects at different plunge depths is shown in the Table 4. When the macrostructures are compared, defect size is more at 1.6 mm plunge depth and less at 1.9 mm plunge depth with a tool of 15 mm shoulder diameter, tool rotation speed of 1100 rpm and welding speed of 90 mm/min. So with increase in plunge depth, the defect size decreases, but the defect is not vanished. But by increasing the rotation speed to 1300 rpm, defects are not formed; eventhough the plunge depth and shoulder diameter are reduced.

Similar exercise has been carried out for different welding speeds (Table 4.5) and rotation speeds (Table 4.6) in combination with other three parameters for generating defect free FS welds. In a nutshell, by varying different FSW parameters, the force and torque required for generating defect free FS welds are attained and hence proper stirring action and material plastic deformation occurs during welding. The formation of defects is mainly because of improper combination of welding parameters resulting in insufficient stirring action and plastic deformation.

4.2.2 Effect of FSW parameters on axial force and torque during welding

The defective weld and defect free weld formation can also be observed through the axial forces (forces in Z-direction) and their corresponding torque with respect to the four FSW parameters. The axial force is monitored through a load sensor and torque by the current and voltage from the servo motor. Figure 4.5 to 4.8 shows the influence of varied FSW parameters on the variation of axial force and torque. The formation of the defective welds can also be related to this. It has been found from Fig. 4.5 that with increase in tool rotation

speed, the axial force and torque decreases. The data given in this Figure is for constant welding speed (90 mm/min), shoulder diameter (18 mm) and plunge depth (1.9 mm). It is observed in the present work, for the base material chosen, the defective welds are formed below a tool rotation speed of 1300 rpm, above which defect free welds are formed. The axial force and torque requirement is substantial during welding and hence defect free welds are formed beyond a critical limit. The decrease in axial force and torque with increase in rotational speed is because of the heat input during welding. With increase in heat input, contact area below the shoulder area or stir zone becomes softer resulting in reduced strength in this region. The axial force and torque requirements will not be large if the strength of the stir zone is less. For good quality welds without internal defects, higher tool rotation speed yielding lesser axial force and torque is recommended.

In the same way, effect of variation in welding speeds (60 to 120 mm/min) using a FSW tool of 18 mm shoulder diameter and 1.9 mm plunge depth at 1350 rpm rotation speed on the weld formation is evaluated through axial force and torque as shown in Fig. 4.6. The defective welds are observed upto a welding speed of 80 mm/min. It is observed that an opposite effect is seen while increasing the welding speed as compared to tool rotation speeds. By increasing the welding speed, the axial force and torque are increased. Till a critical welding speed (80 mm/min) is reached, the axial force and torque requirements are insufficient to form a defect free weld. Once sufficient axial force and torque are reached, defect free welds are generated. This suggests for defect free welds, higher welding speeds generating higher axial forces and torques are recommended. With increase in welding speed, heat input decreases resulting in higher strength at stir zone. For a stronger stir zone, the axial force and torque requirements are large leading to increase in the magnitudes.

In addition to this, in the present work, effect of pin plunge depth and shoulder diameter is also analyzed on the axial force, torque and defect formation. The axial forces and torque variations are plotted in Fig. 4.7 for variable pin plunge depths from 1.6 to1.9 mm by using a tool of 18 mm shoulder diameter, at 1100 rpm tool rotation speed and 90 mm/min welding speed. It is observed that axial force at a plunge depth of 1.6 mm is lesser, whereas at 1.9 mm plunge depth, it is higher. It means with increase in plunge depth the axial force increases. But torque has not shown much variation with pin plunge depth. It remains constant for all plunge depths considered and welds obtained with these parameter combinations are defective. With increase in plunge depth, the reaction force given by the material to the tool will be higher resulting in increased axial force. As a consequence, axial force and torque are monitored at tool rotation speed of 1300 rpm, welding speed of 90 mm/min with plunge

depth variation of 1.85-1.95 mm. It is found that all the welds are defect free and axial load and torque are almost constant as shown in Fig. 4.8. Similar observations are also seen with other two tool shoulder diameters (12 and 15 mm). Finally the effect of shoulder diameter on axial force and toque is shown in the Fig. 4.9. The effect of these three FSW tool shoulder (12, 15, 18 mm) diameters is analyzed at fixed tool rotation speed of 1300 rpm, welding speed of 90 mm/min and plunge depth of 1.9 mm. In this condition, defect free welds are formed for all three shoulder diameter. The observation made is that when tool shoulder diameter is increased, higher axial force and torque values are observed because of the higher reaction force given by the material to the tool and higher friction existing at the interface.

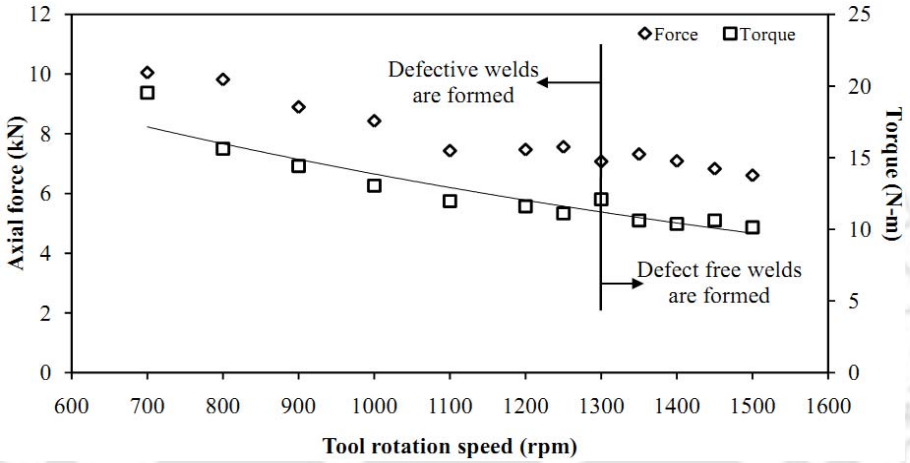

Fig. 4.5 Variations in force and torque at variable tool rotation speed (700-1500 rpm) by using FSW tool of 18 mm shoulder diameter, 1.9 mm plunge depth and 90 mm/min welding speed. Error variation in Force and torque is ±1 kN and ±0.5 Nm

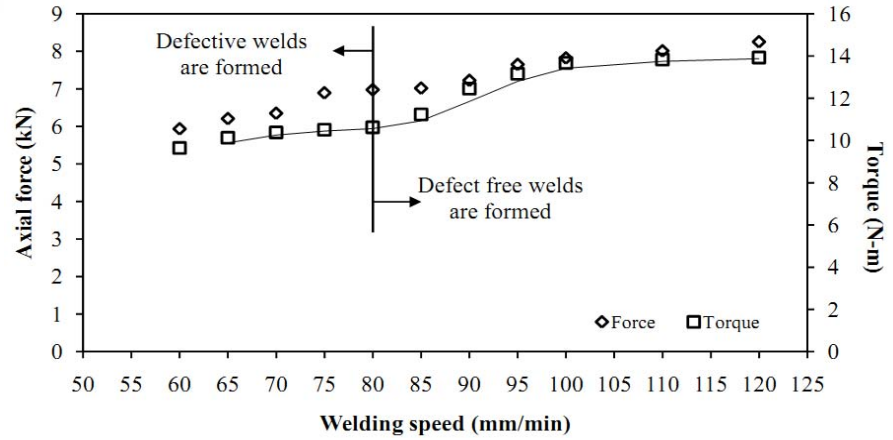

Fig. 4.6 Variations in force and torque at variable welding speed (60-120 mm/min) by using FSW tool of 18 mm shoulder diameter, 1.9 mm plunge depth and 1350 rpm tool rotation speed. Error variation in Force and torque is ±1 kN and ±0.5 Nm

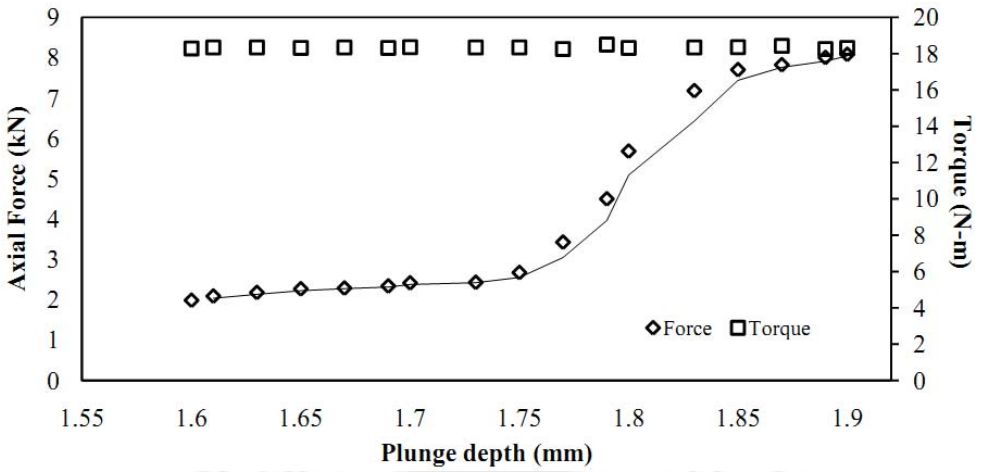

Fig. 4.7 Variations in force and torque at variable plunge depth (1.6-1.9 mm) by using FSW tool of 18 mm shoulder diameter, at 1100 rpm tool rotation speed and 90 mm/min welding speed; *Defective welds are formed*. Error variation in Force and torque is ±1 kN and ±1 Nm

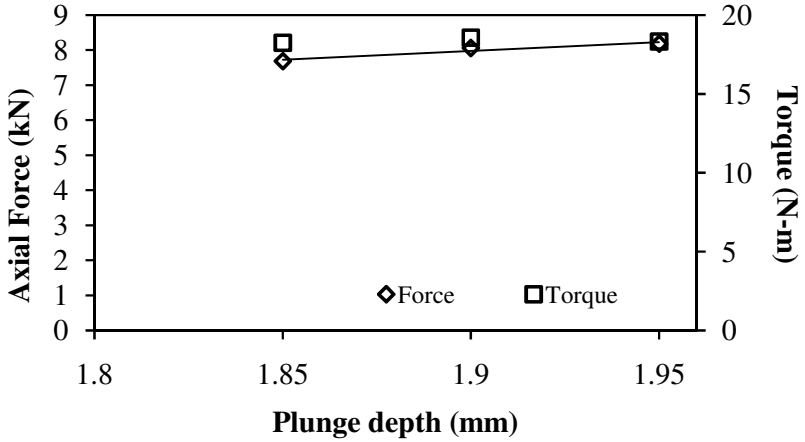

Fig. 4.8 Variations in force and torque at variable plunge depth (1.85-1.95 mm) by using FSW tool of 18 mm shoulder diameter, at 1300 rpm tool rotation speed and 90 mm/min welding speed; *Defect free welds are formed*. Error variation in force and torque is ±1 kN and ±1 Nm

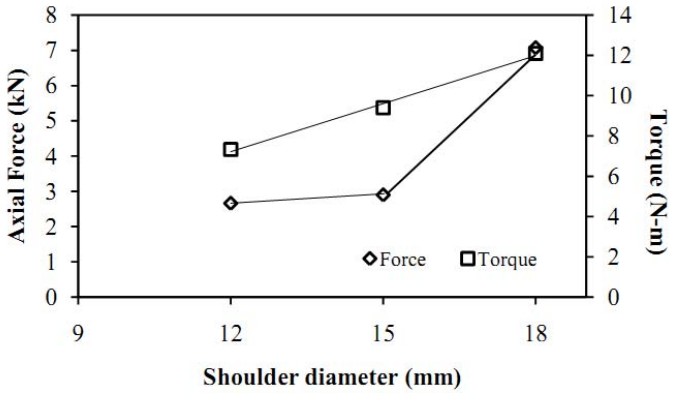

Fig. 4.9 Variations in force and torque of different FSW tool shoulder diameters (12, 15, 18 mm) at 1300 rpm tool rotation speed and 90 mm/min welding speed and 1.9 mm plunge depth. Error variation in force and torque is ±1 kN and ±1 Nm

Some of the results are consistent with results in literature. Ulysse, 2002 developed a model for the FSW process using three-dimensional visco-plastic modeling for butt joints made of aluminum plates and studied the effect of tool speed on temperature distribution and forces acting on the tool for various welding and rotational speeds. It is found that pin forces increase with increasing welding speeds, but the opposite effect is observed for increasing rotational speeds. Peel *et al.*, 2006 studied to produce good quality welds for the friction stir welding of AA5083 to AA6082 at three different tool rotation speeds and welding speeds. They observed and compared the downward force; torque and power are at higher welding speed and lower rotational speed and vice versa. Cavaliere *et al.*, 2008 evaluated the welding speed effect on mechanical and microstructural behavior of AA6082 welded plates with thickness 4 mm. In addition they also observed from the experimental results that force in Z-direction with increasing welding speeds (40 to 460 mm/min) at fixed rotational speed of 1600 rpm is increasing. Cui *et al.*, 2010 studied on FSW of aluminum alloy over a wide range of rotational speed and welding speed and measured the torque. It is found that an exponential decay model would be appropriate to describe the variation of torque with rotational speed and a linear fit for torque variation with respect to welding speed. Similar observation is seen in the present work also (see Fig. 4.5 and Fig. 4.6). But it is found from the present work that the torque variation with respect to welding speed is not purely linear. Upadhyay and Reynolds, 2010 studied the effects of thermal boundary conditions in friction stir welded AA7050-T7 sheets and observed that the torque decreases with increasing tool rotation speed.

From the analysis, two different domains of FSW parameters are defined as shown in Fig. 4.10 for the formation of defective or defect free welds. In order to have defect free welds, the welding should be performed at rotation speed: 1300-1500 rpm, welding speed: 80-120 mm/min, plunge depth: 1.85-2 mm for three different shoulder diameters (12, 15, 18 mm).
From the results, the effect of plunge depth, shoulder diameter of tool, welding speed and tool rotation speed play a vital role to fabricate defect free FSW joints. The function of the non-consumable rotating tool pin is to stir the plasticized metal and move the same behind it. For this material flow should be proper which depends on the welding speed and tool rotation speed. They provide sufficient axial force, torque and heat resulting in defect free welds. The tool shoulder diameter also affects the heat generated due to friction between the tool and sheet surface. The defects seen in FSW joints are due to lesser plunge depth, lesser shoulder contact area, slower welding speed, and low tool rotation speed. From the macrostructures, axial force and torque analysis, the optimum range of welding parameters required for defect

free welds are obtained as shown in Table 4.7 for defect free joints of AA 6061-T651 sheet material. It is also observed that the axial force and torque variation saturates after defect free welds are formed as shown in Fig. 4.5-4.8. The axial force and torque saturates once a tool rotation speed of 1300 rpm, welding speed of 95 mm/min and plunge depth of 1.85 mm is reached. Before this critical limit, a large variation in force and torque are witnessed. In fact this is very clear from Fig. 4.8 where the axial force is almost a constant in the defect free region with respect to plunge depth varying from 1.85 to 1.95 mm.

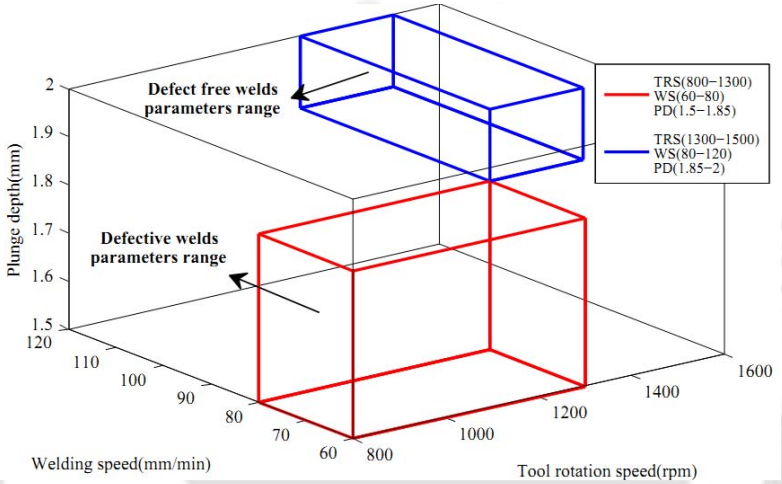

Fig. 4.10 Domains of FSW parameters representing defective and defect free weld parameters

Table 4.7 Selected optimum range of process parameters for FSW of AA 6061 sheets with 2.1 mm thickness (defect free weld formation range)

Shoulder diameter (mm)	Plunge depth (mm)	Rotation speed (rpm)	Welding speed (mm/min)
12, 15, 18	1.85-2.0	1300-1500	80-120

4.2.3 Condition for defect free weld formation in FSW

In order to analyze the influence of rotational speed, welding speed and plunge depth on the axial force and torque during the formation of defect free welds, two trials have been carried out in the optimized range with 12 and 18 mm shoulder diameter tools by varying tool rotation speed within 1300-1800 rpm at 90 mm/min welding speed and 1.9 mm plunge depth; 80-150 mm/min welding speed at tool rotation speed of 1300 rpm and 1.9 mm plunge depth; plunge depth 1.85-2 mm at tool rotation speed of 1300 rpm and 90 mm/min welding speed. At different position of rotational speeds and welding speeds, axial force and torque are noted and plotted for both the shoulder diameters as shown in Fig. 4.11 and Fig. 4.12. It is understood from Fig. 4.11 that by increasing the tool rotation speed at constant welding speed and plunge depth, the change in the axial force and torque is relatively less and it is almost a

constant. This is just opposite to the change in the axial force and torque presented in Fig. 4.5. Similar observations are seen with welding speed and plunge depth where defect free welds are formed by comparing Fig.4.6 with Fig. 4.12 and Fig. 4.7 with Fig. 4.13. Lesser variation in axial force and torque are observed in Fig. 4.12 and Fig. 4.13, while large variation is observed in the defective weld cases shown in Fig. 4.6 and Fig. 4.7.

From Fig. 4.5-4.8 and Fig. 4.11-4.13, it is observed that the change in the axial force (∂F) and torque ($\partial \tau$) with respect to these three parameters (∂p) is high in defective FS welds and less in defect free FS welds. Therefore a simple criterion for identifying the defect free weld region during FSW is given by,

$$\left(\frac{\partial \tau}{\partial p}\right)_{defective} > \left(\frac{\partial \tau}{\partial p}\right)_{defect\ free}$$
$$and \qquad (4.1)$$
$$\left(\frac{\partial F}{\partial p}\right)_{defective} > \left(\frac{\partial F}{\partial p}\right)_{defect\ free}$$

Where ∂p is change in welding speed or tool rotation speed or plunge depth.

If the material volume available below the tool is less, which is the case in defective welds, the axial force, torque will increase or decrease till it reaches an optimum parametric condition which gives defect free weld. Once the defect free weld is attained, the material volume present below the tool will be a constant, and hence the axial force, torque values will be maintained at a constant level relatively.

The criterion proposed should be independent of the materials that are fabricated by FSW process. This can be used as initial index to identify the onset of defect free weld region. Later metallographic analysis can be performed within a small range of welding parameters as part of characterization. The axial force variation during actual welding trial is shown Fig. 4.14 and Fig. 4.15, in which Fig. 4.14 is for defective weld with rotational speed starting at 700 rpm and ending at 1300 rpm and Fig. 4.15 is for defect free weld with rotational speed starting at 1300 rpm and ending at 1800 rpm. The data shown is directly obtained from the FSW machine. More variation in the force and torque is observed in the case of defective weld, whereas with rotational speed varying from 1300 rpm to 1800 rpm, force and torque are relatively uniform, and in this range defect free welds are formed.

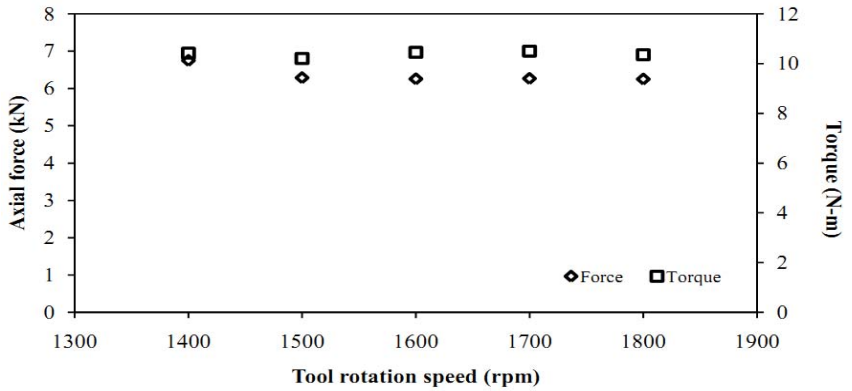

(a) 18 mm shoulder diameter. Error variation in force and torque is ±1.5 kN and ±0.2 Nm

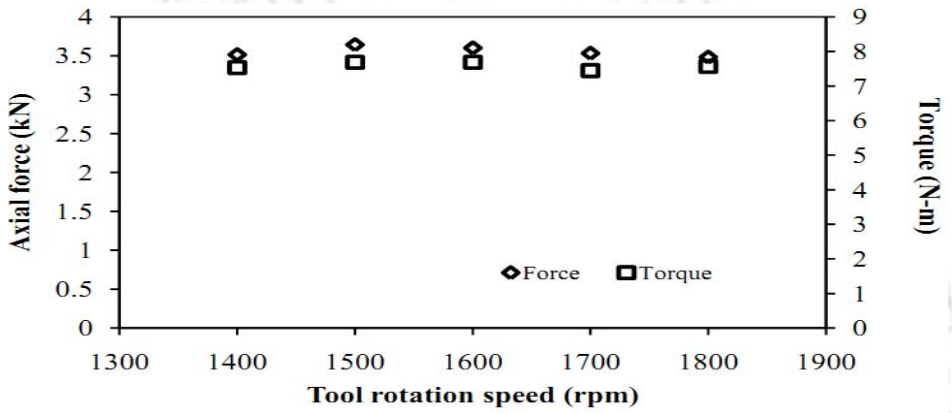

(b) 12 mm shoulder diameter. Error variation in force and torque is ±1 kN and ±0.5 Nm

Fig. 4.11 Variations in force and torque generating defect free welds at rotational speed of 1400-1800 rpm, welding speed 90 mm/min and plunge depth of 1.9 mm

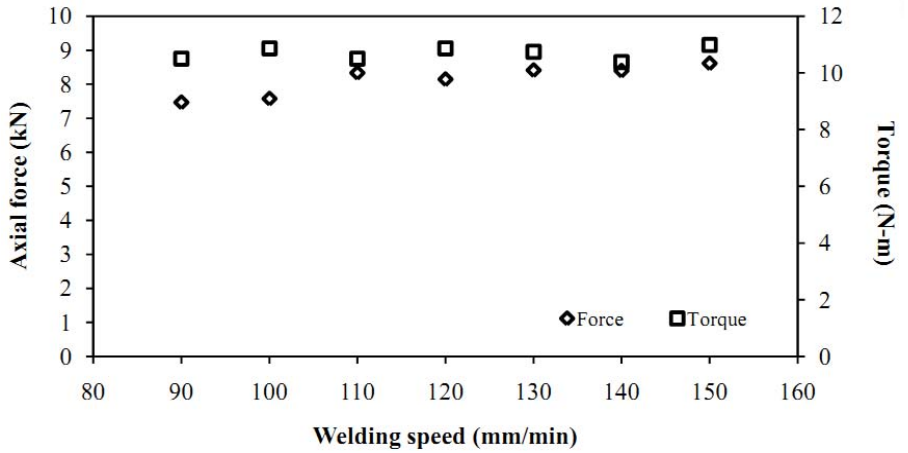

(a) 18 mm shoulder diameter. Error variation in force and torque is ±0.2 kN and ±0.2 Nm

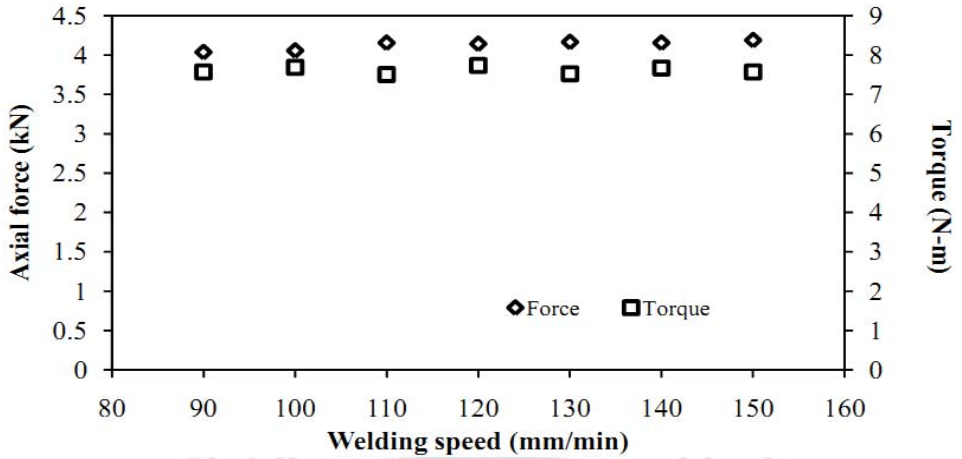

(b) 12 mm shoulder diameter. Error variation in force and torque is ±1 kN and ±0.5 Nm

Fig. 4.12 Variations in force and torque generating defect free welds at welding speed of 90-150 mm/min, tool rotation speed of 1300 rpm and plunge depth of 1.9 mm

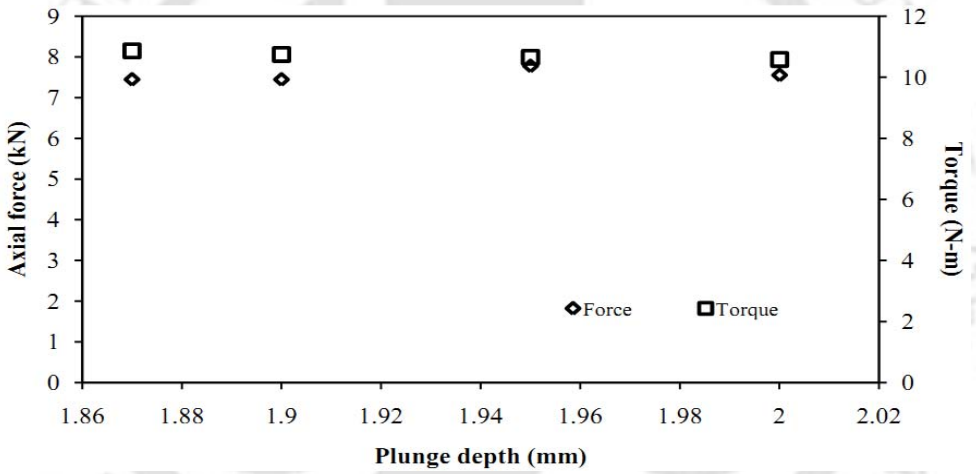

(a) 18 mm shoulder diameter. Error variation in force and torque is ±1 kN and ±0.2 Nm

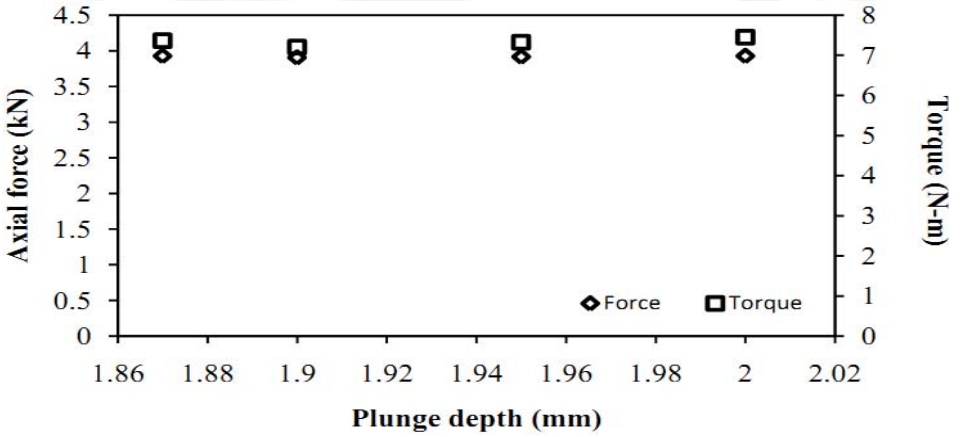

(b) 12 mm shoulder diameter. Error variation in force and torque is ±0.5 kN and ±0.5 Nm

Fig. 4.13 Force and torque variations generating defect free welds at plunge depth of 1.85-2 mm, tool rotation speed of 1300 rpm and welding speed of 90 mm/min

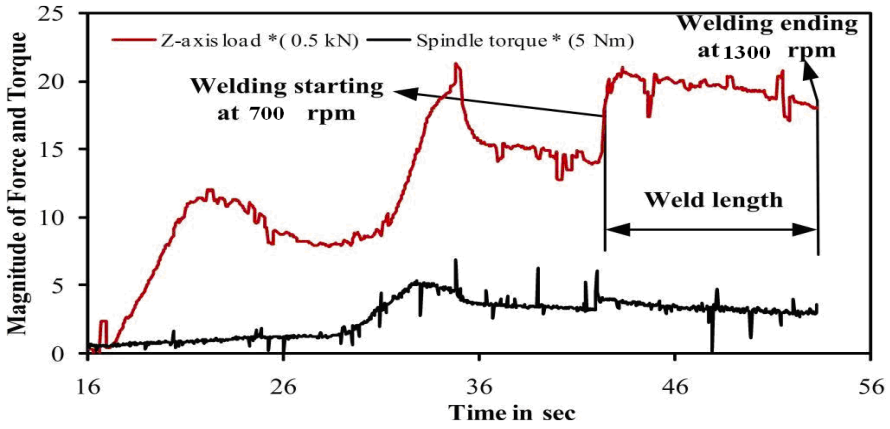

Fig. 4.14 Data obtained from machine for *defective weld*. Error variation in force and torque is ±1 kN and ±0.5 Nm

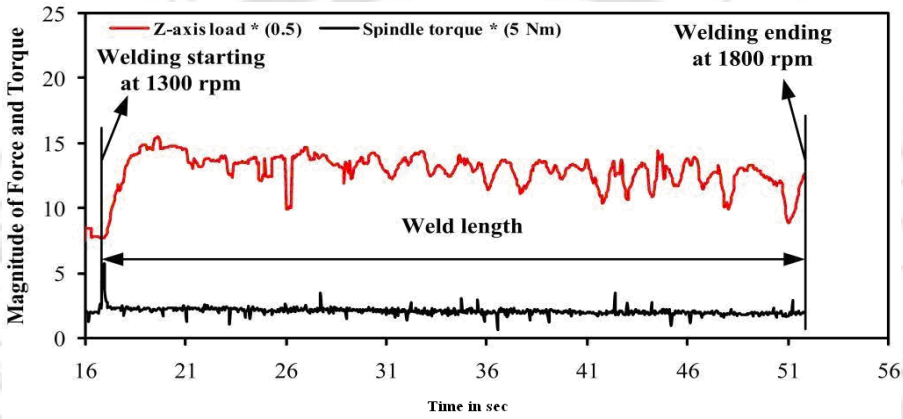

Fig. 4.15 Data obtained from machine for *defect free weld*. Error variation in Force and torque is ±1.5 kN and ±0.2 Nm

A similar observation is also seen in the case of FSW blanks with AA 5xxx as base material. Figure 4.16 shows the variations of force and torque in the defect free welds at plunge depth range of 1.85-2 mm, tool rotation speed of 1300 rpm and welding speed of 90 mm/min using two different shoulder diameters (12 and 18 mm). It is observed that variations in force and torque are almost constant. Figure 4.17 shows the variations of force and torque in the defect free welds at rotational speed of 1400-1800 rpm, plunge depth 1.9 mm and welding speed of 90 mm/min using two different shoulder diameters (12 and 18 mm). Even in this case, force and torque are almost constant. From these observations, it is likely that the proposed criterion (equation 4.1) is independent of the material. In the defect free range, axial force and torque remains constant, this can be considered as an initial index to identify the onset of defect free weld region. Figure 4.18 (a) and 4.18 (b) show the macrostructures of FSW blanks made of Al 5xxx using 12 mm and 18 mm shoulder diameters at 1.95 plunge

depth indicating the absence of defects in the weld region. Similar results are seen in case of Fig. 4.19 (a) and 4.19 (b).

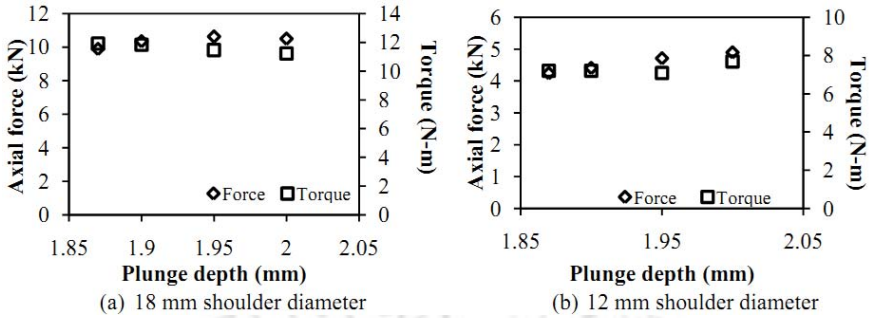

Fig. 4.16 Force and torque variations in the defect free welds at plunge depth of 1.85-2 mm, tool rotation speed of 1300 rpm and welding speed of 90 mm/min (for 5xxx base material)

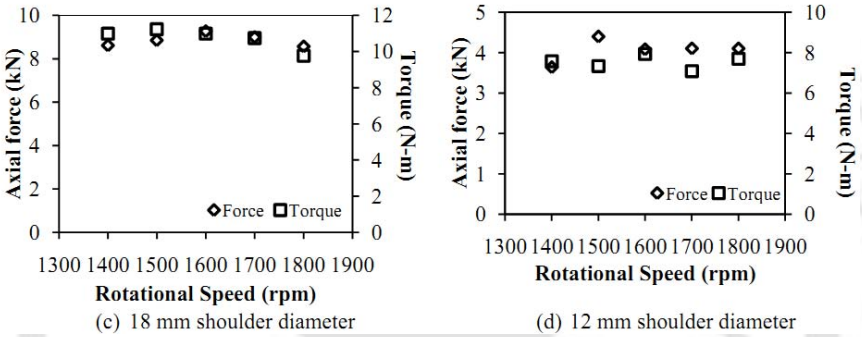

Fig. 4.17 Variations in force and torque in defect free welds at rotational speed of 1400-1800 rpm, welding speed 90 mm/min and plunge depth of 1.9 mm (for 5xxx base material)

(a) Macrostructure at 12 mm shoulder diameter and 1.95 mm plunge depth

(b) Macrostructure at 18 mm shoulder diameter and 1.95 mm plunge depth

Fig. 4.18 Macrostructure of FSW blanks made of AA 5xxx using different shoulder diameters at constant plunge depth

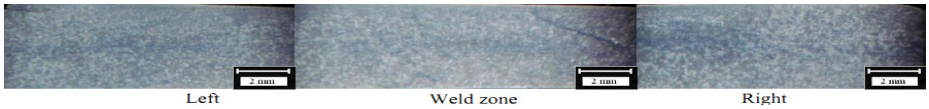

(a) Macrostructure at 12 mm shoulder diameter at 1600 rpm rotation speed

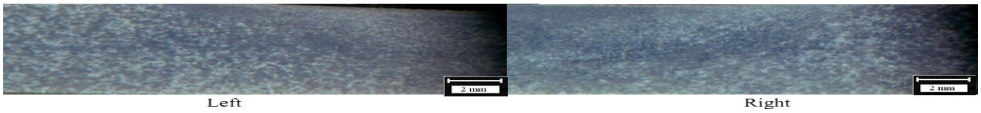

(b) Macrostructure at 18 mm shoulder speed at 1600 rpm rotation speed

Fig. 4.19 Macrostructure of FSW blanks made of AA 5xxx using different shoulder diameters at constant tool rotation speed

4.3 Conclusions

From the present work, the following important conclusions are made:

- It is found from the analysis that, within the welding parameters range chosen, a higher welding speed (80-120 mm/min), a higher rotation speed (1300-1500 rpm) and a higher plunge depth (1.85-2 mm) is preferred for producing a weld without internal defects. In the mean time, all the shoulder diameters (12, 15, 18 mm) produced defect free welds for AA6061-T6 sheet with 2.1 mm thickness used in the present work.
- The axial force and torque are found to increase with increase in welding speed and shoulder diameter. A decreasing trend is observed in axial force and torque while increasing the rotation speed. The axial force is found to increase with increase in plunge depth, while there is no effect of plunger depth on the torque generated in FSW. These are the results observed during the formation of defective welds.
- Once the optimized welding parameters are reached, there are no internal defects in the weld region. In this range of parameters, the axial force and torque are almost constant, indicating that they are insensitive to the change in welding parameters.
- A simple criterion is proposed by observing the variation of axial force (F) and torque (τ) with respect to welding parameters (p) for identifying the onset of defect free weld region. The criterion is stated as:

$$\left(\frac{\partial \tau}{\partial p}\right)_{defective} > \left(\frac{\partial \tau}{\partial p}\right)_{defect\ free}$$

$$and$$

$$\left(\frac{\partial F}{\partial p}\right)_{defective} > \left(\frac{\partial F}{\partial p}\right)_{defect\ free}$$

- The criterion is validated with welds made of different base material (Al 5xxx) and the axial force and torque are found to remain constant while forming a defect free weld region, indicating the validity of the criterion for another base material.

Chapter 5

Influence of few process parameters on the tensile behavior of friction stir welded AA 6061-T6 sheets

5.1 Experimental procedure

5.1.1 Base Material and FSW experiments

The base material details with nominal chemical composition and its mechanical properties evaluation through tensile test in different rolling direction are discussed in Chapter 4 in section 4.1. In the same section FSW process also explained. The optimized process parameters are shown in Table 4.7 in Chapter 4. By using these optimized parameters, the welding was done at two levels with all combinations by tools having different shoulder diameters (12, 18 mm), different plunge depths (1.85, 1.9 mm), welding speeds (90, 100 mm/min) and tool rotation speeds (1300, 1400 rpm) within optimized range. A third trial has also been made with 15 mm shoulder diameter, at plunge depth of 1.95 mm, welding speed of 120 mm/min and tool rotation speed of 1500 rpm as listed in Table 5.1. These parameters were optimized through macrostructures to make sure that the welds are internal defect free. In whole 17 different types of joints were fabricated.

Table 5.1 Selected optimum range of process parameters for FSW of AA 6061 (defect free weld formation range)

Shoulder diameter (mm)	Plunge depth (mm)	Tool Rotation speed (rpm)	Welding speed (mm/min)
12 and 18	1.85 and 1.9	1300 and 1400	90 and 100
15	1.95	1500	120

5.1.2 Testing of FSW sheets

5.1.2.1 Micro hardness test

Samples of FSW joints were polished using different grades of emery papers to measure the micro hardness. The grades of emery papers were varied from 200 to1000 for polishing FSW joints. Finally cloth polishing was done to make surface dents free. Micro hardness profiles were taken across the welded joint, at different locations on the transverse cross-section of the joints. A 50 gf load was used for the Vickers micro hardness measurements. Three trials were made and an averaged hardness value was used for analysis. Figure 5.1

shows the schematic representation of micro hardness indent locations in transverse cross section of the FSW joints during hardness measurement.

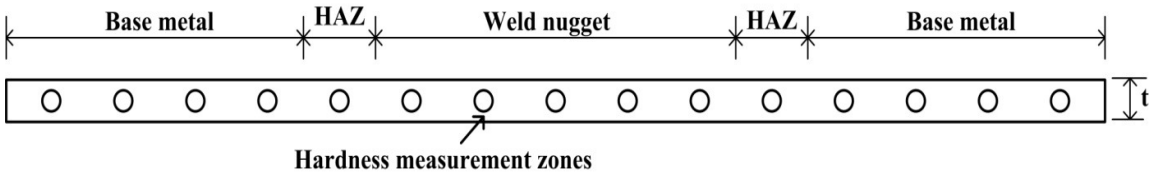

Fig. 5.1 Schematic representation of micro hardness measurement locations in transverse cross section of the FSW joints; t: thickness of sheet

5.2.1.2 Tensile test of FSW sheets and only weld zone FSW sheets

All the FSW blanks and weld zone tensile samples were made parallel to the loading direction (longitudinal direction) only, so that both the weld and base metal participate in deformation during tensile testing. Tensile tests were performed at a nominal cross-head speed of 1 mm/min, at room temperature on an INSTRON 8801 tensile testing machine and repeated twice for each set to check the reproducibility. Failure from grip or slippage during testing was not observed. Fig. 5.2 (a) shows the schematic representation of the FSW tensile sample and (b) tested samples FSW blank and sample with weld zone. The mechanical properties of FSW sheets like yield strength, ultimate tensile strength, total elongation, uniform elongation, strain hardening coefficient (n) and strength coefficient (K) were evaluated as per the standard procedure after testing the samples till failure. The load-stroke behavior obtained during testing was converted into engineering stress - strain and true stress-strain plot for evaluating the mechanical properties. The plastic strain ratios at different rolling directions were obtained after testing the base material to 12 % plastic strain.

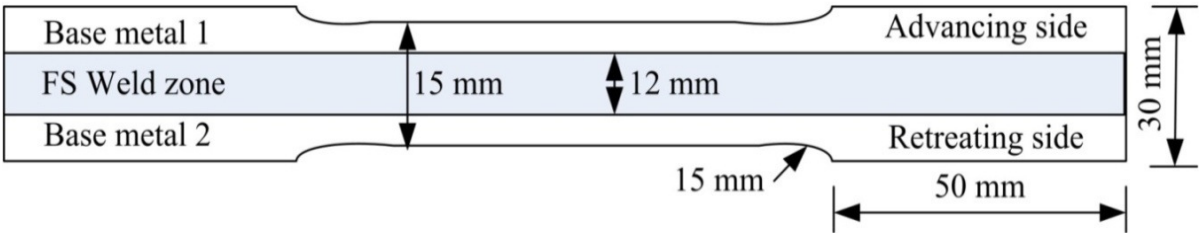

(a)

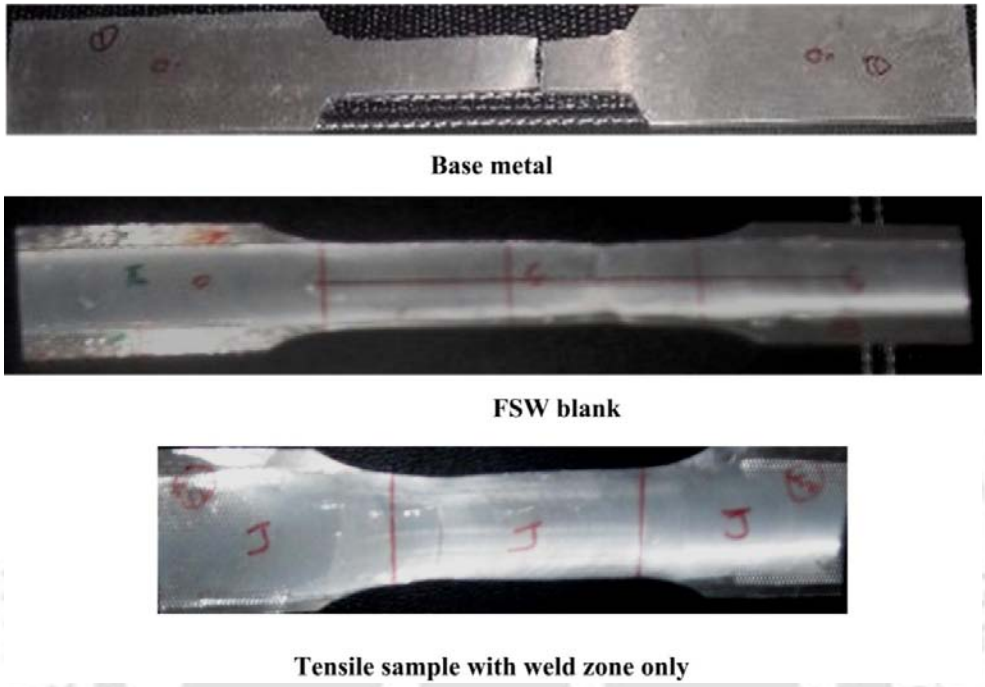

(b)

Fig. 5.2 (a) Schematic representation of FSW tailored blank tensile sample, (b) Tensile tested samples of FSW tailored blank and sample with weld zone

5.3 Results and discussion

5.3.1 Mechanical properties of base material and FSW sheets

The base material engineering stress-strain behavior at different rolling directions is shown in Fig. 5.3 (a). From the summarized the mechanical properties of AA 6061 base material as discussed in Chapter 4 Table 4.2, the yield strength and ultimate tensile strength are found to be within 258-277 MPa and 290-310 MPa respectively. The total elongation and strain hardening exponent are about 11.5% and 0.1 respectively in all the rolling directions. Figure 5.3 (b) shows the micro hardness profile of base material measured at equal distances. The average micro hardness of the base material is about 104.6 VHN.

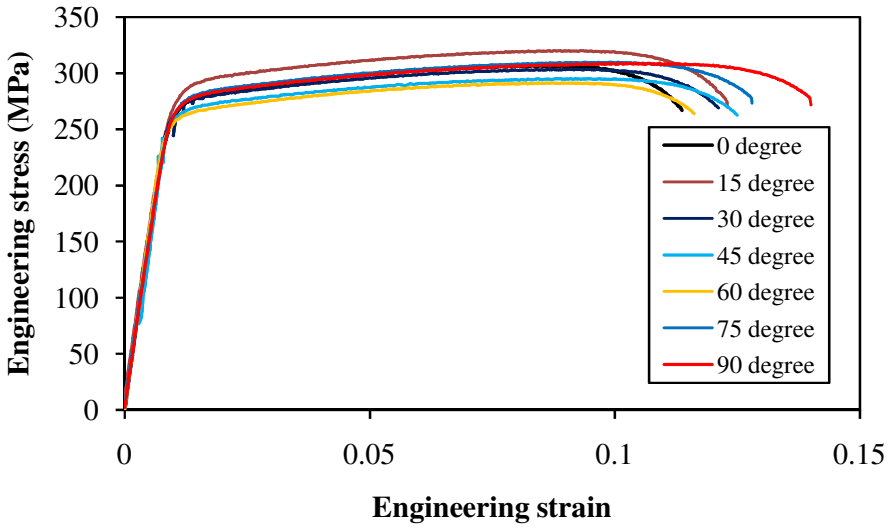

(a)

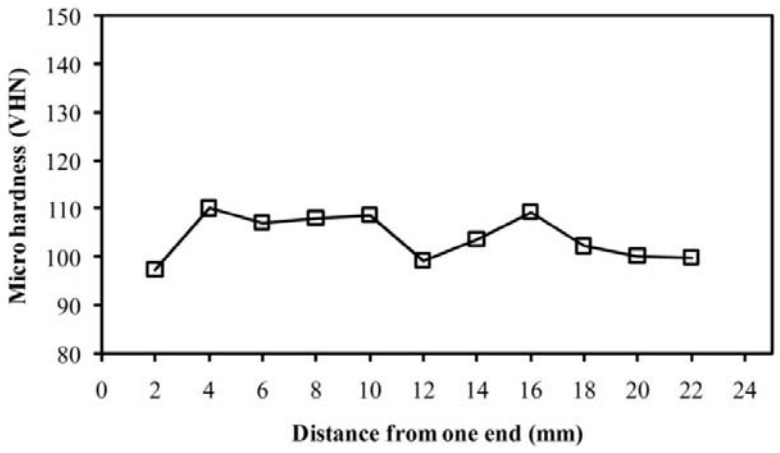

(b)

Fig. 5.3 (a) Tensile behavior of base metal (AA 6061- T651) in different rolling directions and (b) micro hardness profile of base material

In the similar fashion, hardness and mechanical properties of FSW blanks and only weld zone are found at different shoulder diameter, plunge depth, welding speeds and tool rotation speeds. The influence of these parameters on the hardness and mechanical properties are discussed further with base metal properties comparison. Table 5.2 and 5.3 shows the mechanical properties of FSW blanks and weld zone at different FSW conditions.

In Table 5.2, FSW conditions 1 to 16 show data for different shoulder diameters, plunge depths, tool rotation speed and welding speeds combinations at two levels and condition 17 shows the third level FSW condition. From tensile tests, it is observed that among all the FSW conditions, maximum yield strength of 146±4 MPa occurs at FSW condition 8, ultimate

tensile strength of 253±1 MPa at FSW condition 14, uniform elongation (e_u) of 23.3%, total elongation (e_t) of 26.83% and strain hardening exponent (n) of 0.28 at FSW condition 16, and strength coefficient (K) of 472±1 MPa at FSW condition 9. In case of only weld zone from the mechanical properties shown in Table 5.3, maximum yield strength of 189±4 MPa occur at FSW condition 14, ultimate tensile strength of 294±5 MPa at FSW condition 6, uniform elongation of 29.3%, total elongation of 32.3% at FSW condition 10, strain hardening exponent (n) of 0.3 at FSW condition 8, and strength coefficient (K) of 548±14 MPa at FSW condition 14. Another important observation is that the mechanical properties of FSW sheets and weld zone are maximum at a shoulder diameter of 18 mm and it is independent of other welding parameters.

Table 5.2 Mechanical properties of FSW blanks at different FSW conditions

FSW condition	FSW parameters				YS (MPa)	UTS (MPa)	UE (%)	TE (%)	n	K (MPa)
	SD (mm)	PD (mm)	TRS (rpm)	WS (mm/min)						
1	12	1.85	1300	90	139±1	227±5	17.0	18.5	0.24	417±10
2	18				144±4	247±5	21.0	23.1	0.26	458±7
3	12	1.85	1400	90	135±5	227±5	18.3	19.5	0.25	415±7
4	18				142±3	228±9	22.2	23.6	0.27	419±11
5	12	1.9	1300	90	139±1	223±7	18.9	19.5	0.24	408±9
6	18				139±2	241±3	19.6	21.1	0.26	442±1
7	12	1.9	1400	90	137±4	230±5	18	19.5	0.25	430±6
8	18				146±4	245±1	19.3	20.7	0.25	448±2
9	12	1.85	1300	100	135±9	241±5	20.4	20.7	0.27	457±13
10	18				134±4	233±2	20.6	20.7	0.26	434±2
11	12	1.85	1400	100	134±10	229±10	18.3	21.1	0.26	428±15
12	18				135±2	234±2	22.2	23.4	0.26	430±1
13	12	1.9	1300	100	134±3	225±10	18.7	20.3	0.25	417±13
14	18				144±1	253±1	21.9	22.3	0.27	472±1
15	12	1.9	1400	100	134±3	229±4	17.9	20.3	0.25	436±2
16	18				136±4	249±1	23.3	26.8	0.28	465±1
17	15	1.95	1500	120	139±1	237±4	20.1	21.1	0.26	441±12

SD: shoulder diameter; PD: plunge depth; TRS: tool rotational speed; WS: welding speed; YS: yield strength; UTS: ultimate tensile strength; UE: uniform elongation; TE: total elongation; n: strain hardening coefficient; K: strength coefficient

Table 5.3 Mechanical properties of weld zone at different FSW conditions

FSW condition	FSW parameters				YS (MPa)	UTS (MPa)	UE (%)	TE (%)	n	K (MPa)
	SD (mm)	PD (mm)	TRS (rpm)	WS (mm/min)						
1	12	1.85	1300	90	161±1	255±2	20.9	22.7	0.25	468±4
2	18				174±8	282±10	28.7	31.3	0.27	494±20
3	12	1.85	1400	90	150±2	248±2	23.2	25	0.25	461±3
4	18				168±4	279±3	27.3	31.3	0.28	519±4
5	12	1.9	1300	90	165±2	258±2	23.1	25.8	0.24	457±15
6	18				181±2	294±5	25.9	29.7	0.27	539±15
7	12	1.9	1400	90	164±10	257±13	22.1	24.2	0.25	446±20
8	18				180±3	287±2	27.0	31.3	0.3	530±10
9	12	1.85	1300	100	169±2	271±6	22.8	25	0.26	498±5
10	18				165±4	279±1	29.3	32.3	0.28	520
11	12	1.85	1400	100	166±7	269±2	24.6	27.3	0.25	510±20
12	18				165±4	273±1	27.2	31.3	0.27	502
13	12	1.9	1300	100	160±2	249±3	20.8	23.4	0.25	452±14
14	18				189±4	291±2	27.5	29.7	0.26	548±14
15	12	1.9	1400	100	163±4	263±5	23.4	25.8	0.25	478±12
16	18				181±6	290±10	27.3	28.1	0.28	530±10
17	15	1.95	1500	120	174±3	270±13	27.8	29.7	0.27	514±6

SD: shoulder diameter; PD: plunge depth; TRS: tool rotational speed; WS: welding speed; YS: yield strength; UTS: ultimate tensile strength; UE: uniform elongation; TE: total elongation; n: strain hardening coefficient; K: strength coefficient

5.3.2 Micro-hardness distribution in FSW sheets

In order to analyze the effect of shoulder diameter, two FSW blanks corresponding to FSW conditions 7 and 8 (Table 5.2) are considered. They are fabricated with different tool shoulder diameters (12 and 18 mm) at 1400 rpm rotational speed, 90 mm/min welding speed and 1.9 mm plunge depth. It is seen from Fig. 5.4 that hardness values are more in case of 18 mm shoulder diameter as compared to 12 mm shoulder diameter and a maximum hardness of 126.4 VHN is found at transition zone, between base metal and weld zone, in the retreating side of FSW joint. In both the cases, maximum hardness occurs at retreating side compared to advancing side and minimum hardness of 94.3 VHN is reported at the weld centre for 18 mm shoulder diameter. Similar hardness behavior has been observed in all other FSW conditions. Even in other welding conditions, the hardness values are more at higher shoulder diameter. This is in good correlation with flow strength values in Table 5.2 and 5.3 that with increase in shoulder diameter, the yield strength and ultimate tensile strength have improved in most of the cases. This is true for all the FSW conditions used in the present work.

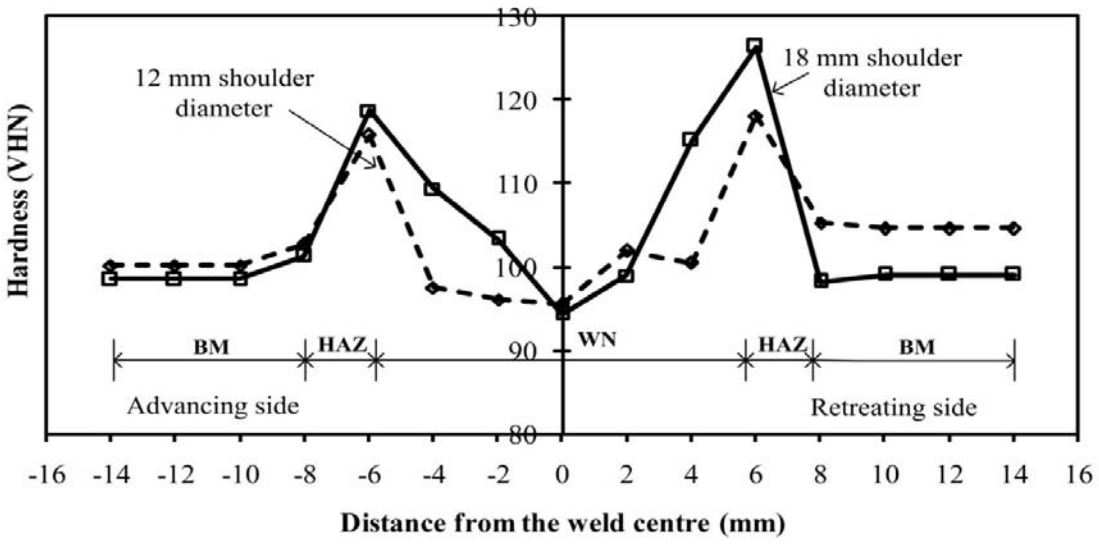

Fig. 5.4 Micro-hardness distribution of FSW joints made with different shoulder diameters, 12 and 18 mm, corresponding to FSW conditions 7 and 8 in Table 5.2. Hardness varied from HAZ to WN ±2 to ±1. BM: base metal; HAZ: heat affected zone; WN: weld nugget

To study the effect of plunge depth, two FSW blanks corresponding to FSW conditions 1 and 5 (from Table 5.2) which are fabricated at different plunge depths, 1.85 and 1.9 mm, at 1300 rpm rotational speed, 90 mm/min welding speed and using 12 mm shoulder diameter are considered for comparison. It is observed from Fig.5.5 that though hardness values are more in case of 1.85 mm plunge depth, the variation is very less. A maximum hardness of 121.8 VHN is found at the transition zone, between base metal and weld zone, in the retreating side of FSW joint for 1.85 mm plunge depth. At the same location, there is only a slight decrease in maximum hardness to 118.2 VHN for 1.9 mm plunge depth. The maximum hardness values corresponding to 1.85 and 1.9 mm plunge depth are almost same in the advancing side. In both plunge depths, hardness values are more in retreating side compared to advancing side and the minimum hardness of 95.4 VHN for 1.9 mm plunge depth value is seen at the weld centre. Similar hardness behavior has been observed in all other FSW conditions. So the effect of plunge depth on hardness distribution is not pronounced, unlike the effect in flow strength. When yield strength and ultimate strength are compared from Table 5.2 and 5.3, it is observed that in few cases there is not much variation in the strength values of FSW sheets when plunge depth is changed, while there is a considerable variation in strength values in the case of only weld zone.

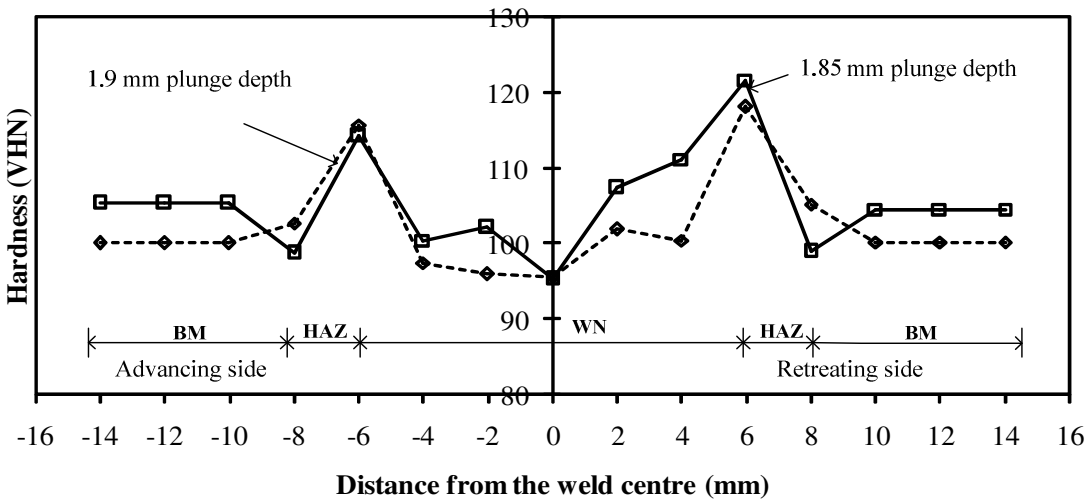

Fig. 5.5 Micro-hardness distribution of FSW joints made at different plunge depths, 1.85 and 1.9 mm, corresponding to FSW conditions 1 and 5 in Table 5.2. Hardness varied from HAZ to WN ±0.5 to ±2. BM: base metal; HAZ: heat affected zone; WN: weld nugget

The FSW sheets corresponding to FSW conditions 5 and 7 in Table 5.2 which are fabricated at different rotational speeds, 1300 and 1400 rpm, 90 mm/min welding speed and 1.9 mm plunge depth with tool shoulder diameter 12 mm are compared to study the effect of rotational speed. It is seen from Fig. 5.6 that hardness values are more in case of 1300 rpm rotational speed as compared to 1400 rpm and also a maximum hardness value of 118.2 VHN is found at transition zone in the retreating side of FSW joint. In both the rotational speeds, hardness values are more in retreating side compared to advancing side and minimum hardness values of 95.6 and 89.3 VHN are found at weld nugget in both the cases. A similar result of decrease in hardness with increase in rotational speed is seen in 18 mm shoulder diameter also. A similar effect is observed in all other FSW conditions too. It can be understood from Table 5.2 and 5.3 that in most of the cases, the yield strength and ultimate tensile strength values are decreased with increase in rotational speed. The effect is more pronounced in the case of weld zone as compared to FSW sheets.

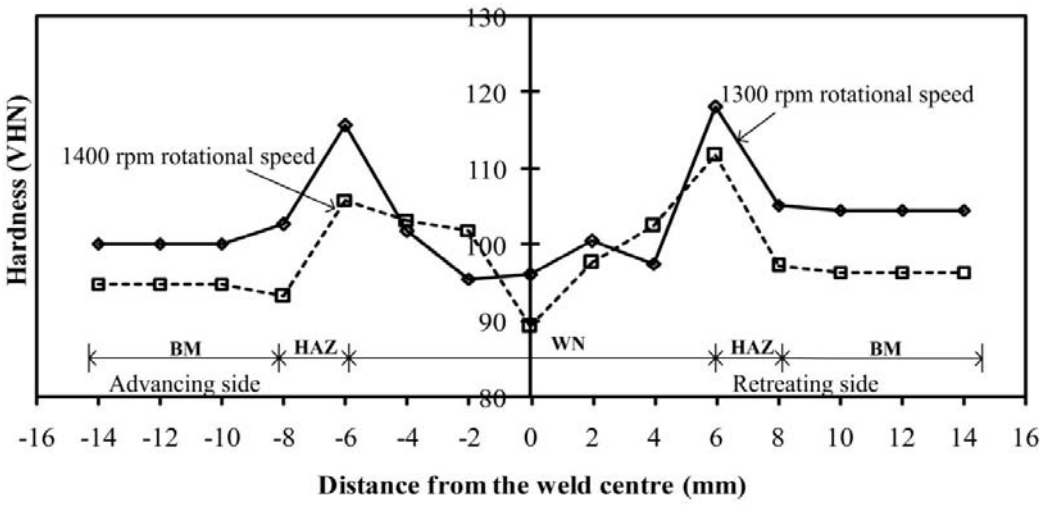

Fig. 5.6 Micro hardness distribution of FSW joints at different tool rotation speeds, 1300 and 1400 rpm, corresponding to FSW conditions 5 and 7 in Table 5.2. Hardness varied from HAZ to WN ±1 to ±4 BM: base metal; HAZ: heat affected zone; WN: weld nugget

The FSW sheets corresponding to FSW conditions 8 and 14 in Table 5.2 at different welding speeds, 90 and 100 mm/min, 1400 rpm rotational speed and 1.9 mm plunge depth with tool shoulder diameter 18 mm are compared to study the effect of welding speed. It is seen in Fig. 5.7 that hardness values are more in case of 100 mm/min welding speed compared to the welding speed at 90 mm/min and also a maximum hardness of 116.3 VHN is found in the retreating side of FSW joint. In both the cases hardness values are more in retreating side compared to advancing side and minimum hardness value 93.33 VHN is seen for 90 mm/min at the weld centre. The increase in hardness with increase in welding speed correlates mostly with the flow strength variation with respect to welding speed presented tin Table 5.2 and 5.3. For example, condition 8 and 14 depict that with increase in welding speed, the yield strength and ultimate tensile strength improved, with significant improvement in the case of weld zone (in Table 5.3) as compared to FSW sheet. A similar improvement in strength values is observed in conditions 1 and 9 for 12 mm shoulder diameter.

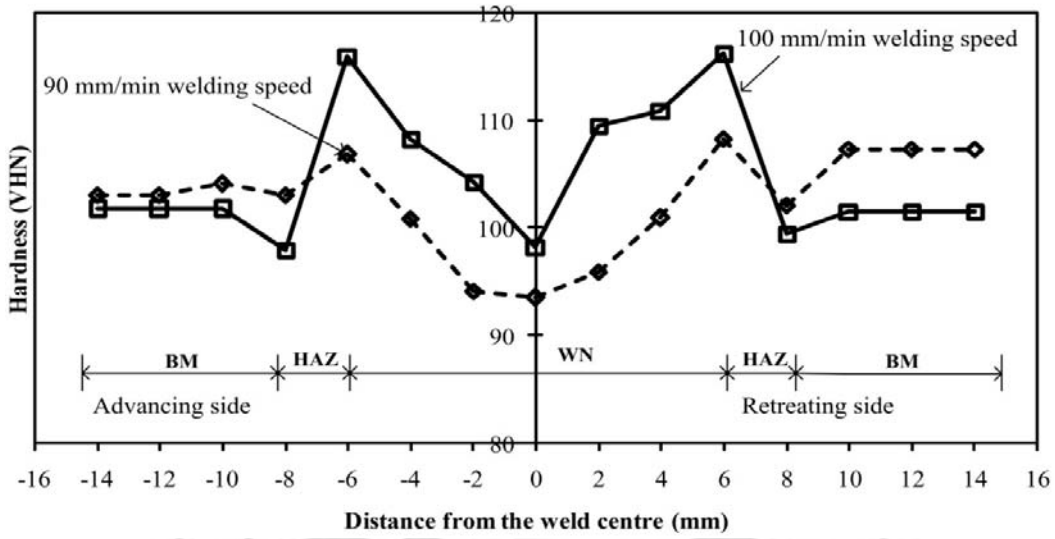

Fig. 5.7 Micro-hardness distribution of FSW joints at different welding speeds, 90 and 100 mm/min, corresponding to FSW conditions 8 and 16 in Table 5.2. Hardness varied from HAZ to WN ±1.5 to ±3.5. BM: base metal; HAZ: heat affected zone; WN: weld nugget

5.3.3 Tensile behavior of FSW sheets

The selected and optimized FSW conditions are listed in Table 5.2 and 5.3 through which all the FSW joints were fabricated. Figure 5.8 shows the effect of shoulder diameters, 12 mm and 18 mm, on the engineering stress–strain behavior on FSW blanks at a constant welding speed of 90 mm/min, tool rotation speed of 1300 rpm and plunge depth of 1.9 mm, i.e., FSW conditions 5 and 6 in Table 5.2 and 5.3. It is observed that the base material mechanical properties like yield strength and ultimate strength are more compared to the FSW blanks and weld zone in all FSW conditions shown in Table 5.2 and 5.3. The other properties like uniform elongation, total elongation, and strain hardening exponent (n) of FSW blanks and weld zone are more compared to base metal. When FSW blanks are compared, 18 mm shoulder diameter FSW blank has more flow strength and more elongation compared to the FSW sheet made at 12 mm shoulder diameter. The same has been observed in weld zone properties as 18 mm shoulder diameter has more strength and more elongation compared to the case of 12 mm shoulder diameter. Even in other FSW combinations, say condition 1 and 2, and condition 13 and 14, the uniform elongation, total elongation and strain hardening exponent increased with increase in shoulder diameter. There is about 5% improvement in elongation in these two cases.

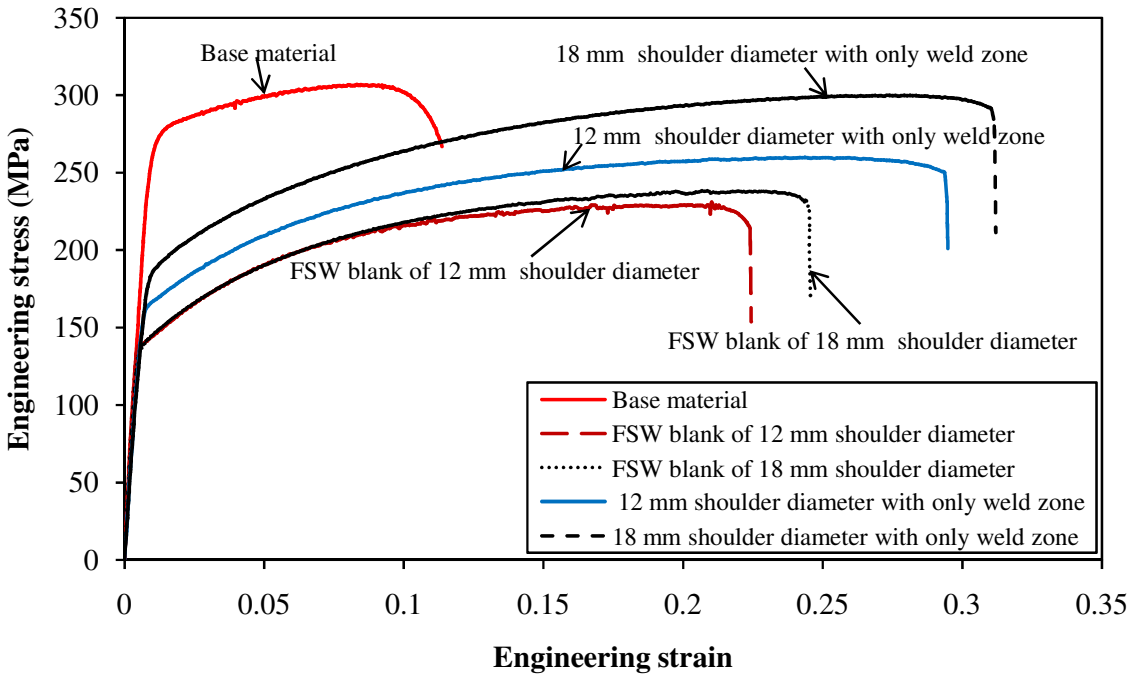

Fig. 5.8 Tensile behavior of base metal, FSW sheets and weld zone made with different shoulder diameters, 12 and 18 mm, at constant welding speed of 90 mm/min, tool rotation speed of 1300 rpm and plunge depth of 1.9 mm

Figure 5.9 shows the engineering stress–strain behavior of FSW sheets presenting the effect of different plunge depths, 1.85 and 1.9 mm, at a constant welding speed of 90 mm/min, and tool rotation speed of 1300 rpm using shoulder diameter of 12 mm (FSW conditions 1 and 5 in Table 5.2 and 5.3). The FSW sheets exhibit lesser yield strength and ultimate tensile strength as compared to base materials. This is evident from Table 5.2 and 5.3. The other properties like uniform elongation, total elongation, and strain hardening exponent (n) of FSW blanks and weld zone are more compared to base metal. When FSW sheets are compared, 1.9 mm plunge depth has got more elongation and almost equal flow strength as compared to 1.85 mm plunge depth. A similar behavior is also observed in weld zone properties. But the 'n' values of FSW sheets and weld zone are observed to be almost equal in both the plunge depths. The hardness distribution shown in Fig. 5.5 to study the effect of plunge depths correlation with the flow strength comparison shown in Fig. 5.9. There is not much variation in hardness distribution with increase in plunge depth.

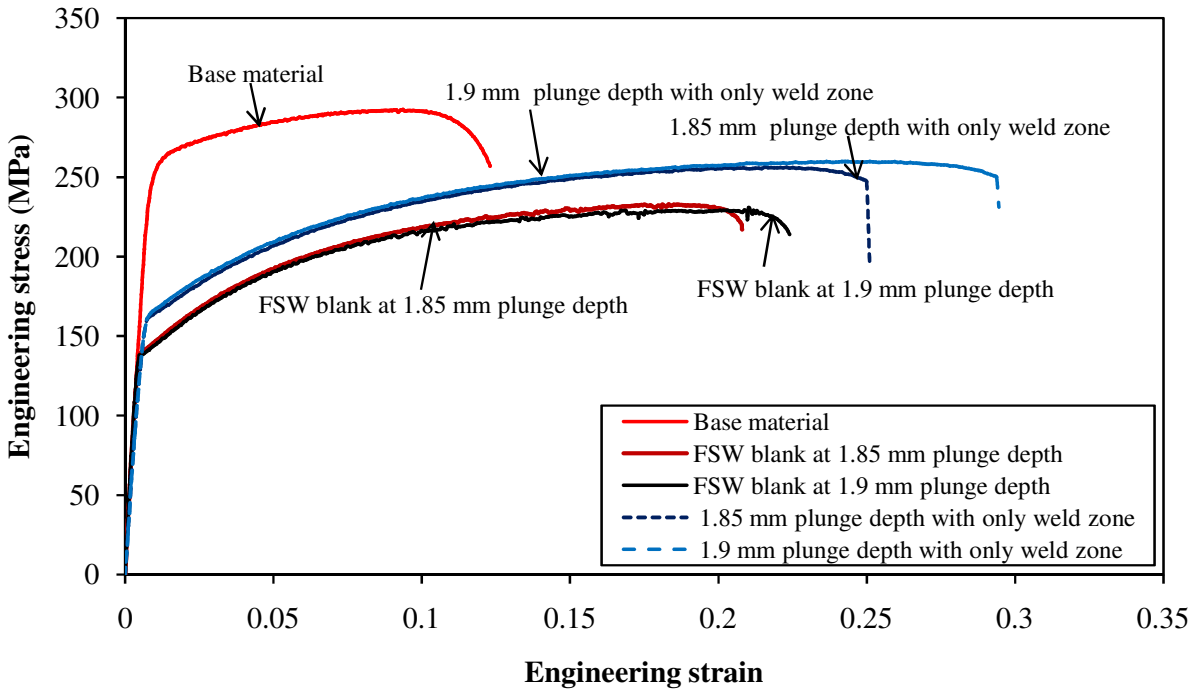

Fig. 5.9 Tensile behavior of base metal, FSW sheets and weld zone made at different plunge depths, 1.85 and 1.9 mm, at constant welding speed of 90 mm/min, and tool rotation speed of 1300 rpm using 12 mm tool shoulder diameter

Figure 5.10 shows the engineering stress–strain behavior presenting the effect of different tool rotation speed, 1300 and 1400 rpm, at a constant welding speed of 100 mm/min, and plunge depth 1.9 mm using shoulder diameter of 18 mm (FSW conditions 14 and 16 in Table 5.2 and 5.3). The uniform elongation, total elongation, and strain hardening exponent (n) of FSW blanks and weld zone are more compared to base metal. When FSW blanks are compared, 1400 rpm tool rotation speed FSW blank has slightly less strength and more elongation compared to the 1300 rpm tool rotation speed FSW blank. Similar behavior is also observed in the case of only weld zone. The same trend is observed in few other welding combinations like condition 1 and 3, and condition 6 and 8 in Table 5.3 for weld zone. There is improvement of about 3% in elongation with increase in rotational speed. Similarly improvement in elongation is witnessed in FSW sheets under few other conditions shown in Table 5.2 with increase in rotational speed.

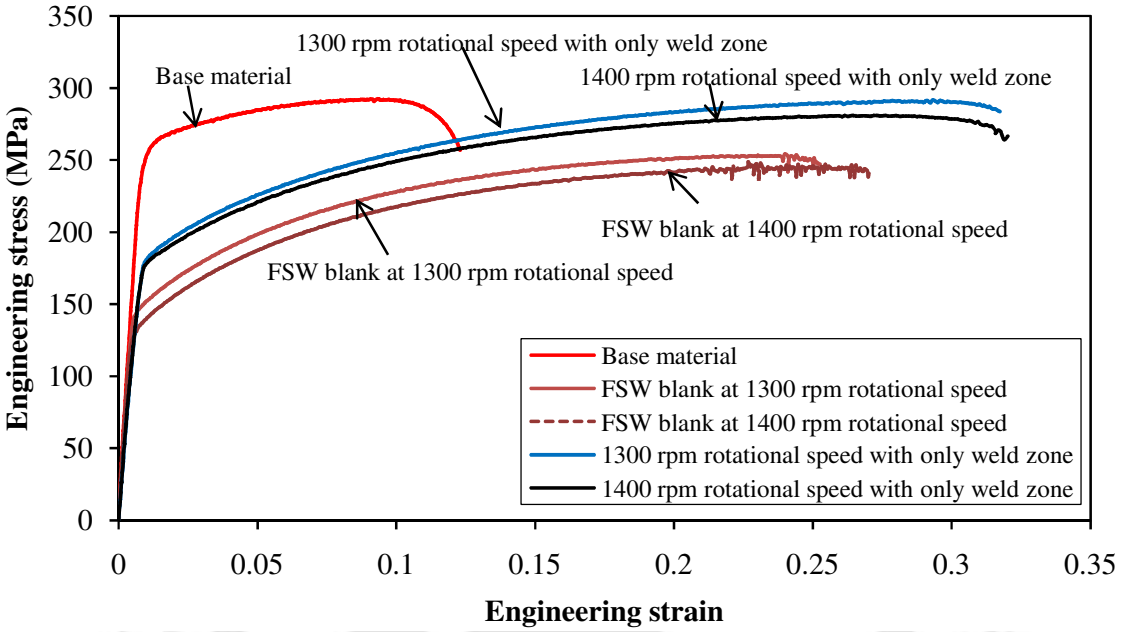

Fig. 5.10 Tensile behavior of base metal, FSW sheets and weld zone made at different tool rotation speeds, 1300 and 1400 rpm, at constant welding speed of 100 mm/min, and plunge depth of 1.9 mm using 18 mm tool shoulder diameter

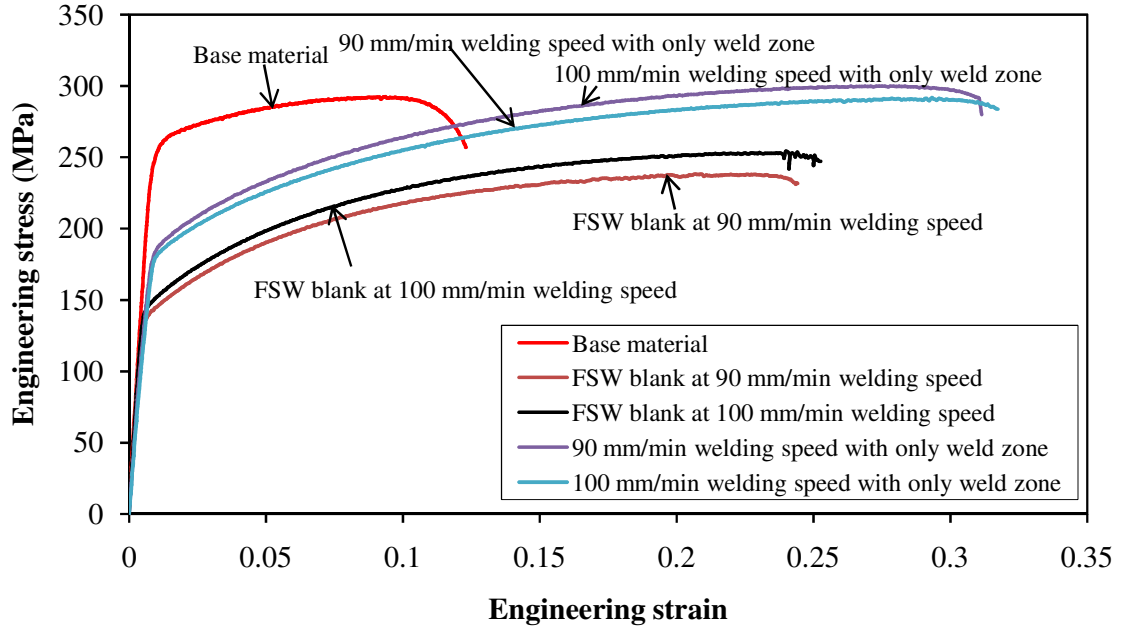

Fig. 5.11 Tensile behavior of base metal, FSW sheets and weld zone made at different welding speeds, 90 and 100 mm/min, at constant tool rotation speed of 1300 rpm, and plunge depth of 1.9 mm using 18 mm tool shoulder diameter

Figure 5.11 shows the engineering stress–strain behavior of FSW sheets made at different welding speeds, 90 and 100 mm/min, at constant tool rotation speed of 1300 rpm, and plunge depth 1.9 mm using tool shoulder diameter of 18 mm (FSW conditions 6 and 14 in Table 5.2

and 5.3). Similar to the previous cases, the FSW sheets and weld zone exhibit lesser flow strength as compared to base material. But, uniform elongation, total elongation, and strain hardening exponent (*n*) of FSW blanks and weld zone are more compared to base metal. When FSW sheets are compared, there is not much variation in strength and elongation when welding speed is changed from 90 mm/min to 100 mm/min though decrease in elongation is expected. This is evident from strain hardening exponent (*n*) values shown in Table 5.2 and 5.3. There is a very small variation in '*n*' values between 0.26 and 0.27 when welding speed is varied. Similar effect is seen in the case of only weld zone. Even in other FSW conditions, total elongation, and strain hardening exponent (*n*) of FSW blanks and are not changing much when welding speed is increased from 90 mm/min to 100 mm/min. In whole there is hardly 0.5-1.5 % change in elongation values in most of the cases of FSW sheets.

5.3.4 Relating the thinning behavior and formability of FSW sheets

In general, 'necking' can be understood as a phenomenon occurring in sheets because of the presence of initial thickness heterogeneity in the material, as a result of which material thinning occurs during the course of deformation in tensile test. The more the thinning gradient, the earlier the failure will be reached. In the case of FSW blanks, the presence of weld region and the properties of weld region can result in an increased or decreased thinning gradient in comparison with that of the unwelded blank. This, in turn, depends on the process parameters that are used to fabricate the FSW joints during welding.

In this section, an attempt has been made to relate the change in elongation of FSW sheets with the thinning behavior during tensile test. Elongation in tensile test is equivalent to forming limit in actual stamping operations. So elongation is an index of formability of FSW blanks. The thinning behavior is evaluated by monitoring the thickness distribution of the FSW sheets after tensile test, perpendicular to the necked region. The averaged thickness data is recorded at a point for three repetitions. The thinning behavior of FSW blanks made at condition 5 and 6 in Table 5.2 with variable shoulder diameters in comparison with that of the unwelded blank is presented in Fig. 5.12. Only the thickness difference distribution is shown with respect to the sample geometry. It is observed that FSW blanks made with 12 mm and 18 mm shoulder diameters have minimum thickness difference of 0.24 mm (for 12 mm shoulder diameter) near to fracture as compared to base metal thickness difference of 0.35 mm near fracture. This has resulted in increased elongation and strain hardening exponent (*n*) for FSW blanks compared to the base metal as described in Fig.5.8. FSW blank of 18 mm shoulder diameter exhibit more elongation and strain hardening exponent (*n*) as

compared to FSW blank of 12 mm shoulder diameter which correlates with the lesser thickness gradient in the case of FSW sheets made with 18 mm shoulder diameter (Fig. 5.12).

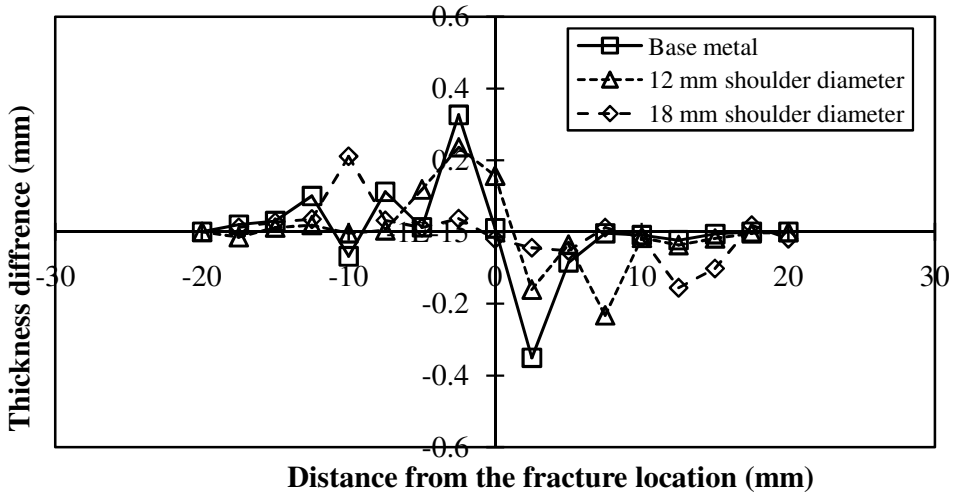

Fig. 5.12 Comparison of thickness difference of FSW blanks made using different shoulder diameters, 12 and 18 mm, corresponding to FSWconditions 5 and 6 in Table 5.2 to base material

The thickness difference plots of FSW sheets made at different plunge depths, and different rotational speed are shown in Fig.5.13 and Fig. 5.14 respectively. It is observed that with increase in plunge depth and tool rotation speed, the thickness difference (or gradient) decreases improving their elongation. This is evident from earlier discussions with respect to Fig. 5.9 and Fig. 5.10.

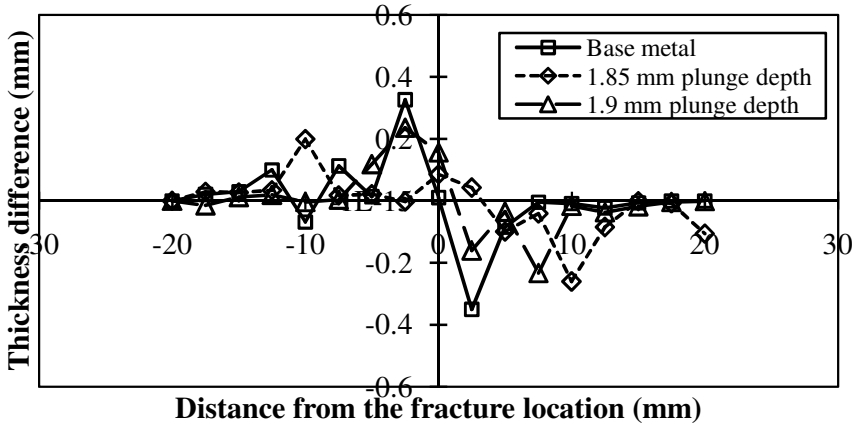

Fig. 5.13 Comparison of thickness difference of FSW blanks made at different plunge depths, 1.85 and 1.9 mm, corresponding to FSWconditions 1 and 5 in Table 5.2 to base material

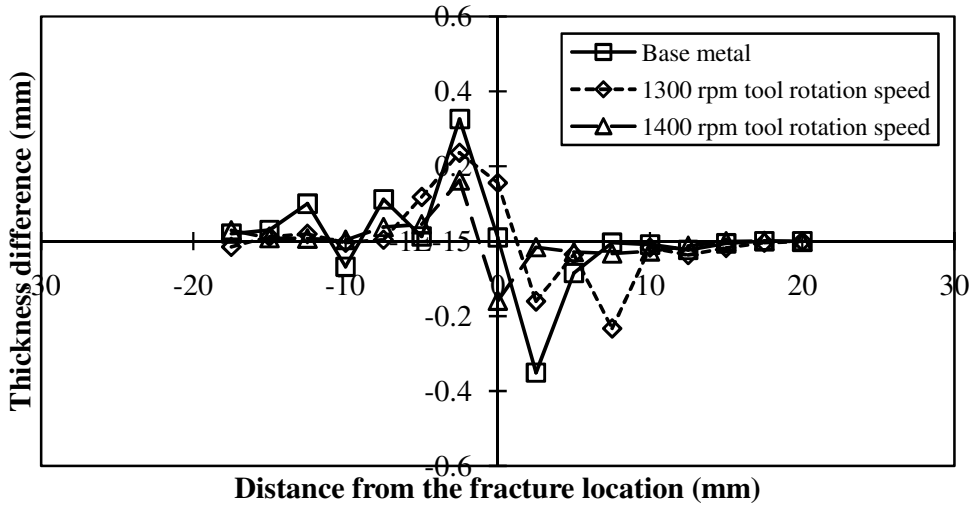

Fig. 5.14 Comparison of thickness difference of FSW blanks made at different tool rotation speeds, 1300 and 1400 rpm, corresponding to FSWconditions 14 and 16 in Table 5.2 to base material

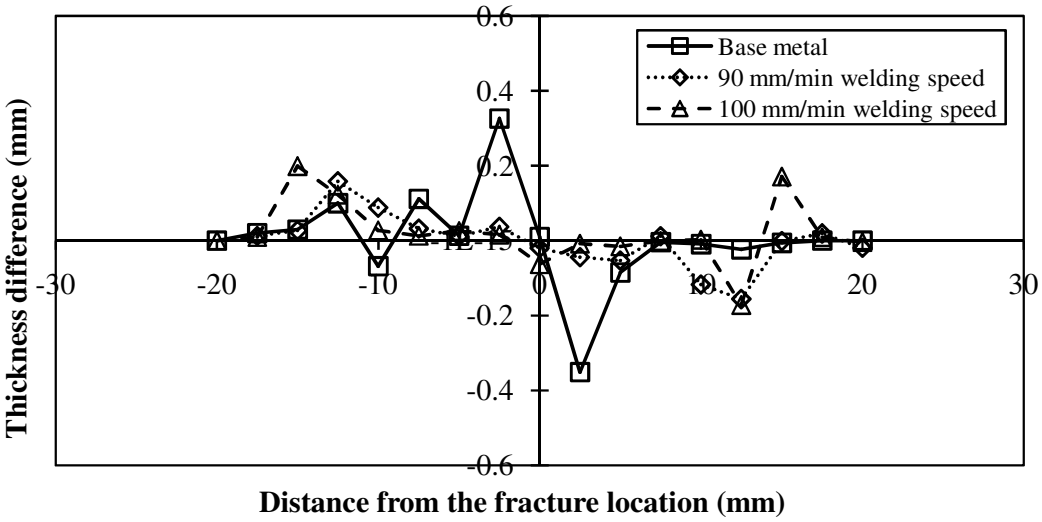

Fig. 5.15 Comparison of thickness difference of FSW blanks made at different welding speeds, 90 and 100 mm/min, corresponding to FSWconditions 6 and 14 in Table 5.2 to base metal

On the other hand, it is observed from Fig. 5.15 that there is not much variation seen in thickness gradient between FSW sheets made at 90 mm/min and 100 mm/min welding speeds. This has resulted in negligible difference in elongation and strain hardening exponent (n) values shown in Fig. 5.11 and in Table 5.2 when welding speed is changed.

In general, the thickness gradient of FSW sheets is much better as compared to unwelded base material (Fig. 5.13-5.15) resulting in more elongation as presented earlier with respect to Fig. 5.9-5.11. For conditions 17 in Table 5.2 and 5.3, it is observed that the yield strength,

ultimate tensile strength, elongation and strain hardening exponent (n) of FSW sheets and only weld zone are in between 12 mm shoulder diameter and 18 mm shoulder diameter in most of the cases irrespective of other parameters.

5.4 Conclusions

The main aim of this work is to investigate the effect of shoulder diameter, plunge depth, tool rotation speed, and welding speed on the tensile behavior of FSW sheets made of AA6061-T6. The following conclusions are drawn from the present work.

- Micro-hardness showed a decreasing trend, from the base material to the middle line of the nugget zone, except near the transition zone. With increase in shoulder diameter and welding speed, hardness has increased. But with increase in plunge depth and rotational speed, hardness has decreased with plunge depth showing relatively subtle effect.

- The FSW sheets showed a decreased flow stress and improved elongation when compared to base material. With increase in plunge depth, shoulder diameter, rotational speed, the elongation of FSW sheets and weld zone is found to improve, while welding speed has shown insignificant effect. The change in flow strength properties (like yield strength, UTS) of FSW sheets with respect to welding conditions is consistent with change in hardness values.

- The thinning gradient has shown significant effect changing the overall elongation with change in welding conditions. The thickness gradient is found to be severe in un-welded blanks as compared to FSW blanks. The thickness gradient is severe in FSW sheets made at lower levels of shoulder diameter, plunge depth and rotation speed, while welding speed showed negligible effect.

- Thinning gradient is dependent on the strain hardening exponent (n). With improvement in strain hardening exponent of FSW sheets (and weld zone) with respect to changing welding conditions, the thinning gradient is less and vice versa, consequently improving the overall elongation of welded sheets in most of the cases.

Chapter 6

Influence of shoulder diameter and plunge depth on the forming limit of friction stir welded 6061 aluminum alloy sheet

6.1 Experimental procedure

6.1.1 Base material properties

The base material properties and methodology to evaluate the mechanical properties are explained in Chapter 4 in section 4.1.

6.1.2 Welding experiments

The FSW is done using the optimized process parameters are shown in Table 4.7 in Chapter 4. From that range of optimized parameters, some of the FSW conditions are considered such that the effect of shoulder diameter and plunge depth on the forming limit strain is focused. The selected FSW conditions are tabulated in Table 6.1 in which FSW conditions from 1 to 4 are for different shoulder diameters and from conditions 5 to 8 are for different plunge depths. The FSW condition 9 is made as third trial with tool of 15 mm shoulder diameter to check the forming limit at a third level.

Table 6.1 Different optimized welding conditions used for formability evaluation of FSW blanks

FSW condition	Shoulder diameter (mm)	Plunge depth (mm)	Tool rotation speed (rpm)	Welding speed (mm/min)
1	12, 18	1.85	1300	90
2	12, 18	1.9	1300	90
3	12, 18	1.85	1400	90
4	12, 18	1.9	1400	90
5	12	1.85, 1.9	1300	90
6	12	1.85, 1.9	1400	90
7	18	1.85, 1.9	1300	90
8	18	1.85, 1.9	1400	90
9	15	1.95	1500	120

6.1.3 Evaluating the strain hardening exponent (n) of weld zone

The strain hardening exponent (n) of FS weld region was evaluated through tensile tests using tensile samples containing weld zone only as shown in Fig. 6.1. The tests were performed at a nominal cross-head speed of 1 mm/min and at room temperature on an

INSTRON 8801 tensile testing machine and repeated twice for each condition to check the reproducibility. Failure from grip or slippage during testing was not observed. The strain hardening coefficient (n) values were evaluated as per the standard procedure after testing the samples till failure. The load-stroke behavior obtained during testing was converted into engineering stress – strain and true stress – strain behavior. The strain hardening exponent (n) value was calculated from the slope of natural logarithm plot of true stress and true strain ($ln\ \sigma$- $ln\ \varepsilon$) in which the σ- ε values in plastic deformation region were considered. The same procedure is repeated for all the combinations of shoulder diameter and plunge depth.

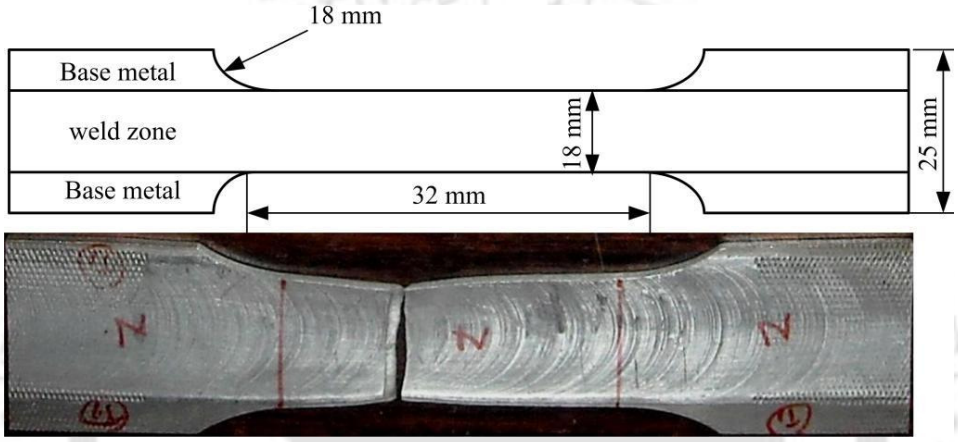

Fig. 6.1 Top: Representation of FSW tensile sample with only weld zone **Bottom:** FSW tested tensile sample of 18 mm weld width

6.1.4 Limit dome height (LDH) test for forming limit evaluation

In order to study the influence of FSW parameters, viz; shoulder diameter, plunge depth on the formability, limit dome height (LDH) tests were performed on the welded and unwelded blanks. Standard LDH test tool geometry was used for the formability tests. Few different sheet widths (like 100 x 200 mm, 125 x 200 mm etc.) with three lubrication (dry, grease and oil) conditions simulating six different predefined strain paths in stretching side were deformed to construct an FLC. During the LDH test, samples were first thoroughly cleaned with acetone to remove oil and dust particles on the sheet surface. Dot grids of diameter 1 mm with 2.5 mm distance was printed on sheet surface for both the welded and the unwelded sheet. The samples were placed on the die surface and sufficient blank holding pressure (≈ 40 kN) was applied such that the blank neither draws in nor fails near the holding region. All the blanks (both welded and unwelded) were deformed until failure (or necking) occurs and repeated twice for each condition. The true major strains and true minor strains of the ellipses, near to the failure and away from the failure, were measured using an optical

strain analyzer in all the strain paths. These major and minor strain data were plotted on a major strain (y-axis)–minor strain (x-axis) graph. All the failed strains and safe strains were incorporated in the same graph. The FLCs were plotted such that they separate all the failed strains from the safe strains. The forming-limit diagram (FLD) of the unwelded blank is shown in Fig. 6.2 for illustration. In this figure, the major strain and minor strain values above FLC are considered as failed strains and those below FLC are considered as safe strains. This procedure is followed for the unwelded blank and the welded blanks.

The FLCs of the welded blanks were compared with each other and also with that of the unwelded blank to investigate the influence of the shoulder diameter and plunge depth on the forming-limit strains of FSW blanks. The obtained major limit strains at different FSW conditions are tabulated in the Table 6.2 including the third level of experiment. Thickness distribution was measured on both sides of the neck towards peak of the dome with sharp edged micrometer perpendicular to the fracture. The thickness distribution was measured at regular intervals at the weld center, near the advancing side of the weld and retreating side of the weld as shown in Fig. 6.3. Three trials were considered for averaging the thickness values at each location. The dome height at failure was measured using a vernier height gauge for all the FSW conditions at different strain paths tested.

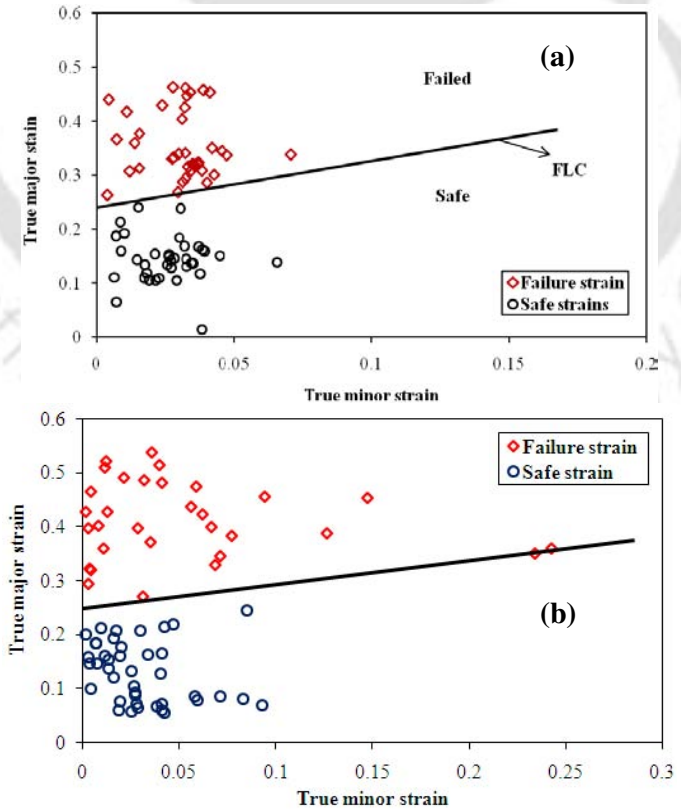

Fig. 6.2 FLD of the (a) unwelded blank and (b) FSW blank of condition 1 from Table 6.2

Table 6.2 Major limit strain values of different FSW conditions

FSW conditions	Shoulder diameter (mm)	Plunge depth (mm)	Rotational speed (rpm)	Welding speed (mm/min)	Limiting major strain values	
					Near plane-strain strain path	Biaxial strain path
Unwelded blank					0.23	0.33
1	12	1.85	1300	90	0.22	0.36
	18	1.85	1300	90	0.22	0.42
2	12	1.9	1300	90	0.25	0.4
	18	1.9	1300	90	0.2	0.48
3	12	1.85	1400	90	0.26	0.38
	18	1.85	1400	90	0.27	0.48
4	12	1.9	1400	90	0.24	0.44
	18	1.9	1400	90	0.2	0.5
5	15	1.95	1500	120	0.2	0.44

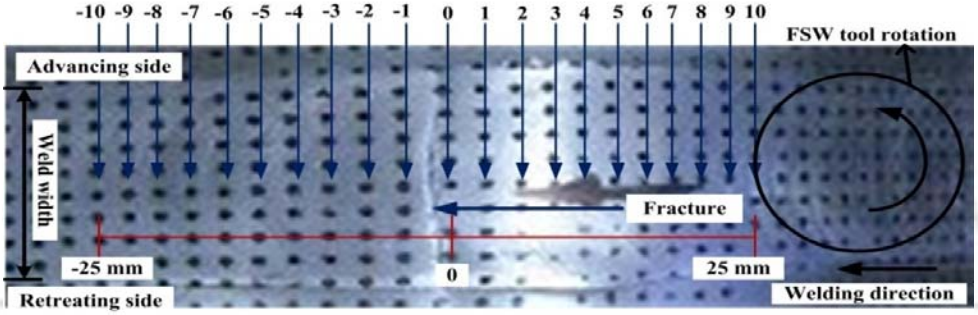

Fig. 6.3 Thickness measurement method for FSW sheets and unwelded sheets

6.2 Results and discussion

6.2.1 Failure pattern during limit dome height (LDH) test of unwelded and FSW blanks

In order to investigate the overall formability performance of the FSW blanks during stretching and also to analyze the effects of shoulder diameters and plunge depths, LDH tests were performed experimentally with different lubricants and sheet dimensions for the welded and unwelded sheets. The sheet dimension and lubrication together have generated few different strain paths required for forming limit evaluation. Two strain paths with sheets having 100 mm x 200 mm and 125 mm x 200 mm dimensions were considered. Deformed unwelded blanks and FSW blanks with different lubricants are shown in the Fig. 6.4 to 6.6 for illustration. Failure pattern in unwelded blanks is same in all the strain paths during LDH test as shown Fig. 6.4. The failure observation, near punch nose region, agrees with expected result that is generally seen in other base materials also. In the case of FSW blanks, failure pattern in 100 mm x 200 mm strain path is perpendicular to the weld like in unwelded blanks,

whereas in 125 mm x 200 mm strain path failure is seen at interface of weld as shown in Fig. 6.5 and 6.6. The main reason behind the change in failure pattern is due to the change in strain path from near plane strain (100x200 mm) to stretching (125x200 mm). Failure is expected to occur along the weld region even in other stretching strain paths generated by different lubricants and sheets dimensions (like 150x200, 175x200, and 200x200 mm). The failure pattern is correlating with the results shown in Miles *et al.*, 2005 work where in all the FSW specimens of AA 6022 failed on either side of the weld. The data containing major strain and minor strain from the deformed sheets for constructing FLCs is analyzed further to study the formability of FSW blanks.

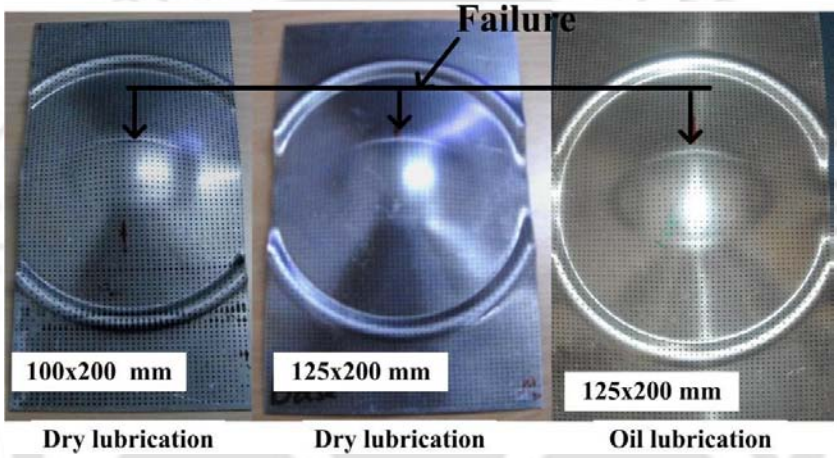

Fig. 6.4 Deformed samples of unwelded blanks at different lubrication conditions

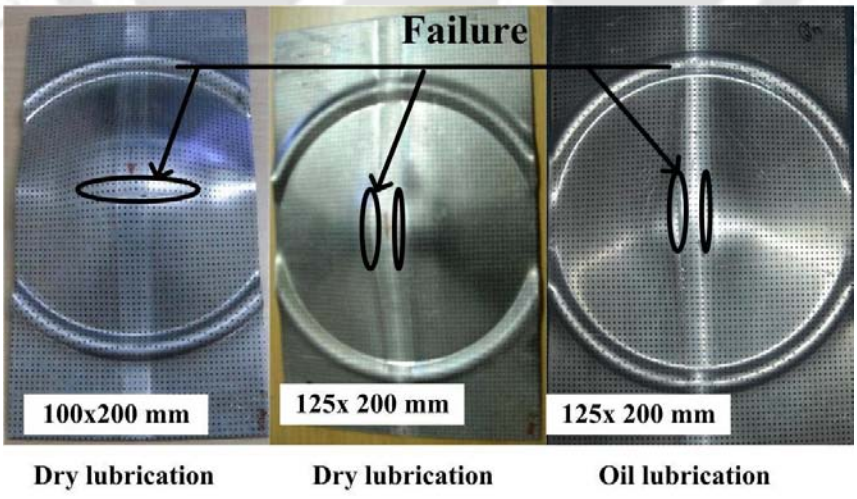

Fig. 6.5 Deformed FSW blanks made at 1.9 mm plunge depth with 12 mm shoulder diameter, 1300 rpm tool speed and 90 mm/min welding speed at different lubrication conditions and strain paths

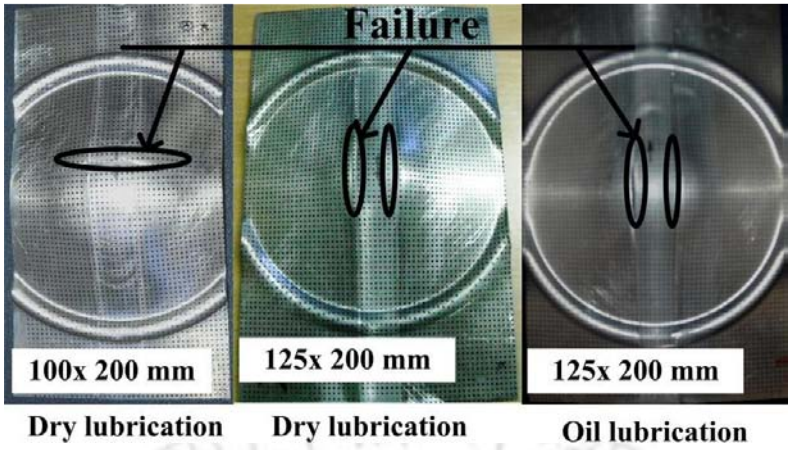

Fig. 6.6 Deformed FSW blanks made at 1.85 mm plunge depth with 18 mm shoulder diameter, 1300 rpm tool speed and 90 mm/min welding speed at different lubrication conditions and strain paths

6.2.2 Influence of shoulder diameter on the forming limit of FSW blanks

The shoulder diameter of the tool is an important parameter because it generates most of the heat, and its grip on the plasticized materials largely establishes the material flow field (Elangovan and Balasubramanian, 2008). Experimental investigations of Elangovan and Balasubramanian, 2008 have shown that shoulder diameter plays a vital role in the FSW to make high strength joints. If joint strength is good, then the formability of the joint improves because of the delayed failure. In this section, for defect free FSW condition, the influence of shoulder diameter on the forming limit of FSW blanks is analyzed.

The selected different welding conditions are listed in Table 6.1 by which all the FSW joints were fabricated. The influence of the shoulder diameter with different FSW conditions (1 to 4 in Table 6.1) on FLC of FSW blanks are compared with unwelded blank FLC as shown in the Fig. 6.7 to 6.10. Figure 6.7 shows the master FLD presenting the effect of different shoulder diameters (12 mm and 18 mm) on the FLCs of FSW blanks at constant welding speed of 90 mm/min, tool rotation speed of 1300 rpm and plunge depth of 1.85 mm (FSW condition 1 in Table 6.1). It is observed that forming limit of the unwelded blank and two FSW blanks are almost same in near plane-strain (100 x 200 mm) strain path and base material formability decreases significantly in stretching strain paths, reducing its overall formability. When FSW blank FLCs are compared, FSW sheets made with 18 mm shoulder diameter has better forming limit than FLC of 12 mm shoulder diameter in stretching strain paths. The percentage difference in true major strain values between base material and FSW blank with 12 mm shoulder diameter is 3% and with 18 mm shoulder diameter is 9%. When percentage difference is seen within the FSW blanks, there is no difference in the plane-strain

strain path and 6% difference is witnessed in stretching side. This percentage difference is calculated from major strain values presented in Table 6.2.

Likewise it is observed from Fig. 6.8 that the forming limit of the FSW blanks fabricated with different shoulder diameters (12 mm and 18 mm) at 1300 rpm rotational speed, 90 mm/min welding speed and plunge depth 1.9 mm (FSW condition 2 in Table 6.1) is better than un-welded blank, with higher tool shoulder diameter (18 mm) showing a better forming limit. It is observed that forming limit of the FSW blank made of 12 mm shoulder diameter has better forming limit than other two FLCs in near plane strain path and it decreases significantly in stretching strain paths, whereas unwelded blank has lower FLC in stretching side. A percentage difference of 2% and 3% is seen in the plane strain stretching strain paths between the FSW sheets made with 12 mm and 18 mm shoulder diameter tool and base material. In stretching strain paths a much larger difference (about 15% and 7%) is found between FSW blanks and base materials. There is about 5-8% difference between the forming limit major strains of FSW sheets made with 12 mm and 18 mm shoulder diameter tools.

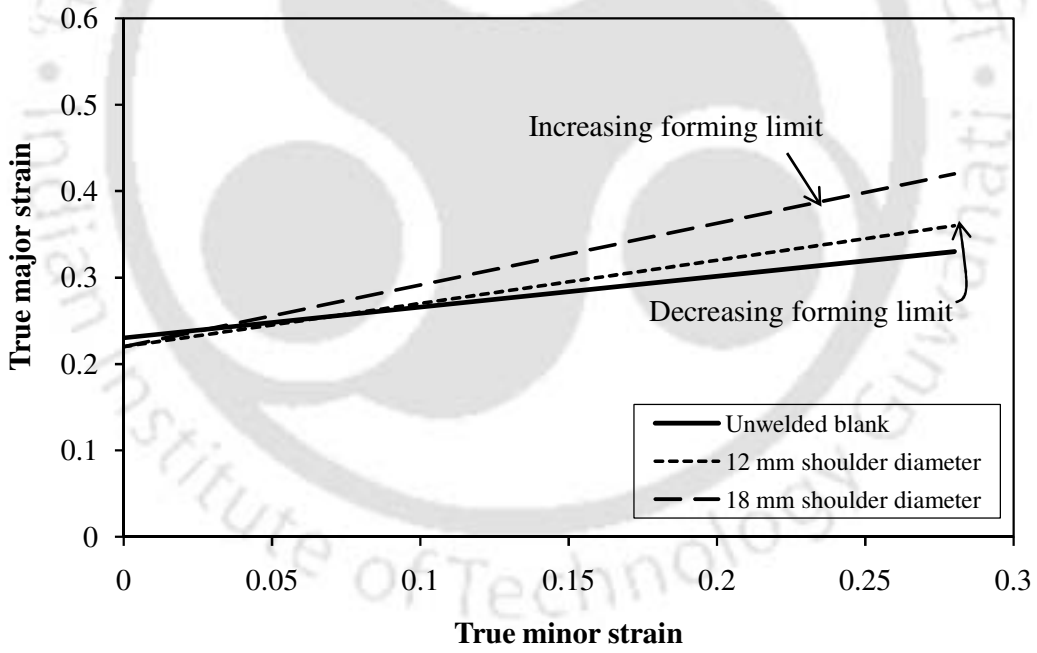

Fig. 6.7 Influence of shoulder diameter on forming limit strains of FSW blanks at plunge depth of 1.85 mm, tool rotation speed 1300 rpm and welding speed 90 mm/min

Similar formability tests were carried out for other two FSW conditions (3 and 4 in Table 6.1) with 1400 rpm rotation speed. In general, it is found that the forming limit of FSW blank is better than that of base material. Moreover the forming limit of FSW blank made with 18 mm shoulder diameter is better than FSW blank made with 12 mm shoulder diameter (Fig.

6.9 and 6.10). Similar results are observed in the case of FSW blanks made with 1300 rpm rotation speed discussed earlier. It should be noted that for FSW blank made at 1.9 mm plunge depth, the forming limit in the case of FSW sheet made with 18 mm shoulder diameter is lower than at 12 mm in near plane-strain condition, but improves in the stretching side (Fig. 6.10).

In whole, the forming limit of FSW blanks is higher than that of base material. With increase in shoulder diameter, the forming limit is found to improve considerably. In two cases, the forming limit of FSW blanks made with 12 mm shoulder diameter tool, in plane-strain stretching condition, is better than FSW blanks made with 18 mm shoulder diameter, while a considerable improvement in forming limit is seen on the stretching side with increase in shoulder diameter.

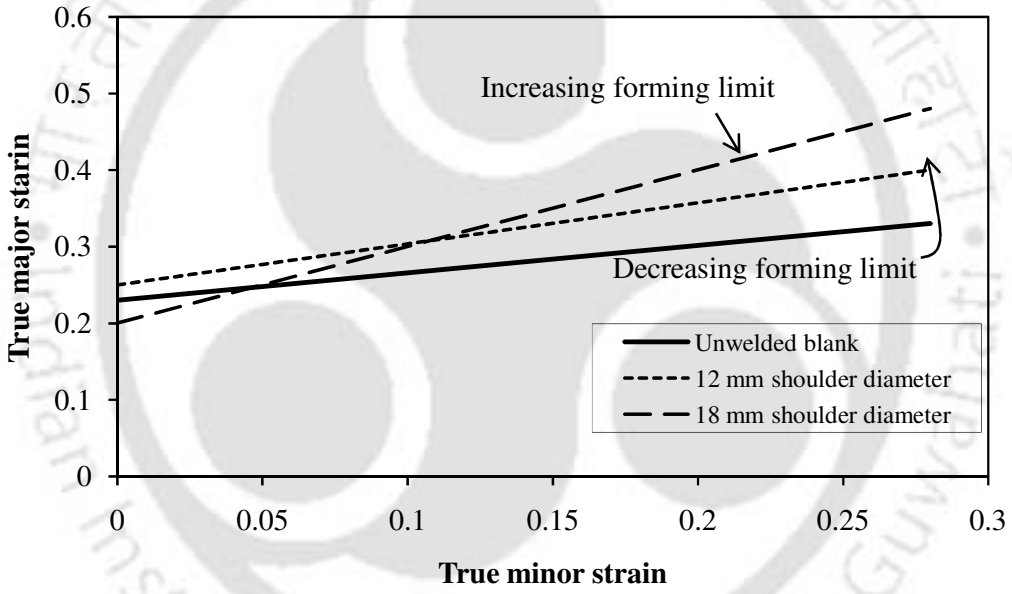

Fig. 6.8 Influence of shoulder diameter on forming limit strains of FSW blanks at plunge depth of 1.9 mm, tool rotation speed 1300 rpm and welding speed 90 mm/min

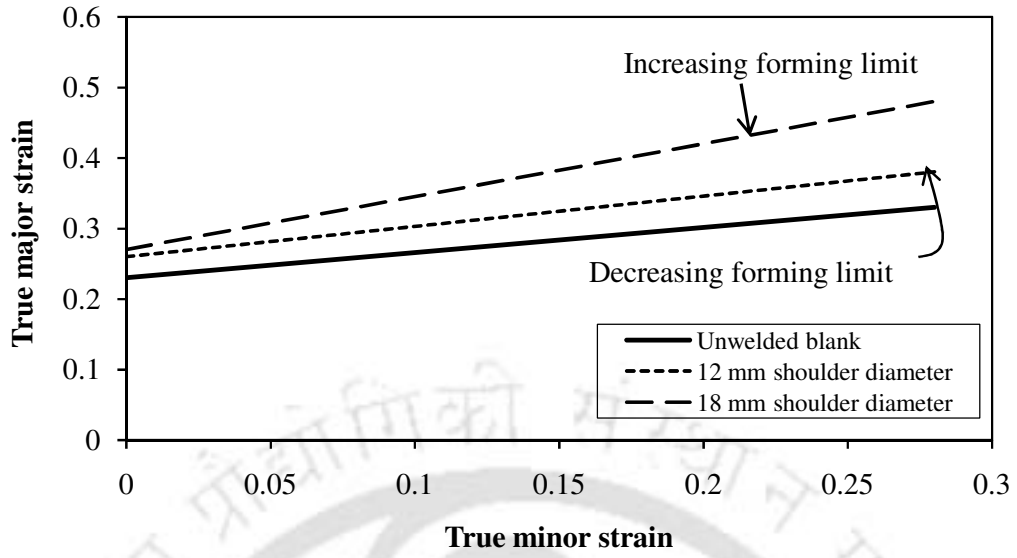

Fig. 6.9 Influence of shoulder diameter on forming limit strains of FSW blanks at plunge depth of 1.85 mm, tool rotation speed 1400 rpm and welding speed 90 mm/min

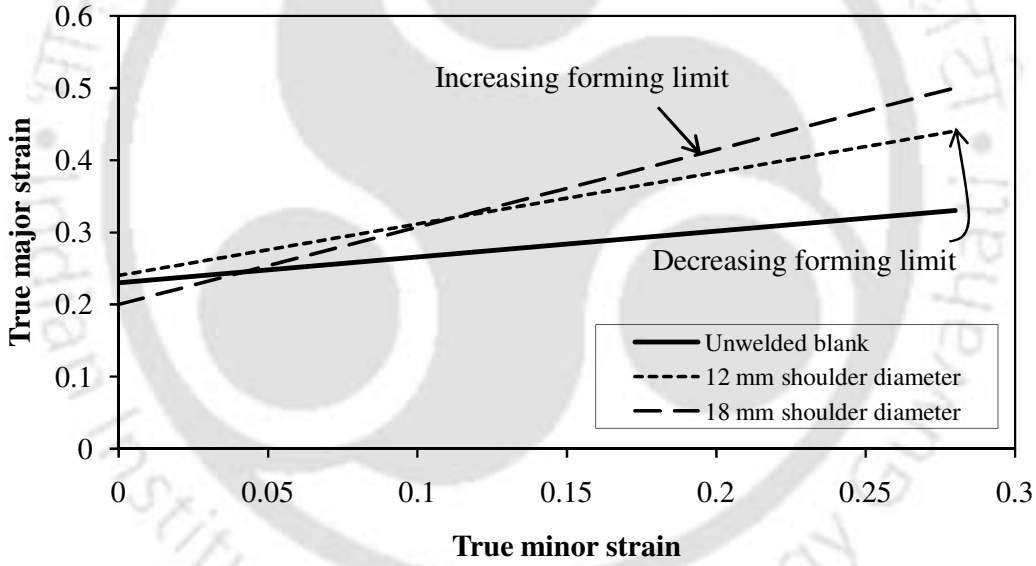

Fig. 6.10 Influence of shoulder diameter on forming limit strains of FSW blanks at plunge depth of 1.9 mm, tool rotation speed 1400 rpm and welding speed 90 mm/min

6.2.3 Influence of plunge depth on the forming limit of FSW blanks

The plunge depth is the depth of the lowest point of the FSW tool below the surface of the welded material and has been found to be a critical parameter for ensuring weld quality. During welding, plunging the shoulder below the weld material surface increases the force below the tool and helps in ensuring adequate forging of the material at the bottom of the tool. Because of this frictional heat and deformation heat develops adequately. These

frictional heat and deformation heat are utilized for the perfect bonding under the applied axial force. In this section, plunge depth is changed within the optimized range at which defect free welds are formed. The plunge depth is varied from 1.85 to 1.9 mm and the influence on FLCs was observed.

The influence of the plunge depth on the forming limit of FSW blanks and their comparison with unwelded blank FLC is depicted in Fig. 6.11 to 6.14. Fig. 6.11 shows the master FLD presenting the effect of different plunge depths (1.85 mm and 1.9 mm) on the FLCs of FSW blanks which are fabricated at 90 mm/min welding speed, 1300 rpm tool rotation speed and tool with 12 mm shoulder diameter (FSW condition 5 in Table 6.1). It can be observed that forming limit of the FSW blanks are better than that of the unwelded blank and percentage difference in plane-strain stretching between the true major strain values of base material and FSW blanks is about 1-2%. But in stretching side, an improvement of 3% and 7 % in major limit strain is seen in both the plunge depths as compared to base metal. So with the increase in plunge depth, the forming limit has increased with a difference of 4 % between the FSW blanks in the stretching side. With increase in the shoulder diameter to 18 mm (condition 7 in Table 6.1), the forming limit of FSW blanks has improved as compared base material (Fig. 6.12) for different plunge depths. There is a large improvement of forming limit (approximately 15%) in stretching side, while the limit strains of FSW blanks are same, as that of base material in the plane-strain stretching condition.

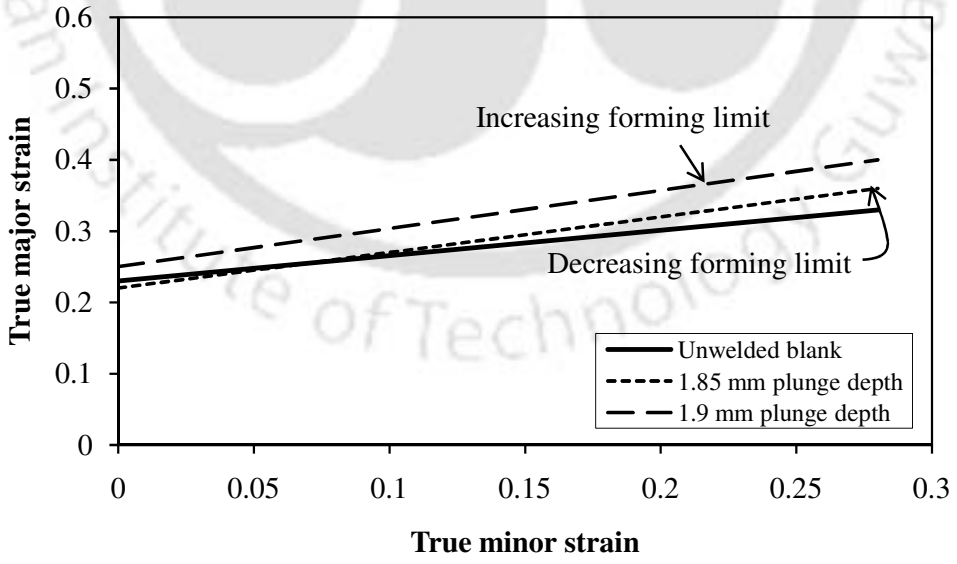

Fig. 6.11 Influence of plunge depth on forming limit strains of FSW blanks with 12 mm shoulder diameter at tool rotation speed of 1300 rpm and welding speed of 90 mm/min

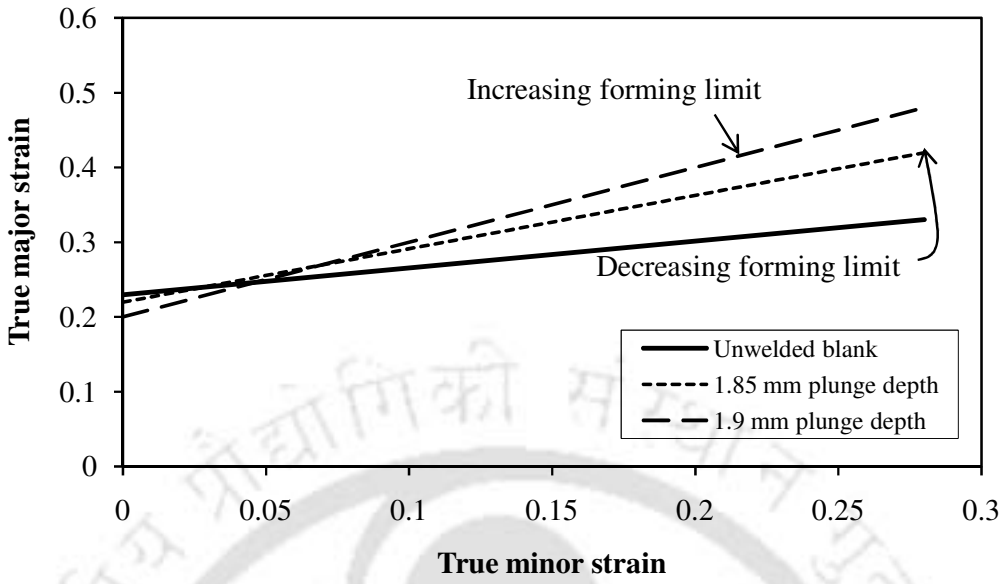

Fig. 6.12 Influence of plunge depth on forming limit strains of FSW blanks with 18 mm shoulder diameter at tool rotation speed of 1300 rpm and welding speed of 90 mm/min

Similar formability tests were carried out for other two FSW conditions (conditions 6 and 8 Table 6.1) with 1400 rpm rotation speed. In general, it is found that the forming limit of FSW blank is better than that of base material. Moreover the forming limit of FSW blank made at 1.9 mm plunge depth is better than FSW blank made at 1.85 mm plunge depth (Fig. 6.13 and 6.14). A similar result is observed in the case of FSW blanks made with 1300 rpm rotation speed discussed earlier.

It should be noted that for FSW blank made with 12 mm shoulder diameter tool, the forming limit of FSW blank made at 1.9 mm plunge depth is lower than at 1.85 mm plunge depth in near plane-strain condition, but improves in the stretching side (Fig. 6.13). Whereas in case of FSW blanks made with 18 mm shoulder diameter tool, the forming limit at 1.9 mm plunge depth and 1.85 mm plunge depth are same in near plane-strain condition, but 1.9 mm plunge depth showed an improved forming limit on the stretching side (Fig. 6.14).

In whole, the forming limit of FSW blanks is higher than that of base material. With increase in plunge depth, the forming limit is found to improve considerably. In two cases, the forming limit of FSW blanks made at 1.85 mm plunge depth, in near plane-strain condition, is better than at 1.9 mm plunge depth and later in stretching side the performance is vice-versa.

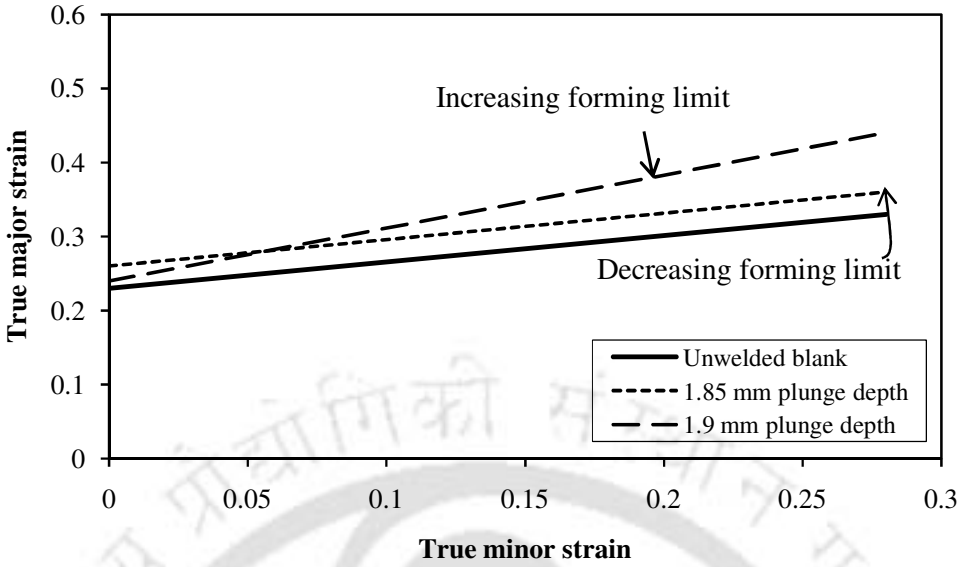

Fig. 6.13 Influence of plunge depth on forming limit strains of FSW blanks with 12 mm shoulder diameter at tool at tool rotation speed of 1400 rpm and welding speed of 90 mm/min

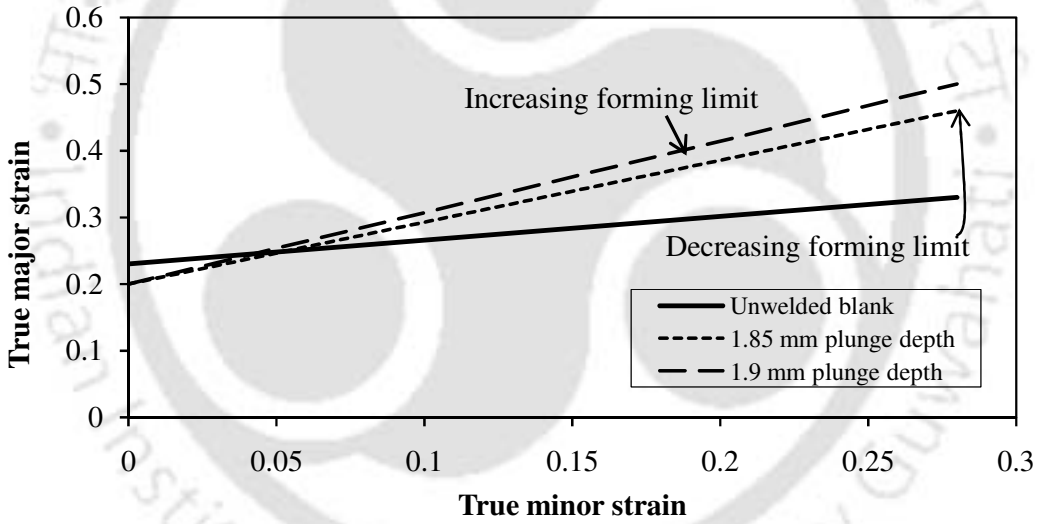

Fig. 6.14 Influence of plunge depth on forming limit strains of FSW blanks with 18 mm shoulder diameter at tool rotation speed of 1400 rpm and welding speed of 90 mm/min

In the third level, FSW blank is made with a tool of 15 mm shoulder diameter at 1500 rpm rotational speed, 120 mm/min welding speed and 1.95 mm plunge depth (FSW condition 9 in Table 6.1). The overall formability of the FSW sheets is better than the unwelded blank and when all FSW sheets FLCs are compared, 15 mm shoulder diameter FLC is in between 12 mm and 18 mm shoulder diameter FLCs in the stretching side strain path. This comparison is shown in Fig. 6.15.

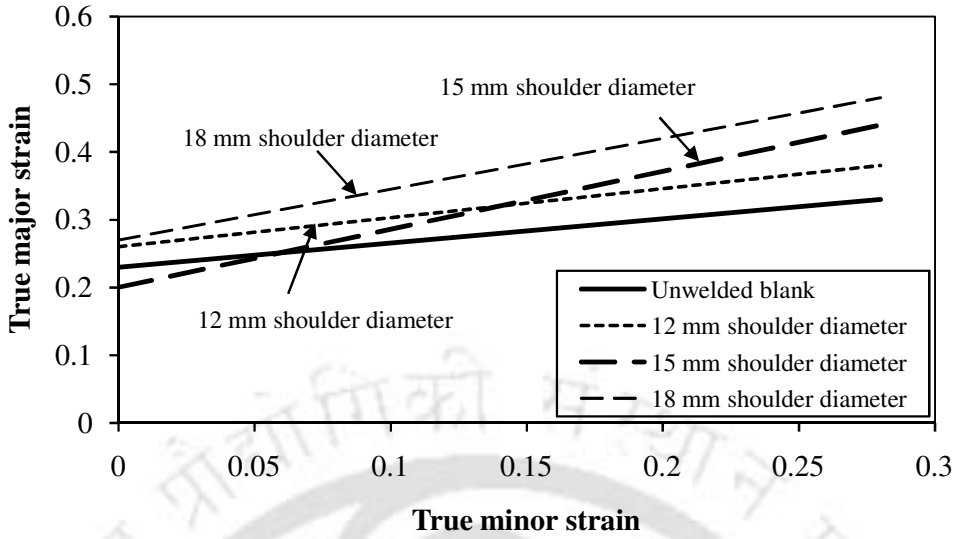

Fig. 6.15 Forming limit strains of FSW blanks made at condition 9 in Table 3 and comparison with 12 mm, 18 mm shoulder diameter and unwelded sheet FLCs

6.2.4 Thinning behavior of FSW sheets

In general, 'necking' can be understood as a phenomenon occurring in sheets because of the presence of initial thickness heterogeneity in the material, as a result of which material thinning occurs during the course of deformation or forming. The more the thinning gradient (at a particular punch travel), the earlier the limits strain will be reached, and hence a lower formability or forming limit is expected. In the case of FSW blanks, the presence of weld region and the properties of weld region can result in an increased or decreased thinning gradient in comparison with that of the unwelded blank. This, in turn, depends on the process parameters that are used to fabricate the FSW joints. Moreover thickness distribution during the sheet forming is an important index that quantifies the formability of sheet material. Even in industrial practice, thinning percentage or gradient is generally mentioned as a parameter that has to be monitored for the quantification of formability. A better or uniform thinning behavior implies a better formability of that sheet material.

In this section, an attempt has been made to relate the change in forming limit of FSW sheets with the thinning behavior during forming. The thinning behavior is evaluated by monitoring the thickness distribution after forming the FSW sheets described earlier.

6.2.4.1 Thinning behavior of FSW blanks made with different shoulder diameters

The thinning behavior of FSW blanks made with variable shoulder diameters in comparison with that of the unwelded blank is presented in Fig. 6.16 to 6.19. The thickness is

measured normal to the necked region using a micrometer with reference to the dot grids marked on the deformed surface at an interval of 2.5 mm sheet surface. The averaged thickness data is recorded at a point for three repetitions. Figure 6.16 shows the thickness distribution of unwelded blank and FSW blanks made at condition 1 in Table 6.1. It is observed that FSW blanks of 12 mm and 18 mm shoulder diameters have minimum thinning gradient as compared to unwelded blank near fracture. This resulted in reduced FLC for the unwelded blanks when compared to FSW blanks of 12 mm and 18 mm shoulder diameters as described in Fig. 6.7. The uniformity in thinning gradient of unwelded blank and FSW blanks can be understood from Fig. 6.17. It shows that the thinning gradient from one end to other end of unwelded blank and FSW blanks is almost similar, except in the fracture region at which thinning gradient is very sensitive. There is a sudden drop in the thickness variation in all the cases because of necking and hence a sudden and localized shoot up is observed in the thickness difference. When thickness difference is observed among three blanks, unwelded sheet has more thickness difference (0.47 mm) near to fracture; whereas in FSW blanks, 12 mm shoulder has more thickness difference (0.19 mm) as compared to 18 mm shoulder diameter which exhibit 0.14 mm thickness difference only. This implies that FSW blanks made at 18 mm shoulder diameter exhibit uniform thickness distribution as compared to the other two cases. The uniform thickness distribution has improved the forming limit of FSW blanks made at 18 mm shoulder diameter as presented in Fig. 6.7.

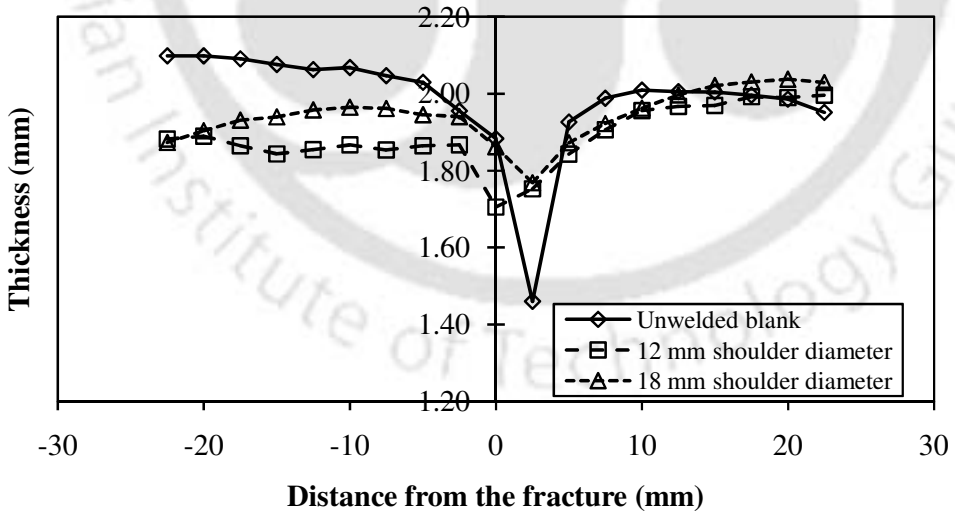

Fig. 6.16 Comparison of experimental thickness distribution of FSW blanks of different tool shoulder diameters (12 and 18 mm) at 1.85 mm plunge depth, rotational speed of 1300 rpm and welding speed of 90 mm/min to unwelded blank in the LDH test

Figure 6.18 shows the thinning behavior comparison of unwelded blank with FSW blanks at 1400 rpm for different shoulder diamters (condition 4 in Table 6.1). Even in this case, it is

observed that unwelded blanks has more thinning gradient than FSW blanks; whereas in FSW blanks, 12 mm shoulder diameter FSW blank has more thinning gradient than 18 mm shoulder diameter FSW blank near to fracture irrespective of other process parameters. When thickness difference (Fig. 6.19) is observed, unwelded blank has more thickness difference (0.47 mm) near to fracture; whereas in FSW blanks, 12 mm shoulder has more thickness difference (0.28 mm) as compared to 18 mm shoulder diameter. This resulted in reduced FLC for the unwelded blanks when compared to FSW blanks as shown in Fig. 6.10.

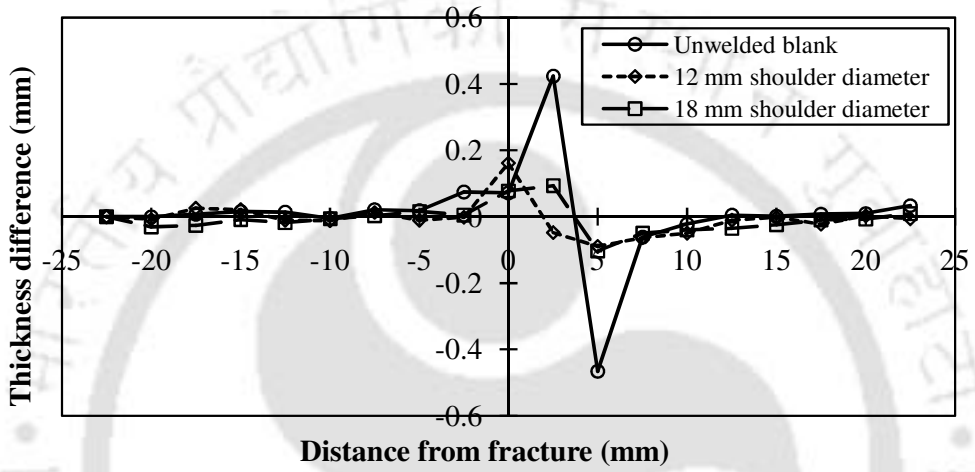

Fig. 6.17 Comparison of thickness gradient uniformity of FSW blanks of different tool shoulder diameters (12 and 18 mm) at 1.85 plunge depth to unwelded blank

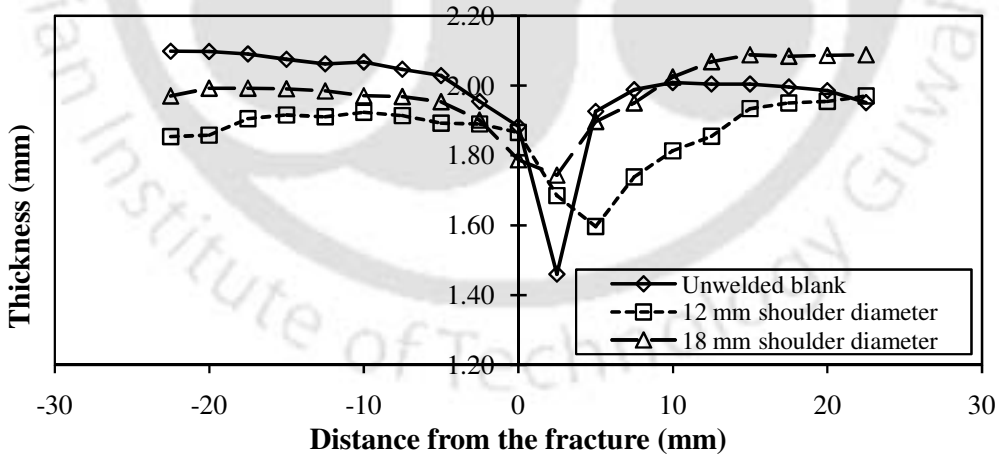

Fig. 6.18 Comparison of experimental thickness distribution of FSW blanks of different tool shoulder diameters (12 and 18 mm) at 1.9 mm plunge depth, rotational speed of 1400 rpm and welding speed of 90 mm/min to unwelded blank in the LDH test

Similar observation is seen in other FSW conditions (condition 2 and 3 in Table 6.1) that thinning gradient is more for unwelded blank than FSW blanks, and then FSW sheet made with tool 12 mm shoulder diameter has more thinning gradient than 18 mm shoulder

diameter FSW blank. Thinning gradient sensitivity is more for 12 mm shoulder diameter in all the cases as compared to 18 mm shoulder diameter. Because of this the overall formability of unwelded blank and 12 mm shoulder diameter FSW blanks is reduced as compared to FSW sheets made with 18 mm shoulder diameter tool.

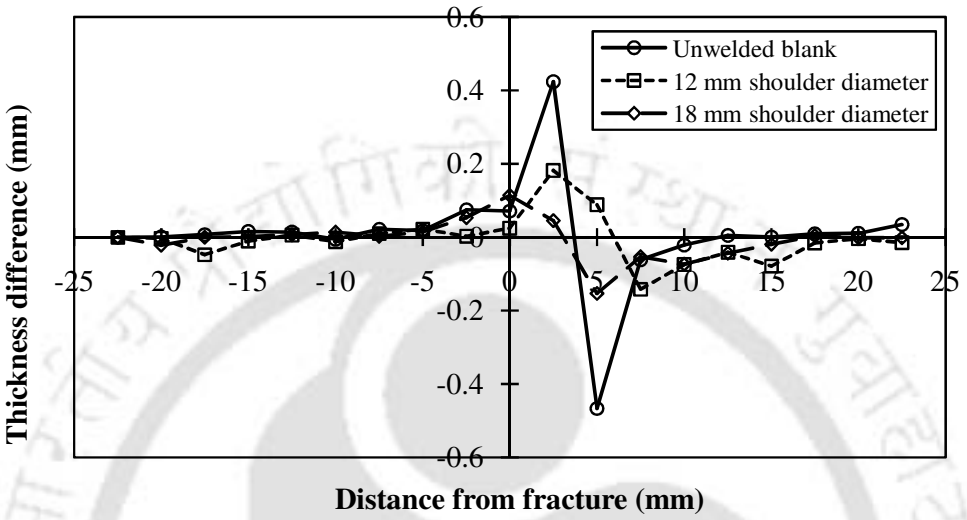

Fig. 6.19 Comparison of thickness gradient uniformity of FSW blanks of different tool shoulder diameters (12 and 18 mm) at 1.9 plunge depth to unwelded blank

6.2.4.2 Thinning behavior of FSW blanks at different plunge depths

The thinning behavior of FSW blanks in comparison with that of unwelded blank by considering the variable plunge depth is presented in Fig. 6.20 to 6.23. Figure 6.20 shows the thickness distribution of unwelded blank and FSW blanks made at FSW condition 6 at different plunge depths (1.85 and 1.9 mm). It is observed that FSW blanks made at 1.85 mm and 1.9 mm plunge depths exhibit minimum thinning gradient as compared to unwelded blank near fracture. This resulted in reduced FLC for the unwelded blanks when compared to FSW blanks as shown in Fig. 6.12. But the thickness distribution of FSW blanks as presented in Fig. 6.21 is almost same. The uniformity in thinning gradient of unwelded blank and FSW blanks can be understood from Fig. 6.21, which shows that the thinning gradient of unwelded blank and FSW blanks is almost similar except near necked region. When thickness difference is observed among three blanks, unwelded blank has more thickness difference (0.47 mm) near to fracture; whereas FSW blanks at different plunge depths show almost same thickness difference distribution (Fig. 6.21). This basically has reflected in forming limit in Fig. 6.12 where in the FLCs of FSW blanks at two different plunge depths are almost same with very less difference between them at near plane-strain strain path.

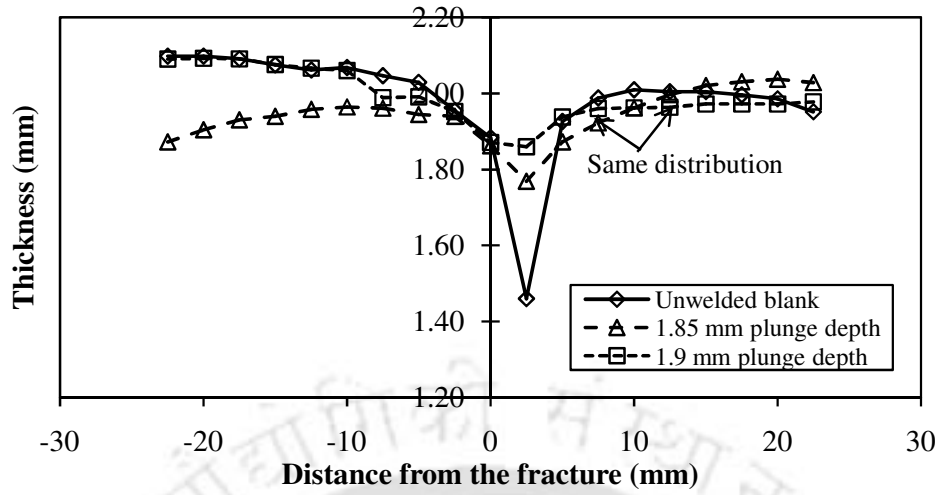

Fig. 6.20 Comparison of experimental thickness distribution of FSW blanks of different plunge depths (1.85 and 1.9 mm) at rotational speed of 1300 rpm and welding speed of 90 mm/min using 18 mm tool shoulder diameter to unwelded blank in the LDH test

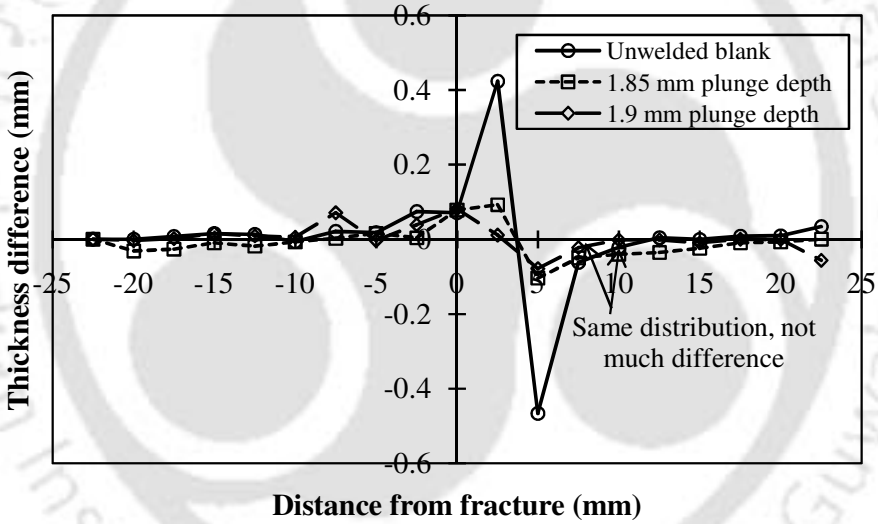

Fig. 6.21 Comparison of thickness gradient uniformity of FSW blanks at different plunge depths (1.85 and 1.9 mm) at 18 mm shoulder diameter to unwelded blank

In the case of FSW condition 8 in Table 6.1, the thinning gradient is more for unwelded blank than FSW blanks at different plunge depths, and then 1.85 mm plunge depth FSW blank has more thinning gradient than 1.9 mm plunge depth FSW blank (Fig. 6.22 and 6.23). The overall formability of 1.85 mm plunge depth FSW blanks and unwelded blank is reduced as compared to 1.9 mm plunge depth FSW blank.

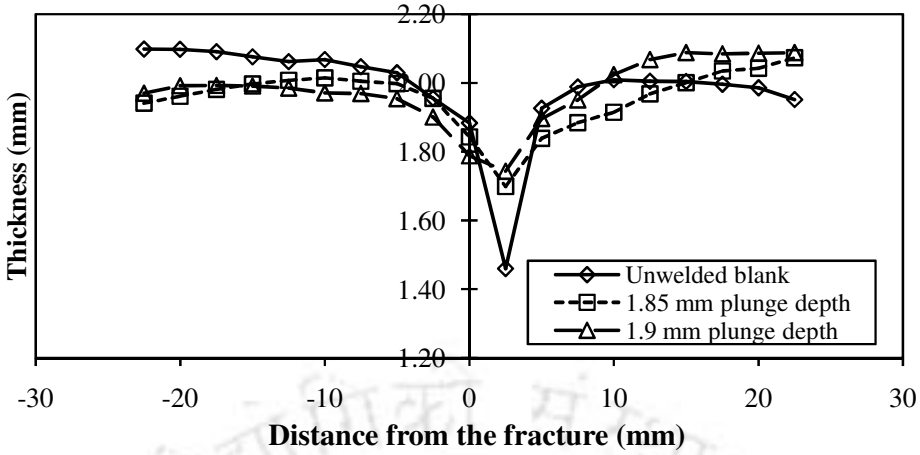

Fig. 6.22 Comparison of experimental thickness distribution of FSW blanks of different plunge depths (1.85 and 1.9 mm) at rotational speed of 1400 rpm and welding speed of 90 mm/min using 18 mm tool shoulder diameter to unwelded blank in the LDH test

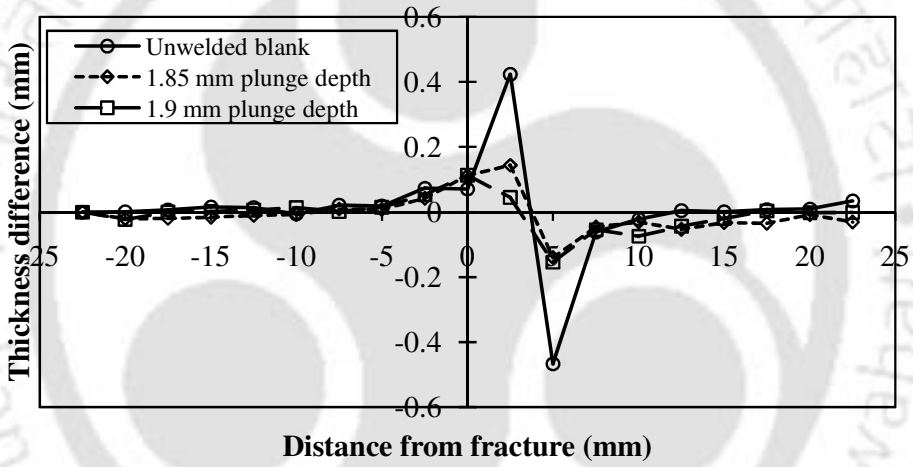

Fig. 6.23 Comparison of thickness gradient uniformity of FSW blanks at different plunge depths (1.85 and 1.9 mm) at 18 mm shoulder diameter to unwelded blank

6.2.5 Effect of shoulder diameter and plunge depth on strain hardening coefficient (*n*) and its relation with forming limit of FSW blanks

The strain-hardening coefficient influences the strain distribution in a forming operation. Increasing '*n*' value distribute the strain and thickness uniformly in sheets during forming. If strain distribution is uniform, then FLC is likely to improve. For example, Fig. 6.24 shows the thickness distribution of a sheet made of a standard steel grade formed at biaxial strain path having different '*n*' values by keeping all other properties constant (namely: Young's modulus, Poission's ratio, density, plastic strain ratio) with initial sheet thickness of 2 mm. The standard LDH test was simulated in PAM STAMP 2G for each blank. The base material

blank was comprised of quadrilateral shell elements of Belytschko-Tsay formulation with five through thickness integration points. Hollomon's strain hardening law and Hill's 1948 isotropic hardening yield criterion was used as the plasticity model. This thickness distribution is measured perpendicular to the failure at same punch travel before failure. It is observed from Fig. 26 that a sheet with n = 0.3 exhibits uniform thickness distribution when comaperd to the case with n = 0.15. So improvement in 'n' value improves the thickness distribution uniformity during sheet forming.

From the earlier sections, it is observed that FSW blanks of higher tool shoulder diameter and plunge depth exhibit better FLC and lesser thinning gradient. Table 6.3 summarises the strain hardening exponent values obtained from tensile test of FSW blnaks with longitudinal weld made at varaible welding conditions.

It is seen from Table 6.3 that FSW blanks with 18 mm tool shoulder diameter exhibits higher 'n' value than 12 mm tool shoulder diameter and unwelded blank. This has resulted in better FLC for FSW blanks made with 18 mm shoulder diameter compared to 12 mm shoulder diameter and unwelded sheet. It should be noted that FSW sheets made using 15 mm shoulder diameter tool is in between 12 mm and 18 mm shoulder diameter tool in the most of the cases.

The effect of plunge depth on the strain hardening exponent of FSW blank is also illustrated in Table 6.3. It can be said that there is not much difference in 'n' values with respect to different plunge depths. The change in 'n' value with respect to plunge depths is relatively less as compared to the changes with respect to shoulder diameter. In the case of 18 mm shoulder diameter, the change in 'n' values with respect to different plunge depths are not much significant which lead in the same thickness gradient (Fig. 6.20, 6.22) and hence same FLCs (Fig. 6.12, 6.14) at near plane-strain strain path of FSW sheets.

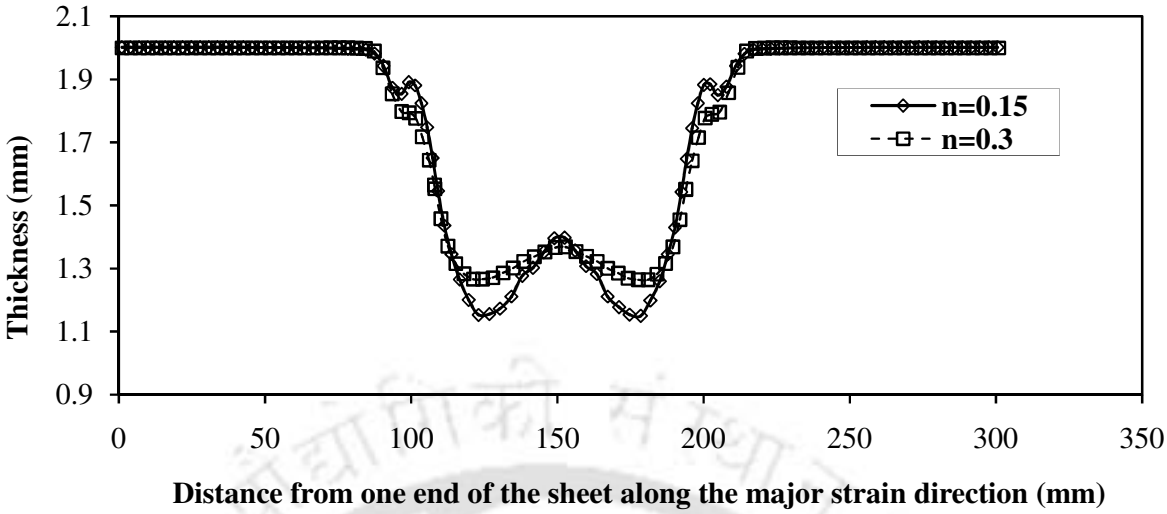

Fig. 6.24 Thickness distribution of unwelded sheet at different '*n*' values at same punch travel for biaxial strain path

Table 6.3 Strain hardening coefficient (*n*) values of FS welded sample at different FSW conditions with variable shoulder diameters and plunge depths

FSW conditions	Shoulder diameter (mm)	Plunge depth (mm)	Tool rotation speed (rpm)	Welding speed (mm/min)	Strain hardening coefficient (*n*)
1	12	1.85	1300	90	0.23
	18				0.27
2	12	1.9	1300	90	0.24
	18				0.28
3	12	1.85	1400	90	0.24
	18				0.27
4	12	1.9	1400	90	0.25
	18				0.3
5	15	1.95	1500	120	0.27

As the shoulder diameter and plunge depth increases, the temperature in the stirring zone is expected to increase. This means that the final grain size would be larger (Kumar and Satish, 2008) and it is also expected that the dislocation density reduces as the temperature increases. It leads to more static recrystallization in the WN region. Strain hardening behavior is typically related to the accumulation and interaction of the dislocations. If the dislocation density is lower more strain can be induced in the material, thus increasing the ductility and so it's forming limit has improved. In contrast, in the base material, the saturation of the dislocation density results in the low strain hardening and poor ductility resulting in less formability. The relation between improvement in strain hardening exponent in weld zone and dislocation density has been studied by Woo *et al.*, 2008 through X-ray peak profile analyses.

6.2.6 Effect of shoulder diameter and plunge depth on dome height

Table 6.4 shows dome height comparison of all FSW sheets deforemd at different lubricants (dry, oil and grease). It can be observed that dome height of FSW blanks is more compared to the unwelded blank in near plane-strain strain path, whereas in 125x200 mm strain path unwelded blank has more dome height than all FSW sheets. This is mainly due to the failure occuring in the weld region parallel to the major strain direction in stretching strain path. But in the case of near plane-strain strain path, failure is witnessed normal to the weld region. It is also observed that there is not much variation in dome height with respect to varied plunge depth and shoulder diameter, unlike in forming limit curve and thickness distribution. There is hardly 1-2 mm variation in dome height in all FSW cases.

Table 6.4 Dome height of FSW blanks at different FSW conditions

FSW conditions	Shoulder diameter (mm)	Plunge depth (mm)	Tool rotation speed (rpm)	Welding speed (mm/min)	Dome height (mm) at two strain paths at three lubricant conditions					
					100x200 mm			125x200 mm		
					Dry	Oil	Grease	Dry	Oil	Grease
Base material					27.1	27.04	27.02	28	28.08	28
1	12	1.85	1300	90	29.1	28.03	29.08	18.1	19.08	17.06
	18				28.1	28.14	29	19.1	18.08	18
2	12	1.9	1300	90	29.1	28.02	29	19.1	19.1	17.18
	18				28.2	28.14	28.1	19	19.08	17.1
3	12	1.85	1400	90	28.2	28.1	28.08	20	18.08	17.1
	18				28.	27.02	29.06	19	18.14	17.16
4	12	1.9	1400	90	29.2	28.1	28.14	19.2	19.14	17.16
	18				29.1	29.06	30.16	19.2	19.16	18.06
5	15	1.95	1500	120	31.1	29.12	29.12	23.1	18.16	17.06

6.2.7 Effect of shoulder diameter and plunge depth on thickness distribution in advancing side (AS) and retreating side (RS) of FSW blanks

In general, welds produced by FSW are asymmetric. Since on one side of the weld called as advancing side (AS), the direction of rotation of the tool coincides with the welding direction, while on the other side, the retreating side (RS), the direction of rotation of the tool is opposite to the welding direction (Heurtier *et al.*, 2006). Therefore, a material element on the advancing spends a longer time and is more influenced by the vortex velocity field than on the retreating side. As a result, the strain, grain structure refinement (Heurtier *et al.*, 2006), temperature (Song and Kovacevic, 2003; Kim et al., 2009), shear rate, friction bonding, material flow (Leal *et al.*, 2008; Kumar and Kailas, 2008), residual stresses (Scialpi *et al.*, 2007), mechanical properties [Mahoney *et al.*, 1998; Sato and Kokawa, 2001; Heinz and

Skrotzki 2002; Liu *et al.*, 2003; Simalr *et al.*, 2008; Zadpoor *et al.*, 2010; Rajakumar *et al.*, 2011) are higher on the advancing side than on the retreating side. For example, for FSW 6063 aluminum alloy, after post weld heat treatments, the maximum hardness found in the advancing side and retreating side is 82 and 78 HV respectively (Sato and Kokawa, 2001). Similarly, in the case of FSW of AA 6005A-T6 aluminum alloy, a hardness of 110 HV is seen in AS and 104 HV in RS (Simalr *et al.*, 2008). Since the asymmetric properties are preserved in the weld region before forming, there are possibilities that it will affect the thickness distribution and strain distribution after forming. Hence the thickness distribution along the AS and RS of the weld region is monitored and compared for analysis.

The thickness distribution is compared for different shoulder diameters (12 mm and 18 mm) and at different plunge depths (1.85 and 1.9 mm). Figure 6.25 illustrates the thickness distribution comparison in AS and RS of FSW blanks made at different shoulder diameters at rotational speed of 1300 rpm and welding speed of 90 mm/min using 1.85 mm plunge depth. It is observed that for 12 mm shoulder diameter (Fig. 6.25 a), the thickness gradient is severe in RS as compared to AS. But in 18 mm shoulder diameter, both the sides show almost same thinning gradient (Fig. 6.25 b).

It is also seen from Table 6.5 that maximum thickness difference is higher in the RS, rather than in AS of the weld, independent of FSW parameters chosen. This maximum thickness difference is obtained between the consecutive data from left to right side in the respective thickness distributions. The effect of plunge depth is also seen from the maximum thickenss difference shown in Table 6.5. At a shoulder diameter of 12 mm, with increase in plunge depth from 1.85 to 1.9 mm, the maximum thickness distribution is found to decrease. At 18 mm shoulder diameter, though the maximum thickness difference is found to decrease with increase in plunge depth for 1300 rpm rotation speed, it has increased with increase in plunge depth for 1400 rpm rotation speed.

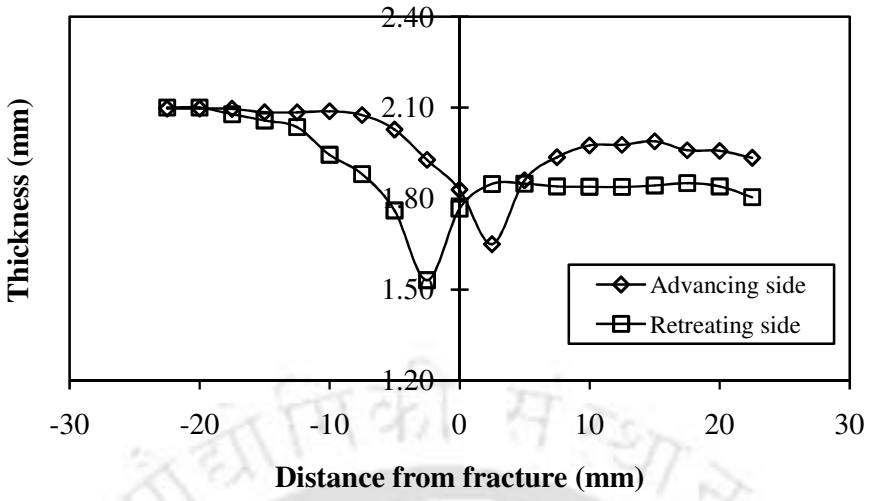

(a) 12 mm shoulder diameter

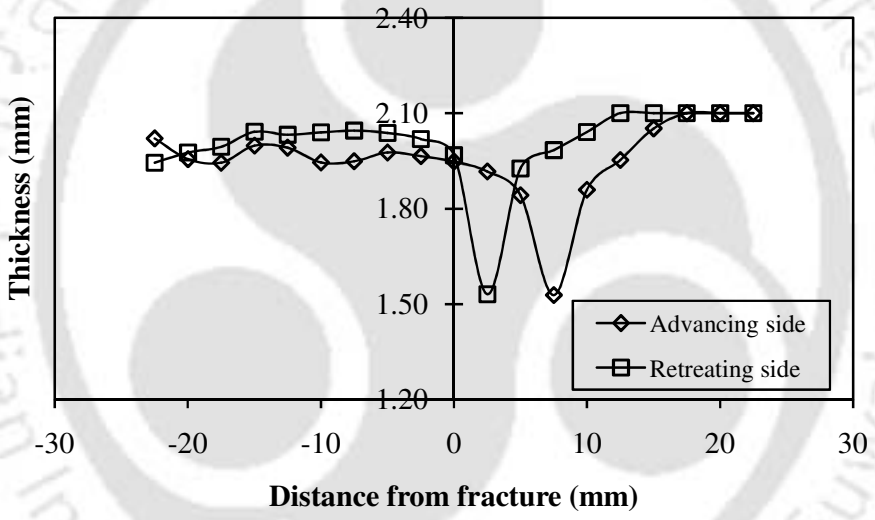

(b) 18 mm shoulder diameter

Fig. 6.25 Comparison of thickness distribution in AS and RS of FSW blanks of different shoulder diameters at rotational speed of 1300 rpm and welding speed of 90 mm/min using 1.85 mm plunge depth in the LDH test

Table 6.5 Thickness difference in AS and RS of FSW blanks at different conditions

FSW blank conditions				Maximum thickness difference (mm)	
Shoulder diameter (mm)	**Plunge depth (mm)**	**Tool rotation speed (rpm)**	**Welding speed (mm/min)**	**AS**	**RS**
12	1.85	1300	90	0.21	0.24
18	1.85	1300	90	0.33	0.44
12	1.9	1300	90	0.13	0.12
18	1.9	1300	90	0.08	0.14
12	1.85	1400	90	0.11	0.19
18	1.85	1400	90	0.10	0.16
12	1.9	1400	90	0.13	0.17
18	1.9	1400	90	0.39	0.49
15	1.95	1500	120	0.09	0.16

From the earlier discussion, it can be understood that the thickness distribution and maximum thickness difference is not same in advancing and retreating side of the weld. The main reason behind this is due to the differential straining attained by both the sides during FSW. It has been shown by Heurtier *et al.*, 2006, through numerical simulations that because of difference in material flow during welding, the advancing side exhibits higher strain than the retreating side. Since strain in higher is advancing side after FSW, lesser amount of strain would be sufficient to increase the existing strain to a higher strain level (say limit strain) during actual forming trials (or in LDH test). On the other hand, imparting larger strain during forming is required on the retreating side in order to reach the same limit strain. Imparting larger strain on the retreating side is like imparting more plastic deformation as compared to advancing side during forming. This difference in plastic deformation levels has generated extra thinning and hence larger thinning gradient is seen in the retreating side of the weld. Finally the difference in the thickness distribution depends on the welding conditions.

6.3 Conclusions

The main aim of this Chapter is to investigate the effect of tool shoulder diameter and plunge depth on the forming limit of FSW blanks. The following conclusions are drawn from this Chapter.

- The FSW sheets exhibit better formability than un-welded sheets at different welding conditions.

- By increasing the shoulder diameter from 12 to 18 mm, formability of FSW blank is found to improve. When plunge depth is increased from 1.85 mm to 1.9 mm, forming limit of FSW blanks has increased. This is mainly due to the evolution of thickness gradient during necking of un-welded and welded sheets.

- The thickness gradient is found to be severe in un-welded blanks as compared to FSW blanks. With increase in shoulder diameter and plunge depth, the thickness distribution becomes uniform and hence improvement in forming limit is witnessed.

- The improvement in forming limit of FSW sheets is also due to the increase in strain hardening exponent of weld region as compared to un-welded sheets.
- The dome height difference between the FSW sheets and un-welded sheets is not very different in plane-strain strain path. But in stretching side, due to failure in weld region, the dome height of un-welded sheets is more than that of welded sheets. There is not much variation in dome height with respect to varied plunge depth and shoulder diameter, unlike in forming limit curve and thickness distribution. There is hardly 1-2 mm variation in dome height in all FSW cases.
- Thickness distribution in advancing side and retreating side is not same and more thinning gradient is seen in the retreating side of the weld. This is mainly due to the differential straining attained by both the sides during FSW. The hardness difference between the retreating side and advancing side also affects the thickness evolution during forming along with the strains. Finally the thickness gradient depends on the welding conditions also.

Chapter 7

Influence of tool rotation speed and welding speed on forming limit of friction stir welded AA6061-T6 sheets

7.1 Experimental procedure

7.1.1 Base material properties

The base metal and its mechanical properties are already discussed in Chapter 4 in section 4.1.

7.1.2 Welding experiments

The FSW is done using the optimized process parameters are shown in Table 4.7 in Chapter 4. From that range of optimized parameters, some of the FSW conditions are considered such that the effect of tool rotation speed and welding speed on the forming limit strain is focused. The selected parameters are given in Table 7.1. The FSW condition 9 is made as third trial at 1500 rpm rotational speeds and 120 mm/min welding speed.

Table 7.1 Different optimized FSW conditions used for welding trials

FSW conditions	Rotational speed (rpm)	Welding speed (mm/min)	Shoulder diameter (mm)	Plunge depth (mm)
1	1300, 1400	90	12	1.9
2	1300, 1400	90	18	1.9
3	1300, 1400	100	12	1.9
4	1300, 1400	100	18	1.9
5	1300	90, 100	12	1.9
6	1400	90, 100	12	1.9
7	1300	90, 100	18	1.9
8	1400	90, 100	18	1.9
9	1500	120	15	1.95

7.1.3 Formability testing and forming limit evaluation

As discussed in the previous Chapter 6 in section 6.1.4, the similar formability test and thickness measurement method was followed and evaluated the limit strains and thickness difference with respect to tool rotation speed and welding speed. The obtained limiting major strain values at different strain paths are tabulated in Table 7.1

Table 7.2 Major limit strain values of different FSW conditions

FSW conditions	Rotational speed (rpm)	Welding speed (mm/min)	Shoulder diameter (mm)	Plunge depth (mm)	Limiting major strain values	
					Near plane–strain strain path	Biaxial stretching strain path
Unwelded blank					0.23	0.33
1	1300	90	12	1.9	0.25	0.4
	1400				0.24	0.44
2	1300	100	12	1.9	0.24	0.34
	1400				0.25	0.42
3	1300	90	18	1.9	0.2	0.48
	1400				0.2	0.5
4	1300	100	18	1.9	0.3	0.46
	1400				0.28	0.48
5	1500	120	15	1.95	0.2	0.44

7.2 Results and discussion

7.2.1 Effect of tool rotation speed on forming limit of FSW blanks

The overall formability performance of FSW blanks in stretching deformation was investigated through limit dome height (LDH) formability test with different lubricant conditions for the welded sheets and unwelded sheets experimentally.

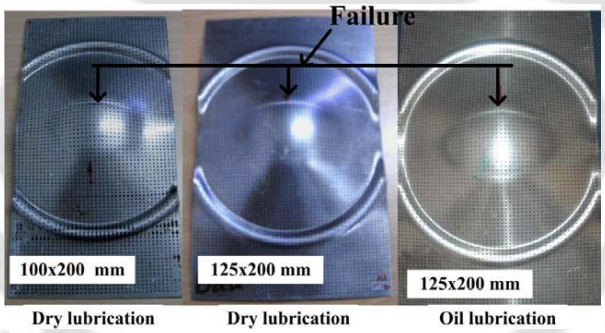

Fig. 7.1 Deformed samples of unwelded blanks different lubrication conditions

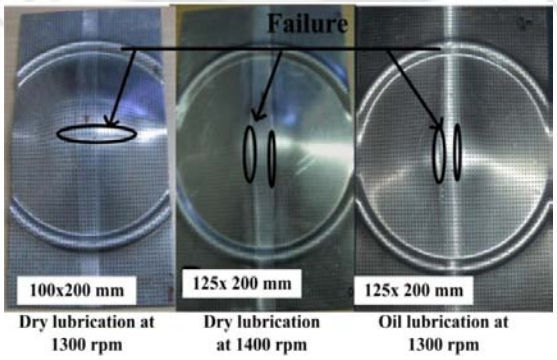

Fig. 7.2 Deformed FSW blanks at different tool rotation speeds, 90 mm/min welding speed and 1.9 mm plunge depth with 12 mm shoulder diameter at different lubrication conditions

Deformed unwelded blanks and FSW blanks with different lubricant condition are shown in the Fig. 7.1 and 7.2 for illustration. Failure pattern in unwelded blanks is same in all the strain paths during LDH test as shown Fig. 7.1. In case of FSW blanks made at different tool rotation speeds failure pattern in 100 mm x 200 mm strain path is perpendicular to the weld like unwelded blanks whereas in 125 mm x 200 mm failure is at interface of weld as shown in Fig. 7.2

The influence of the tool rotation speed under different FSW conditions (1 to 4 in Table 7.1) on FLC of FSW blanks is compared with unwelded blank FLC initially. Figure 7.3 shows the master FLD presenting the effect of tool rotation speeds on the FLCs of FSW blanks which are made using different tool rotation speeds (1300 and 1400 rpm), at constant 90 mm/min welding speed, and 1.9 mm plunge depth with 12 mm shoulder diameter (FSW condition 1 in Table 7.1). It is observed that forming limit of the unwelded blank and two FSW blanks are almost same in near plane–strain strain-path and FSW sheets formability has improved significantly in stretching strain paths, increasing its overall formability. When FSW blank FLCs are compared, FLC at 1400 rpm is better than at 1300 rpm tool rotation speed in stretching strain paths. The percentage difference in true major strain values between base material and FSW blank made at 1300 rpm is 7% and with 1400 rpm is 11%. When percentage difference is seen within the FSW blanks, about 4% difference is witnessed in stretching side. The percentage difference is calculated from major strain values presented in Table 7.2.

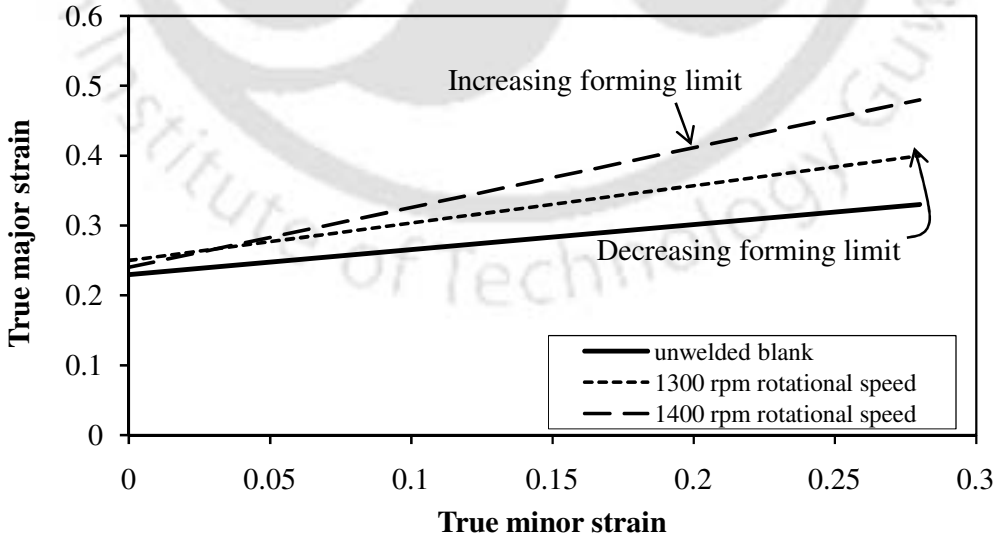

Fig. 7.3 Influence of tool rotation speeds (1300 and 1400 rpm) on forming limit strains at welding speed of 90 mm/min, 12 mm shoulder diameter and 1.9 mm plunge depth

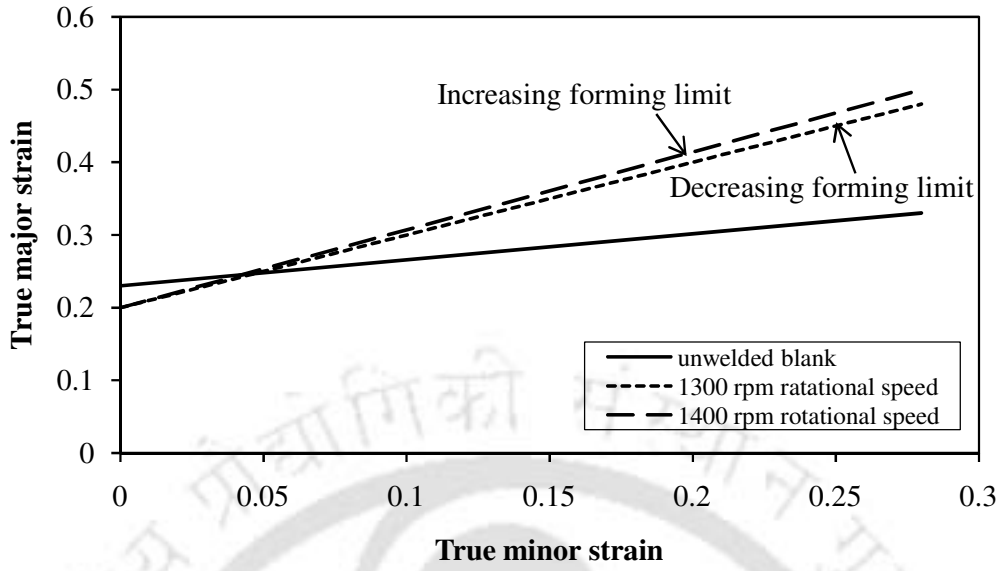

Fig. 7.4 Influence of tool rotation speeds (1300 and 1400 rpm) on forming limit strains at welding speed of 90 mm/min, 18 mm shoulder diameter and 1.9 mm plunge depth

Likewise, it is observed from Fig. 7.4 that the forming limit of the FSW blanks fabricated at different tool rotation speeds, 1300 rpm and 1400 rpm, with 18 mm shoulder diameter at constant welding speed of 90 mm/min and plunge depth of 1.9 mm (FSW condition 2 in Table 7.1) is better than un-welded blank; with higher tool rotation speed (1400 rpm), showing a better forming limit. It is observed that forming limit of the unwelded blank is slightly better than FSW sheets in near plane-strain strain-path and it decreases significantly in stretching strain paths. The percentage difference in true major strain values between base material and FSW blanks is 3% approximately in near plane-strain stretching condition, whereas in stretching side, 1300 rpm and 1400 rpm showed a considerable difference of 15% and 17% respectively.

Similarly formability tests were carried out for other two FSW conditions (3 and 4 in Table 7.1) with 100 mm/min welding speed. In general, it is found that the forming limit of FSW blank is better than that of base material. Moreover the forming limit of FSW blank made at 1400 rpm tool rotation speed is 8% more than FSW blank made at 1300 rpm tool rotation speed (Fig. 7.5 and 7.6). Similar results are observed in the case of FSW blanks made at 90 mm/min welding speed as discussed earlier. It should be noted that for FSW blank made at 90 mm/min welding speed, the forming limit in the case of FSW sheet made at 1400 rpm is 1% lesser than at 1300 rpm in near plane–strain condition, but improves in the stretching side by about 4% (Fig. 7.3).

In whole, the forming limit of FSW blanks is higher than that of base material. With increase in tool rotation speed, the forming limit is found to improve considerably about 2% in near plane–strain condition and 2-8% in the stretching side.

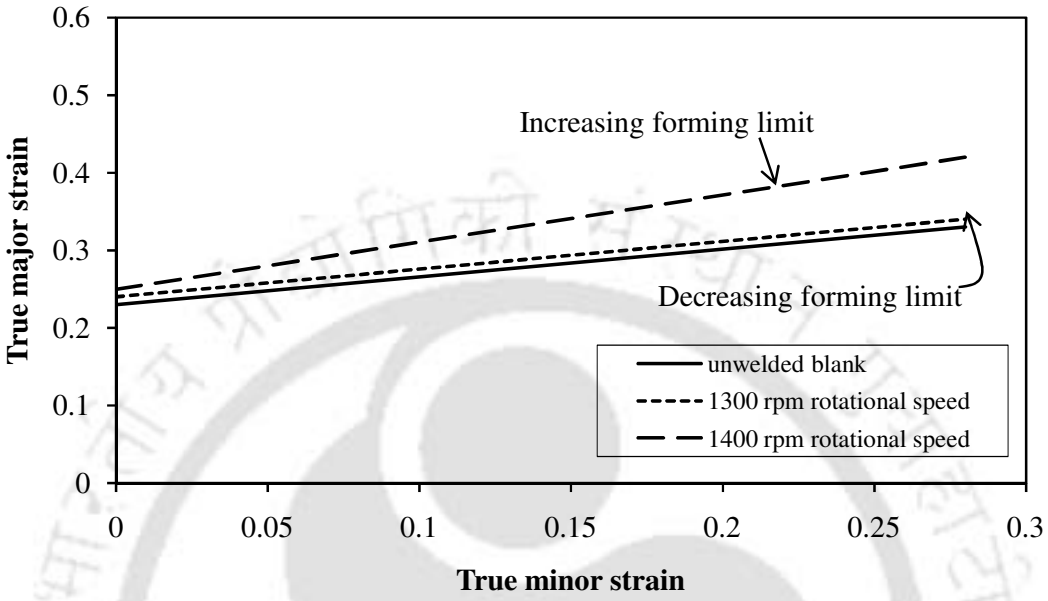

Fig. 7.5 Influence of tool rotation speeds (1300 and 1400 rpm) on forming limit strains at welding speed of 100 mm/min, 12 mm shoulder diameter and 1.9 mm plunge depth

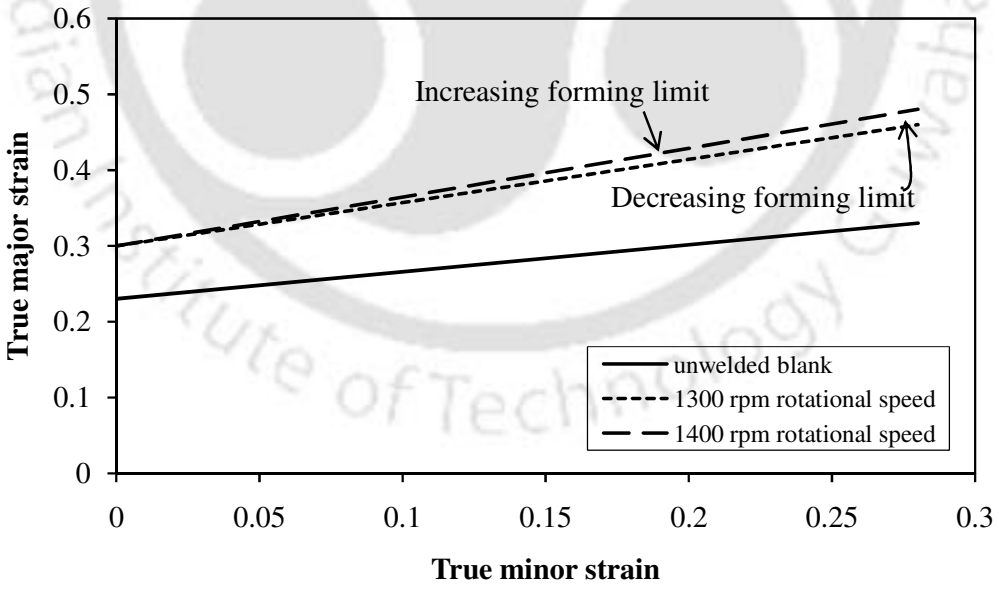

Fig. 7.6 Influence of tool rotation speeds (1300 and 1400 rpm) on forming limit strains at welding speed of 100 mm/min, 18 mm shoulder diameter and 1.9 mm plunge depth

7.2.2 Influence of welding speed on forming limit of FSW blanks

The deformed FSW blanks made at different welding speeds with different lubricants are shown in the Fig. 7.7 for illustration. The failure pattern is found to be same as that of FSW sheets made at different rotation speeds.

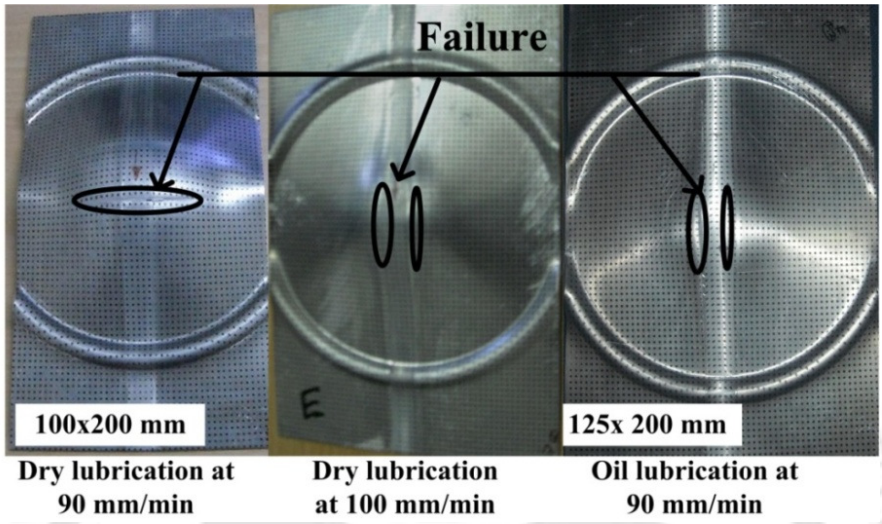

Fig. 7.7 Deformed FSW blanks at different welding speeds, 1300 rpm tool rotation speed and 1.9 mm plunge depth with 12 mm shoulder diameter at different lubrication conditions

The influence of welding speed on the FLC of FSW blanks made at different welding conditions and is compared with unwelded blank FLC in Fig. 7.8 to 7.11. Figure 7.8 shows the master FLD presenting the effect of different welding speeds (90 and 100 mm/min) on the FLCs of FSW blanks which are fabricated at 1300 rpm tool rotation speed, 1.9 mm plunge depth and tool with 12 mm shoulder diameter (FSW condition 5 in Table 7.1). It is observed that forming limit of the FSW blanks is better than that of the unwelded blank. The percentage difference in near plane–strain stretching condition between the true major strain values of base material and FSW blanks made at 90 mm/min and 100 mm/min welding speeds is 2% and 1% respectively. But in stretching side, an improvement of 7% and 1% in major limit strain is seen for 90 mm/min and 100 mm/min welding speed as compared to base metal. So with the increase in welding speed, the forming limit has decreased with a difference of 6 % between the FSW blanks in the stretching side.

Similar behavior is seen in Fig. 7.10 for FSW condition 7 in Table 7.1 that with increasing welding speed, forming limit has decreased. It is observed that forming limit of FSW sheets made at 90 mm/min welding speed is same as that of other two forming limit in near plane-strain strain-path, but found to improve on the stretching strain path.

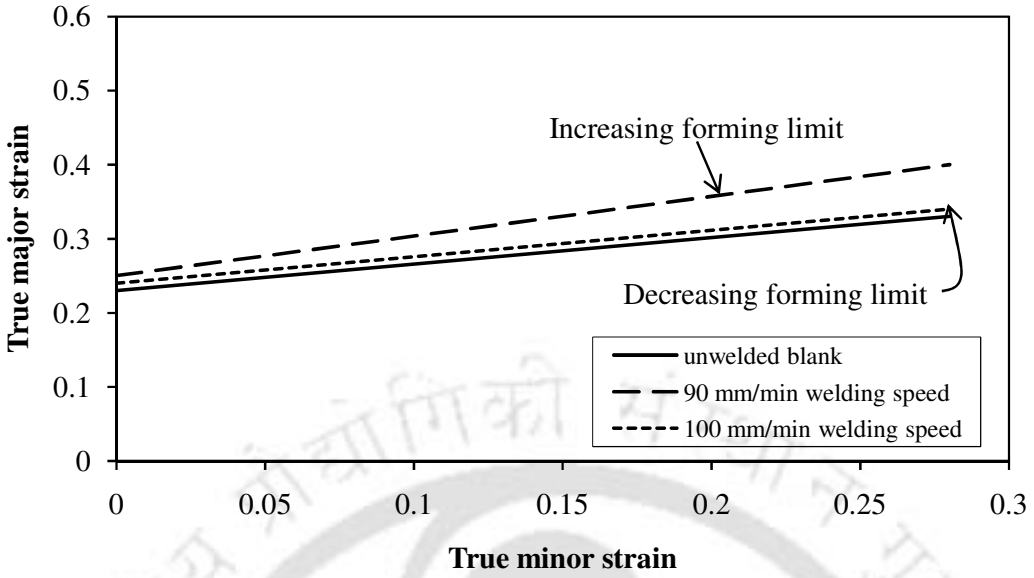

Fig. 7.8 Influence of welding speeds (90 and 100 mm/min) on forming limit strains at tool rotation speed of 1300 rpm, 12 mm shoulder diameter and 1.9 mm plunge depth

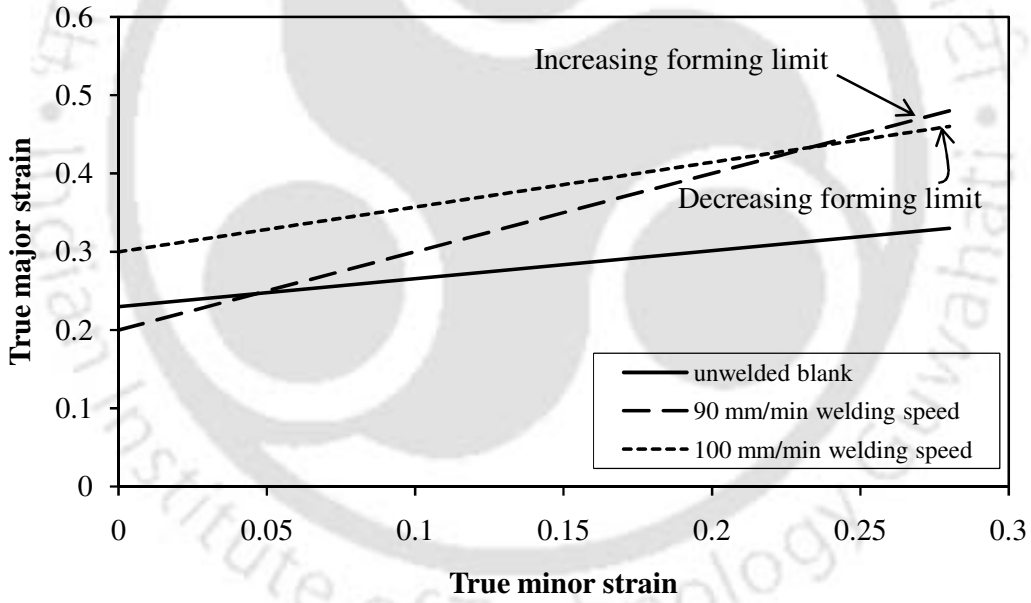

Fig. 7.9 Influence of welding speeds (90 and 100 mm/min) on forming limit strains at tool rotation speed of 1300 rpm, 18 mm shoulder diameter and 1.9 mm plunge depth

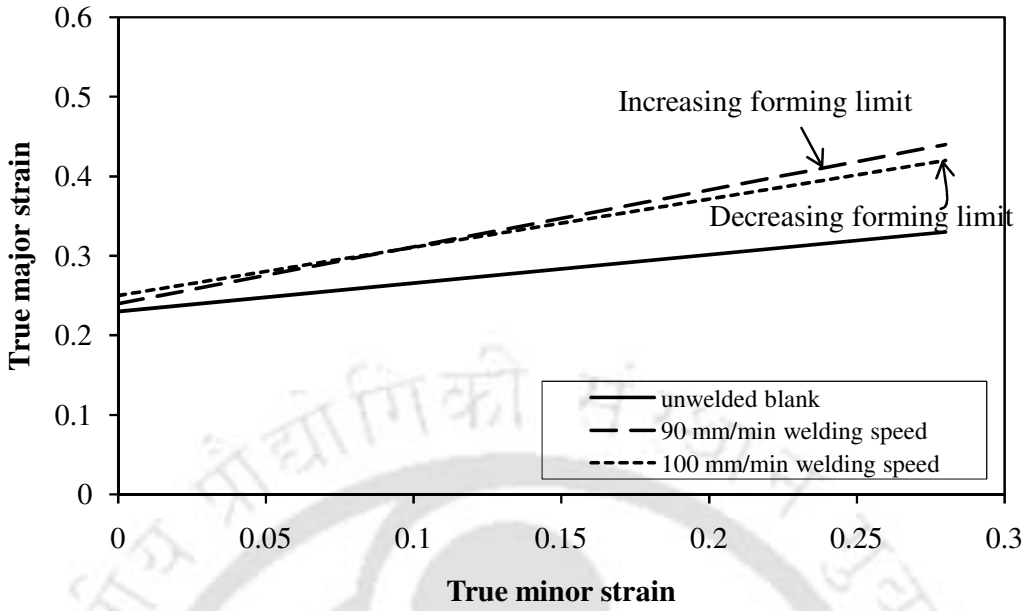

Fig. 7.10 Influence of welding speeds (90 and 100 mm/min) on forming limit strains at tool rotation speed of 1400 rpm, 12 mm shoulder diameter and 1.9 mm plunge depth

Similarly formability tests were carried out for other two FSW conditions (condition 6 and 8 in Table 7.1) with different tool rotation speed (1400 rpm). In general, it is found that the forming limit of FSW blank is better than that of base material. Moreover the forming limit of FSW blank made at 90 mm/min welding speed is better than FSW blank made at 100 mm/min welding speed. A similar result is observed in the case of FSW blanks made with 1300 rpm tool rotation speed presented earlier. It should be noted that for FSW sheet made with 18 mm shoulder diameter tool, the forming limit in the case of 90 mm/min welding speed FSW blank is lower than at 100 mm/min welding speed in near plane–strain strain condition, but improves in the stretching side as shown in Fig. 7.9 and 7.11.

In whole, the forming limit of FSW blanks is higher than that of base material. With increase in welding speed, the forming limit is found to decrease. In three cases, the forming limit of FSW blanks made at 100 mm/min welding speed, in near plane–strain condition is slightly better than at 90 mm/min welding speed and considerable improvement is seen on the stretching side for 90 mm/min welding speed.

In the third level, FSW blank is made with a tool of 15 mm shoulder diameter at 1500 rpm rotational speed, 120 mm/min welding speed and 1.95 mm plunge depth (FSW condition 9 in Table 7.1). The overall formability of the FSW sheets is better than the unwelded blank and when FSW sheet FLCs are compared, 120 mm/min welding speed FLC has lower

formability than 90 mm/min and 100 mm/min welding speed FLCs in the stretching strain-path (see Fig. 7.12).

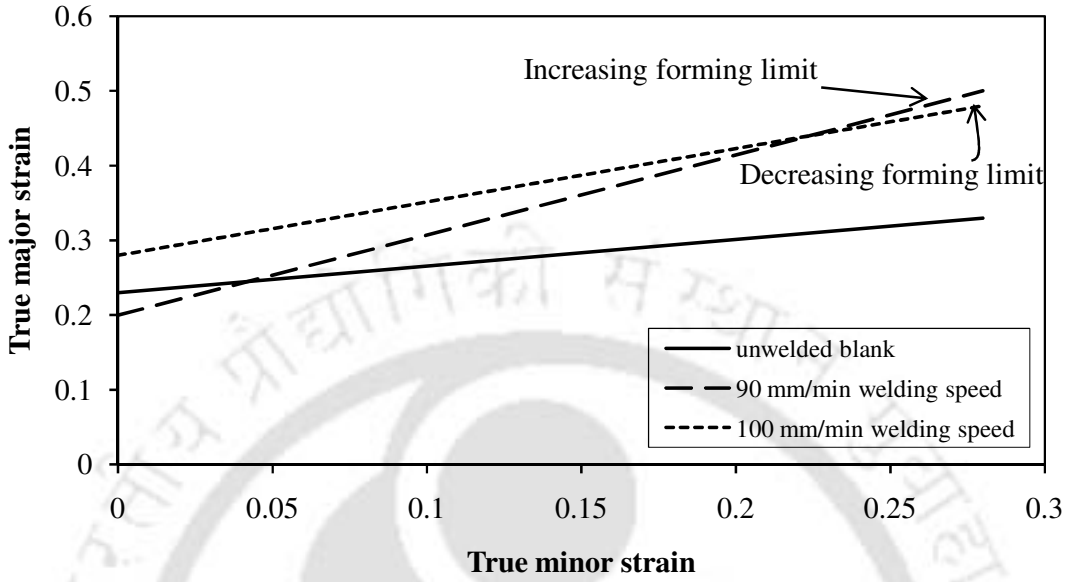

Fig. 7.11 Influence of welding speeds (90 and 100 mm/min) on forming limit strains at tool rotation speed of 1400 rpm, 18 mm shoulder diameter and 1.9 mm plunge depth

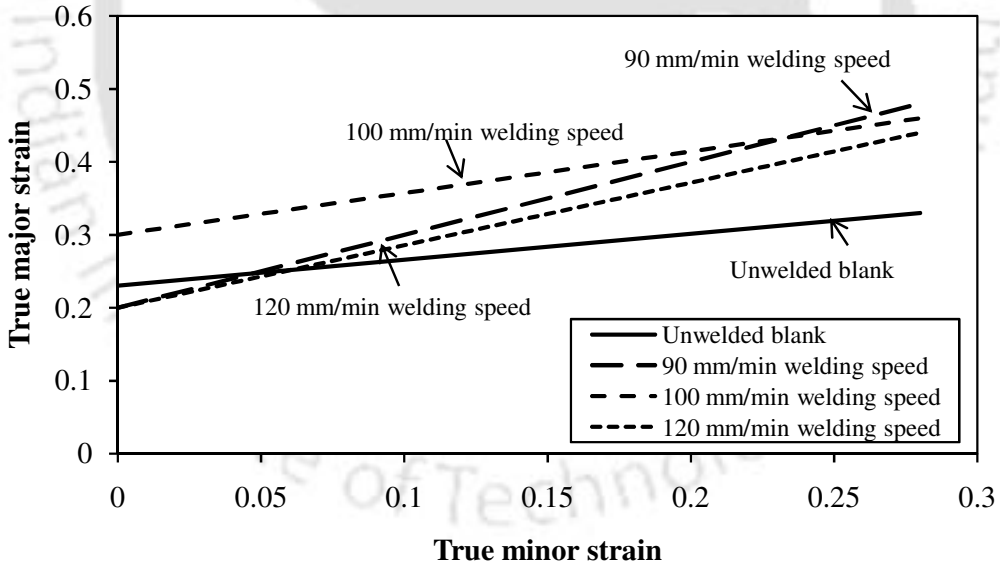

Fig. 7.12 Forming limit curves of FSW blanks made at condition 9 in Table 3 and comparison with 90 mm/min, 100 mm/min welding speed and unwelded sheet FLCs

7.2.3 Thinning behavior of FSW sheets and its relation with forming limit

It is described in the earlier Chapter 6 in section 6.2.4.

7.2.3.1 Thinning behavior of FSW blanks made at different tool rotation speeds

The thinning behavior of FSW blanks made at different tool rotation speed in comparison to that of the unwelded blank is presented in Fig. 7.13 to 7.16. Figure 7.13 shows the thickness distribution of unwelded blank and FSW blanks made at FSW condition 1 in Table 7.1. It is observed that FSW blanks made at 1300 rpm and 1400 rpm have lesser thinning gradient as compared to unwelded blank near fracture. This resulted in reduced FLC for the unwelded blanks when compared with FSW blanks as presented in Fig. 7.3. The uniformity in thinning gradient of unwelded blank and FSW blanks can be understood from Fig. 7.14. It is seen that thinning gradient is very sensitive in the fracture region. There is a sudden change in the thickness variation in all the cases because of necking and hence a sudden and localized shoot up in observed in the thickness difference. When thickness difference is observed among three blanks, unwelded blank has more thickness difference of 0.47 mm near to fracture; whereas in FSW blanks, 1300 rpm has more thickness difference of 0.20 mm as compared to 1400 rpm case which exhibits 0.18 mm thickness difference. This implies that FSW blanks made at 1400 rpm tool rotation speed exhibit uniform thickness distribution as compared to the other two cases. The uniform thickness distribution has improved the forming limit of FSW blanks made at 1400 rpm tool rotation speed as presented in Fig. 7.3.

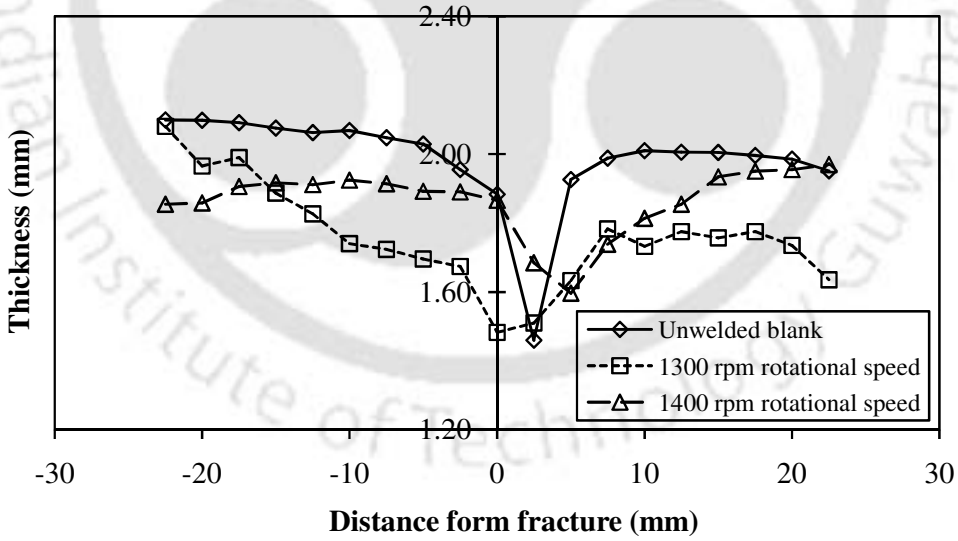

Fig. 7.13 Comparison of experimental thickness distribution of FSW blanks made at different rotational speed (1300 and 1400 rpm) using 12 mm tool shoulder diameter at plunge depth 1.9 mm and welding speed of 90 mm/min to unwelded blank in the LDH test

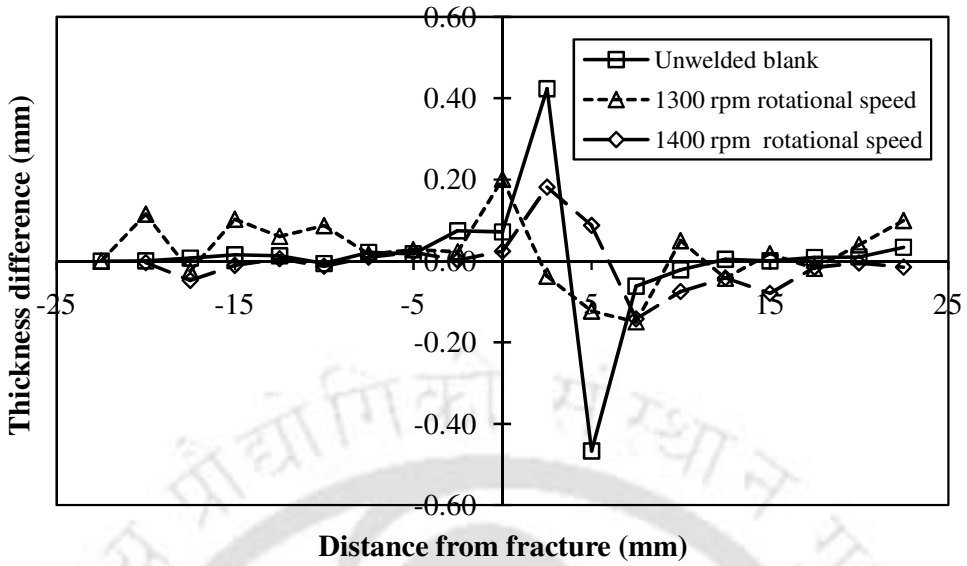

Fig. 7.14 Comparison of thickness gradient uniformity of FSW blanks of different tool rotation speed (1300 and 1400 rpm) at 90 mm/min welding speed to unwelded blank

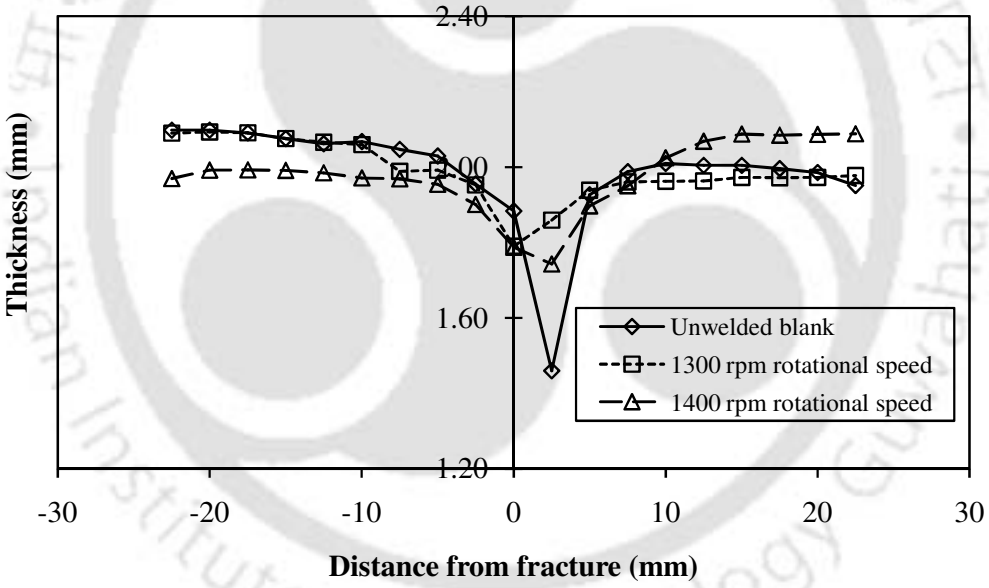

Fig. 7.15 Comparison of experimental thickness distribution of FSW blanks made at different rotational speed (1300 and 1400 rpm) using 18 mm tool shoulder diameter at plunge depth 1.9 mm and welding speed of 90 mm/min to unwelded blank in the LDH test

Figure 7.15 shows the other case on thinning behavior comparison of unwelded blank with FSW blanks made by using condition 2 in Table 7.1 with different rotational speeds. In this case also, it is observed that unwelded blanks has more thinning gradient than FSW blanks; whereas in FSW blanks, 1300 rpm case has more thinning gradient than 1400 rpm case near to fracture irrespective of other process parameters. When thickness difference (Fig. 7.16) is observed unwelded blanks has more thickness difference (0.47 mm) near to fracture;

whereas in FSW blanks, 1300 rpm case has more thickness difference (0.16 mm) as compared to 1400 rpm rotational speed.

Similar observations are seen in other FSW conditions 3 and 4 in Table 7.1 that thinning gradient is more for unwelded blank than FSW blanks. FSW sheet made at 1300 rpm rotational speed has more thinning gradient than 1400 rpm FSW blank. Thinning gradient sensitivity is more for 1300 rpm rotational speed in all the cases as compared to 1400 rpm rotational speed. Because of this, the overall formability of unwelded blank and FSW sheet made at 1300 rpm has reduced as compared to FSW sheets made at 1400 rpm rotational speed.

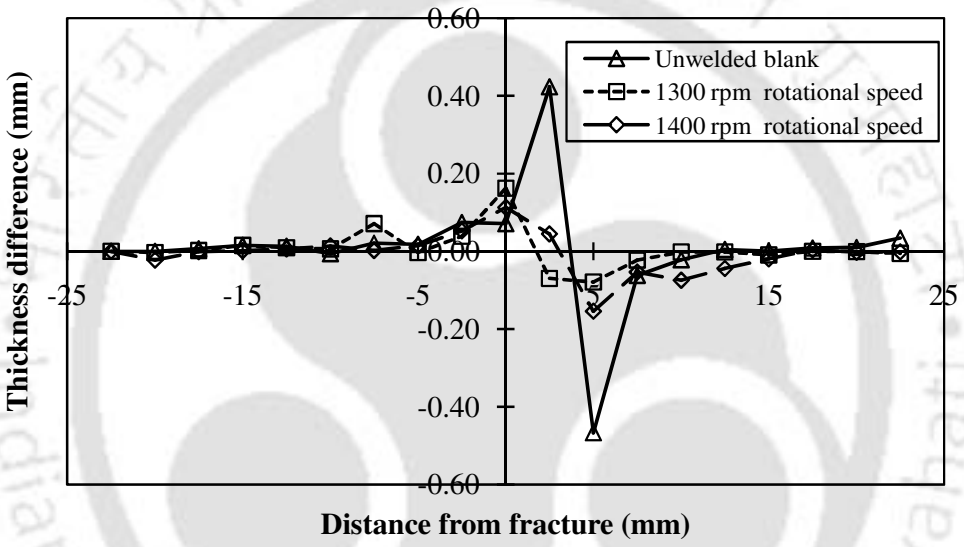

Fig. 7.16 Comparison of thickness gradient uniformity of FSW blanks of different tool rotation speed (1300 and 1400 rpm) at 90 mm/min welding speed to unwelded blank

7.2.3.2 Thinning behavior of FSW blanks made at different welding speeds

The thinning behavior of FSW blanks in comparison with that of unwelded blank by considering the variable welding speed is presented in Fig. 7.17 to 7.20. Figure 7.17 shows the thickness distribution of unwelded blank and FSW blanks with FSW condition 5 in Table 7.1 at different welding speeds 90 and 100 mm/min. It is observed that FSW blanks made at 90 mm/min welding speed and 100 mm/min welding speed have minimum thinning gradient as compared to unwelded blank near fracture. This resulted in reduced FLC for the unwelded blanks when compared to FSW blanks at 90 mm and 100 mm/min welding speed as shown in Fig. 7.7. The uniformity in thinning gradient of unwelded blank and FSW blanks can be understood from Fig. 7.18, which shows that thinning gradient from one end to other end of

unwelded blank and FSW blanks is almost similar except near necked region. When thickness difference is observed among three blanks, unwelded blank has more thickness difference (0.47 mm) near to fracture; whereas FSW blanks at 90 mm/min and 100 mm/min welding speed have 0.19 mm and 0.24 mm (Fig. 7.18). This basically has reflected in forming limit as shown in Fig. 7.7. Similar results are seen in the case of FSW conditions 6 to 8 in Table 7.1 that thinning gradient is more for unwelded blank than FSW blanks at different welding speeds, and FSW blanks made at 100 mm/min welding speed has more thinning gradient than 90 mm/min welding speed FSW blank (Fig. 7.19 and 7.20 for FSW condition 8).

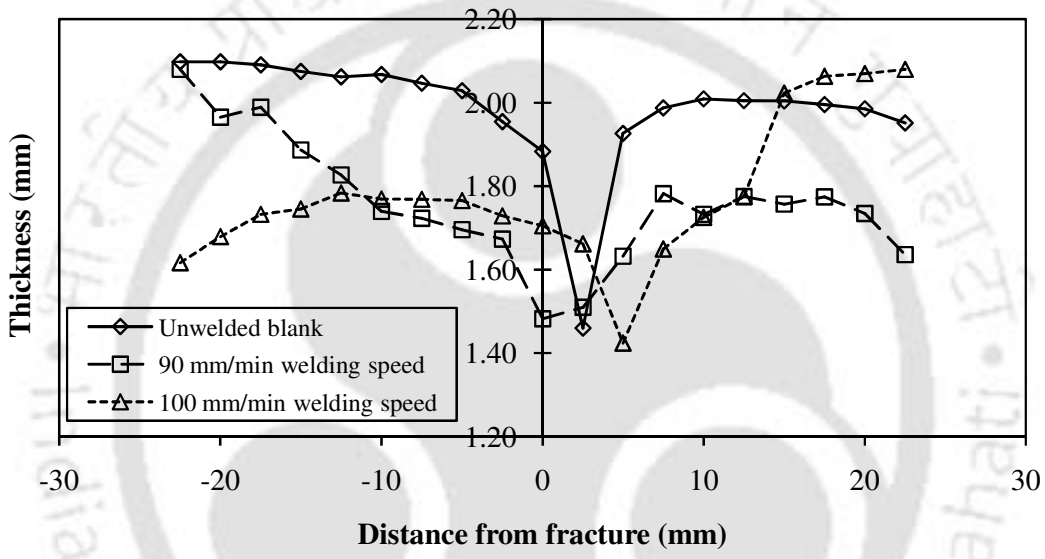

Fig. 7.17 Comparison of experimental thickness distribution of FSW blanks made at different welding speeds (90 and 100 mm/min) using 12 mm tool shoulder diameter at plunge depth 1.9 mm and rotational speed of 1300 rpm to unwelded blank in the LDH test

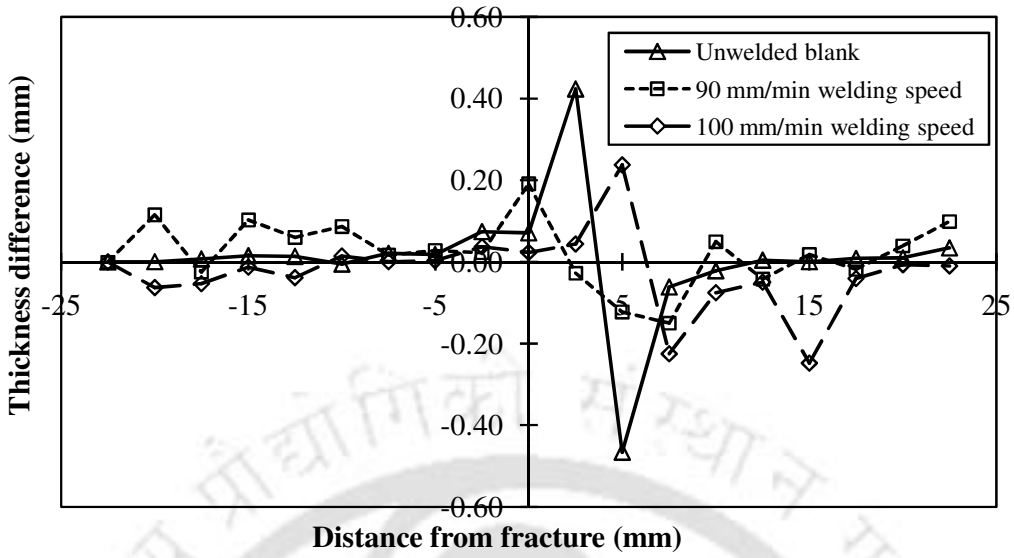

Fig. 7.18 Comparison of thickness gradient uniformity of FSW blanks of different tool welding speeds (90 and 100 mm/min) at 1300 tool rotation speed to unwelded blank

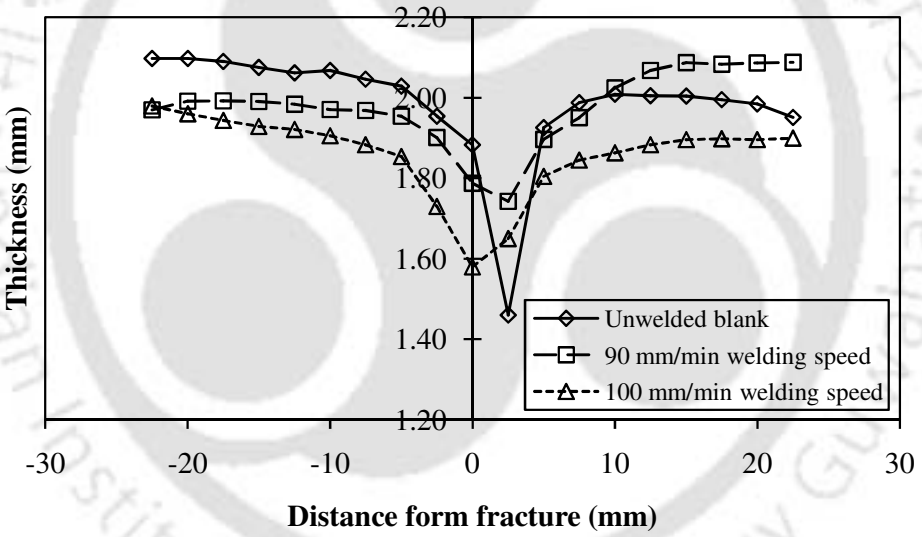

Fig. 7.19 Comparison of experimental thickness distribution of FSW blanks made at different welding speeds (90 and 100 mm/min) using 18 mm tool shoulder diameter at plunge depth 1.9 mm and rotational speed of 1400 rpm to unwelded blank in the LDH test

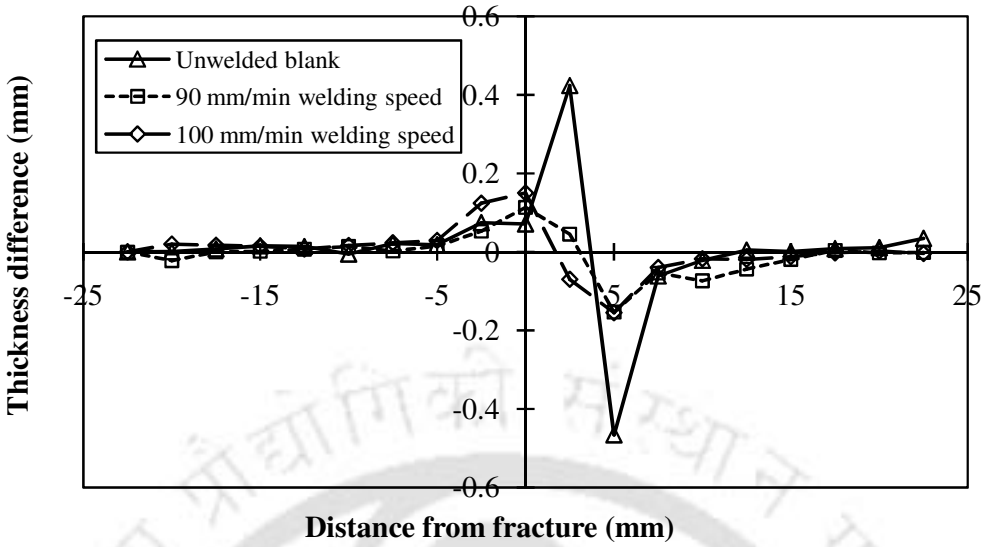

Fig. 7.20 Comparison of thickness gradient uniformity of FSW blanks of different tool welding speeds (90 and 100 mm/min) at 1400 tool rotation speed to unwelded blank

7.2.4 Effect of tool rotation speed and welding speed on strain hardening coefficient (*n*) and its relation with forming limit of FSW blanks

The same has explianed in Chapter 6 in section 6.2.5 in Fig. 6.24 for steel grade and now it is Fig. 7.21 (a) and effect of '*n*' value in other material Al sheet is also seen in Fig. 7.21 (b). In which '*n*' value is varied from 0.1 to 0.25, by keeping all other properties constant (namely: Young's modulus, Poission's ratio, density, plastic strain ratio). An initial sheet thickness of 2 mm and 2.1 mm were considered for steel grade and Al sheet respectively. Same LDH test is simulated using PAM STAMP 2G like section 6.2.5 in Chapter 6. The thickness distribution is measured perpendicular to the failure at same punch travel before failure. It is observed from Fig. 7.21 (a) and Fig. 7.21 (b) that steel sheet with n = 0.3 and Al sheet with n = 0.25 exhibit uniform thickness distribution when compared to the cases with n = 0.15 and n = 0.1. So improvement in '*n*' value improves the thickness distribution uniformity during sheet forming.

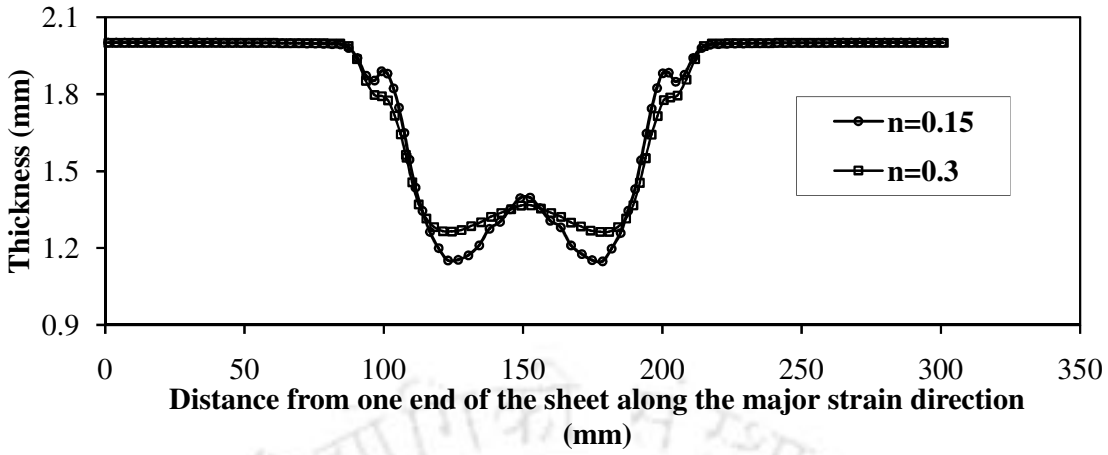

(a) Steel grade sheet

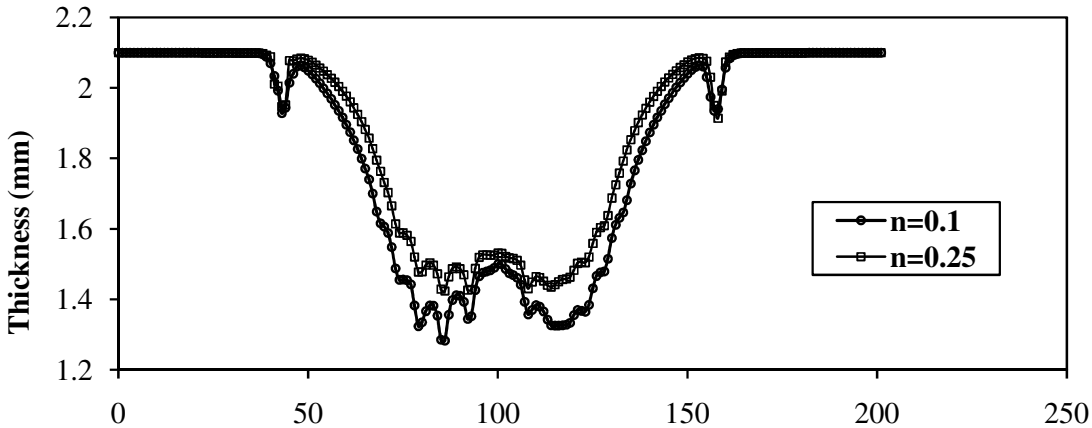

(b) Aluminium alloy sheet

Fig. 7.21 Thickness distribution of unwelded sheet at different '*n*' values at same punch travel

The strain hardening coefficient (*n*) of FS weld region was evaluated through tensile tests using samples containing weld zone only similar to the section 6.1.3 in Chapter 6. Table 7.3 summarises the strain hardening exponent values obtained from tensile test of FSW blanks with longitudinal weld made at variable welding conditions. The values represents '*n*' value of weld zone only.

From the earlier sections, it is observed that FSW blanks of higher tool rotation speed exhibit better FLC and lesser thinning gradient. It is seen from Table 7.3 that the weld zone made at 1400 rpm tool rotation speed exhibits higher '*n*' value than 1300 rpm tool rotation speed at any welding speed and unwelded blank. This has resulted in better FLC for FSW blanks made with 1400 rpm tool rotation speed compared to 1300 rpm tool rotation speed and unwelded sheet. It should be noted that the *n*-value of weld zone made at 1500 rpm is in

between '*n*' values obtained for 1300 rpm and 1400 rpm. But in few cases, it is almost same as that of values obtained for 1400 rpm. The effect of welding speed on the strain hardening exponent of weld zone is also illustrated in Table 7.3. It is seen that with increase in welding speed from 90 mm/min to 100 mm/min, the strain hardening exponent is found to decrease in most of the cases. Because of the decrease in '*n*' value, the forming limit has decreased with increasing welding speed.

With the increase in tool rotation speed and decrease in welding speed, temperature in the stirring zone is expected to increase. This means that the final grain size would be larger (Kumar and Kailas, 2008) and the dislocation density reduces because of static recrystallization in the nugget region. The strain hardening behavior can then be related to the accumulation and interaction of the dislocations. If the dislocation density is lower, more strain can be induced in the material, thus increasing the ductility and strain hardening exponent and hence the forming limit. In contrast, in the base material, the saturation of the dislocation density results in lower strain hardening and poor ductility making it less formable (Afrin *et al.*, 2007; Woo *et al.*, 2008; 2010). The improvement in strain hardening exponent in Al alloys was presented by Woo *et al.*, 2008; 2010; Afrin *et al.*, 2007 for Al 6061-T6 and Magnesium alloys respectively. Woo *et al.*, 2008 showed, through X-ray peak profile analysis, a clear improvement of strain hardening exponent of nugget zone by three times as compared to base material. The low initial dislocation density in the recrystallized region is believed as the main reason for the improvement is '*n*' value in the nugget zone as compared to base material in their work. A similar result was presented by Afrin *et al.*, 2008 for AZ31B-H24 Mg alloy.

Table 7.3 Strain hardening exponent (*n*) values of weld zone at different FSW conditions with variable shoulder diameter

FSW conditions	Tool rotation speed (rpm)	Welding speed (mm/min)	Shoulder diameter (mm)	Plunge depth (mm)	Strain hardening exponent (*n*)
Un-welded blank					0.1
1	1300	90	12	1.9	0.24
	1400				0.25
2	1300	100	12	1.9	0.25
	1400				0.25
3	1300	90	18	1.9	0.27
	1400				0.3
4	1300	100	18	1.9	0.26
	1400				0.28
5	1500	120	15	1.95	0.27

7.2.5 Effect of tool rotation speed and welding speed on dome height

Table 7.4 shows the dome height comparison of all FSW sheets deformed at different strain paths using different lubricants (dry, oil and grease). It is observed that dome height of FSW blanks is more compared to the unwelded blank in near plane-strain strain path, whereas in 125×200 mm strain path unwelded blank has more dome height than all FSW sheets. This is mainly due to the failure occuring in the weld region parallel to the major strain direction in stretching strain paths. But in the case of near plane-strain strain path, failure is witnessed normal to the weld region. It is also observed that there is not much variation in dome height with respect to varied welding speed and tool rotation speed, unlike in forming limit curve and thickness distribution. There is hardly 1-2 mm variation in dome height in all FSW cases and at different lubricant conditions.

Table 7.4 Dome height of FSW blanks at different FSW conditions

FSW conditions	Tool rotation speed (rpm)	Welding speed (mm/min)	Shoulder diameter (mm)	Plunge depth (mm)	Dome height (mm) at varied strain-paths					
					100×200mm			125×200mm		
					Dry	Oil	Grease	Dry	Oil	Grease
Base material					27.1	27.04	27.02	28	28.08	28
1	1300	90	12	1.9	29.1	28.02	29	19.1	19.12	17.18
	1400				29.2	28.1	28.14	19.2	19.14	17.16
2	1300	100	12	1.9	28.1	27.14	28.14	19.1	18.14	17.08
	1400				28.1	29.06	29.12	19.2	17.096	17.09
3	1300	90	18	1.9	28.2	28.14	28.1	19	19.08	17.1
	1400				29.1	29.06	30.16	19.2	17.16	18.06
4	1300	100	18	1.9	29	29.18	30.02	19.2	18.1	21
	1400				29.1	30.1	28.06	21.1	20.08	18.18
5	1500	120	15	1.95	31.1	29.12	29.12	23.1	18.16	17.06

7.3 Conclusions

The main aim of this Chapter is to investigate the effect of tool rotation speed and welding speed on the forming limit of FSW blanks. The following are the conclusions made from this Chapter analyses.

- The FSW sheets made at few welding speeds and rotation speeds exhibit higher forming limit as compared to un-welded sheets. By increasing the tool rotation speed and decreasing the welding speed, forming limit of FSW blanks is found to improve.

- It has been demonstrated that this is mainly due to the evolution of thickness gradient during necking of FSW sheets and strain hardening exponent of weld region.

- The thickness gradient is found to be severe in un-welded blanks as compared to FSW blanks. Similar observation is seen in cases of FSW sheets made at higher welding speed and lower rotation speed.

- There is an increase in strain hardening exponent (n) of weld region with increase in tool rotation speed and decrease in welding speed. The improvement in strain hardening exponent in weld zone is believed to occur because of lower dislocation density in the recrystallized region. If the dislocation density is lower, more strain can be induced in the material, thus improving the forming limit.

- There is not much variation in dome height among the welded sheets. There is hardly 1-2 mm variation in dome height in all FSW cases. In the stretching strain-paths, the dome height of welded sheets is lower than that of base material.

Chapter 8

Forming limit of friction stir welded sheets made of AA 6061-T6: Effect of weld orientation and weld location

8.1 Experimental methodology

8.1.1 Base material and FSW experiments

Base metal details are discussed in Chapter 4 in section 4.1. FSW blanks were welded at two different levels by varying welding speed from 90 mm/min (Level-I) to 100 mm/min (Level-II) at a constant plunge depth of 1.9 mm, tool rotation speed of 1400 rpm and tool shoulder diameter of 18 mm, while the tool tilt angle (2.5°) was kept constant throughout the process. These levels of parameters were selected by conducting a series of experiments with different parameters to achieve the 'internal defect free' joints in Chapter 4 and the better mechanical properties in Chapter 5 among the all 17 FSW conditions. In this, the effect of weld location and orientation is studied under two different welding conditions fabricated using two different welding speeds.

8.1.2 Weld orientation and location

FSW sheets made at different welding locations and weld orientations are considered for studying the influence on the limit strains. The longitudinal weld orientation includes weld parallel to major straining direction (0°); the transverse weld, perpendicular to major straining direction (90°) and 45° to major straining direction. In the case of longitudinal welds, the weld zone was located at three different positions including one at the geometric centre and other two 5mm and 10mm offset as shown in Fig. 8.1 (a). Fig. 8.1 (b) shows the schematic of weld orientations used for LDH testing. The weld locations are selected such that they are placed at strain localization regions during LDH tests. The transverse welds and 45° welds are located at geometric centre of FSW sheets.

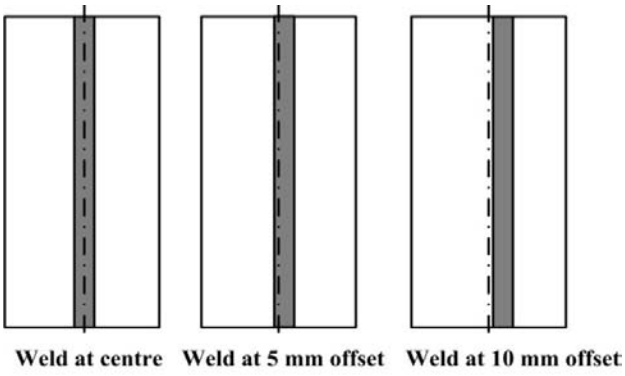

(a) Weld locations (with longitudinal welds)

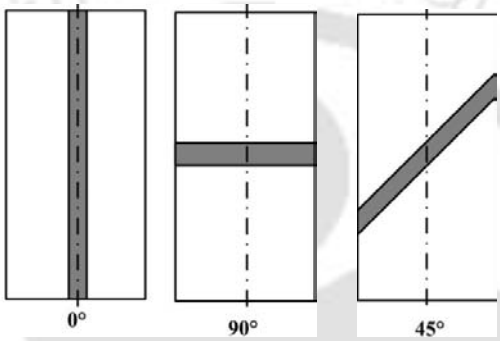

(b) weld orientations

Fig. 8.1 Schematic diagram of the weld locations and orientations (in 100×200 mm strain path of LDH test)

8.1.3 Formability testing

The standard limit dome height (LDH) tests were performed on the welded and unwelded sheets as explained in Chapter 6 in section6.1.4 and studied the influence of weld orientation and location. In the case of 45° orientation, only plane-strain (100x200 mm) strain path was deformed due to unavailability of welded samples. The deformation of the welded and unwelded sheets was analyzed through the online deformation system with help of GOM made ARGUS software. The pixel size in the spackle pattern was fixed at 15×6 with a 0.6 deviation before deformation for FSW sheets with different weld orientation and location.

After deformation, the true major and true minor strains, near to the failure and away from the failure, were measured in all the strain paths automatically using deformed pixels on the sheet. The major and minor strain data were plotted on a single graph such that the forming limit curve separates the failed and safe strain values. This procedure is followed for the unwelded blank and the welded blanks. The FLCs of the welded blanks are compared with each other and also with that of the unwelded blank to investigate the influence of the

weld location and weld orientation on the forming-limit strains. The major limit strains thus obtained at different FSW conditions are tabulated in Table 8.1.

Table 8.1 Major limit strain values of different weld conditions of FSW blanks

Strain path	Base metal	Weld location						Weld orientation			
		Centre / 0 degree		5 mm offset		10 mm offset		45 degree		90 degree	
		Level-I	Level-II	Level-I	Level-II	Level-I	Level-II	Level-I	Level-II	Level-I	Level-II
Near plane stain	0.23	0.2	0.3	0.19	0.18	0.18	0.17	0.28	0.24	0.25	0.21
Biaxial stretching	0.33	0.5	0.48	0.38	0.36	0.37	0.34	—	—	0.35	0.34

8.2 Results and discussion

8.2.1 Failure pattern of friction stir welded and un-welded sheets

The deformed unwelded blanks and FSW blanks with different strain paths and lubricants are shown in the Fig. 8.2 to Fig. 8.4. Failure pattern in unwelded blanks is same in all the strain paths during LDH test as shown Fig. 8.2. The failure observation, near punch nose region, agrees with expected result that is generally seen in other base materials also. The failure pattern in 100 mm x 200 mm strain path (plane-strain condition) is perpendicular to the weld like in all the unwelded blanks in three weld locations, viz., geometric centre, 5 mm and 10 mm offsets. In 125 mm x 200 mm strain path, failure is seen at the interface of weld as shown in Fig. 8.3 in all the locations. In the case of weld orientations, weld in 0° orientation has encountered failure perpendicular to the weld in 100 mm x 200 mm strain path. The strain path of 125 mm x 200 mm in 0° weld orientation has also failed along the weld interface. In 45° orientation failure is observed at the weld interface, independent of the strain paths deformed. The main reason behind the change in failure pattern is due to the change in strain path from near plane strain (100x200 mm) to stretching (125x200 mm). Failure is expected to occur along the weld region even in other stretching strain paths generated by different lubricants and sheets dimensions (like 150x200, 175x200, and 200x200 mm). In the case of transverse weld (90° orientation), failure is observed at the weld interface like in 45° weld orientation (Fig. 8.4).

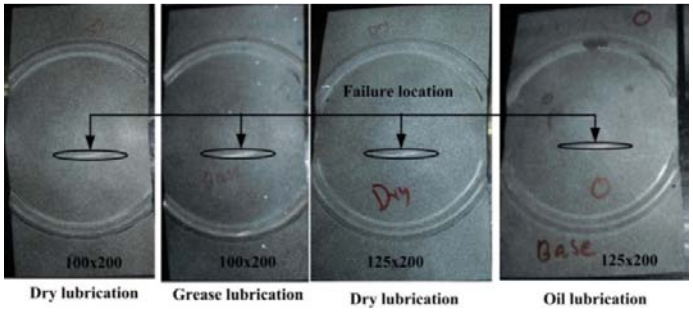

Fig. 8.2 Failure pattern in unwelded blanks at different lubricant conditions and strain paths during LDH test

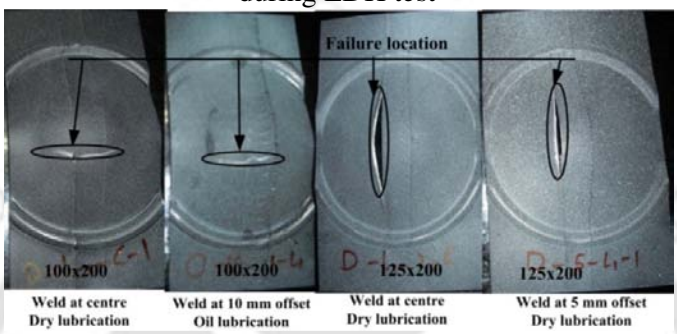

Fig. 8.3 Failure pattern in FSW sheets with weld at 0° orientation, i.e., in longitudinal weld orientation

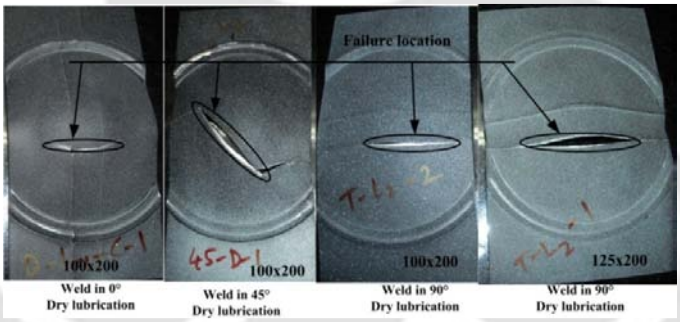

Fig. 8.4 Failure pattern in FSW sheets with weld at 0°, 45° and 90° weld orientations

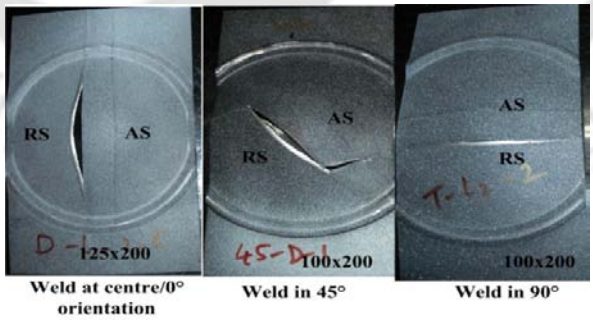

Fig. 8.5 Failure location in FSW sheets at different weld orientation, RS: retreating side; AS: advancing side

The failure location has been observed at the HAZ-BM interface in the retreating side of FSW sheets in case of few weld orientations and locations as presented in Fig. 8.5. Figure 8.6 shows the micro-hardness distribution of FSW sheets at level-I and level-II FSW conditions, measured in the through thickness direction of FSW specimen using Vickers

hardness tester by applying load of 50gf. It is expected that the advancing side would be stronger than the retreating side and is responsible for the failure pattern. This is due to the larger peak hardness value seen in the advancing side from the existing literature (Liu *et al.*, 2003). But the peak hardness value is almost same in both the sides of weld zone.

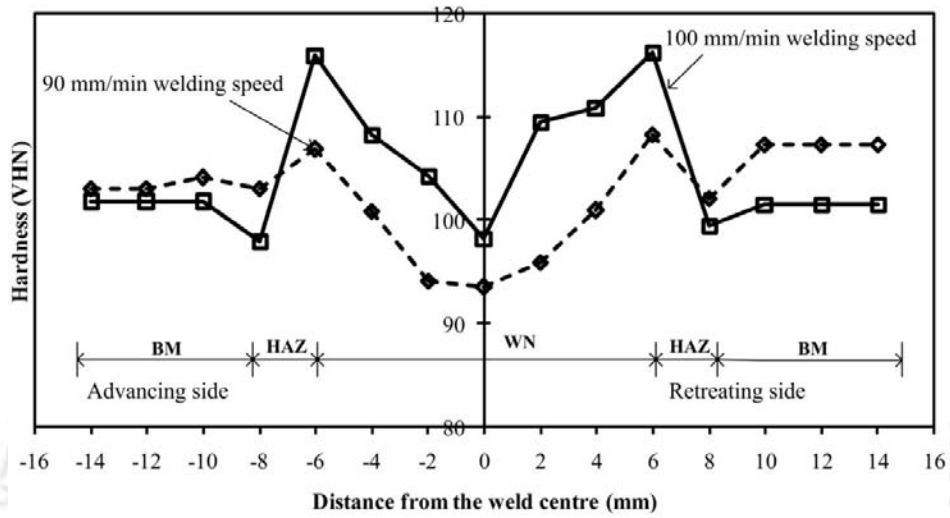

Fig. 8.6 Micro hardness distribution of FSW joints at different welding speeds, 90 and 100 mm/min. Hardness varied from HAZ to WN ±1.5 to ±3.5. BM: base metal; HAZ: heat affected zone; WN: weld nugget

The maximum hardness is found as 106.9 VHN for 90 mm/min and 116 VHN for 100 mm/min welding speed in advancing side, whereas 108.3 VHN and 116.3 VHN for 90 mm/min and 100 mm/min welding speed in the retreating side which has been discussed in Chapter 5 in section 5.3.2. Then it was believed that the strain localization during LDH test (or forming) would be responsible for the failure pattern and hence thickness distribution was monitored in the advancing side and retreating side. It is understood that more the thinning gradient in the sheet, earlier the failure will be reached. From the thickness distribution, the thickness difference, a measure of thickness gradient, is observed to evaluate the maximum thickness difference. The thickness difference near failure in the retreating side, 0.49 mm for 90 mm/min and 0.33 mm for 100 mm/min welding speeds, is larger than in advancing side having 0.39 mm and 0.14 mm for 90 and 100 mm/min welding speeds (Table 8.2). The larger thinning gradient in the retreating side has initiated failure in that side as compared to advancing side, for the same forming levels. The larger thinning gradient on retreating side is due to the larger strain levels attained in the side during welding (Heurtier *et al.*, 2006). Similar observations are also seen in the work of Lee *et al.*, 2009; Chung *et al.*, 2010; Kim *et*

al., 2010a, b. They have studied the failure mode in tensile test and hemispherical dome height test and all the failures are found in the retreating side.

Table 8.2 Thickness difference in AS and RS of FSW blanks

Welding conditions				Maximum thickness difference (mm)	
Shoulder diameter (mm)	**Plunge depth (mm)**	**Tool rotation speed (rpm)**	**Welding speed (mm/min)**	**AS**	**RS**
18	1.9	1400	90	0.39	0.49
18	1.9	1400	100	0.14	0.33

8.2.2 Influence of weld location on the forming limit of FSW sheets

In this section the influence of the weld location on the forming limit curve (FLC) of FSW sheets is discussed. The three different weld locations namely weld at geometric centre, 5 mm offset and 10 mm offset in 0° orientation (weld is parallel to loading direction) are considered. Figure 8.7 and Fig. 8.8 show the influence of weld location on the FLCs at two different welding speeds, 90 mm/min and 100 mm/min. It can be observed from Fig. 8.7, for FSW sheets made at level-I, that among all the FLCs unwelded sheet FLC has better forming limit near to plane-strain (100 mm x 200 mm) strain path and formability decreases significantly in stretching strain paths, reducing its overall formability. When FSW sheets FLCs are compared, the case with weld at centre has better forming limit than the other two locations. The percentage differences in true major strain values between unwelded sheet and FSW sheets in near plane-strain strain path are 3%, 4% and 5% for weld at centre, 5 mm offset and 10 mm offset respectively. Similarly, the percentage differences in stretching strain paths are: 17%, 5% and 4% for weld at centre, 5 mm offset and 10 mm offset respectively. These percentage differences are calculated from major strain values presented in Table 8.1. The decrease in forming limit of FSW sheets with weld at offset locations (5mm and 10mm from center) is due to the localization of strain during forming. The offset weld locations are the locations at which actual failure would occur if there is no weld region. By locating the weld region at these critical positions, the strain gradient and hence the thickness distribution severity during forming will increase. This has been discussed already by Ganesh Narayanan and Narasimhan, 2008a with respect to laser welded steel sheets. The same is believed to be responsible for the forming limit decrease in the case of offset weld locations compared to centre weld.

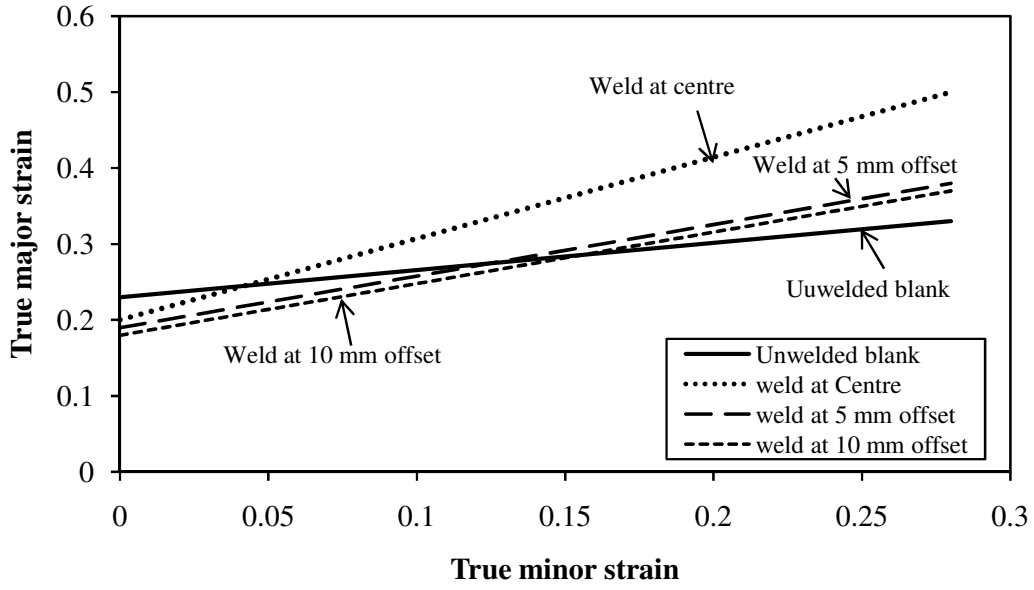

Fig. 8.7 Forming limit comparison of FSW blanks with different weld locations made at level-I FSW condition

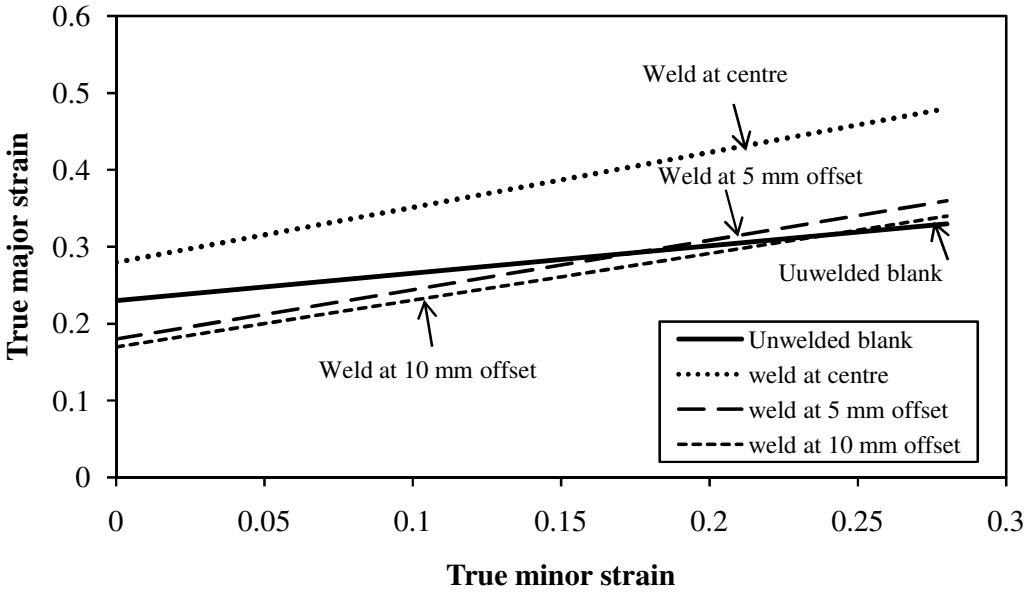

Fig. 8.8 Forming limit comparison of FSW blanks with different weld locations made at level-II FSW condition

A similar result is observed in the case of level-II FSW condition as shown in Fig. 8.8 in which the case with weld at centre exhibits higher forming limit as compared to other cases. The FSW sheet with weld at 5 mm offset shows a better forming limit than the case with 10 mm offset weld, but there is not much difference in the values. A percentage difference of 7% for weld at centre, 5% for weld at 5 mm offset and 6% for weld at 10 mm offset is seen in the plane-strain strain paths as compared to unwelded sheet. In stretching strain paths, percentage

differences compared to unwelded blank are: 15%, 3% and 1%, found between FSW sheets with weld at centre, at 5 mm offset and at 10 mm offset.

8.2.3 Effect of weld orientation on the forming limit of FSW sheets

Figure 8.9 shows the forming limit of FSW sheets made at level-I welding condition and unwelded blank. It is observed from FLC data that the case with weld at 0° orientation, i.e., longitudinal weld, has better forming limit compared to FSW sheets with 90° orientation and unwelded sheet. Since at 0° weld orientation, failure is seen perpendicular to the weld region and weld region being more ductile because of high strain hardening exponent, the forming limit is improved. Moreover, failure is observed along the weld region in the cases of 45° and 90° weld orientations because of which their forming limit is closer to each other and lesser than that of 0° weld orientation. The percentage differences in true major strain values between unwelded sheet and FSW sheets at near plane-strain strain path are: 3%, 5% and 2% in 0°, 45° and 90° weld orientations respectively. So there is not much difference in the forming limit strain values in near plane-strain condition. The percentage differences in stretching strain paths are: 17% and 2% in 0° and 90° weld orientations.

A similar observation is seen in the level-II case also with 0° weld orientation showing better forming limit compared to the other three as shown in Fig. 8.10. The forming limit of FSW sheet with 45° orientation and 90° orientation are almost same in plane-strain strain path. A percentage difference of 7%, 1% and 2% in 0°orientation, 45° orientation and 90° orientation is observed among the FSW sheets in the plane-strain strain paths. In stretching strain path a percentage difference of about 15% and 1% is found in 0° orientation and 90° orientation as compared to unwelded sheet.

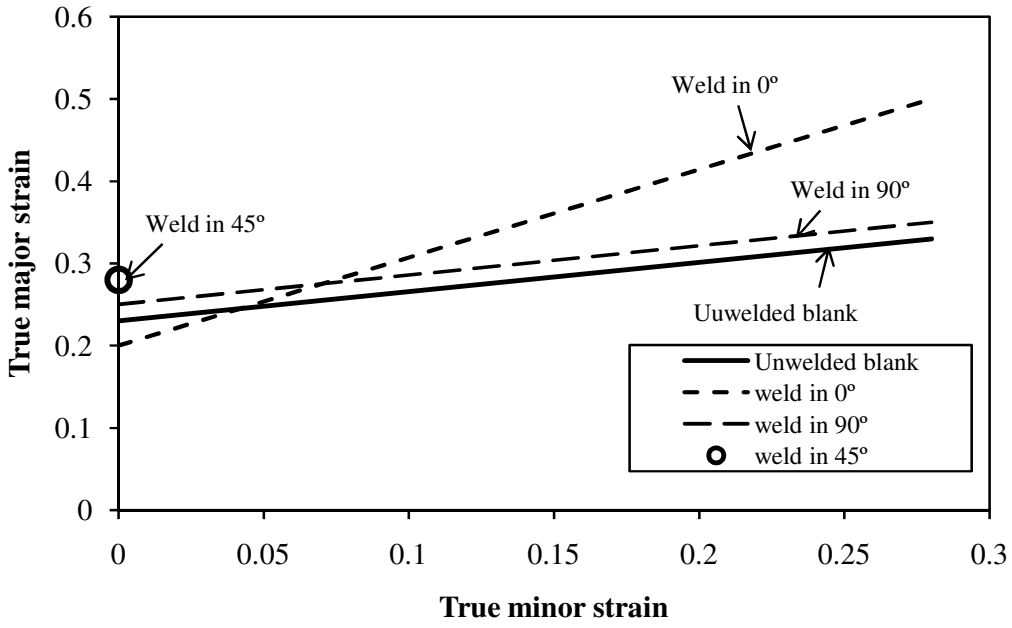

Fig. 8.9 Forming limit strains comparison of FSW blanks with different weld orientations made at level-I FSW condition

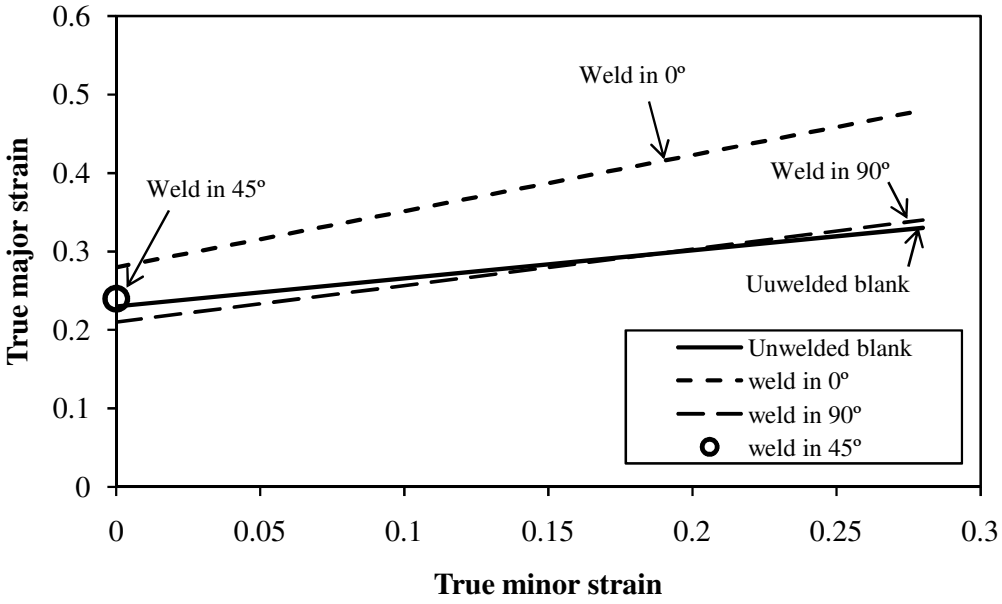

Fig. 8.10 Forming limit strains comparison of FSW blanks with different weld orientations made at level-II FSW condition

8.3 Conclusions

The following conclusions are drawn from this Chapter analysis.

- The FSW sheets show a better forming limit as compared to base material. FSW sheet with weld at center location shows better forming limit as compared to 5 mm and 10 mm weld offset location cases. This is mainly due to the localization of strains and larger thickness distribution severity at these offset locations. There is not much difference in the forming limit of FSW sheets with welds at 5 mm and 10 mm offset locations showing their insensitivity.
- In the case weld orientations, FSW sheets with 0° weld orientation possess improved formability as compared to 45° and 90 ° weld orientation cases. This is due to the change in failure mode, from normal to weld region to parallel to weld zone, when the weld orientation is changed. There is not much change in limit strains between 45° and 90° weld orientations as the failure pattern is same.
- The failure pattern at different weld orientations and weld locations plays a significant role in deciding the forming limit of FSW sheets. The failure location is found to be at the retreating side of the weld zone, at the HAZ-BM interface and this mainly due to the larger thickness gradient existing at this side as compared to advancing side during forming.
- The effect of weld orientation and weld location is independent of FSW parameters chosen.

Chapter 9

Predicting the forming limit strains of FSW blanks made of AA 6061-T6 sheets at different weld orientations and weld locations

9.1 Methodology

9.1.1 Experimental material and mechanical properties

The base material details are discussed in Chapter 4 in section 4.1. The experimental forming limit strains of varied welding speed at 90 mm/min (Level-I) and 100 (Level-II) mm/min as discussed in Chapter 8 in section 8.1.1 are considered for prediction comparison.

9.1.2 Weld nugget and heat affected zone properties evaluation

The mechanical properties of full weld zone, weld nugget (WN) and heat affected zone (HAZ) are evaluated through tensile tests like base material. The tensile samples were made with total weld zone, weld nugget (WN) and HAZ as per the ASTM- B557M with reduced scale ratio as shown in Fig. 9.1 a, b, c. All the samples were prepared using laser cutting machine. The WN and HAZ were identified from the total weld zone through the microstructure. Figure 9.2 shows the macrostructure of different zones like weld nugget (WN) and heat affected zone (HAZ) and their geometric configuration. Tensile tests were performed at a nominal cross-head speed of 1 mm/min, at room temperature on an INSTRON 8801 tensile testing machine and repeated twice for each set to check the repeatability. All the tensile tests specimens with total weld zone, WN and HAZ were made such that weld zone is parallel to the loading direction (longitudinal direction). The engineering stress-strain curves are compared in Fig. 9.3 for base metal, total weld zone, weld nugget and heat affected zone. Table 9.1 summarizes the mechanical properties of total weld zone, WN and HAZ obtained in the present work.

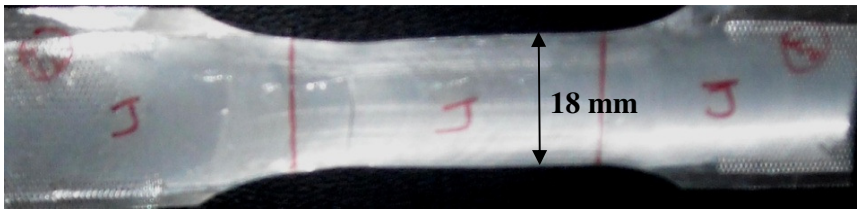

(a)

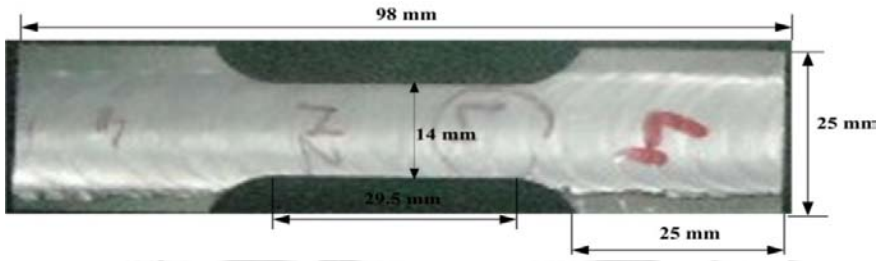

(b)

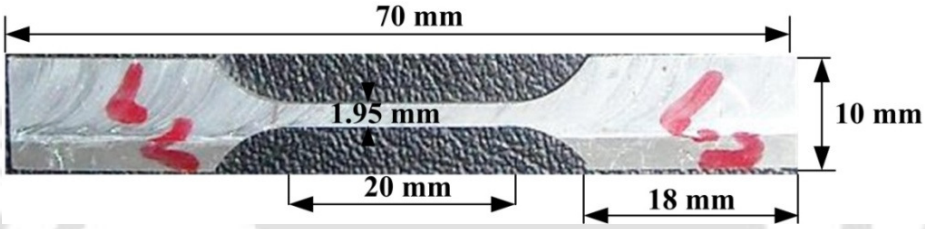

(c)

Fig. 9.1 Tensile samples of (a) tested sample of total weld zone (a) only WN (b) only HAZ

Fig. 9.2 Macrostructure at 10x magnification showing dimensions of different zones in FSW sheets

It is observed that mechanical properties like $\sigma_{YS,}$ UTS, and K are more for HAZ at level-I than total weld zone and weld nugget. The uniform elongation (e_u) of total weld zone and WN are almost same and are better than HAZ at both the conditions. The total elongation (e_t) is more in WN at level-I condition. The strain hardening exponent (n) is more for total weld zone at level-I condition and less in HAZ at level-II. In summary, in many of the cases the mechanical properties are slightly better for level-I condition compared to level-II. The HAZ properties are considered same on advancing side and retreating side of weld zone during simulation.

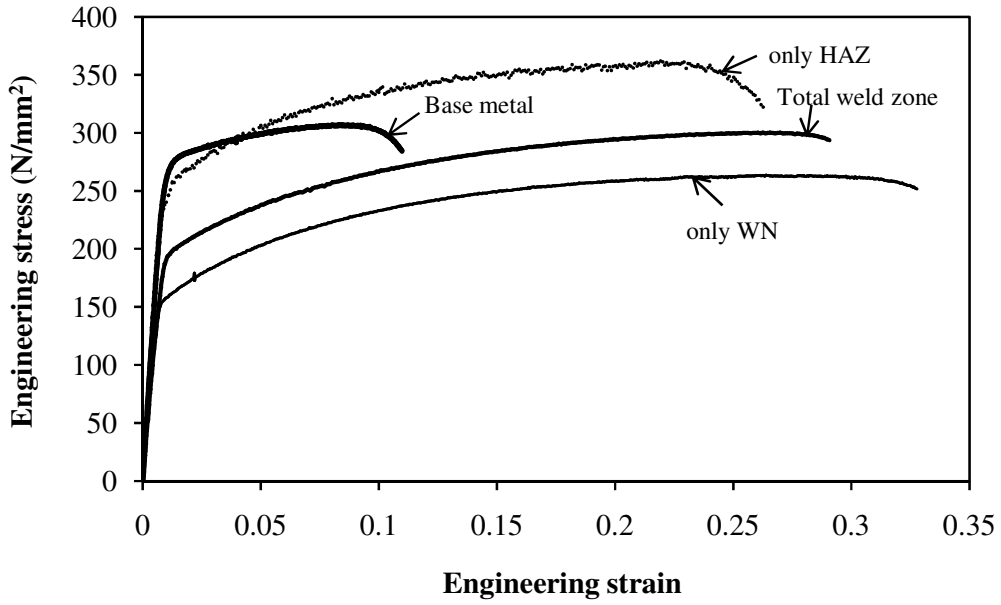

Fig. 9.3 Engineering stress-strain behavior comparison of base material, total weld zone, only weld nugget (WN) and only heat affected zone (HAZ)

Table 9.1 Mechanical properties summary of total weld zone, weld nugget, heat affected zone

Mechanical properties	Total weld zone		Weld nugget		Heat affected zone	
	Level-I	Level-II	Level-I	Level-II	Level-I	Level-II
σ_{YS} (MPa)	182	181	153	154	239	238
UTS (MPa)	289	291	262	264	373	362
e_u (%)	27.3	27.3	27.4	26.4	23	21.9
e_t (%)	31.3	31.3	35.6	32.2	30	27.5
K (MPa)	531	530	488	490	633	611
n	0.3	0.28	0.28	0.27	0.22	0.21
R	0.86	0.84	-	-	-	-

σ_{YS}: yield strength; UTS: ultimate tensile strength; e_u: uniform elongation; e_t: total elongation; K: strength coefficient; n: strain hardening coefficient; R: plastic strain ratio

9.1.3 Plastic strain ratio (R) evaluation for total weld zone of FSW sheets

The plastic strain ratio (R) of weld was evaluated through tensile tests on rectangular samples. The samples were cut from FSW sheet (Fig. 9.4 (a)) in the weld zone using a shear cutting machine and made as per ASTM- E517 (Fig. 9.4 (b)). Figure 9.4 (c) represents the schematic of sheared rectangular tension test sample along with dimensions. Tensile tests were performed at a nominal cross-head speed of 1 mm/min, at room temperature on an INSTRON 8801 tensile testing machine and repeated twice for each condition, to level-I and

level-II, check the repeatability. All the tests were stopped at 12% elongation giving sufficient plastic deformation and measured the changes in dimensions along the length and width directions from marked points with help of profile projector. The true strains in width and in length direction were measured and the true strain along the thickness direction was evaluated by volume constancy principle. The plastic strain ratio was obtained by the ratio of true strain in width direction to true strain in thickness direction. The plastic strain ratio of total weld zone was obtained as 0.86 for level-I and 0.84 for level-II welding conditions.

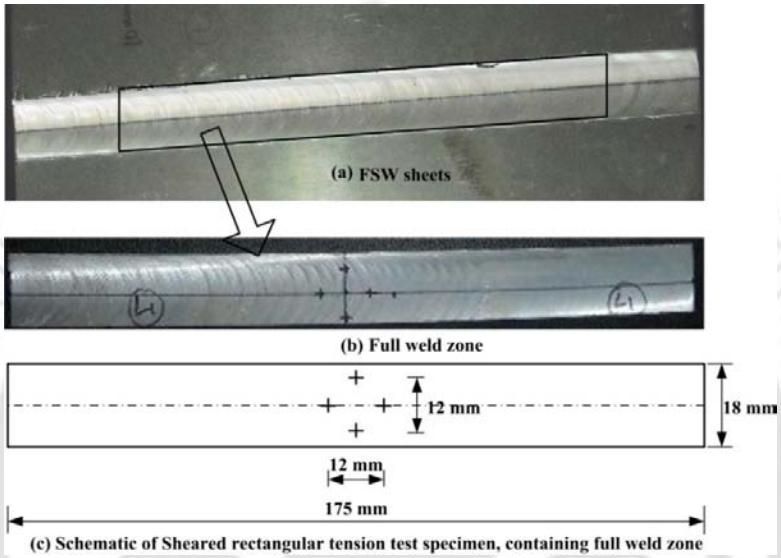

Fig. 9.4 FSW sample for evaluating plastic strain ratio

9.2 Simulation methodology for formability prediction of FSW blanks

9.2.1 Incorporating mechanical properties of weld zone and base metal

The limiting dome height (LDH) test simulation was performed using PAMSTAMP 2G, an elasto-plastic finite element code. The methodology of constructing the tools and welded blanks required for LDH test simulation is described in Chapter 2 in section 2.1. The different strain paths (100x200 to 175x200 mm) for un-welded and welded sheets having different weld locations and orientations, but one during a simulation, were simulated to predict the FLC. Limit strains were obtained using thickness gradient-based necking criterion (TNGC) and major strain rate ratio criterion (MSRC), explained in next sub-section. Friction coefficient 'μ' was assumed to be 0.12, and was kept constant throughout the simulations. This particular 'μ' value closely simulates the dry friction condition existing at the sheet-punch interface in experiments. Optimal blank holder force (BHF) (~40 kN) was chosen such that the blank neither draws-in nor tears near draw beads during forming simulation.

During simulation of FSW blanks, the weld zone is modeled in two methods mainly single zone model, i.e., with total weld zone only, there is no WN and HAZ separately, and double zone model, i.e., WN and HAZ are modeled separately as shown in Fig. 9.5. For single zone model, total weld width is fixed as 18 mm, whereas for double zone model, WN width is 14 mm and HAZ width is assumed 2 mm on both sides of WN during simulation. The properties given in Table 9.1 for both single zone and double zone models are considered for simulation, and for base metal, 0° rolling direction properties from Table 4.2 in Chapter 4 are considered. The other properties assumed are: Young's modulus 69.44 GPa; Poisson's ratio 0.33; thickness of the base metal and weld region: 2.1 mm.

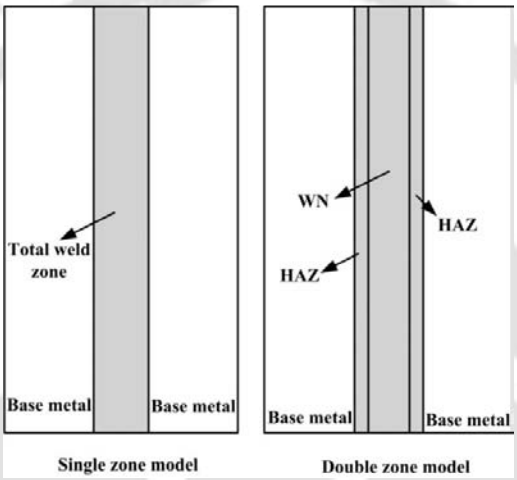

Fig. 9.5 Schematic representations of weld zone models during simulation

9.2.2 Strain hardening law and yield criterion

During simulation trials, the weld region is modeled as single and double zone models as shown in Fig. 9.5. The base material and weld zone model consisted of quadrilateral shell elements of the Belytschko–Tsay formulation with five through thickness integration points. Mesh size of 1 mm was kept constant in the weld region and base metal. Hollomon's power law ($\sigma = K\varepsilon^n$, where σ *is* true stress, K is the strength coefficient, ε true strain and n is the strain-hardening exponent) was used as the strain hardening law. The predicted, simulated tensile behavior using Hollomon's law is found to match with experimental data as shown in Fig. 9.6. Hill's 1990 isotropic hardening yield criterion was used as the plasticity model. This yield criterion is more suitable for aluminum alloys rather than Hill's 1948, and Hill's 1979 criteria. Hill's 1948 is not suitable for aluminum sheets which shows anomalous behavior (Banabic, 2010). Hill's 1979 yield criterion is suitable for aluminum sheets, but it is

applicable in specific principal axes only. Later Hill's proposed a new yield criterion in 1990 (Hill, 1990) which is suitable for any orientation by defining non-quadratic yield parameter (M) called as Hill's non-quadratic yield parameter. This parameter can be evaluated through few different experimental methods including balanced biaxial stretch test and through thickness compression tests (Mulder et al. 2012). For Hill's 1990 yield criterion the inputs have given to base material as yield strength and plastic strain ration in seven different (0º, 15º, 30º, 45º, 75ºand 90º) rolling directions as shown in Table 4.2 in Chapter 4 whereas for weld zone only one yield strength and plastic strain ratio given to all rolling directions corresponding to welding conditions as shown in Table 9.1.

In this Chapter M was found by varying in a specified range based on available data Lin and Ding, 1996; Keum and Lee, 2000; Leacock, 2006) during simulations. Plane-strain strain path (100x200 mm) was simulated by changing various M-values. Some of the varied values and their corresponding obtained limit strains are tabulated in Table 9.2 for base metal and weld zone. From these results, limit strain values at M-value 2.2 for base material was very close to the experimental limit strain at plane-strain condition and this value is found to satisfy with other strain paths. When M-value is above 2.2, sheets were drawing in during simulation. If M-value is below 2.2, plane-strain strain path showed less error but other strain paths were not satisfied and showed larger error. So, M-value is fixed at 2.2 for all the simulations of unwelded sheets and similar method was followed for fixing M-value for weld zone. It is fixed at 1.5 which has given closer limit strain when compared with experimental limit strain.

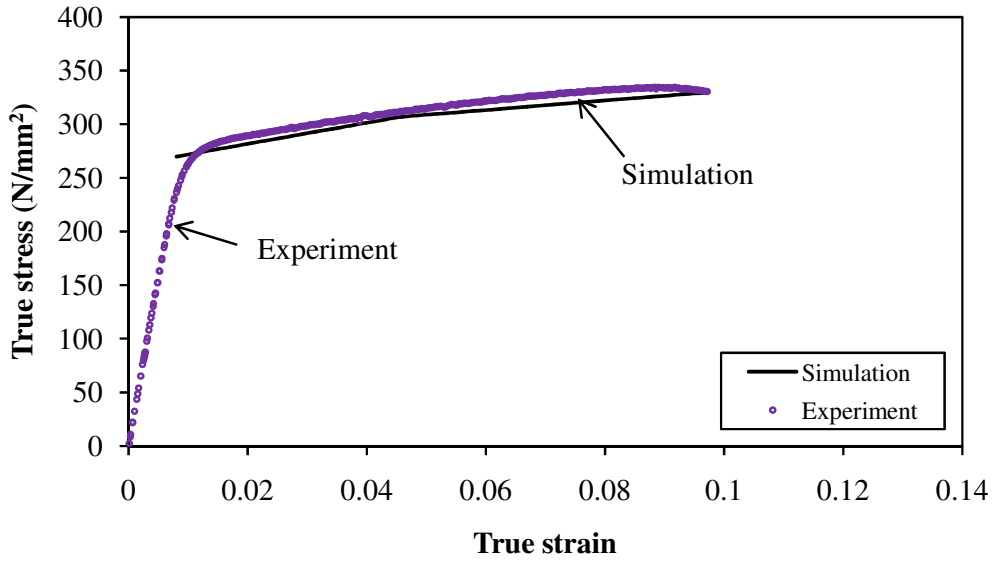

Fig. 9.6 Experimental tensile behavior of base metal comparison with simulation results

Table 9.2 Hill's non-quadratic yield parameter (M) evaluation

M-value	Prediction limit strains	Experimental limit strain
	Major limit strain for unwelded sheets	
1.8	0.264	0.23
1.9	0.278	
2.0	0.177	
2.1	0.189	
2.2	**0.198**	
	Major limit strain of weld zone(FSW sheets)	
1.4	0.184	0.2
1.5	**0.2**	
1.6	0.193	

9.3 Failure criteria used for FLC prediction

9.3.1 Thickness gradient-based necking criterion (TGNC)

This has been discussed in Chapter 2 section 2.1.3

9.3.2 Major strain-rate ratio based criterion (MSRC)

Narasimhan and Wagoner, 1991 developed this criterion, which described that the ratio of major principal strain rate in the neck to that in the bulk, R_1, increases unstably during necking and the criterion is defined as below for necking to occur.

$$R_1 = \frac{\text{Major strain rate in notch}}{\text{Major strain rate in bulk}} \geq 10 \Rightarrow \text{material failure or necking}$$

The validation of MSRC in unwelded and FSW sheets are shown in the Fig. 9.7 to 9.9. In Fig. 9.7 two strain paths namely 100x200 mm and 125x200 mm of unwelded sheets are shown for illustration. The graph is plotted between the ratio "R_1" along y-axis and major strain in the necked element along the x-axis. It is observed that the ratio 8.01 is less than the critical ratio in 100x200 mm strain path, after that the ratio becomes 16.01 which is more than critical ratio. So, the major and minor strain values are noted, as limit strain, corresponding to the ratio of 8.01 for FLC plotting. Similarly in case of 125x200 mm strain path, the major and minor strain values are noted corresponding to the ratio of 9.45. It should also be noted from Fig. 9.7 that beyond the critical ratios (8.01, 9.45), there is a sudden and unstable increase in the major strain ratio indicating the onset of necking.

In the similar manner, the evolution of MSRC is also shown for the FSW blanks at different weld locations; weld at centre, at 5 mm offset and at 10 mm offset and at different welding conditions level-I and II. In Fig. 9.8 three cases are considered for illustration. In all the cases, critical ratios are 9.17, 7.84 and 9.34 for single zone models of 175x 200 mm strain

path with weld at centre, 125x200 mm strain path with weld at 5 mm and 10 mm offset locations at level-II welding conditions respectively. After the critical limit, it becomes very large of about 320.3, 270.9 and 111.3, which are more than the critical ratio. The major and minor strain values corresponding to the critical ratios are considered for evaluating limit strain. The same has observed in case of different weld orientations. The ratios are 9.22 for 45º orientation at level-II in 100 x 200 strain path, and 7.1 and 9.34 for transverse weld orientation at level-I in 150x200 mm and for transverse weld orientation at level-II in 100x200 mm strain path respectively shown in Fig. 9.9.

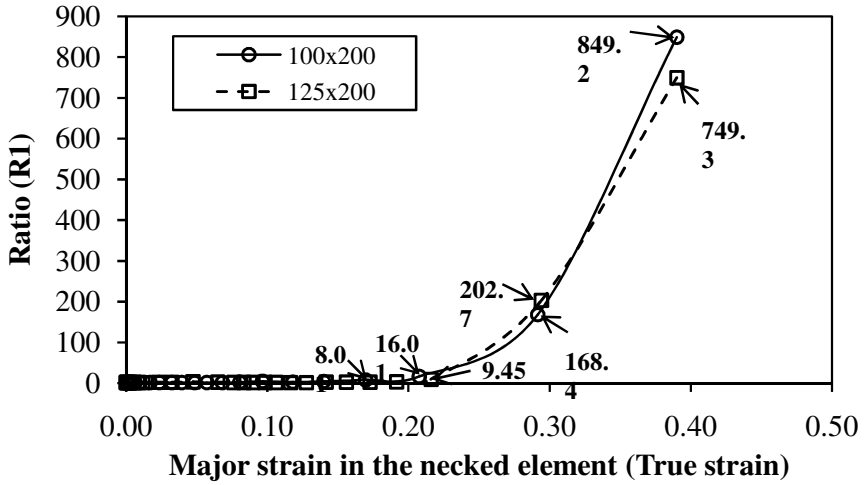

Fig. 9.7 MSRC evolution in unwelded blank

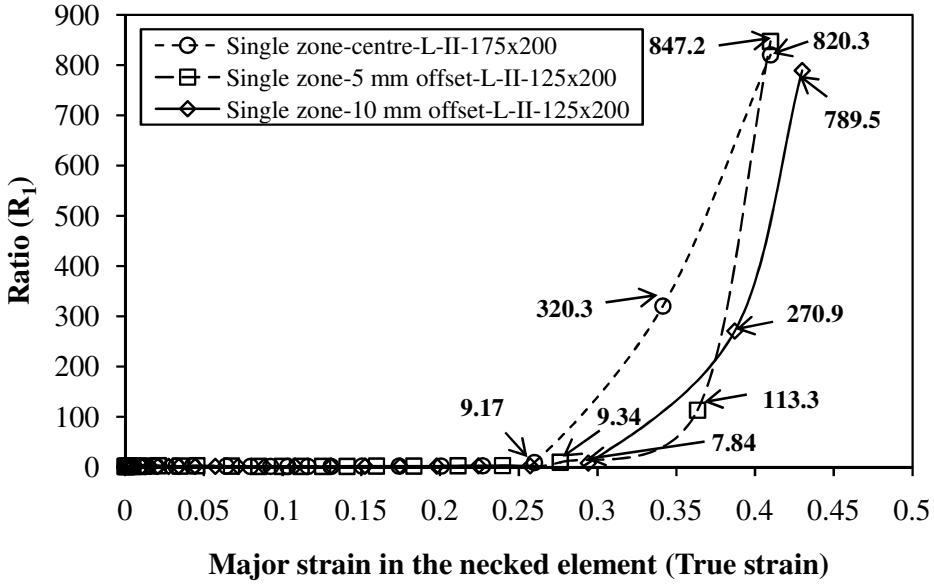

Fig. 9.8 MSRC evolution in FSW blanks at different weld locations

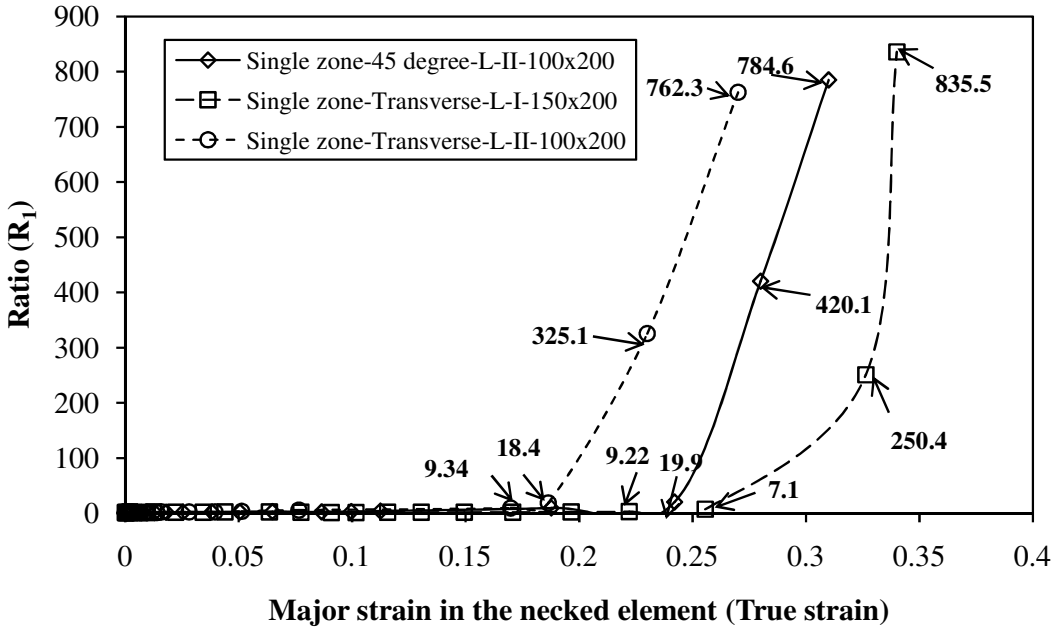

Fig. 9.9 MSRC evolution in FSW blanks at different weld orientations

9.4 Results and Discussion

9.4.1 Comparison of experimental and predicted FLCs of unwelded sheet and FSW sheets at different weld conditions

A comparison has been made between experimental and predicted FLCs of unwelded and FSW sheets with different weld locations, at centre, at 5 mm, at 10 mm offset and at different orientations, 0°, 45° and 90°. For all the weld locations, longitudinal weld orientation is maintained constant. Figure 9.10 shows the experimental and predicted forming limit curves (FLCs) of un-welded sheets. The predicted limit strains are evaluated by thickness gradient based necked criterion (TGNC) and major strain rate ratio based criterion (MSRC). It is observed that the FLC predicted by TGNC is very closer to the experimental FLC as compared to the one predicted by MSRC. The percentage differences of 3% and 6% are seen between TGNC and MSRC and experimental limit strain in plane-strain condition. Towards stretching side, the predicted limit strain values from both the criteria are coinciding with experimental limit strain.

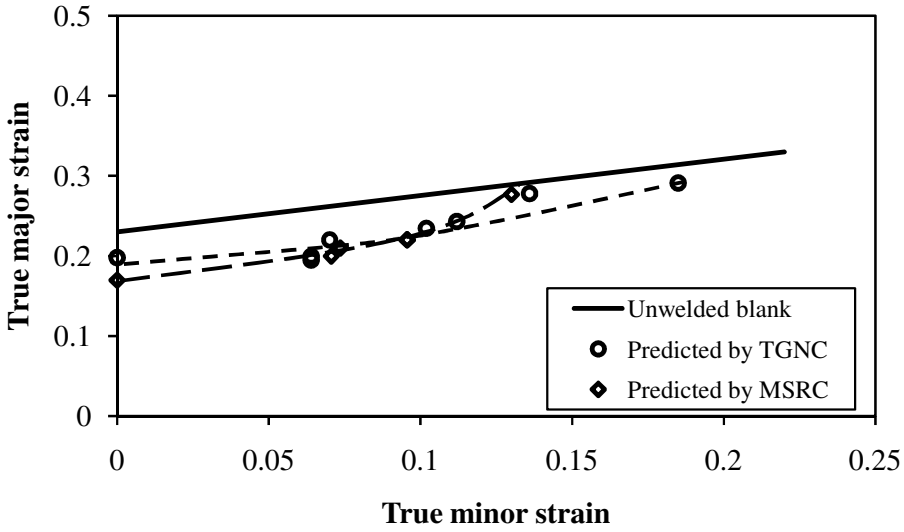

Fig. 9.10 Predicted and experimental FLCs of unwelded sheets

In the case of FSW sheets made at level-I condition with longitudinal weld at centre, as shown in Fig. 9.11, predicted FLCs from both the failure criteria agree well with the experimental result, with MSRC showing 1% difference near to plane-strain condition. When stretching side is considered, predicted FLCs are coinciding well with experimental FLC. FLC predicted by TGNC is slightly better than MSRC when compared with experimental FLC. In level-II, as shown in Fig. 9.12, FLC predicted by MSRC is better than TGNC. The percentage differences are 6% with TGNC and 5% with MSRC, when compared with experimental result.

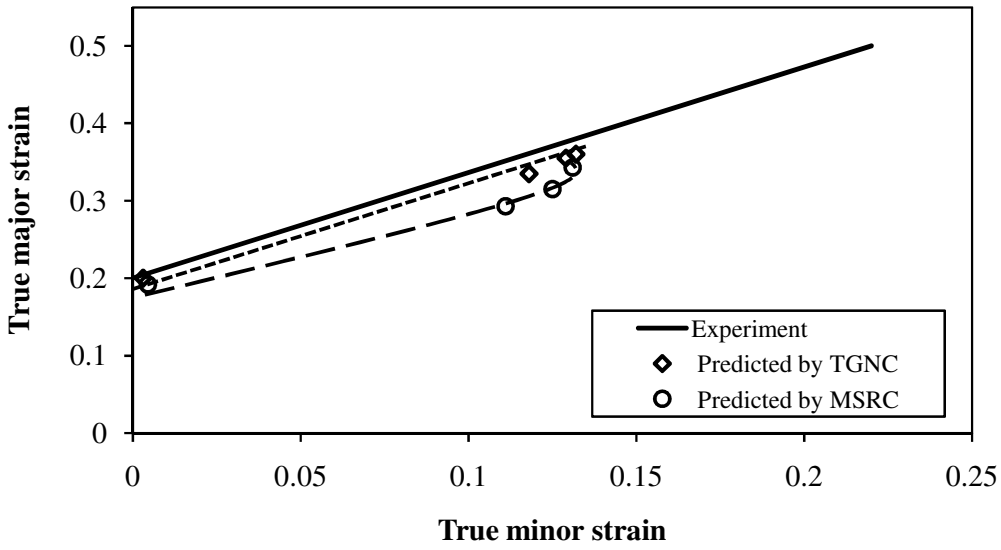

Fig. 9.11 Predicted and experimental FLCs of FSW sheets made at level–I welding condition with longitudinal weld

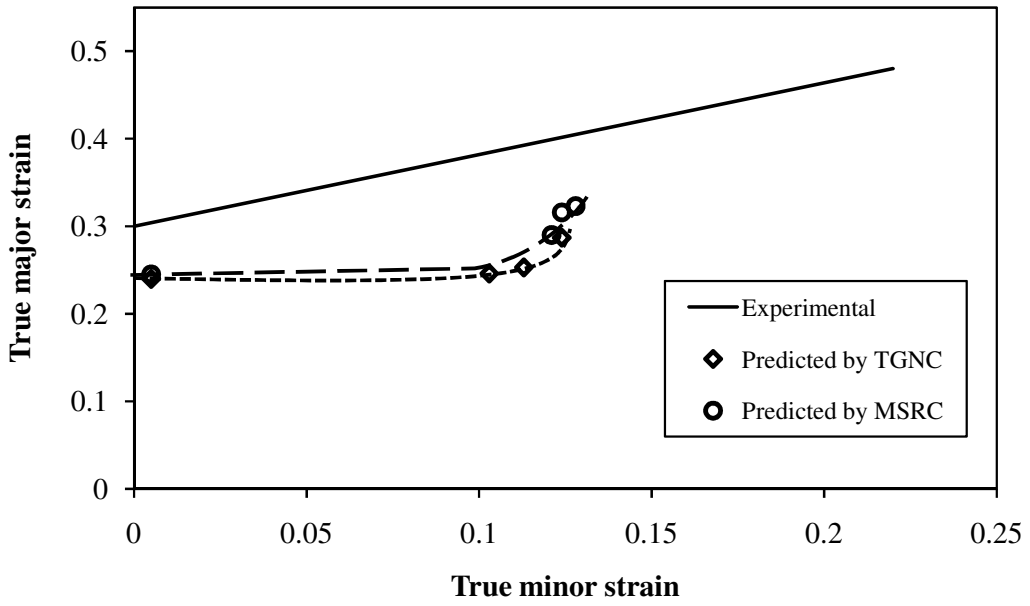

Fig. 9.12 Predicted and experimental FLCs of FSW sheets made at level-II weld condition with longitudinal weld

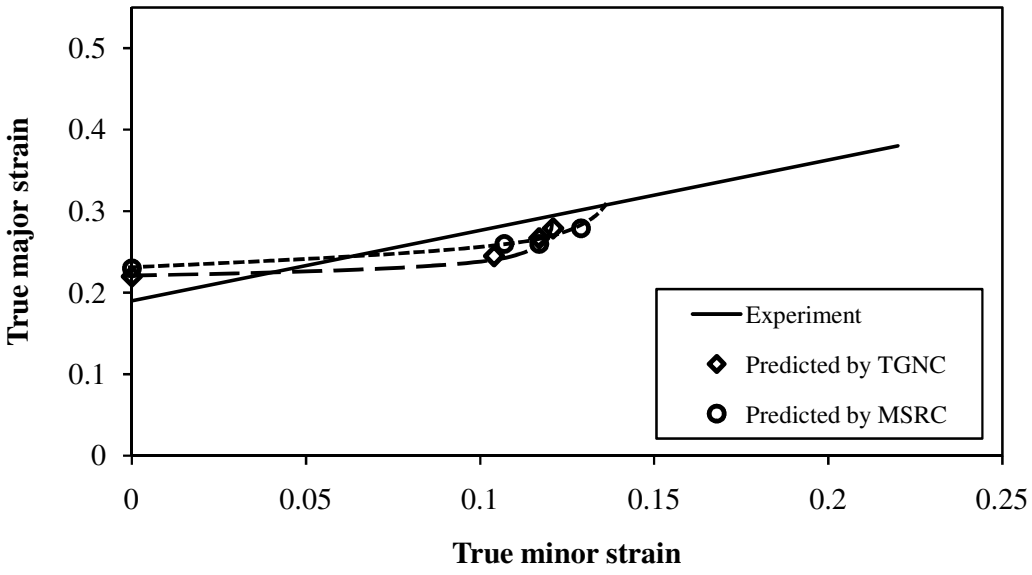

Fig. 9.13 Predicted and experimental FLCs of FSW blanks with 5 mm offset weld location at level-I (longitudinal weld orientation)

Figure 9.13 shows the predicted FLCs of FSW sheets with weld location at 5 mm offset from center distance compared with experimental FLC at level-I condition. It is observed that the predicted FLCs from TGNC and MSRC have better formability near plane-strain condition as compared to experimental FLC and have percentage difference of 3% and 4%

respectively. The overall FLC is coinciding with experimental FLC on the biaxial stretching side. It is also observed that the forming limit prediction is accurate at level-II condition. In case of weld location at 10 mm offset, predicted FLCs are almost same compared to experimental FLC near plane-strain condition and biaxial stretching conditions as shown in Fig. 9.14 for level-I condition. When FLCs from TGNC and MSRC are compared, they predict almost same FLC as compared to experimental FLC. A similar accuracy level is also observed between the experimental and predicted FLCs in level-II condition.

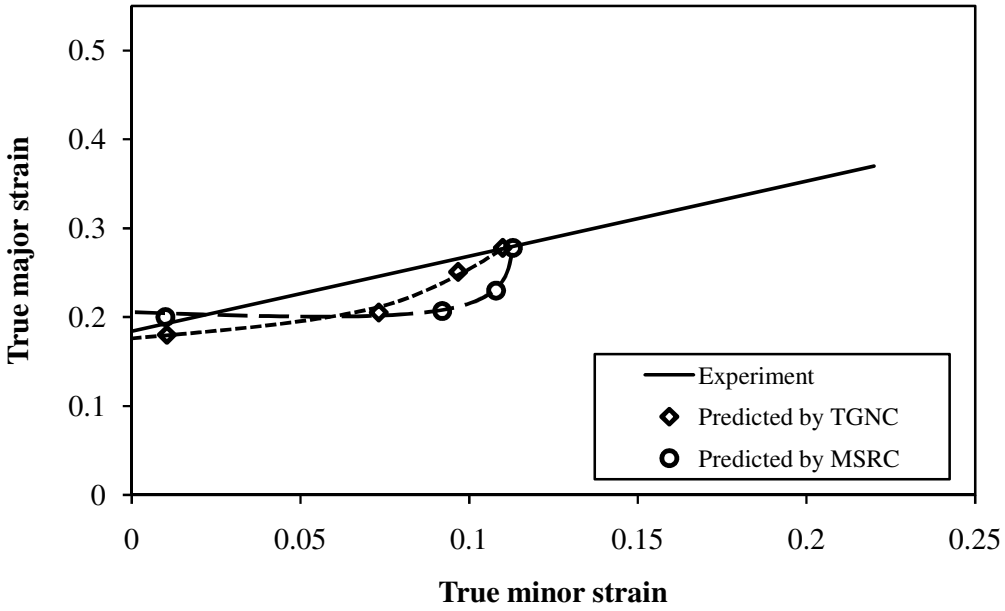

Fig. 9.14 Predicted and experimental FLCs of FSW blanks with longitudinal weld at 10 mm offset made at level-I weld condition

9.4.2 Predicting FLC of FSW sheets with different weld orientations

The weld orientation is kept in three orientations namely 0°, 45° and 90°. Predicting FLCs of FSW sheets with weld orientation at 0° has been discussed in Fig. 9.11 and Fig. 9.12. Figure 9.15 a, b compares the FLCs predicted for transverse weld orientation at level-I and II weld conditions. The FLCs are matching well in the stretching side with slight deviation of the order of 3% and 5% for TGNC and MSRC respectively in plane-strain condition. The same observation is witnessed at level-II condition. In 45º weld orientation, only plane-strain limit strain has been predicted because of experimental material restriction. The TGNC prediction is found to be better than MSRC when compared to experimental limit strain as shown in Fig. 9.16 a, b for level-I and level-II welding conditions respectively.

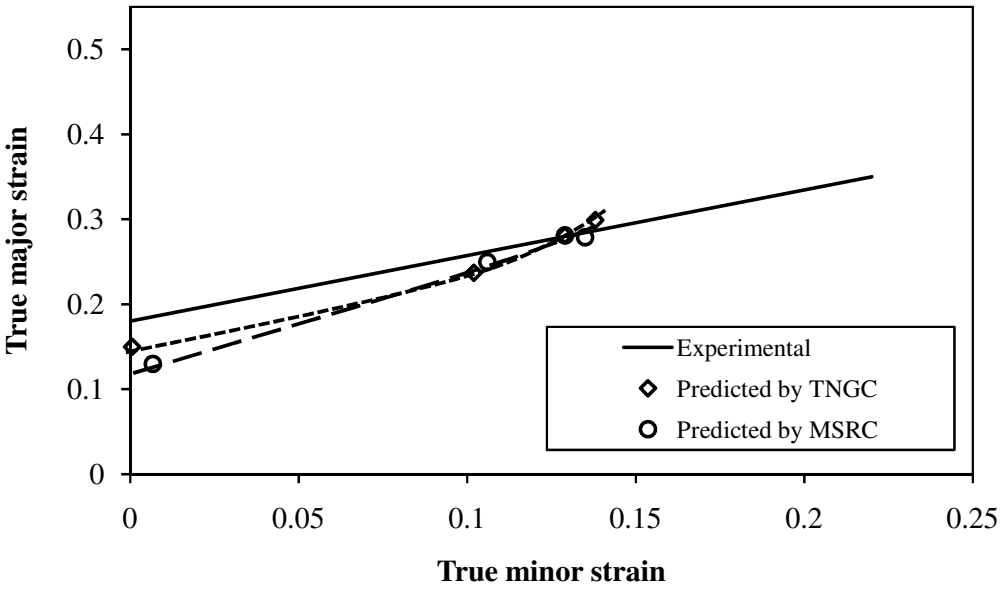

(a) Level-I weld condition

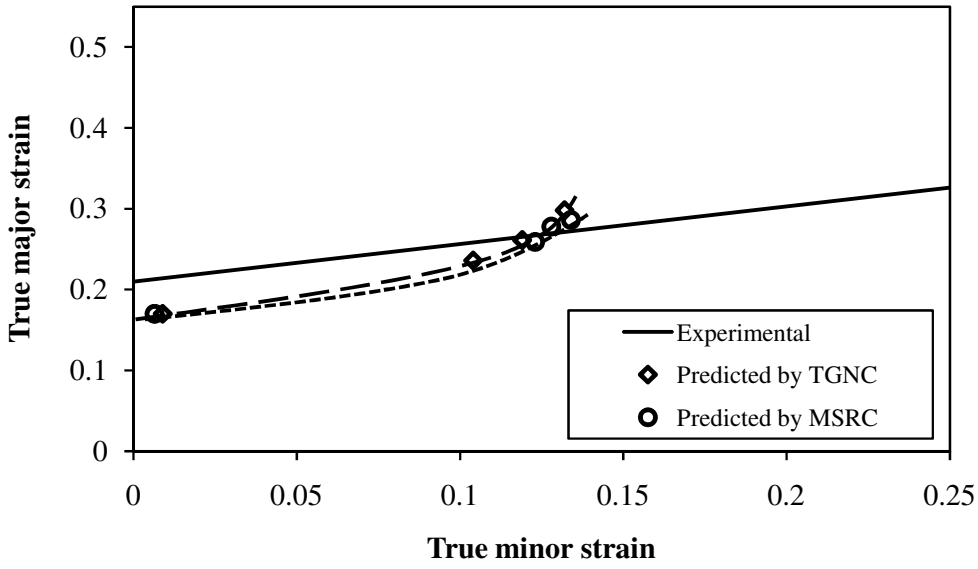

(b) Level-II weld condition

Fig. 9.15 Predicted and experimental FLCs of FSW blanks weld in transverse orientation at different weld conditions

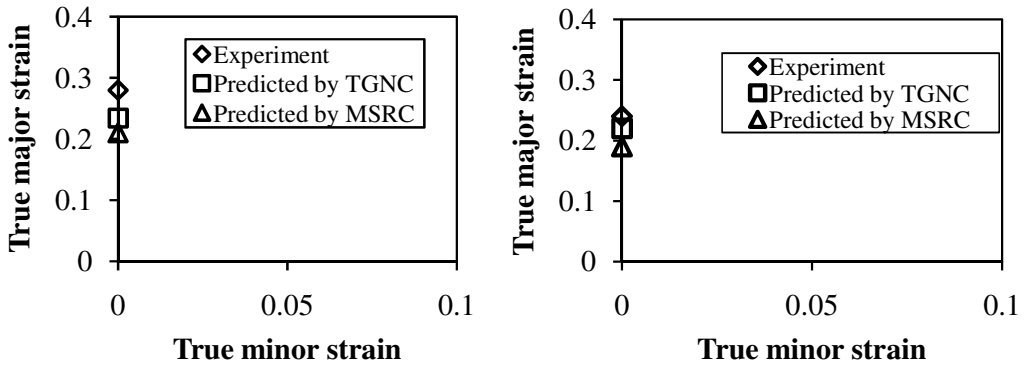

(a) Level-I weld condition (b) Level-II weld condition

Fig. 9.16 Predicted and experimental FLCs of FSW blanks with weld in 45° weld orientation at different welding conditions

9.4.3 Influence of weld zone representation methods on forming limit strain prediction

The weld zone representation methods play a significant role for accurate formability prediction of FSW sheets. The essentiality of weld zone representation has been demonstrated in Chapter 2 and 3. From these Chapters, it has been observed that the weld zone model essentiality depends on the weld geometry, mechanical properties of weld zone, and weld orientation in a synergetic manner. Generally it is expected that the formability prediction accuracy would be better with the double zone models, while in some of the cases single zone model has proved to be sufficient. This critical issue is further discussed in the present work with different weld conditions namely weld orientations, weld locations and welding conditions as presented in Fig. 9.17 to 9.21. The predicted FLCs are compared with experimental results to address this issue.

Figure 9.17 shows the comparison of predicted FLCs having single zone and double zone models, with experimental FLCs for FSW sheets with longitudinal weld orientation at centre location made at level-I welding condition. In this case, the single zone models are showing better forming limit and are closer to experimental limit strains than double zone models. When double zone models are compared, TGNC performs better than MSRC. It can be said that single zone model is sufficient for prediction in this welding condition. In case of weld location at 5 mm offset, FSW sheets made at level-II condition shows that double zone models are essential during formability prediction (Fig. 9.18). The forming limit predicted by MSRC is better than TGNC using double zone models. FSW sheets made at level-II condition in which weld located at 10 mm offset distance from centre in longitudinal direction is shown in Fig. 9.19. It can be observed that FLCs predicted using double zone

models agree well with experimental FLC than single zone models from both TGNC and MSRC.

From the discussion, it is understood that double zone models are more accurate than single zone model at offset weld locations and single zone models are sufficient at centre location. Though performance of double zone models are better than single zone model in few cases, there is only slight deviation between them, independent of weld location and welding conditions.

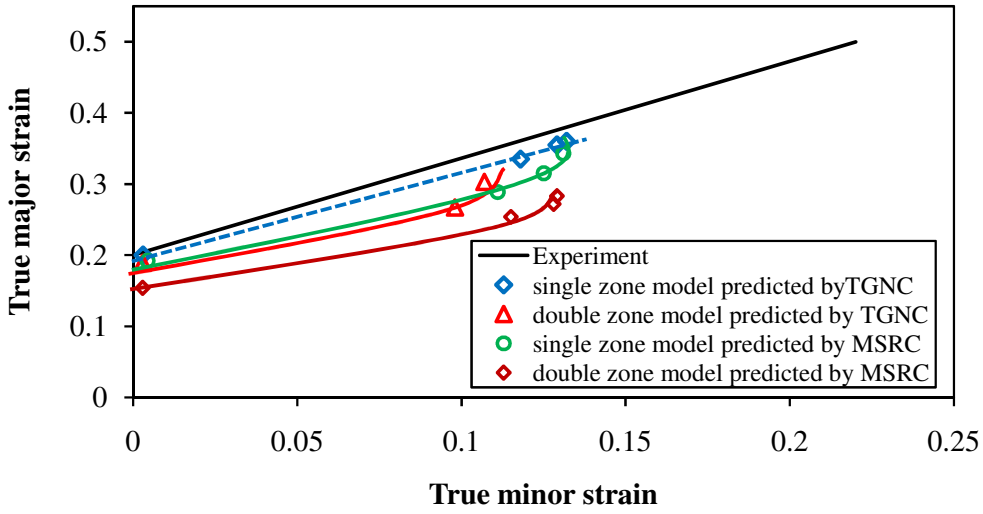

Fig. 9.17 Predicted FLCs of FSW sheets with single zone and double zone models and comparison with experimental FLC of FSW sheet with longitudinal weld at centre made at level-I welding condition

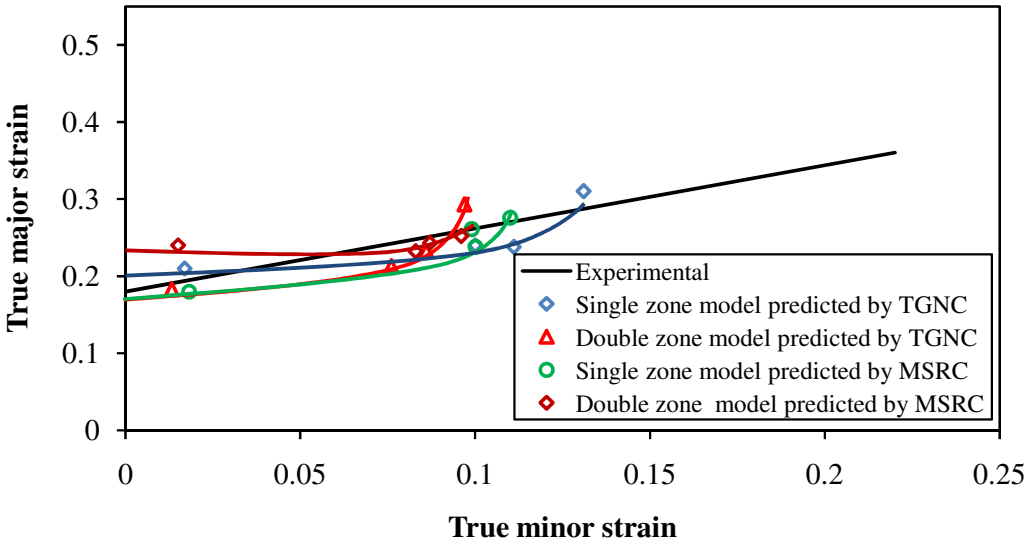

Fig. 9.18 Predicted FLCs of FSW sheets with single zone and double zone models and comparison with experimental FLC of FSW sheet with longitudinal weld at 5 mm offset distance made at level-II welding condition

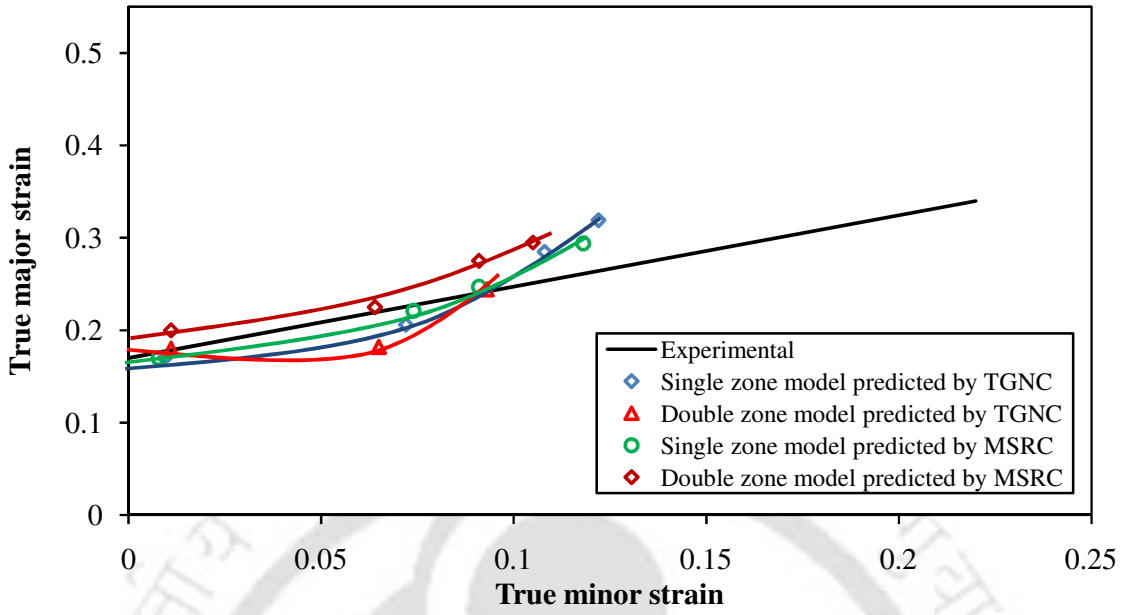

Fig. 9.19 Predicted FLCs of FSW sheets with single zone and double zone models and comparison with experimental FLC of FSW sheet with longitudinal weld at 10 mm offset distance made at level-II welding condition

The other weld condition is about weld orientation, in which weld is kept at three orientations like 0°, 45° and 90° at centre location. The longitudinal weld orientation is already discussed in Fig. 18. In case of FSW sheets with 90° weld orientation (transverse weld orientation), it is observed from Fig. 9.20 (for level-II condition) that double zone models are essential for formability prediction during simulation as their forming limit prediction is closer to experimental FLC. The accurate prediction is seen in double zone models by MSRC. Similarly in case FSW sheets with 45° weld orientation, double zone models predict accurately and are essential for a better forming limit prediction by both TGNC and MSRC (Fig. 9.21). A summarized assessment of weld zone representation methods under different weld conditions (orientation, location, weld properties) is shown in Table 9.3.

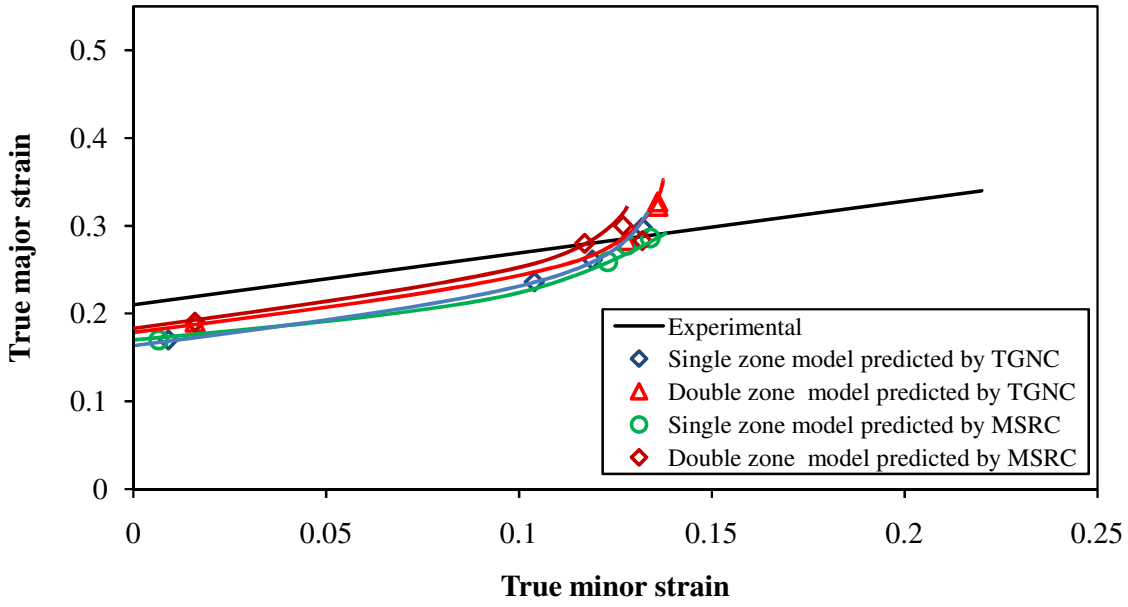

Fig. 9.20 Predicted FLCs of FSW sheets with single zone and double zone models and compared with experimental FLC of FSW sheet in transverse orientation at level-II welding condition

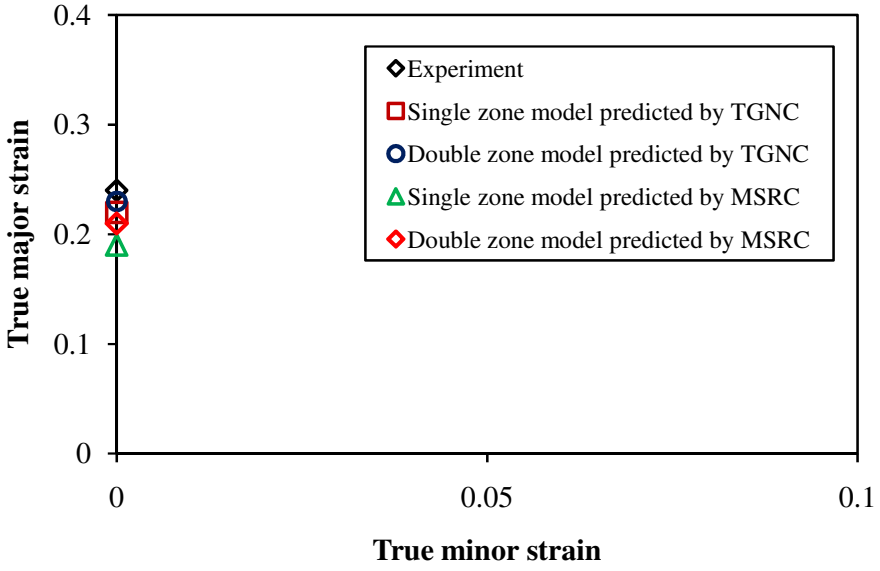

Fig. 9.21 Predicted FLCs of FSW sheets with single zone and double zone models and compared with experimental FLC of FSW sheet in 45° orientation at level-II welding condition

Table 9.3 Assessment of weld zone representation methods during formability prediction of FSW sheets at different weld conditions

Weld zone model	Weld locations												Weld orientations							
	Centre / 0º				5 mm offset				10 mm offset				45º				90º			
	TGNC		MSRC		TGNC		MSRC		TGNC		MSRC		TGNC		MSRC		TGNC		MSRC	
	L-I	L-II	L-I	L-II	L-I	L-II	L-I	L-II	L-I	L-II	L-I	L-II	L-I	L-II	L-I	L-II	L-I	L-II	L-I	L-II
Single zone	√	×	√	×	√	×	×	×	√	×	×	×	×	×	×	×	×	×	√	×
Double zone	×	√	×	√	×	√	√	√	×	√	√	√	√	√	√	√	√	√	×	√

From the obtained mechanical properties of the weld zone, WN and HAZ from Table 9.1, the width ratio between WN width (w_{WN}) and HAZ width (w_{HAZ}), that is $w_r = w_{WZ}/w_{HAZ}$, is obtained as 3.5 approximately; ratio of yield strength of WN (σ_{NZ}) to HAZ (σ_{HAZ}), $\sigma_r = \sigma_{NZ}/\sigma_{HAZ}$; is 0.64; and ratio of strain hardening exponent of WN (n_{NZ}) to HAZ (n_{HAZ}), $n_r = n_{NZ}/n_{HAZ}$, is 1.28 for level-I FSW condition. Similarly for level-II condition: w_r = 3.5; σ_r = 0.65; n_r= 1.29. The three weld conditions (σ_r, n_r, w_r) influence the validity of single zone or double zone in a compounding fashion as discussed in Chapter 2 and 3. From the Chapter 2 and 3, it has been demonstrated that when these ratios $\sigma_r=1$, $n_r=1$, $w_r=4$ are near to single zone model then single zone model is sufficient, otherwise double zone model would be essential. From the present work, the ratios σ_r and n_r are not very close to single zone model, so in all cases double zone model is essential. The same has been observed in Table 9.3 that in most of cases double zone models delivered better formability prediction than single zone models. Also since offset weld locations are critical when compared to centre weld location and failure is seen most often in the interface of HAZ and base material, double zone models would provide accurate FLCs as compared to single zone models as presented in Table 9.3. This is true in the cases of 45º and 90º weld orientations also, where double zone models are more accurate than single zone models.

9.4.4 Failure location comparison

Failure location plays a vital role in deciding the limit strains of welded blanks. It gives idea about localizations of strain and thickness evolution during forming. The following are some of the important observation in this context.

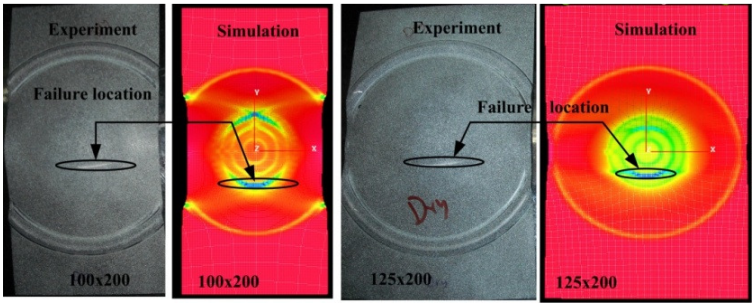

Fig. 9.22 Failure locations comparison in experimental and predicted unwelded sheets

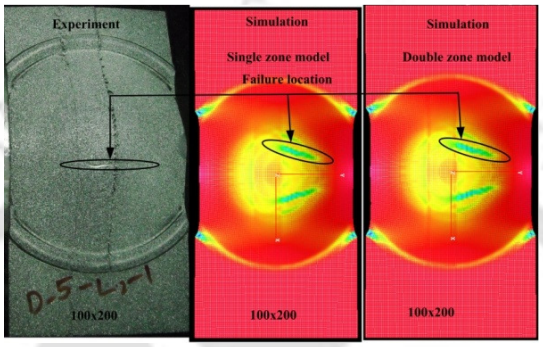

(a) Plane-strain strain paths

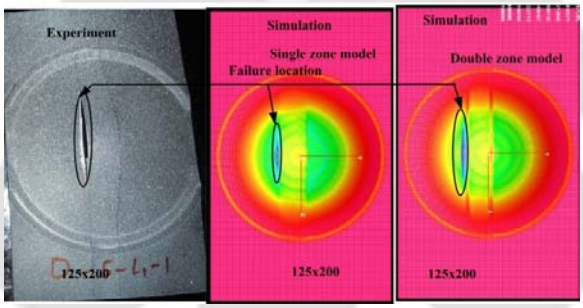

(b) Stretching strain paths

Fig. 9.23 Comparison of failure location in experimental and predicted FSW sheets with weld at 5 mm offset location

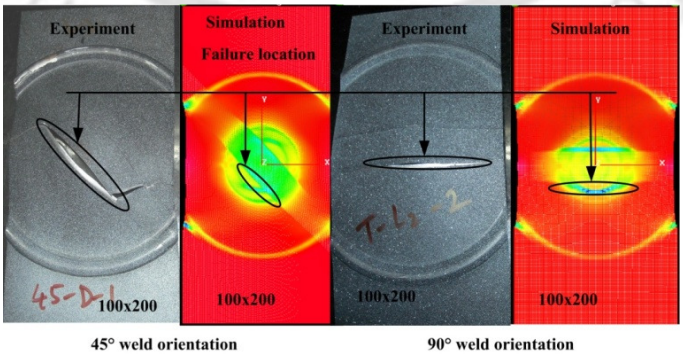

Fig. 9.24 Comparison of failure location in experimental and predicted FSW sheets with weld in 45° and 90° orientations

Figure 9.22 shows the comparison between experimental and predicted failure location in unwelded sheet. It is observed that failure pattern is same in both the strain paths. Similar consistent failure pattern prediction is seen in case of plane-strain (100 x 200 mm) strain paths of FSW sheets (Fig. 9.23 (a)). During predictions in plane-strain strain paths, failure has occurred in the base metal first and then propagated towards weld zone. This has happened in both single zone and double models irrespective of the weld location. In case of stretching strain paths (125x200 mm, 150x200 mm and 175x200 mm) failure pattern in FSW sheets is along the weld interface shown in Fig. 9.23 (b). The same failure pattern is seen in the cases of 45° and 90° weld orientation (Fig. 9.24) irrespective of the weld zone models. All the predicted failure pattern and locations in unwelded and FSW sheets are well matched with experimentally tested FSW sheets. Due to this the FLCs predictions are also matching well with experimental results as discussed in sections 9.4.1, 9.4.2 and 9.4.3.

9.5 Conclusions

The following conclusions are made from this Chapter

- The forming limit predicted by TGNC and MSRC coincide well with experimental forming limit of un-welded sheet. In the meantime, the TGNC predictions are slightly better than MSRC predictions.
- The FSW sheet FLCs predicted at different weld locations, weld at centre, at 5 mm offset, and at 10 mm offset, are agreeing well with the experimental results, except in level-II welding condition for centre weld location. The predicted FLCs from TGNC and MSRC are equally accurate as compared to experimental FLCs.
- In general, the predicted FLCs for different weld orientations, say 0°, 45° and 90°, are coinciding well with the experimental results. Both TGNC and MSRC predict almost the same forming limit in 90° weld orientation, while TGNC showed better prediction in 45° weld orientation. Only plane-strain forming limit is measured and predicted in 45° weld orientation because of material restriction.
- FSW sheets with double zone models show better prediction accuracy than single zone models in most of the cases. Single zone model is found to be sufficient in case of weld at centre location and at longitudinal orientation.
- Since weld at 5 mm and 10 mm offset are at critical locations and failure is observed along the weld region, double zone models are found to be more accurate than single zone models. Though double zone models perform better than single zone models in these

cases, there is only slight deviation between them, independent of weld location and welding conditions.

- The failure location and failure pattern predicted are same as compared to experimental results for varied weld location, weld orientations, and welding conditions.

Chapter 10

Conclusions from the present work

The conclusions drawn from the present work are:

- The weld zone representation methods affect the accuracy of forming limit prediction significantly. For representing the single zone or double zone models, multiple domains are possible due to the parametric changes in weld conditions and such changes affects the local and global deformation, like thickness distribution, influencing the model representation.

- The three weld conditions namely YS_r, n_r, and w_r influence the validity of single zone or double zone in a compounding fashion. If these weld conditions are closer to reference model weld condition, then single zone model is found to be valid. If the weld conditions are very different from the reference model, it breaks down the single zone model so that double zone model is valid in those cases. These failure locations or initiations also affect the weld zone representation along with the critical error percentage difference between reference model (single zone) and double zone model FSW blanks.

- The failure initiations are observed at different locations of weld in transverse and longitudinal orientations for different weld conditions of FSW blanks. In the case of transverse weld orientation, failure initiations are in weld nugget and HAZ only. In longitudinal weld orientation, failure initiation is not only in weld zones but also in base materials, and failure is normal to the weld zone. In addition, the base metal properties and thickness could also affect the methods of weld zone representation during formability prediction.

- The number of single zone models has increased in transverse weld orientation and number of double zone models has increased in longitudinal weld orientation in the case of FSW blank with dissimilar thicknesses as compared to similar thickness FSW blanks. This is due to the change in failure location during forming of FSW blanks.

- The optimized welding parameters chosen for the experimental work are, welding speed: 80-120 mm/min, tool rotation speed: 1300-1500 rpm, plunge depth: 1.85-2 mm. This range is

preferred for producing a weld without internal defects. This range is valid for all the shoulder diameters, 12, 15, 18 mm, for welding AA6061-T6 sheet with 2.1 mm thickness.

- The axial force and torque are found to increase with increase in welding speed and shoulder diameter. A decreasing trend is observed in axial force and torque while increasing the rotation speed. The axial force is found to increase with increase in plunge depth, while there is no effect of plunger depth on the torque generated in FSW. Once the optimized welding parameters are reached, since there are no internal defects in the weld region, the axial force and torque are almost constant.

- A simple criterion is proposed by observing the variation of axial force (F) and torque (τ) with respect to welding parameters (p) for identifying the onset of defect free weld region for any base material. The criterion is stated as:

$$\left(\frac{\partial \tau}{\partial p}\right)_{defective} > \left(\frac{\partial \tau}{\partial p}\right)_{defect\ free}$$

$$and$$

$$\left(\frac{\partial F}{\partial p}\right)_{defective} > \left(\frac{\partial F}{\partial p}\right)_{defect\ free}$$

- The micro-hardness showed a decreasing trend, from the base material to the middle line of the nugget zone, except near the transition zone. With increase in shoulder diameter and welding speed, hardness has increased. But with increase in plunge depth and rotational speed, hardness has decreased with plunge depth showing relatively subtle effect. The FSW sheets showed a decreased flow stress and improved elongation when compared to base material. With increase in plunge depth, shoulder diameter, rotational speed, the elongation of FSW sheets and weld zone is found to improve, while welding speed has shown insignificant effect.

- The thinning gradient has shown significant effect changing the overall elongation with change in welding conditions. The thickness gradient is found to be severe in un-welded blanks as compared to FSW blanks. The thickness gradient is severe in FSW sheets made at lower levels of shoulder diameter, plunge depth and rotation speed, while welding speed showed negligible effect. Thinning gradient is dependent on the strain hardening exponent

(n). With improvement in strain hardening exponent of FSW sheets (and weld zone) with respect to changing welding conditions, the thinning gradient is less and vice versa, consequently improving the overall elongation of welded sheets in most of the cases.

- The FSW sheets exhibit better formability than un-welded sheets at different welding conditions. By increasing the shoulder diameter, plunge depth and tool rotation speed, and by decreasing the welding speed, the formability of FSW blank is found to improve. With increase in shoulder diameter, plunge depth, and tool rotation speed, the thickness distribution becomes uniform and hence improvement in forming limit is witnessed.

- The improvement in forming limit of FSW sheets is also due to the increase in strain hardening exponent of weld region as compared to un-welded sheets. The increase in strain harening exponent of weld region is believed to happen because of reduction in dislocation density in the recrystallized zone. With increase in weld zone strain hardening exponent, the thickness distribution becomes uniform, improving the overall forming limit of FSW sheets.
- The dome height difference between the FSW sheets and un-welded sheets is not very different in plane-strain strain path. But in stretching side, due to failure in weld region, the dome height of un-welded sheets is more than that of welded sheets. There is not much variation in dome height with respect to varied plunge depth and shoulder diameter, unlike in forming limit curve and thickness distribution. There is hardly 1-2 mm variation in dome height in all FSW cases.
- Thickness distribution in advancing side and retreating side is not same and more thinning gradient is seen in the retreating side of the weld. This is mainly due to the differential straining attained by both the sides during FSW. The hardness difference between the retreating side and advancing side also affects the thickness evolution during forming along with the strains. Finally the thickness gradient depends on the welding conditions also.

- FSW sheet with weld at centre location shows better forming limit as compared to 5 mm and 10 mm weld offset location cases. This is mainly due to the localization of strains and larger thickness distribution severity at these offset locations. There is not much difference in the forming limit of FSW sheets with welds at 5 mm and 10 mm offset locations showing their insensitivity.

- In the case of weld orientations, FSW sheets with 0° weld orientation possess improved formability as compared to 45° and 90 ° weld orientation cases. This is due to the change in failure mode, from normal to weld region to parallel to weld zone, when the weld orientation is changed. There is not much change in limit strains between 45° and 90° weld orientations as the failure pattern is same.

- The failure pattern at different weld orientations and weld locations plays a significant role in deciding the forming limit of FSW sheets. The failure location is found to be at the retreating side of the weld zone and this mainly due to the larger thickness gradient existing at this side as compared to advancing side during forming.

- In general, the predicted FLCs for different weld orientations, say 0°, 45° and 90°, are coinciding well with the experimental results. Both TGNC and MSRC predict almost the same forming limit in 90° weld orientation, while TGNC showed better prediction in 45° weld orientation. Only plane-strain forming limit is measured and predicted in 45° weld orientation because of material restriction.

- The FSW sheet forming limit predicted at different weld locations, weld at centre, at 5 mm offset, and at 10 mm offset, are agreeing well with the experimental results, except in level-II welding condition with centre weld. The predicted FLCs from TGNC and MSRC are equally accurate as compared to experimental FLCs.

- The failure location and failure pattern predictions of FSW sheets are same as compared to experimental results for varied weld location, weld orientations, and welding conditions.

- FSW sheets with double zone models have the better formability prediction than single zone models with respect to weld locations and orientations. It is seen that defining the properties for WN and HAZ separately makes a significant contribution to the accuracy of formability prediction.

Future work

The following recommendations could be applied to future work in this area.

- The formability evaluation of FSW sheets can also be studied through different forming tests like bending tests, in-plane plane-strain forming tests and deep drawing tests. Weld zone representation prediction can be verified by simulating bending test, in-plane plane-strain forming test and deep drawing behavior of FSW sheets and can be verified with experimental results. Spring back analysis can be studied through numerical simulation and experiments for FSW sheets.

- In the present work all the friction stir welds were fabricated in load controlled mode, whereas there is a provision the FS welds can also be fabricated in process control mode. By which an optimized axial load and torque can be identified for making defect free welds and influence of axial load and torque on formability of FSW sheets can be observed.

- In this work, the influence of forming behavior of FSW sheets with respect to shoulder diameter, plunge depth, tool rotation speed and welding speed only. There are few other process parameters like tilt angle, axial load, overlap, feed rate, axial load etc., which are also affecting the FSW joint performance. A separate study can be made on forming behavior with respect to these process parameters.

- In the present work, study of the effect of shoulder diameter, plunge depth, tool rotation speed and welding speed was carried out for formability evaluation of FSW sheets made AA 6061-T6 with similar thickness. The work can be extended to other materials having similar and dissimilar quality/ thickness with different shoulder diameter, plunge depth, tool rotation speed and welding speed and their combinations. The optimum relationships can be formulated for the best formability of FSW sheets.

- In the present study, formability prediction of FSW sheets was studied using different failure criteria by modeling weld zone as single zone and double zone model. The mechanical properties were evaluated for heat affected zone and weld nugget of FS weld zone for modeling double zone model. The investigation showed that for accurate formability

prediction double zone model is essential. This can be extended further by evaluating mechanical properties of heat affected zone in advancing side and retreating side separately.

- The formability can also be observed after post weld heat treatments of FSW sheets with respect to all the FSW process parameters. The formability can be correlated with respect to microstructural changes during post weld heat treatments.

- An expert system can be developed for optimizing the process parameters, mechanical properties and formability by artificial neural networks. This can be used as an initial index for selecting optimum range to fabricate defect free welds and also avoiding more number of trials by which material can be saved.

- The influence of process parameters on the residual stresses after forming of FSW sheets can be addressed.

References

Abbasi Gharacheh M, Kokabi AH, Daneshi GH, Shalchi B, Sarrafi R (2006) The influence of the ratio of ‘‘rotational speed/traverse speed’ on mechanical properties of AZ31 friction stir welds. International Journal of Machine Tools & Manufacture 46:1983–1987.

Afrin N, Chen DL, Cao X, et al. (2007) Strain hardening behavior of a friction stir welded magnesium alloy. Scripta Materialia 57:1004–1007.

Ahn BW, Choi DH, Kim DJ, Jung SB (2012) Microstructures and properties of friction stir welded 409L stainless steel using a Si3N4 tool. Materials Science and Engineering A 532:476– 479.

Akinlabi ET (2012) Effect of Shoulder Size on Weld Properties of Dissimilar Metal Friction Stir Welds. Journal of Materials Engineering and Performance 21:1514–1519.

Amancio-Filho ST, Sheikhi S, Dos Santos JF, Bolfarini C (2008) Preliminary study on the microstructure and mechanical properties of dissimilar friction stir welds in aircraft aluminium alloys 2024-T351 and 6056-T4. Journal of Materials Processing Technology 206:132-142.

Arbegast WJ (2008) A flow-partitioned deformation zone model for defect formation during friction stir welding. Scripta Materialia 58:372–376.

Arora A, De A, DebRoy T (2011) Toward optimum friction stir welding tool shoulder diameter. Scripta Materialia 64:9–12.

Aval HJ, Serajzadeh S, Kokabi AH (2010) The influence of tool geometry on the thermo-mechanical and microstructural behaviour in friction stir welding of AA5086. Proceedings of IMechE Part C: Journal of Mechanical Engineering Science 225:1-16.

Azizieh M, Kokabi AH, Abachi P (2011) Effect of rotational speed and probe profile on microstructure and hardness of AZ31/Al_2O_3 nano-composites fabricated by friction stir processing. Materials and Design 32:2034–2041.

Badarinarayan H, Shi Y, Li X, Okamoto K (2009 a) Effect of tool geometry on hook formation and static strength of friction stir spotweldedaluminum5754-O sheets. International Journal of Machine Tools & Manufacture 49:814–823.

Badarinarayan H, Yang Q, Zhu S (2009 b) Effect of tool geometry on static strength of friction stir spot-welded aluminum alloy. International Journal of Machine Tools & Manufacture 49:142–148.

Banabic D (2010) Sheet Metal Forming Processes: Constitutive Modeling and Numerical Simulation: Formability of Sheet Metals. Springer Heidelberg 141-204.

Banabic D, Bunge HJ, Pohalandt K, Tekkaya AE (2000) Formability of metallic materials: Plastic Anisotropy, Formability Testing, Forming Limit. Springer-Verlag Berlin Heidelberg, 61-108 and 173-209.

Barcellona A, Buffa G, Fratini L, Palmeri D (2006) On microstructural phenomena occurring in friction stir welding of aluminium alloys. Journal of Materials Processing Technology 177:340–343.

Buffa G, Campanile G, Fratini L, Prisco A (2009) Friction stir welding of lap joints: Influence of process parameters on the metallurgical and mechanical properties. Materials Science and Engineering A 519:19-26.

Buffa G, Fratini L, Merklein M, Staud D (2007) Investigations on the Mechanical Properties and Formability of Friction Stir Welded Tailored Blanks. Key Engineering Materials 344:143-150.

Buffa G, Hua J, Shivpuri R, Fratini L. A continuum based fem model for friction stir welding—model development. Materials Science and Engineering A. 419:389–396.

Cabibbo M, McQueen HJ, Evangelista E, Spigarelli S, Paola DM, Falchero A (2007) Microstructure and mechanical property studies of AA6056 friction stir welded plate. Materials Science and Engineering A 460-461:86-94.

Caizhi Zhou , Xinqi Yang Guohong Luan (2006) Effect of root flaws on the fatigue property of friction stir welds in 2024-T3 aluminum alloys. Materials Science and Engineering A 418:155-160.

Cao X and Jahazi M (2011) Effect of tool rotational speed and probe length on lap joint quality of a friction stir welded magnesium alloy. Materials and Design 32:1-11.

Cavaliere P, Campanile G, Panella F, Squillace A (2006) Effect of welding parameters on mechanical and microstructural properties of AA6056 joints produced by Friction Stir Welding. Journal of Materials Processing Technology 180:263–270.

Cavaliere P, Squillace A, Panella F (2008) Effect of welding parameters on mechanical and microstructural properties of AA6082 joints produced by friction stir welding. Journal of Materials Processing Technology 200:364-372.

Cerri E, Leo P, Wang X, Embury JD (2011) Mechanical Properties and Microstructural Evolution of Friction-Stir-Welded Thin Sheet Aluminum Alloys. Metallurgical and Materials Transactions A 42A:1283-1295.

Chen HB, Yan K, Lin T, Chen SB, Jiang CY, Zhao Y (2006) The investigation of typical welding defects for 5456 aluminum alloy friction stir welds. Materials Science and Engineering A 433:64–69.

Chen YC and Nakata K (2009) Effect of tool geometry on microstructure and mechanical properties of friction stir lap welded magnesium alloy and steel. Materials and Design 30:3913–3919.

Chen ZW, Pasang T, Qi Y (2008) Shear flow and formation of Nugget zone during friction stir welding of aluminum alloy 5083-O. Materials Science and Engineering A 474:312–316.

Cheng CH, Chan LC, Chow CL, Lee TC (2005) Experimental investigation on the weldability and forming behavior of aluminum alloy tailor-welded blanks. Journal of Laser Applications 17(2):81-88.

Choi Y, Heo Y, Kim YH, Seo D (2000) Investigations of weld-line movements for the deep drawing process of tailor welded blanks. Journal of Materials Processing Technology 108:1-7.

Chowdhury SM, Chen DL, Bhole SD, Cao X (2010) Tensile properties of a friction stir welded magnesium alloy: Effect of pin tool thread orientation and weld pitch. Materials Science and Engineering A 527:6064-6075.

Chung K, Lee W, D. Kim D, Kim J, Chung KH, Kim C, Okamoto K, Wagoner RH (2010) Macro-performance evaluation of friction stir welded automotive tailor-welded blank sheets: Part I–Material properties. International Journal of Solids and Structures 47:1048-1062.

Colegrove PA, Shercliff HR (2005) 3-Dimensional CFD modelling of flow round a threaded friction stir welding tool profile. Journal of Materials Processing Technology. 169:320–327.

Colligan KJ and Mishra RS (2008) A conceptual model for the process variables related to heat generation in friction stir welding of aluminum. Scripta Materialia 58:327-331.

Commin L, Dumont M, Masse JE, Barrallier L (2009) Friction stir welding of AZ31 magnesium alloy rolled sheets: Influence of processing parameters. Acta Materialia 57:326-334.

Cui L, Yang X, Zhou G, Xu X, Shen Z (2012) Characteristics of defects and tensile behaviors on friction stir welded AA6061-T4 T-joints. Materials Science and Engineering A 543:58-68.

Cui S, Chen ZW, Robson JD (2010) A model relating tool torque and its associated power and specific energy to rotation and forward speeds during friction stir welding/processing. International Journal of Machine Tools and Manufacture 50:1023 –1030.

D'Urso G and Giardini C (2010) The influence of process parameters and tool geometry on mechanical properties of friction stir welded aluminum lap joints. International Journal of Material Forming 3(1):1011-1014.

D'Urso G, Ceretti E, Giardini C, Maccarini G (2009) The effect of process parameters and tool geometry on mechanical properties of friction stir welded aluminum butt joints. International Journal of Material Forming 2(1):303-306.

De Giorgi M, Scialpi A, Panella FW, De Filippis LAC (2009) Effect of shoulder geometry on residual stress and fatigue properties of AA6082 friction stir welded joints. Journal of Mechanical Science and Technology 23:26-35.

Derry CG and Robson JD (2008) Characterisation and modelling of toughness in 6013-T6 aerospace aluminium alloy friction stir welds. Materials Science and Engineering A 490:328–334.

Elangovan K and Balasubramanian V (2007) Influences of pin profile and rotational speed of the tool on the formation of friction stir processing zone in AA2219 aluminium alloy. Materials Science and Engineering A 459:7-18.

Elangovan K and Balasubramanian V (2008 a) Influences of post-weld heat treatment on tensile properties of friction stir-welded AA6061 aluminum alloy joints. Materials Characterization 59:1168-1177.

Elangovan K and Balasubramanian V (2008 b) Influences of tool pin profile and welding speed on the formation of friction stir processing zone in AA2219 aluminium alloy. Journal of Materials Processing Technology 200:163-175.

Elangovan K and Balasubramanian V (2008 c) Influences of tool pin profile and tool shoulder diameter on the formation of friction stir processing zone in AA6061 aluminium alloy. Materials and Design 29:362-373.

Elangovan K, Balasubramanian V, Valliappan M (2008 d) Influences of tool pin profile and axial force on the formation of friction stir processing zone in AA6061 aluminium alloy. International Journal of Advanced Manufacturing Technology 38:285-295.

Ericsson M and Sandstrom R (2003) Influence of welding speed on the fatigue of friction stir welds, and comparison with MIG and TIG. International Journal of Fatigue 25:1379-1387.

Feng AH, Chen DL, Ma ZY (2009) Effect of Welding Parameters on Microstructure and Tensile Properties of Friction Stir Welded 6061 aluminum joints. Materials Science Forum 618-619:41-44.

Fersini D and Pirondi A (2008) Analysis and modeling of fatigue failure of friction stir welded aluminum alloy single-lap joints. Engineering Fracture Mechanics 75:790-803.

Fonda RW, Bingert JF, Colligan KJ (2004) Development of grain structure during friction stir welding. Scripta Materialia 51:243-248.

Forcellese A and Simoncini M (2012) Plastic flow behaviour and formability of friction stir welded joints in AZ31 thin sheets obtained using the ''pinless'' tool configuration. Materials and Design 36:123-129.

Forcellese A, Gabrielli F, Simoncini M (2012) Mechanical properties and microstructure of joints in AZ31 thin sheets obtained by friction stir welding using ‘‘pin’’ and ‘‘pinless’’ tool configurations. Materials and Design 34:219–229.

FU Zhi-hong, HE Di-qiu, Wang Hong (2004) Friction Stir Welding of Aluminum Alloys. Journal of Wuhan University of Technology, Material Science Edition 19:61-64.

Gan W, Okamoto K, Hirano S, Chung K, Kim C, Kim C, Wagoner RH (2008) Properties of friction-stir welded AA 6111 and 5083. Journal of Engineering Materials and Technology 130:31007-1-15.

Ganesh Narayanan R and Narasimhan K (2006) Weld region representation during the simulation of TWB forming behavior. International Journal of Forming Processes 9:491-518.

Ganesh Narayanan R and Narasimhan K (2008 a) Influence of the weld conditions on the forming-limit strains of tailor-welded blanks. The Journal of Strain Analysis for Engineering Design 43:217-227.

Ganesh Narayanan R and Narasimhan K (2008 b) Predicting the forming limit strains of tailor-welded blanks. Journal of strain analysis for engineering design 43:551-563.

Ghosh M, Kumar K, Kailas SV, Ray AK (2010) Optimization of friction stir welding parameters for dissimilar aluminum alloys. Materials and Design 31:3033-3037.

Grant G, Davies R, Stephens E, Wazny S, Kaunitz L, Waldron D (2005) The Formability of Friction Stir Welds in Automotive Stamping Environments, SAE World Congress, April 11-14.

Greitmann MJ and Peter Deimel (2005) Friction stir welding-Innovative Technology for Joining Aluminuim Components. Otto-Graf journal 16:185-192.

Guerdoux S, Fourment L (2009) A 3D numerical simulation of different phases of friction stir welding. Modelling and Simulation of Material Science and Engineering. 17: 32.

Guerra M, Schmidt C, McClure JC, Murr LE, Nunes AC (2003) Flow patterns during friction stir welding. Materials Characterization 49:95-101.

Gurmeet Singh, Kulwant Singh, Jagtar Singh (2011) Effect of Process Parameters on Microstructure and Mechanical Properties in Friction Stir Welding of Aluminum Alloy. Transactions of Indian Institute of Metals. 64(4–5):325-330.

Haşim K and Nuran AY (2009) Mechanical Properties of 6013-T6 Aluminium Alloy Friction Stir Welded Plate. 13th International Conference on Aerospace Sciences & Aviation Technology May 26–28.

Heinz A, Haszler A, Keidel C, Moldenhauer S, Benedictus R, Miller WS (2000) Recent development in aluminium alloys for, aerospace applications. Materials Science and Engineering A 280:102-107.

Heinz B and Skrotzki B (2002) Characterization of a friction stir welded aluminum alloy 6013. Metallurgical and Materials Transactions B 33B:489-498.

Heurtier P, Jones MJ, Desrayaud C, Driver JH, Montheillet F, Allehaux D (2006) Mechanical and thermal modelling of friction stir welding. Journal of Materials Processing Technology 171:348–357.

Hidetoshi Fujii, Ling Cui, Masakatsu Maeda, Kiyoshi Nogi (2006) Effect of tool shape on mechanical properties and microstructure of friction stir welded aluminum alloys. Materials Science and Engineering A 419:25–31.

Hill R (1990) Constitutive modeling of orthotropic Plasticity in sheet metals. Journal of Mechanical Physics of Solids 38:405-417.

Hirata T, Oguri T, Hagino H, Tanaka T, Chung SW, Takigawa Y (2007 a) Influence of friction stir welding parameters on grain size and formability in 5083 aluminum alloy. Material Science Engineering A 456:344-349.

Hirata T, Oguri T, Hagino H, Tanaka T, Wook CS, Tsujikawa M (2007 b) Formability of friction stir welded and arc welded 5083 aluminum alloy sheets. Key Engineering Materials 340-341:1473-1478.

Hua-Bin Chen, Keng Yan, Tao Lin, Shan-Ben Chen, Cheng-Yu Jiang, Yong Zhao (2006) The investigation of typical welding defects for 5456 aluminum alloy friction stir welds. Materials Science and Engineering A 433:64-69.

Hussain AK and Quadri SAP (2010) Evaluation of parameters of Friction stir welding for AA 6351 aluminum alloy. International Journal of Engineering Science and Technology 2(10):5977-5984.

James MN, Hattingh DG, Bradley GR (2003) Weld tool travel speed effects on fatigue life of friction stir welds in 5083 aluminum. International Journal of Fatigue 25:1389–1398.

Jamshidi Aval H, Serajzadeh S, Kokabi AH (2011) Evolution of microstructures and mechanical properties in similar and dissimilar friction stir welding of AA5086 and AA6061. Materials Science and Engineering A 528:8071–8083.

Jiahu Ouyang, Eswar Yarrapareddy, Radovan Kovacevic (2006) Microstructural evolution in the friction stir welded 6061-T6 aluminum alloy to copper. Journal of Materials Processing Technology 172:110-122.

Jones MJ, Heurtier P, Desrayaud C, Montheillet F, Allehaux D, Driver JH (2005) Correlation between microstructure and microhardness in a friction stir welded 2024 aluminium alloy. Scripta Materialia 52:693-697.

Kang SH, Chung SH, Han NH, Oh HK, Lee GC, Kim JS (2007) Relationship between formability and microstructure of Al alloy sheet locally modified by friction stir processing. Scripta Materialia 57:17-20.

Kazanowski P (2006) Sheet Forming of Specific Metals: Froming of Aluminum alloys. ASM Handbook Metal forming: sheet metal forming 14B:583-598.

Keum YT and Lee KB (2000) Sectional finite element analysis of forming processes for aluminum-alloy sheet metals. International Journal of Mechanical Sciences 42:1911-1933.

Kim D, Lee W, Kim J, Chongmin Kim, Kwansoo Chung (2010 a) Formability evaluation of friction stir welded 6111-T4 sheet with respect to joining material direction. International Journal of Mechanical Sciences 52:612–625.

Kim D, Lee W, Kim J, Kyung-Hwan Chung, Chongmin Kim, Kazutaka Okamoto, Wagoner RH, Kwansoo Chung (2010 b) Macro-performance evaluation of friction stir welded automotive tailor-welded blank sheets: Part II–Formability. International Journal of Solids and Structures 47:1048-1062.

Kim JH, Barlat F, Kim C, Chung K (2009) Themo-Mechanical and Microstructural Modeling of Friction Stir Welding of 6111-T4 Aluminum Alloys. Metals and Materials International 15:125-132.

Kim YG, Fujii H, Tsumura T, Komazaki T, Nakata K (2006) Three defect types in friction stir welding of aluminum die casting alloy. Materials Science and Engineering A 415:250-254.

Kinsey B, Krishnan N, Jian J (2004) A Methodology to Reduce and Quantify Wrinkling in Tailor Welded Blank Forming. International Journal of Materials and Product Technology 21:154-168.

Kinsey B, Viswanathan V, Cao J (2001 a) Forming of Aluminum Tailor Welded Blanks. Journal of Materials and Manufacturing 110: 673-679.

Kinsey B, Viswanathan V, Cao J (2001 b) Forming of Aluminum Tailor Welded Blanks. SAE 2001 World Congress 822:1-9.

Kinsey BL and Cao J (2005) An Analytical Model for Tailor welded Blank Forming. Journal of Manufacturing Science and Engineering 125:344-351.

Kumar K and Kailas SV (2008 a) On the role of axial load and the effect of interface position on the tensile strength of a friction stir welded aluminium alloy. Materials and Design 29:791-797.

Kumar K and Kailas SV (2008 b) The role of friction stir welding tool on material flow and weld formation. Materials Science and Engineering A 485:367-374.

Lakshminarayanan AK, Balasubramanian V, Elangovan K (2009) Effect of welding processes on tensile properties of AA6061 aluminium alloy joints. International Journal of Advanced Manufacturing Technology 40:286-296.

Leacock GA (2006) A mathematical description of orthotropy in sheet metals. Journal of the Mechanics and Physics of Solids 54:425-444.

Leal RM, Leitao C, Loureiro A, Rodrigues DM, Vilaca P (2008) Material flow in heterogeneous friction stir welding of thin aluminium sheets: Effect of shoulder geometry. Materials Science and Engineering A 498:384-391.

Lee W, Chung KH, Kim D, Kim C, Okamoto K, Wagoner, RH, Chung K (2009) Experimental and numerical study on formability of friction stir welded TWB sheets based on hemispherical dome stretch tests. International Journal of Plasticity 25:1626–1654.

Lee WB, Lee CY, Chang WS, Yeon YM, Jung SB (2005) Microstructural investigation of friction stir welded pure titanium. Materials Letters 59:3315 – 3318.

Lee WB, Yeon YM, Jung SB (2004) Mechanical Properties Related to Microstructural Variation of 6061 Al Alloy Joints by Friction Stir Welding. Materials Transactions 45:1700-1705.

Leitao C, Emilio B, Chaparro BM, Rodrigues DM (2009) Formability of similar and dissimilar friction stir welded AA 5182-H111 and AA 6016-T4 tailored blanks. Materials and Design 30:3235–3242.

Li Y, Murr LE, McClure JC (1999) Flow visualization and residual microstructures associated with the friction-stir welding of 2024 aluminum to 6061 aluminum. Materials Science and Engineering A 271:213-223.

Lim S, Kim S, Lee C, Kim S (2004) Tensile Behavior of Friction-Stir-Welded Al 6061-T651. Metallurgical and Materials Transactions A 35A:2829-2835.

Lim S, Kim S, Lee CG, Kim SJ, (2005) Mechanical Properties of Friction Stir Welded Al Alloys with Different Hardening Mechanisms., Metals and Materials International 11:113-120.

Lima EBF, Wegener J, Dalle Donne C, Goerigk G, Wroblewski T, Buslaps T, Pyzalla AR, Reimers W (2003) Dependence of the microstructure, residual stresses and texture of AA 6013 friction stir welds on the welding process. Zeitschrift fuer Metallkunde 94(8):908-915.

Lin BS, Ding LJ (1996) A modified form of Hill's orientation dependent yield criterion for orthotropic sheet metals. Journal of the Mechanics and Physics of Solids 44:1739-1764.

Liu FC, Ma ZY (2008) Influence of tool dimension and welding parameters on microstructure and mechanical properties of friction stir welded 6061-T651 aluminum alloy. Metallurgical and Materials Transactions A 39A:2378-2388.

Liu H, Fujii H, Maeda M, Nogi K (2004) Tensile Fracture Location Characterizations of Friction Stir Welded joints of different aluminum alloys. Journal of Material Science Technology 20:103-105.

Liu HJ, Zhang HJ, Yu L (2011) Effect of welding speed on microstructures and mechanical properties of underwater friction stir welded 2219 aluminum alloy. Materials and Design 32:1548-1553.

Liu S, and Chao, YJ (2005) Determination of global mechanical response of friction stir welded plates using local constitutive properties. Modeling and Simulation of Material Science Engineering 13(1):1–15.

Lockwood WD, Borislav Tomaz, Reynolds AP (2002) Mechanical response of friction stir welded AA2024: experiment and modeling. Materials Science and Engineering A 323:348–353.

Longo M, D'Urso G, Giardini C, Ceretti E (2012) Process Parameters Effect on Mechanical Properties and Fatigue Behavior of Friction Stir Weld AA6060 Joints. Journal of Engineering Materials and Technology 134:021006-1-8.

Ma ZY (2008) Friction Stir Processing Technology: A Review. Metallurgical and Materials Transactions A 39A:642-658.

Ma ZY, Sharma SR, Mishra RS (2006) Microstructural Modification of As-Cast Al-Si-Mg Alloy by Friction Stir Processing. Metallurgical And Materials Transactions A 37a:323-3336.

Mahoney MW, Rhodes CG, Flintoff JG, Spurling RA, Bingel WH (1998) Properties of friction-stir-welded 7075 T651 aluminum alloy, Metallurgical and Materials Transactions A 29A:1955-1964.

Malarvizhi S and Balasubramanian V (2012) Influences of tool shoulder diameter to plate thickness ratio (D/T) on stir zone formation and tensile properties of friction stir welded dissimilar joints of AA6061 aluminum-AZ31B magnesium alloys. Materials and Design 40:453-460.

Melendez M, Tang W, Schmidt C, McClure JC, Nunes AC, Murr LE, Tool Forces Developed During Friction Stir Welding, http://ntrs.nasa.gov/archive/nasa/casi.ntrs.nasa.gov/20030071631_2003069405.pdf.

Miles M (2006 a) Formability Analysis: Formability testing of sheet metals. ASM Handbook Metal forming: sheet metal forming 14B:671-703.

Miles MP, Decker BJ, Nelson, TW (2004) Formability and Strength of Friction Stir Welded Aluminum Sheets. Metallurgical and Materials Transactions 35A:3461-3468.

Miles MP, Melton DW, Nelson TW, (2005) Formability of Friction-Stir-Welded Dissimilar-Aluminum- Alloy Sheets. Metallurgical and Materials Transactions A 36:3335-3342.

Miles MP, Pew J, Nelson TW, Li M (2006 b) Comparison of formability of friction stir welded and laser welded dual phase 590 steel sheets. Science and Technology of Welding and Joining 11(4):384-388.

Milton CH, Dymek S, Blicharski M (2008) A model of material flow during friction stir welding. Materials Characterization 59:1206-1214.

Mishra RS and Ma ZY (2005) Friction stir welding and processing. Materials Science and Engineering R 50:1-78.

Mohamed Assidi, Lionel Fourment, Simon Guerdoux, Tracy Nelson (2010) Friction model for friction stir welding process simulation: Calibrations from welding experiments. International Journal of Machine Tools and Manufacture. 50:143–155.

Mohanty HK, Mahapatra MM, Kumar P, Biswas P, Mandal NR (2012) Effect of Tool Shoulder and Pin Probe Profiles on Friction Stirred Aluminum Welds–a Comparative Study. Journal of Marine Science and Application 11:200-207.

Moreira PMGP, D e Oliveira FMF, D e Castro PMST, (2008) Fatigue behavior of notched specimens of friction stir welded aluminum alloy 6063-T6. Journal of Materials Processing Technology 207:283-292.

Mulder J, Vegter H, Ha JJ, van den Boogaard AH (2012) Determination of flow curves under equibiaxial stress conditions. Key Engineering Materials, Material Forming ESAFORM 2012 504–506:53-58.

Murr LE (2010) A Review of FSW Research on Dissimilar Metal and Alloy Systems. Journal of Materials Engineering and Performance 19:1071–1089.

Murr LE, Liu G, McClure JC (1998) A TEM study of precipitation and related microstructures in friction-stir-welded 6061 aluminium. Journal of Materials Science 33:1243-1251.

Mustafa Boz and Adem Kurt (2004) The influence of stirrer geometry on bonding and mechanical properties in friction stir welding process. Materials and Design 25:343-347.

Mustafa Kemal Bilici, Ahmet Irfan Yukler (2012) Influence of tool geometry and process parameters on macrostructure and static strength in friction stir spot welded polyethylene sheets. Materials and Design 33:145-152.

Nandan R, DebRoy T, Bhadeshia HKDH (2008) Recent advances in friction-stir welding Process, weldment structure and properties. Progress in Materials Science 53:980–1023.

Nandedkar VM, Formability studies on a deep drawing quality steel. PhD Thesis. IIT Bombay. India, 2000.

Narasimhan K and Wagoner RH (1991) Finite element modeling simulation of In-plane forming limit diagrams of sheets containing finite defects. Metallurgical and Materials Transactions A 22A:2355-2665.

Nourani M, Abbas Milani S, Yannacopoulos S (2011) Taguchi Optimization of Process Parameters in Friction Stir Welding of 6061 Aluminum Alloy: A Review and Case Study. Engineering 3:144-155.

Palanivel R, Koshy Mathews P, Murugan N, Dinaharan I (2012) Effect of tool rotational speed and pin profile on microstructure and tensile strength of dissimilar friction stir welded AA5083-H111 and AA6351-T6 aluminum alloys. Materials and Design 40:7-16.

Panda KS and Kumar RD (2009) Study of formability of tailor-welded blanks in plane-strain stretch forming. International Journal of Advanced Manufacturing Technology 44:675-685.

Panda KS, Li J, Hernandez BHV, Zhou Y, Goodwin F (2010) Effect of weld location, orientation, and strain path on forming behavior of AHSS tailor welded blanks. Journal of Engineering Materials and Technology 132:041003-1-11.

Peel M, Steuwer A, Preuss M, Withers PJ (2003) Microstructure, mechanical properties and residual stresses as a function of welding speed in aluminium AA5083 friction stir welds. Acta Materialia 51:4791-4801.

Peel MJ, Steuwer A, Withers PJ, Dicker Son T, Shi Q, Sher Cliff H (2006) Dissimilar friction stir welds in AA5083-AA6082. Part I: Process parameter effects on thermal history and weld properties. Metallurgical and Materials Transactions A 37A:2183-2193.

Rai R, De A, Bhadeshia HKDH, DebRoy T (2011) Review: friction stir welding tools. Science and Technology of Welding and Joining 16:325-342.

Rajakumar S, Muralidharan C, Balasubramanian V (2011) Predicting tensile strength, hardness and corrosion rate of friction stir welded AA6061-T6 aluminium alloy joints. Materials and Design 32:2878-2890.

Rajamanickam N, Balusamy V, Madhusudhanna Reddy G, Natarajan K (2009) Effect of process parameters on thermal history and mechanical properties of friction stir welds. Materials and Design 30:2726–2731.

Rani IM, Marpu RN, Kumar ACS (2011) A Study of Process Parameters of Friction Stir Welded AA 6061 Aluminum Alloy in O and T6 conditions. ARPN Journal of Engineering and Applied Sciences 6:61-66.

Razal Rose A, Manisekar K, Balasubramanian V (2011) Effect of axial force on microstructure and tensile properties of friction stir welded AZ61A magnesium alloy. Transactions of Nonferrous Metals Society China 21:974-984.

Ren SR, Ma ZY, Chen LQ (2007) Effect of welding parameters on tensile properties and fracture behavior of friction stir welded Al–Mg–Si alloy. Scripta Materialia 56:69-72.

Reynolds AP (2008) Flow visualization and simulation in FSW. Scripta Materialia 58:338-342.

Reynolds AP, Wei Tang, Gnaupel-Herold T, Prask H (2003) Structure, properties, and residual stress of 304L stainless steel friction stir welds. Scripta Materialia 48:1289–1294.

Rezaei H, Mirbeik MH, Bisadi H (2011) Effect of rotational speeds on microstructure and mechanical properties of friction stir-welded 7075-T6 aluminum alloy. Proceedings of IMechE Part C: Journal of Mechanical Engineering Science 225:1761-1773.

Rhodes CG, Mahoney MW, Bingel WH, Spurling RA, Bampton CC (1997) Effects of friction stir welding on microstructure of 7075 Aluminum. Scripta Materialia 36:69-75.

Rodrigues DM, Loureiro A, Leitao C, Leal RM, Chaparro BM, Vilaça P (2009) Influence of friction stir welding parameters on the microstructural and mechanical properties of AA 6016-T4 thin welds. Materials and Design 30:1913-1921.

Sakthivel T, Sengar GS, Mukhopadhyay J (2009) Effect of welding speed on microstructure and mechanical properties of friction-stir-welded aluminum. International Journal of Advanced Manufacturing Technology 43:468-473.

Sato YS and Kokawa H (2001) Distribution of Tensile Property and Microstructure in Friction Stir Weld of 6063 aluminum alloy. Metallurgical and Materials Transactions A 32A:3023-3031.

Sato YS, Nelson TW, Sterling CJ, Steel RJ, Pettersson CO (2005) Microstructure and mechanical properties of friction stir welded SAF 2507 super duplex stainless steel. Materials Science and Engineering A 397:376–384

Sato YS, Sugiura Y, Shoji Y, Park SHC, Kokawa H, Ikeda K (2004) Post-weld formability of friction stir welded Al alloy 5052. Material Science and Engineering A 369 (1–2):138-143.

Sato YS, Urata M, Kokawa H (2002) Parameters Controlling Microstructure and Hardness during Friction-Stir Welding of Precipitation-Hardenable Aluminum Alloy 6063. Metallurgical And Materials Transactions A 33A:625-635.

Schmidt H and Hattel J (2006) A local model for the thermomechanical conditions in friction stir welding. Modelling and Simulation of Material Science and Engineering. 13:389-396

Schmidt HNB, Dickerson TL, Hattel JH (2006) Material flow in butt friction stir welds in AA2024-T3. Acta Materialia 54:1199–1209.

Scialpi A, De Filippis LAC, Cavaliere P (2007) Influence of shoulder geometry on microstructure and mechanical properties of friction stir welded 6082 aluminium alloy. Materials and Design 28:1124-1129.

Semiatin SL (2006) Forming of Steel Tailor-Welded Blanks. ASM Handbook Metal forming: sheet metal forming 14B:539-546.

Simar A, Brechet Y, De Meester B, Denquin A, Pardoen T (2008) Microstructure, local and global mechanical properties of friction stir welds in aluminium alloy 6005A-T6. Materials Science and Engineering A 486: 85-95.

Sirong YU, Xianjun C, Zhiqiu H, Yaohui L (2010) Microstructure and mechanical properties of friction stir welding of AZ31B magnesium alloy added with cerium. Journal of Rare Earths 28:316-320.

Song KH, Fujii H, Nakata K (2009) Effect of welding speed on microstructural and mechanical properties of friction stir welded Inconel 600. Materials and Design 30:3972-3978.

Song M and Kovacevic R (2003) Thermal modeling of friction stir welding in a moving coordinate system and its validation. International Journal of Machine Tools and Manufacture 43:605-615.

Srinivas Naik B, Janaki Ramulu P, Ganesh Narayanan R (2010) Application of a few necking criteria in predicting the forming limit of un-welded and tailor-welded blanks. Journal of strain analysis for engineering design 45:79-96.

Steuwer A, Peel MJ, Withers PJ (2006) Dissimilar friction stir welds in AA5083–AA6082: The effect of process parameters on residual stress. Materials Science and Engineering A 441:187-196.

Surekha K, Murty BS, Prasad Rao K (2009) Effect of processing parameters on the corrosion behaviour of friction stir processed AA 2219 aluminum alloy. Solid State Sciences 11:907-917.

Thomas UWM and Nicholas ED (1997) Friction stir welding for the transportation industries. Materials and Design 18:269-273.

Ulysse P (2002) Three-dimensional modeling of the friction stir-welding process. International Journal of Machine Tools and Manufacture 42:1549–1557.

Upadhyay P and Reynolds AP (2010) Effects of thermal boundary conditions in friction stir welded AA7050-T7 sheets. Materials Science and Engineering A 527:1537-1543.

Veera Babu K, Ganesh Narayanan R, Saravana Kumar G (2009) An expert system based on artificial neural network for predicting the tensile behavior of tailor welded blanks. Expert Systems with Applications 36:10683-10695.

Vijay SJ and Murugan N (2010) Influence of tool pin profile on the metallurgical and mechanical properties of friction stir welded Al–10 wt. % TiB_2 metal matrix composite. Materials and Design 31:3585-3589.

Woo W, Balogh L, Ungár T, et al. (2008) Grain structure and dislocation density measurements in a friction-stir welded aluminum alloy using X-ray peak profile analysis. Materials Science and Engineering A 498:308-313.

Woo W, Ungar T, Feng Z, et al. (2010) X-Ray and Neutron Diffraction Measurements of Dislocation Density and Sub-grain Size in a Friction-Stir-Welded Aluminum Alloy. Metallurgical and Materials Transactions A 41:1210-1216.

Xu W, Liu J, Luan G, Dong C (2009 a) Microstructure and mechanical properties of friction stir welded joints in 2219-T6 aluminum alloy. Materials and Design 30:3460-3467.

Xu W, Liu J, Luan G, Dong C (2009 b) Temperature evolution, microstructure and mechanical properties of friction stir welded thick 2219-O aluminum alloy joints. Materials and Design 30:1886-1893.

Yang Q, Li X, Chen K, Shi YJ (2011) Effect of tool geometry and process condition on static strength of a magnesium friction stir lap linear weld. Materials Science and Engineering A 528:2463-2478.

Yan-hua Zhao, San-bao Lin, Lin Wu, Fu-xing Qu (2005) The influence of pin geometry on bonding and mechanical properties in friction stir weld 2014 Al alloy. Materials Letters 59:2948-2952.

Yasunari Tozaki, Yoshihiko Uematsu, Keiro Tokaji (2007) Effect of tool geometry on microstructure and static strength in friction stir spot welded aluminium alloys. International Journal of Machine Tools & Manufacture 47:2230-2236.

Yuan SJ, Hu ZL, Wang XS (2012) Evaluation of formability and material characteristics of aluminum alloy friction stir welded tube produced by a novel process. Materials Science and Engineering A 543:210-216.

Yuan W, Mishra RS, Webb S, Chen YL, Carlson B, Herling DR, Grant GJ (2011) Effect of tool design and process parameters on properties of Al alloy 6016 friction stir spot welds. Journal of Materials Processing Technology 211:972-977.

Zadpoor AA, Sinke J, Benedictus R (2007 a) Spring back behavior of Friction Stir Welded Tailor made blanks. International Deep-drawing Research Group IDDRG 2007 International Conference.

Zadpoor AA, Sinke J, Benedictus R (2007 b), Finite Element Modeling of Transition Zone in Friction Stir Welded Tailor-Made Blanks. CP908, NUMIFORM 2007, Materials Processing and Design: Modeling, Simulation and Applications.

Zadpoor AA, Sinke J, Benedictus R (2008 a) Theoretical prediction of failure in forming of friction stir welded blanks. International Journal of Material Forming Supplement 1:305-308.

Zadpoor AA, Sinke J, Benedictus R (2009) Finite element modeling and failure prediction of friction stir welded blanks. Materials and Design 30:1423-1434.

Zadpoor AA, Sinke J, Benedictus R (2010) Global and Local Mechanical Properties and Microstructure of Friction Stir Welds with Dissimilar Materials and/or Thicknesses. Metallurgical and Materials Transactions A 41A:3365-3378.

Zadpoor AA, Sinke J, Benedictus R, Pieters R (2008 b) Mechanical properties and microstructure of friction stir welded tailor-made blanks. Materials Science and Engineering A 494:281-290.

ZHANG Gui-feng, SU Wei, ZHANG Jun, WEI Zhong-xin, ZHANG Jian-xun (2010) Effects of shoulder on interfacial bonding during friction stir lap welding of aluminum thin sheets using tool without pin. Transactions of Nonferrous Metals Society China 20:2223-2228.

Zhang HW, Zhang Z, Chen JT (2007) 3D modeling of material flow in friction stir welding under different process parameters. Journal of Materials Processing Technology 183:62-70.

Zhang HW, Zhang Z, Chen JT (2008) Corrigendum to "3D modeling of material flow in friction stir welding under different process parameters". Journal of materials processing technology 199:456.

Zhang Z and Zhang HW (2009) Numerical studies on controlling of process parameters in friction stir welding. Journal of materials processing technology 209:241-270.

Zhang Z and Zhang HW (2009) Numerical studies on the effect of transverse speed in friction stir welding. Materials and Design 30:900–907.

Zhang Z, Liu YL, Chen JT (2009) Effect of shoulder size on the temperature rise and the material deformation in friction stir welding. International Journal of Advanced Manufacturing Technology 45:889-895.

Zimmer S, Langlois L, Laye J, Goussain JC, Martin P, Bigot R (2009) Influence of processing parameters on the tool and workpiece mechanical interaction during friction stir welding. International Journal of Material Forming 2(1):299-302.

Zohoor M, Besharati Givi MK, Salami P (2012) Effect of processing parameters on fabrication of Al–Mg/Cu composites via friction stir processing. Materials and Design 39:358–365.